A Quantitative MALDI-MSI Study of the Movement of Molecules in Biological Systems

RUSSO, Cristina

A Quantitative MALDI-MSI Study of the Movement of Molecules in Biological Systems

Cristina Russo

A thesis submitted in partial fulfilment of the requirements of Sheffield Hallam University for the degree of Doctor of Philosophy

September 2019

Candidate Declaration

I hereby declare that:

1. I have not been enrolled for another award of the University, or other academic or professional organisation, whilst undertaking my research degree.

2. None of the material contained in the thesis has been used in any other submission for an academic award.

3. I am aware of and understand the University's policy on plagiarism and certify that this thesis is my own work. The use of all published or other sources of material consulted have been properly and fully acknowledged.

4. The work undertaken towards the thesis has been conducted in accordance with the SHU Principles of Integrity in Research and the SHU Research Ethics Policy.

5. The word count of the thesis is 39153.

Name	*Cristina Russo*
Date	*September 2019*
Award	*PhD*
Faculty	*Health and Wellbeing*
Director(s) of Studies	*Professor Malcolm Clench*

Dedication

To my Father

E ricordati, io ci sarò.
Ci sarò nell' aria.

Allora ogni tanto,
se mi vuoi parlare,
mettiti da parte,
chiudi gli occhi e cercami.

Ci si parla.
Ma non nel linguaggio delle parole.
Nel silenzio.

(Tiziano Terzani)

Acknowledgments

At the end of this long and tortuous journey, thanks are due to everyone who was close to me, supporting and bearing with me in these years.

Firstly, I would like to thank my supervisor Professor Malcolm Clench for giving me the opportunity of being part of his research group. I am truly grateful for all your support, your guidance and especially for your faith in me. I learnt from you what it means to carry out real Research, One without linguistic and geographic barriers.

In addition, I would like to thank the rest of my supervisory team Professor Neil Bricklebank, Dr. Catherine Duckett, Dr. Steve Mellor and Dr. Stephen Rumbelow for the help and advice throughout my PhD. Catherine you have been a perfect mixture between supervisor and friend, thanks for being my confidant and supporter, as well as “crazy” roomie.

Special thanks go to my family, my rock. To my Father, for teaching me that the real tools to be successful in life are honesty, determination and humility. You made me feel always your source of pride and I hope I can always be that for you. To my Mother, my first and biggest supporter. Thanks for encouraging me to always believe in myself and helping me to pursue this career. You were there whenever I needed, taking the first plane without hesitation, to take care of me. To my sisters, Flavia and Anna, for relieving in these years my homesickness with your messages and video calls. Flavia with Antonio’s birth you made me the happiest auntie in the world. Anna your visit at my every birthday, our long conversations despite time difference and finding you waiting for me at the airport are my most lovely memories.

To my friends of adventure, Becky, Ieva and Emma. Becky, I am extremely grateful for all your support. You have been more than just a friend, taking care of me in the hardest time and sharing with me the happiest moments. Ieva, a huge thanks for all your incredible patience and help. I really enjoyed all our trips, for conferences and pleasure. Now I have no excuses anymore, I promise I will come to visit you soon. Emma, I know my strong Italian accent made our communication difficult in the beginning but I really appreciated all of your efforts in making things clear for me, I never will forget that day in the bank.

To Ermanno, my mentor. You have been an incredible guide, your affection and advice have been precious and I hope I can draw from them also in the future.

Also I would like to thank Prof. Simona Francese, for her tips, for the encouragements and comprehension about me finishing my thesis during the post-doc. To Dr. Laura Cole, Dr. Ekta Patel, Dr. Robert Bradshaw and Dr. Amanda Harvey, for offering me help and friendship since the first day I came. To Prof. Christine Le Maitre for her availability and kindness. To Dr. Emily Lewis for all listening and "catch up" lunches and coffees in York.

Special thanks go to the technicians, Dr. Daniel Kingsman and Michael Cox. You have been a huge resource in the laboratory throughout all my PhD, solving instrument “crisis” and answering all my countless questions.

Thanks to all of my BMRC colleagues, old and new, who have represented more a family than just colleagues. To the "MSI geeks". You were really supportive during the last period of my PhD, we shared so much hard work in the mass spec lab but also a lot of fun and laughs. To Paula, it was a joy to be your deskmate my last year. Thanks for coping with my mess and for cheering me up when the stress took over.

Huge thanks to Bruno, for all the love and for putting up with me even when I could not stand myself. Your willpower and your positivity have been inspirational for me and definitely your contribution for the end of this PhD is huge. I cannot wait to start our next chapter together.

Leaving my country, my family and studying a PhD in another language has been an arduous challenge. I am really grateful to those who in one way or another have helped me to face this and offered the opportunity of personal and professional growth, making me the person I am now, without losing my "Italianity", which I am extremely proud of.

An African proverb says "If you want to go quickly, go alone, but if you want to go far, go together" and I couldn't have gone so far without all of you.

Grazie mille dal profondo del cuore.

i. Abstract

The use of mass spectrometry imaging (MSI) for the analysis of 3D tissue models of human skin has been shown to provide an elegant label-free methodology for the study of both drug absorption and drug biotransformation.

The main aim of the work presented in this thesis was to develop methodology for quantitative assessment of percutaneous absorption using matrix assisted laser desorption ionisation mass spectrometry imaging (MALDI-MSI). Quantitative assessment of the absorption of an antifungal agent, terbinafine hydrochloride, into the epidermal region of a commercial full thickness living skin equivalent model (Labskin) was used as a model system.

Different approaches to generate robust and sensitive quantitative mass spectrometry imaging (QMSI) data were developed and compared. The combination of microspotting of analytical and internal standards, matrix sublimation, and recently developed software for quantitative mass spectrometry imaging provided a high-resolution method for the determination of terbinafine hydrochloride in Labskin. A quantitative assessment of the effect of adding a penetration enhancer (dimethyl isosorbide (DMI)) to the delivery vehicle was also performed, and data was compared to LC–MS/MS measurements of isolated epidermal tissue extracts. Comparison of means and standard deviations indicated no significant difference between the values obtained by the two methods.

In this thesis the localisation of hydrocortisone hydrochloride in *ex-vivo* skin was also investigated. Hydrocortisone exhibits a low ionisation efficiency that makes its detection challenging with mass spectrometry techniques. An in-solution and on-tissue chemical derivatisation reaction using the Girard reagent T, a hydrazine based reagent, significantly increased the sensitivity and detection of the respective hydrocortisone-derivative using MALDI-MSI.

In an additional study, MALDI-MSI was used to assess the metabolic activity in Labskin by employing the approach of "substrate-based mass spectrometry imaging" (SBMSI). Preliminary MALDI-MSI data detected the activity of the carboxylesterase 1 enzyme in the epidermal layer of skin. The MALDI-MSI data was supported by preliminary LC-MS/MS analysis. To investigate the reproducibility of the results future investigations are required.

ii. Contents

iii. List of tables

iv. List of figures

v. Abbreviations

α-CHCA: alpha-cyano-4-hydroxycinnamic acid

µg: microgram

µL: microliter

µm: micrometer

2D: two dimensional

3D: three dimensional

3Rs: Replacement, Reduction and Refinement

9-AA: 9-aminoacridine

AC: acetyl-l-carnitine

ACN: acetonitrile

ADE: acoustic droplet ejection

ANI: aniline

AP: atmospheric pressure

API: atmospheric pressure interface

CEM: chain ejection model

CES: carboxylesterase

CPCD: coupled photophysical and chemical dynamics

CPE: chemical penetration enhancer

CRM: charge reduction model

CYP: cytochrome

d: deuterated

DAN: diaminonaphthalene

DC: direct current

DESI: desorption electrospray ionisation

DHB: 2,5-dihydroxybenzoic acid

diH_2O: deionised water

DMI: dimethyl isosorbide

DNPH : dinitrophenylhydrazine

DPK: dermatopharmacokinetics

EGF: epidermal growth factor

ESI: electrospray ionisation

EtOH: ethanol

EU: European Union

FA: formic acid

FFA: free fatty acid

FMPTS: 2-fluoro-1-methylpyridinium p-toluenesulfonate

FT-ICR: fourier transform-ion cyclotron resonance

FWHM: full width at half maximum

g: gram

GirT: Girard's reagent T

H&E: haematoxylin and eosin

HBA: hydroxybenzoic acid

HC: hydrocortisone

HCl: hydrochloride

HDMS: high definition mass spectrometry

HPLC: high performance liquid chromatohraphy

HSE: human skin equivalent

ILMs: ionic liquid matrices

Ims: industrial methylated spirit

IMS: ion mobility separator

IR: infrared

IS: internal standard

ITO: indium tin oxide

K: coefficient of partition

LC-MS: liquid chromatography-mass spectrometry

LESA: liquid extraction surface analysis

LIT: linear ion trap

LOD: limit of detection

LOQ: limit of quantitation

LSEs: living skin equivalents

m/z: mass to charge ratio

M: molar

MALDI: matrix assisted laser desorption ionisation

MeOH: methanol

mg: milligram

mL: milliliter

mm: millimiter

mM: millimolar

mm^2 : millimiter squared

mm^3 : millimiter cubed

MP: methylparaben

MPH: methylphenidate

MRM: multiple reaction monitoring

MS/MS: tandem mass spectrometry

MS: mass spectrometry

MSI: mass spectrometry imaging

MSP: mass spectrometry profiling

NC: national centre

Nd:YAG: neodymium-doped yttrium aluminium garnet

NEDC: N-(1-naphthyl) ethylenediamine dihydrochloride

ng: nanogram

NHDF: normal human dermal fibroblasts

nL: nanoliter

nm: nanometre

PBS: phosphate buffered saline

PC: phosphatidylcholine

ppm: parts per million

Q: quadrupole

QIT: quadrupole ion trap

QMSI: quantitative mass spectrometry imaging

QTOF: quadrupole time of flight

QWBA: quantitative whole-body autoradiography

RA: ritalinic acid

RF: radiofrequency

RHEs: reconstructed human epidermis

ROI: region of interest

RSD : relative standard deviation

RSE: residual standard error

SA: sinapinic acid

SB-MSI: substrate based mass spectrometry imaging

SC: stratum corneum

SIL: stable-isotope labelled

SIMS: secondary ion mass spectrometry

SRIG: stacked ring ion guides

TBF: terbinafine

TEA: triethylamine

TEC: tissue extinction coefficient

TFA: trifluoroacetic acid

TIC: total ion current

TIS: timed ion selector

TOF/TOF: tandem time-of-flight

TOF: time of flight

TWIG: travelling wave ion guides

TWIMS: travelling wave ion mobility separator

UV: ultraviolet

v/v: volume to volume

w/v: weight to volume

w/w: weight to weight

XME: xenobiotic-metabolising enzyme

Chapter 1:Introduction

1.1 Mass spectrometry

Mass spectrometry (MS) is an analytical technique capable of molecular analysis by ionisation of chemical species and subsequent sorting of the ions by their mass to charge ratio (*m/z*). The principal elements of a mass spectrometer instrument include the:

- Ionisation source, where molecules within the sample are ionised.
- Mass analyser, where ions are separated by their mass to charge ratio.
- Detector, for the measurement of ion relative abundance, resulting then in a mass spectrum.
- Data system, which includes computer and software, for the acquisition and processing of data derived from MS.

Commercially available mass spectrometers offer different configurations of ionisation sources, mass analysers and detectors.

A simple diagram of a mass spectrometer is illustrated below (Figure 1.1).

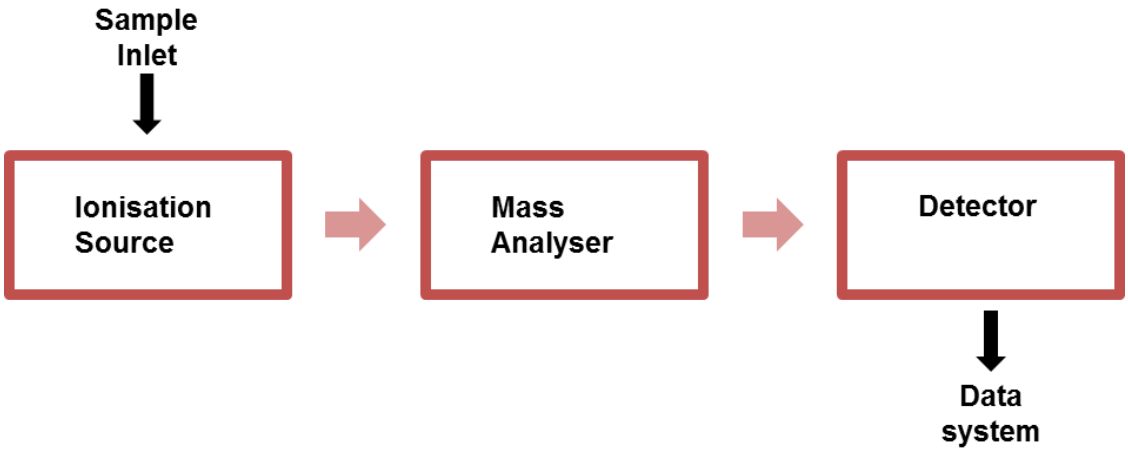

Figure 1.1 *Basic components of a mass spectrometer, including; a sample inlet, an ionisation source, a mass analyser, a detector and a data system (displaying the mass spectrum).*

1.2 Ionisation source

Multiple ionisation sources are associated with mass spectrometry and their different characteristics are mainly related to the exploitable mass range and the energies involved in the ionisation process. The ionisation sources used in the present study are electrospray ionisation (ESI) and matrix assisted laser desorption ionisation (MALDI); they are referred to as "soft" ionisation techniques as they cause little or no fragmentation.

1.2.1 Electrospray ionisation (ESI)

Electrospray ionisation (ESI) was presented in the late 1960's by Dole and co-workers (Dole *et al.*, 1968), and later combined with a quadrupole mass analyser by Yamashita and Fenn (Yamashita and Fenn, 1984).

ESI is an atmospheric pressure ionisation technique produced by injecting an analyte solution through a capillary, to which a high voltage is applied, into a desolvation chamber. The voltage (~ 3-6 kV), which is applied between the capillary and the sampling cone, leads to the formation of a droplet containing an excess of charges (positive or negative) at the tip of the capillary. As a consequence of the strong electric field the shape of the droplet changes to a Taylor cone, from which an aerosol of highly charged droplets is released (Kebarle and Verkcerk, 2009; Hoffmann and Stroobant, 2007).

In the desolvation chamber, the volume of the droplets reduces due to the evaporation of the solvent under the influence of a stream of drying gas/heat. The shrinking of droplet volume leads to an increase of the repulsive force between the charges at the surface until reaching the Rayleigh instability limit, the point at which the surface tension matches Coulombic repulsion. When the Rayleigh limit is exceeded, the droplet undergoes Coulombic explosion, releasing smaller droplets, which undergo further desolvation and coulombic explosion until the formation of gaseous phase analyte ions occurs (Figure 1.2).

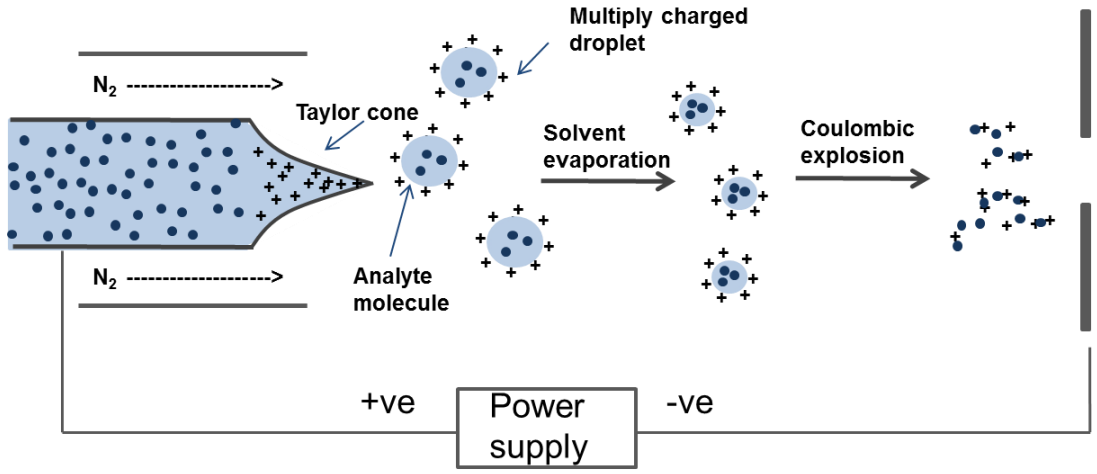

Figure 1.2 *Representation of an electrospray ionisation source. A Taylor cone is formed at the tip of the capillary, from which a spray of charged droplets is expelled due to an applied voltage.*

The advantage of this method is that it requires very little sample preparation and it is able to generate multiply charged ions. Because the analyser in mass spectrometry arrays the ions based on their mass to charge ratio, the ability of electrospray to produce multiply charged ions extends the mass range of analysis up to kDa-MDa orders of magnitude, which makes it possible to observe intact proteins and their associated polypeptide fragments (Ho *et al.*, 2003; Pitt, 2009). Molecules for ESI are already ionised in solution prior to them being transferred to the gas phase, therefore non-polar molecules are not very ionisable by ESI.

Three main mechanisms have been proposed for the process that leads up to the emission of the ions from the charged droplets; these include: the ion evaporation model (IEM); the charge reduction model (CRM) and the chain ejection model (CEM). The IEM model was proposed by Iribarne and Thomas and it is more likely to occur during analysis of small molecular weight compounds (Iribarne and Thomson, 1976). This model suggests that pre-formed solution ions are expelled from nanodroplets, which have reduced their volume by evaporation until the field strength at the surface of the droplet is large enough to assist the desorption of the ions into the gas phase (Nguyen and Fenn, 2007). The CRM model was proposed by Dole *et al.* and it is more likely to occur during analysis of large molecular weight compounds (Dole *et al.*,

1968). The CRM model proposes that nanodroplets, containing a single analyte, fully evaporate and the residual charge is transferred to the analyte (Fernandez de la Mora, 2000). The latest mechanism is the CEM, which was firstly described by Ahadi *et al.* and it is more likely to occur during analysis of unfolded, disordered proteins (Ahadi and Konermann, 2012). This model suggests that an unfolded protein migrates to the surface of the droplet due to the exposure of hydrophobic residues and one chain terminus get partially ejected from the droplet into the gas phase. This is followed by further ejection of the rest of the protein, which will result in highly charged ions (Konermann *et al.*, 2013; Metwally, Duez and Konermann, 2018). A schematic illustration of the main mechanisms responsible of ion formation by ESI is provided in Figure 1.3.

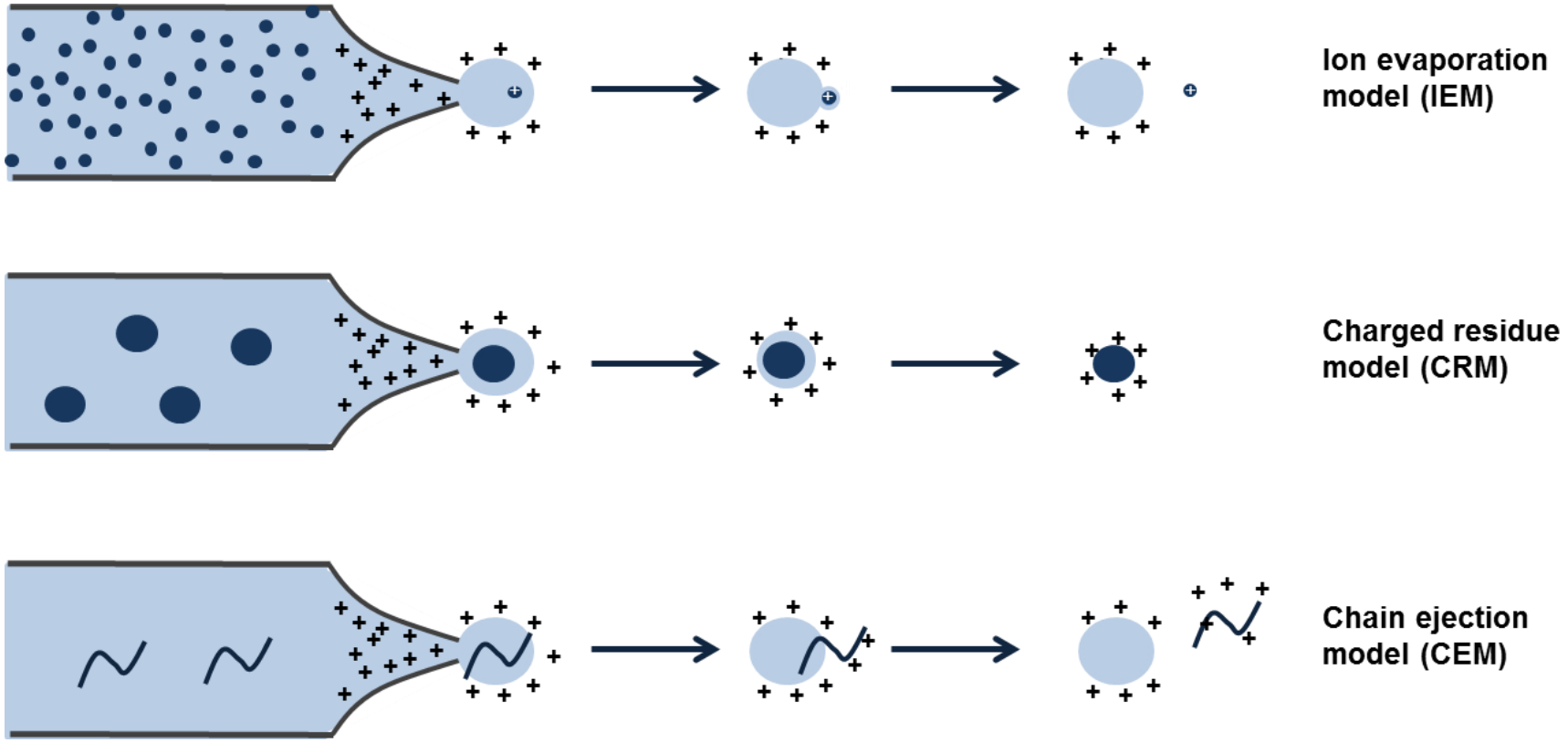

Figure 1.3 *Schematic representation of the three proposed mechanisms of ESI. In the IEM small ions are emitted from droplets which shrink until the field strength at the surface is large enough for ions to be expelled. In the CRM a droplet containing a single analyte evaporates with the residual charge being transferred to the analyte. In the CEM a disordered polymer is partially ejected from the droplet where protons attach to the exposed portion, followed by further extrusion and ultimate ejection of the rest of the protein.*

1.2.2 Matrix assisted laser desorption ionisation (MALDI)

Matrix assisted laser desorption ionisation (MALDI) was developed in the late 1980's by Karas, Hillenkamp and co-workers (Karas, Bachmann and Hillenkamp, 1985). MALDI generates intact gas-phase ions from non-volatile and thermally labile compounds. Initially, it was established as a widespread and powerful source for the detection of macromolecules and biomolecules, such as proteins and polysaccharides (Hoffmann and Stroobant, 2007). However, the application areas have quickly extended and, nowadays, this technique also finds a place into many laboratory's workflow for the analysis of small molecules such as pharmaceuticals, lipids, metabolites and peptides (Amstalden van Hove, Smith and Heeren, 2010) .

MALDI uses a laser to induce ionisation of an analyte, which is mixed with a matrix, typically a molecule with conjugated double bonds. The matrix is a key component of the method, since it acts by absorbing most of the laser energy and promoting analyte ionisation. Although either ultraviolet (UV) or infrared (IR) lasers can be used as light sources, the majority of MALDI sources contain UV lasers, which include nitrogen laser at a wavelength of 337 nm, and neodymium-doped yttrium aluminium garnet (Nd:YAG) laser at a wavelength of 355 nm.

In MALDI mass spectrometry profiling (MSP) experiments, an analyte is first co-crystallised with the matrix, which is usually in high excess. The mixture (analyte embedded in the matrix) is dried and placed under vacuum conditions inside a MALDI source, where it is irradiated by intense laser pulses. Subsequently, high energy excitation of matrix molecules causes rapid heating and ablation of crystals which expand into the gas phase. Ionisation events could happen under vacuum at any time during this process (Hoffmann and Stroobant, 2007).

A schematic overview of the MALDI technique is shown in Figure 1.4**.**

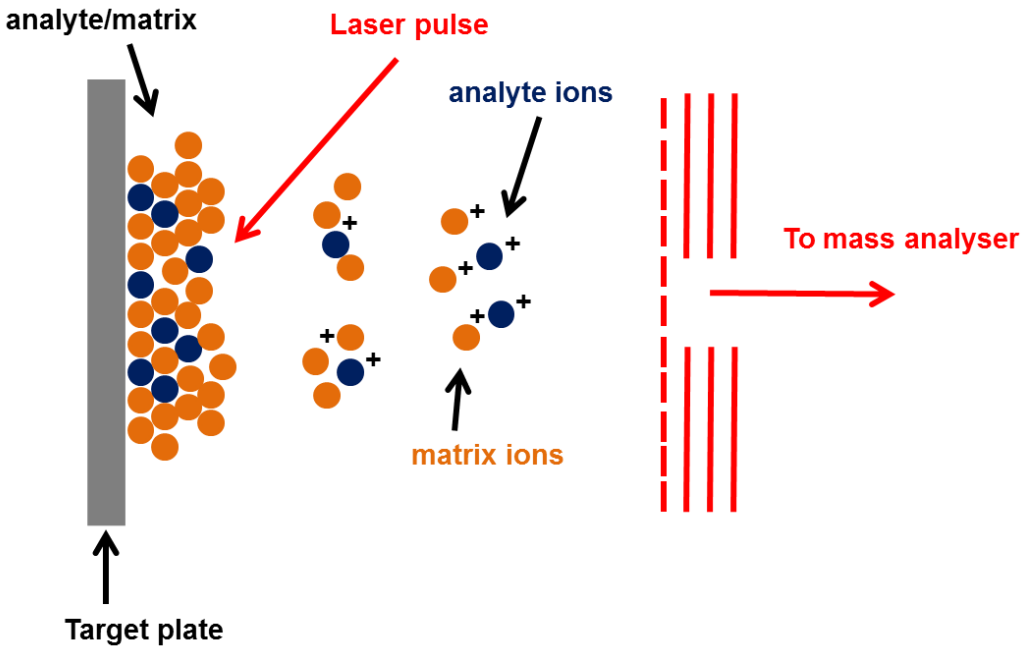

Figure 1.4 *A schematic diagram of the matrix assisted laser desorption ionisation process. The laser fires at the crystals (analyte-matrix) causing the desorption and ionisation of the gas phase ions, which are then directed into a mass analyser.*

However, MALDI source can operate also at atmospheric pressure (AP-MALDI) (Laiko, Moyer and Cotter, 2000; Li *et al.*, 2014). The principles behind the sample preparation and ionisation are the same for both vacuum and AP-MALDI, however in the latter case, the ions are generated under normal atmospheric pressure conditions and their movement into a high vacuum analyser is pneumatically assisted by a stream of dry nitrogen (Laiko, Baldwin and Burlingame, 2000; Hoffmann and Stroobant, 2007). The main advantages of AP-MALDI over conventional vacuum MALDI are associated with the preservation of sample integrity, as well as the higher experimental practicality, indeed AP-MALDI can be easily combined with mass spectrometer equipped with atmospheric pressure interface (API) and interchanged with other AP sources (Hoffmann and Stroobant, 2007).

1.2.2.1 MALDI ionisation

The mechanisms behind the ionisation process in MALDI are not entirely understood yet. However, it is commonly accepted that the ionisation process is separated into two steps: a primary ionisation process during or shortly after the laser pulse and a secondary ionisation process in the expanding plume of desorbed material (Knochenmuss, 2006). Generation of the first ions represents the most disputed part of the ionisation mechanism. Several processes have been proposed, and those considered the most probable are: the Lucky Survivor model (Jaskolla and Karas, 2011), the coupled photophysical and chemical dynamics (CPCD) model (Knochenmuss, 2013, 2016) and the thermal proton transfer model (Chu *et al.*, 2014; Lu *et al.*, 2015).

The Lucky Survivor model proposes that analyte molecules are embedded into the matrix as charged species (Hillenkamp and Peter-Katalinić, 2007). After the ablation upon laser irradiation, clusters of different sizes, containing matrix, analytes and ionic species incorporated in the matrix crystals, are generated. An extensive neutralisation of most of the ions by their counter ions is thought to occur in the plume; only ions that escape the neutralisation can be detected, hence they are called "lucky survivors". This model offers an explanation of the presence of the predominantly singly charged ions observed in MALDI spectra, since they have the greatest chance of "surviving" (Karas, Glückmann and Schäfer, 2000; Karas and Krüger, 2003; Jaskolla and Karas, 2011). In the CPCD model, the photoexcitation of the matrix is principally involved in the ionisation process. First, upon laser irradiation, excitation of matrix molecules takes place, which raise to the first electronically excited state (S_1). This is followed by an energy pooling event defined as redistribution of the total energy of two neighbouring excited matrix molecules leading to a matrix molecule at a higher excited state (S_n), while the other molecule returns to the ground state (S_0). A subsequent pooling event between one matrix molecule in a highly electronic excited state (S_n) with another in the first electronic excited state (S_1) results in the formation of matrix ions. These ions will undergo a set of reactions to generate the final ions (secondary process) (Knochenmuss, 2013, 2016). A diagram of the steps that occur in the CPCD model is illustrated in Figure 1.5.

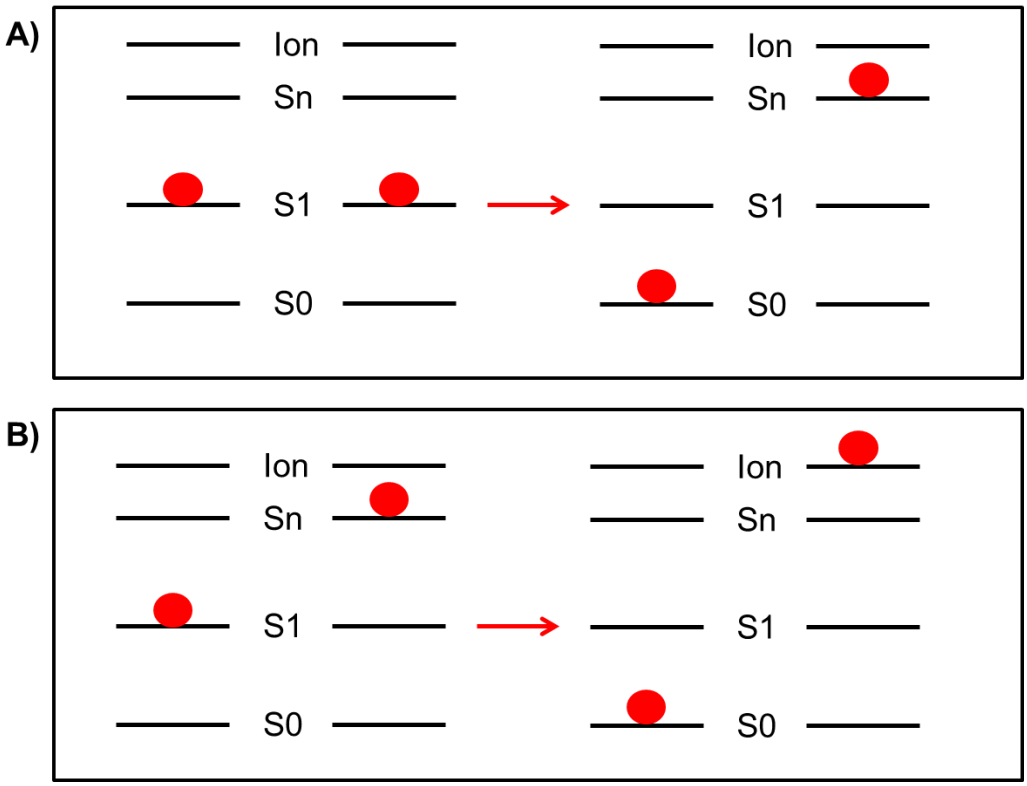

Figure 1.5 *Schematisation of the two energy pooling events, which are the key of the coupled chemical and physical dynamics (CPCD) model: A) S1 + S1 pooling to S0 and Sn. B) S1 + S0 pooling to S0 and ion.*

In the thermal proton transfer model it is important to estimate the ion-to-neutral ratio of matrix and analyte molecules for the MALDI mechanism. The laser energy absorbed by matrix molecules is converted in thermal energy leading to an increase in temperature. The creation of a polar fluid, then, causes a reduction of the ionisation energy of the matrix with consequent formation of free protons. These protons diffuse through the polar fluid and they are trapped by the analyte molecules, causing ionisation of the analyte molecules (Lu *et al.*, 2015).

The ions formed during the primary ionisation will react with neutral molecules present in the expanding plume of desorbed material, causing the formation of the ions which will be detected by the mass spectrometer. The secondary ionisation mechanisms include: proton, cation or electron transfer (Knochenmuss and Zenobi, 2003). Proton transfer is the main secondary

reaction in MALDI and it takes place between protonated matrix and neutral analytes, as shown below:

$$MH^+ + A \rightarrow M + AH^+$$

1.3 MALDI mass spectrometry imaging (MALDI-MSI)

MALDI mass spectrometry imaging (MALDI-MSI) is a relatively new and powerful technique able to study intact biological samples providing ion distribution maps of many non-labelled endogenous and exogenous species simultaneously. This is a distinct advantage in comparison to conventional techniques, such as immunohistochemistry and radiolabelling. The absence of labels or chemical probes makes this technique a fast and relatively inexpensive technique, which can be used to perform *de novo* discoveries.

MALDI-MSI was first illustrated by Spengler *et al.* (Spengler, Hubert and Kaufmann, 1994), while the first full publication was reported by Caprioli and coworkers in 1997 (Caprioli, Farmer and Gile, 1997). In this work, the authors described the development of the MALDI-MSI technique to localise peptides and proteins in biological tissue.

Over the past two decades, MALDI-MSI has become established as a powerful method extensively employed in many applications (Anderson *et al.*, 2010; Francese and Clench, 2010; Solon *et al.*, 2010; Ryan, Spraggins and Caprioli, 2019) and its use to study skin absorption was one of the first applications of MSI in pharmaceutical analysis to be reported (Bunch, Clench and Richards, 2004).

In a typical MALDI-MSI experiment, prior to analysis, an effective sample preparation step is required, which includes: tissue sampling; tissue sectioning and matrix application (Shimma and Sugiura, 2014). An overview of the workflow for the MALDI-MSI analysis of a tissue section is illustrated in Figure 1.6.

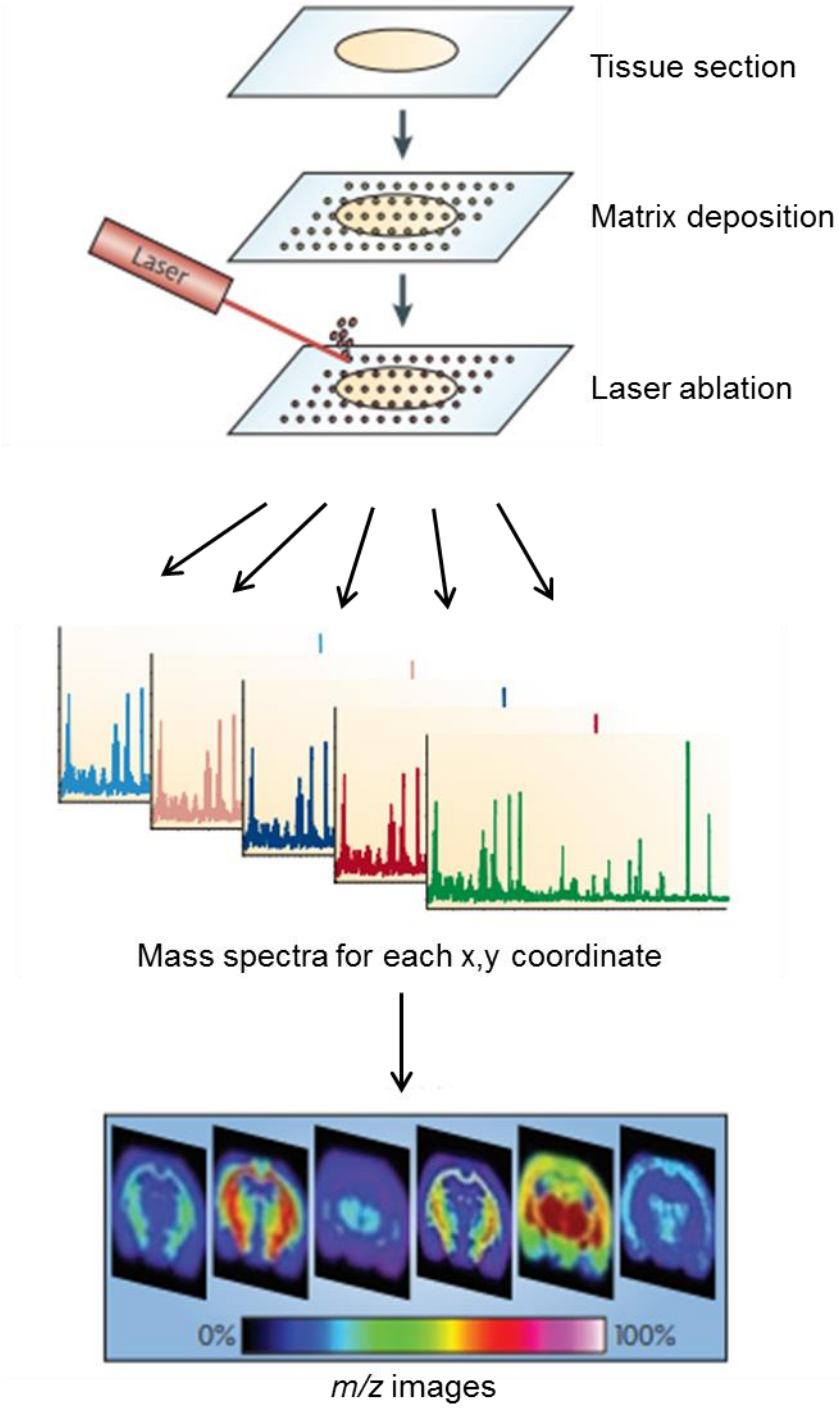

Figure 1.6 *Schematic overview of a MALDI MSI experiment. Figure adapted from (Schwamborn and Caprioli, 2010).*

Matrix deposition technique represents a crucial step in the MSI workflow and can significantly impact MSI results in terms of analyte extraction and spatial localisation (Smith *et al.*, 2017). Several matrix deposition devices, used to generate data in this thesis, will be described later.

The MALDI-MS images presented in this thesis were acquired using the microprobe approach. In this mode, upon co-crystallisation of the matrix with the analytes, the laser is fired at the coated sample, at a series of programmed raster points in an array of two dimensional positions, creating a full mass spectrum at each x,y coordinate. Once the experiment has concluded, the results from individual mass spectra are reconstructed into an image revealing the localisation and the abundance of ions within the sample (Luxembourg *et al.*, 2004). With the microprobe approach, the resolution of the image depends on the laser spot size as well as on the sample stage movement increment; and the throughput time increases significantly with increased resolution. An alternative mode is the microscope mode. In this approach, the laser fires the sample with a large beam (usually 200 µm) and the derived ions maintain their spatial coordinates throughout travel until they reach a position sensitive detector (Luxembourg *et al.*, 2004). In microscope mode the spatial resolution is influenced by the quality of the ion optics and the resolving power of the detector (Luxembourg *et al.*, 2004; Klerk *et al.*, 2009). Figure 1.7 shows a representation of both microprobe and microscope modes for MALDI imaging experiments.

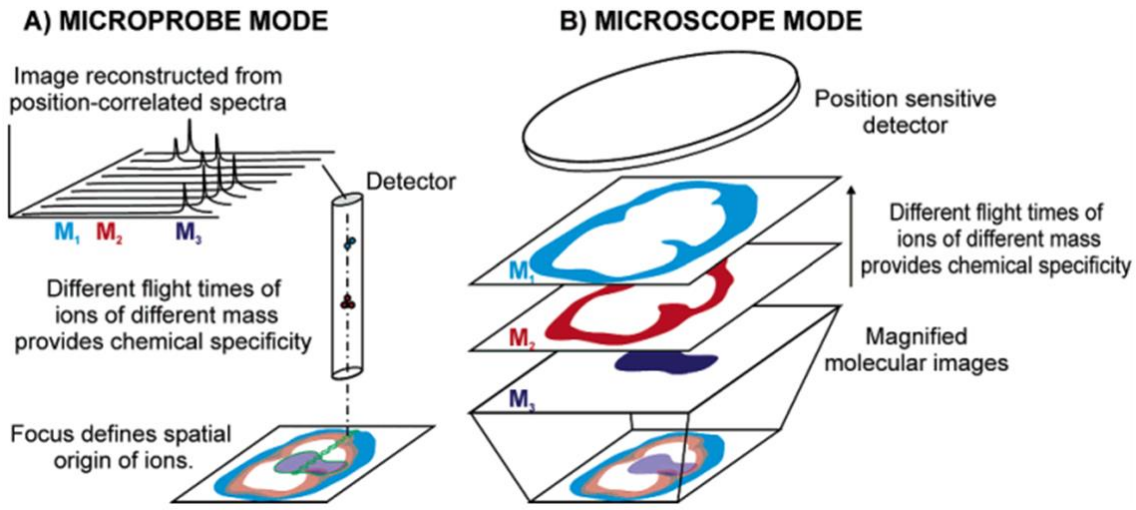

Figure 1.7 *Representation of the two modes used for MALDI-MSI experiments: A) microprobe mode, where a high focus laser is rastered across distinct regions of the sample, and B) microscope mode, where the laser focus is wide and the location of ions is picked up using a position sensitive detector. Image from (Luxembourg et al., 2004).*

Although the microscope technique offers advantages in terms of high-spatial resolution (down to few μm) and high-speed of analysis (Luxembourg *et al.*, 2006; Lee *et al.*, 2012), at present microprobe mode represents the dominant mode for obtaining MALDI-MSI data. This is due to several drawbacks of the microscope mode that hamper its implementation. These include: the risk of a partial sampling of the sample, if the latter is bigger than the entire area of the microscope field of view; the limited *m/z* range and sensitivity; and its compatibility with only analysers that enable ions to preserve the original spatial information (i.e. TOF) (Lee *et al.*, 2012; Gessel, Norris and Caprioli, 2014). In light of these considerations, the employment of microscope mode is currently inappropriate for the image of complex biological sample and, hence, efforts to overcome the limitations are necessary.

1.3.1 Matrix deposition techniques

1.3.1.1 Manual spotting

Manual spotting is the easiest and most practical matrix application technique. This technique includes the deposition of microliter (µL) volumes of matrix using a hand-held pipette. The main disadvantage of this technique is the significant irregularity and inhomogeneity of matrix-analyte crystals, responsible, subsequently, for an intense spot-to-spot irreproducibility. The spot inhomogeneity also results in the analyte signal changing when the laser is fired in different points of an individual spot; the points in which higher analyte sensitivity is detected are known as "sweet spots" (Dai, Whittal and Li, 1996; Fujita and Fujino, 2013).

Different approaches for the deposition of matrix using manual spotting have been investigated, such as dried droplet (Karas and Hillenkamp, 1988), crushed-crystals (Xiang, Beavis and Ens, 1994) and sandwich (Kussmann *et al.*, 1997). The most commonly used method is the dried droplet method, which consists either of pre-mixing the analyte with the matrix or directly depositing the matrix onto the sample surface prior to introduction into the mass spectrometer for analysis (Figure 1.8).

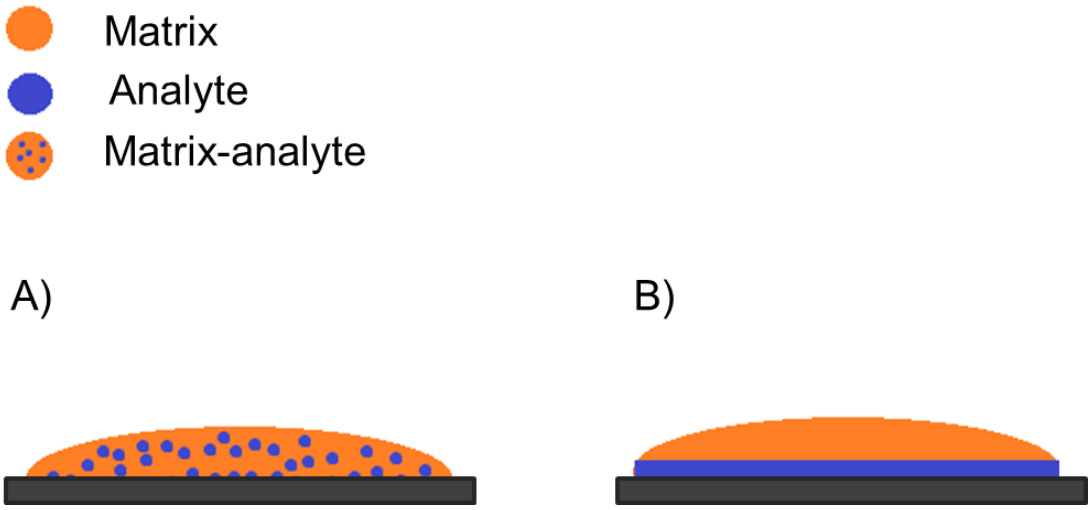

Figure 1.8 *The 'dried droplet' methods. The analyte can be pre-mixed with the matrix (A) or the matrix can be applied onto the analyte surface (B).*

Considering the poor reproducibility in sample preparation, manual spotting is not used for MALDI-MSI experiments, but it finds application in MALDI-MSP in order to assess the best matrix and polarity to use for a specific analysis.

1.3.1.2 Acoustic droplet ejection

Acoustic droplet ejection (ADE) is a technology able to deposit submicroliter volumes (170 picoliter per droplet) of matrix solution onto a sample. In ADE, radio frequency power is converted to ultrasonic energy through a piezoelectric transducer; the ultrasonic energy is spread though the reagent reservoir causing the ejection of small droplets from the fluid surface (Pickett *et al.*, 2006)

A schematic illustration of the ADE mechanism is illustrated in Figure 1.9**.**

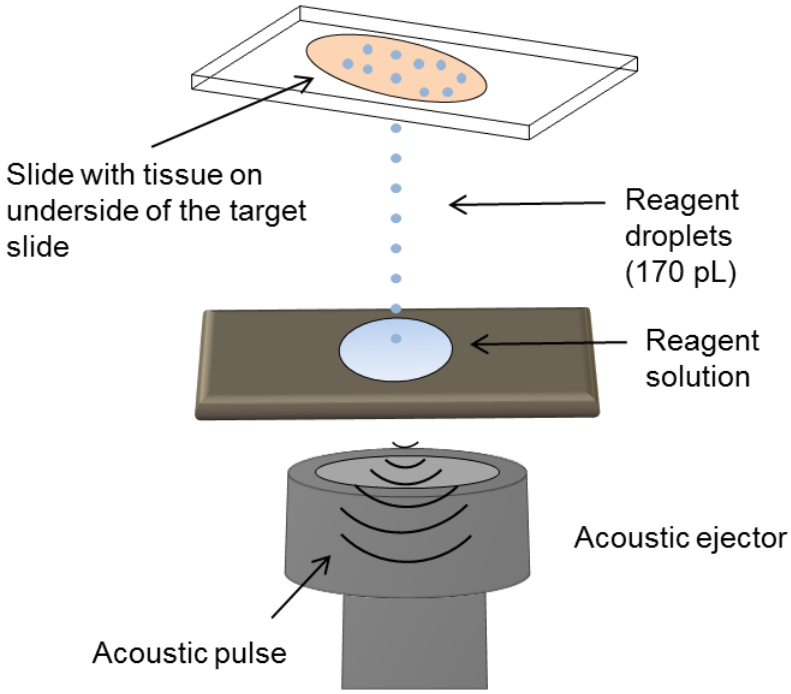

Figure 1.9 *Schematic representation of an acoustic droplet ejector, consisting of a reagent reservoir and acoustic ejector.*

The main advantages of this method are the reproducibility of droplet sizes, the high extraction capabilities and no risk of clogging due to the absence of nozzles (Aerni, Cornett and Caprioli, 2006). The main disadvantages are represented by the fixed distance between the droplets (200 µm), which limits the spatial resolution in MALDI-MSI experiments (Kaletaş *et al.*, 2009). This represents a limiting factor when the acoustic ejector is used as a matrix deposition device, in fact, although several spotting patterns could be overlaid to minimise the distance between the droplets, the entire coverage of a given area is difficult to achieve.

A commercial acoustic spotter, the Portrait® 630 (Labcyte Inc. California, USA), has been employed in this thesis for the work reported in Chapter 3 and Chapter 4.

1.3.1.3 Sprayers

Spraying technology allows the deposition of the matrix onto the sample in the form of small aerosol droplets. This technique offers the advantage of obtaining a uniform matrix coating and it can be accomplished in two ways: manual (pneumatic spray) or automatic. An example of a manual pressurised airbrush is shown below in Figure 1.10.

Figure 1.10 *The Iwata Eclipse manual sprayer (www.iwata-airbrush.com).*

With manual spraying the reproducibility of experiments is not guaranteed due to the difficulty of controlling variables, such as the distance between the sprayer and the sample, the speed of the spraying and the amount of matrix deposited. These issues can be overcome by using an automatic sprayer which permits parameters to be kept constant in multiple experiments with the aid of software.

In the work presented in this thesis, the Sunchrom Suncollect automated sprayer has been used (KR Analytical, Sandbach, UK) (Figure 1.11). This instrument is equipped with a syringe driver, for controlled matrix delivery, and a compressed nitrogen gas line surrounding the needle, enabling ejection of the matrix solution as a fine mist. The matrix can be applied at a specific flow rate and pressure within a predefined area. Unlike the spotting technique, spraying has the advantage of covering the entire sample with matrix, unless clogging occurs.

Figure 1.11 *The SunCollect automated sprayer (www.sunchrom.de).*

1.3.1.4 Sublimation

Sublimation is the transition of a solid directly into a gaseous phase. Among the matrix application techniques investigated, sublimation is the most recently applied to MALDI-MSI. A detailed description of this technique was illustrated in the work by Hankin *et al.*, which reported for the first time the sublimation of matrix onto brain tissue sections for the detection of lipids using MALDI-MSI (Hankin, Barkley and Murphy, 2007).

A typical sublimation apparatus is shown in Figure 1.12. This device consists of a bottom and top section (condenser part). The matrix is inserted in the bottom section, whereas the slide with the sample is fixed on the underside of the top section; the two parts are then assembled and tightly sealed. At this point, under reduced pressure and heat, the matrix starts to sublime and it is deposited onto the sample surface since the condenser is filled with cold water (<15° C).

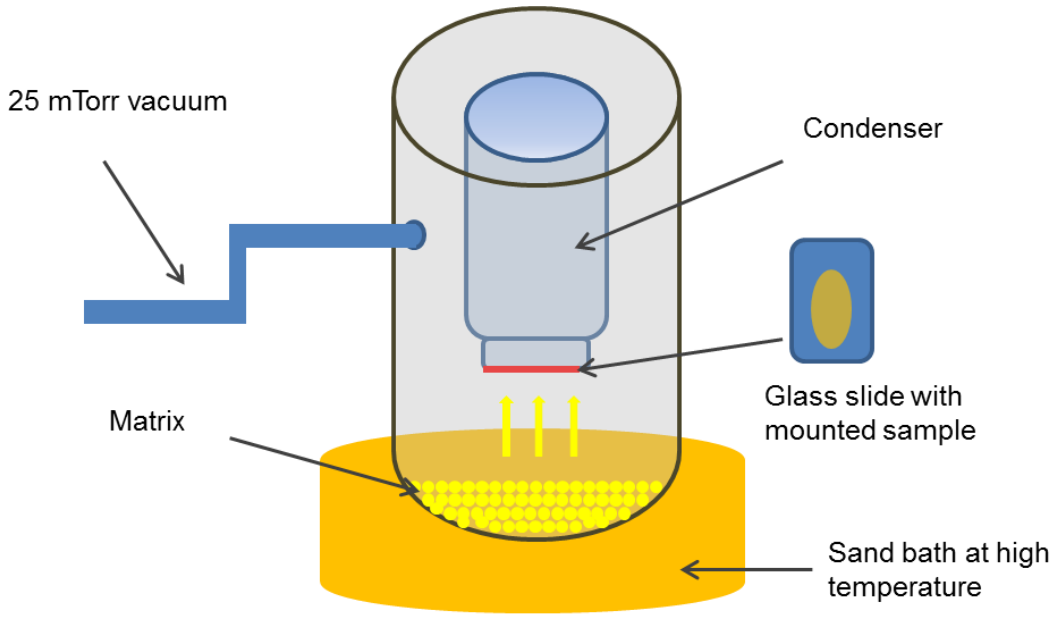

Figure 1.12 *Representation of the sublimation process.*

In Chapter 2 the main advantages of this technique over the spraying technique are discussed and sublimation has been chosen as method of choice for the deposition of the matrix in the work reported in this thesis. In this regard, a commercially available sublimation apparatus available from Sigma-Aldrich, (Gillingham, U.K.) has been used.

1.4 Mass analysers

The mass analyser is the component of a mass spectrometer responsible for separating ions based on their mass to charge ratio (*m/z*). Currently, there are several mass analysers commercially available that differentiate for the upper mass limit and the resolution.

Common commercially available mass analysers include: time of flight (TOF), quadrupole (Q), linear ion trap (LIT), quadrupole ion trap (QIT), fourier transform-ion cyclotron resonance (FT-ICR) and Orbitrap.

1.4.1 Time of flight (TOF)

The concept of a time of flight (TOF) mass analyser was initially introduced by W.E. Stephens (Wolff and Stephens, 1953). The TOF analyser operates by separating ions according to their velocity when they drift in a free-field region, called a flight tube (Hoffmann and Stroobant, 2007). Firstly, ions generated in the source are subjected to an applied voltage, responsible for giving the same kinetic energy to all ions, which are then accelerated into the TOF tube. The velocity and therefore the time that ions take to travel the tube is a function of their *m/z*. The *m/z* of ions can be determined by measuring the time necessary for ions to go through the length of the tube to the detector as reported in Equation 1.1; ions with lower *m/z* will be faster to reach the detector than those with higher *m/z*.

Equation 1.1

$$t^2 = \frac{m}{z}\left(\frac{L^2}{2eV_s}\right)$$

Where t is the time required to cover the distance L before reaching the detector; m = mass of ions; z = number of charges; e = charge of an electron; Vs = acceleration potential.

A representation of a linear TOF is illustrated in Figure 1.13.

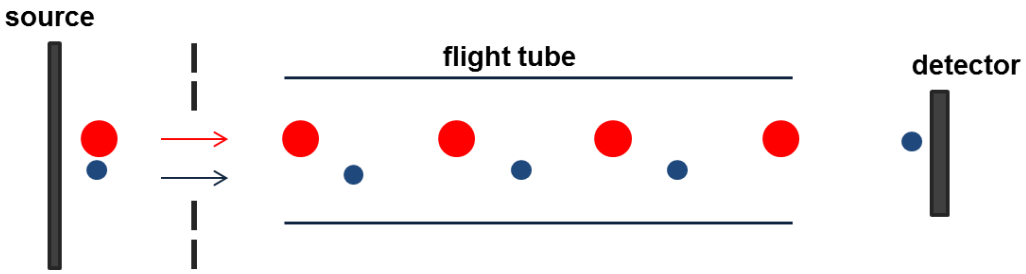

Figure 1.13 *Representation of a linear time of flight mass spectrometer.*

One of the major limitations of linear TOF instruments is the low mass resolution. This aspect is essentially due to the spatial and kinetic energy spread amongst the ion packets generated by the laser-based ion sources.

One approach to increase the resolution is by using a reflectron, or ion mirror (Figure 1.14). The reflectron was proposed by Mamyrin and coworkers in 1973 (Mamyrin *et al.*, 1973) and it consists of a cylinder made up of a series of ring electrodes and grids that are subjected to a gradient voltage. When the ions enter the electrical field, they are deflected back along the flight tube; the ions with higher energy will penetrate further into the reflectron field than those with lower energy, which penetrate the field less. In this way, the spread of kinetic energy of ions with the same *m/z* is corrected and ions will arrive at the detector at the same time (Hoffmann and Stroobant, 2007).

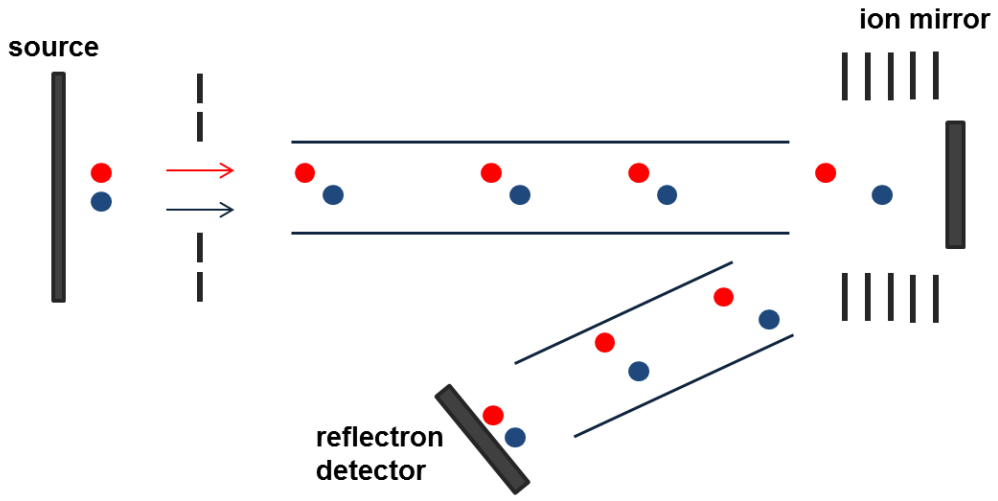

Figure 1.14 *Representation of a reflectron time of flight mass spectrometer.*

TOF is a pulsed ion analyser, and, hence, its coupling with continuous ionisation sources (i.e. ESI) is arduous. A way to overcome this issue is by generation of ion packets from the continuous ion stream. The strategy used is by setting the TOF analyser orthogonally to the axial path of ions derived from the source. Ions are transmitted in a 'pusher' region where ion packets are excised and are accelerated into the orthogonal TOF by a pulsed voltage. The insertion of an orthogonal reflectron TOF analyser after a horizontal path of ion beam confers a V-geometry of the ion trajectory (Hoffmann and Stroobant, 2007; Greaves and Roboz, 2013) (Figure 1.15).

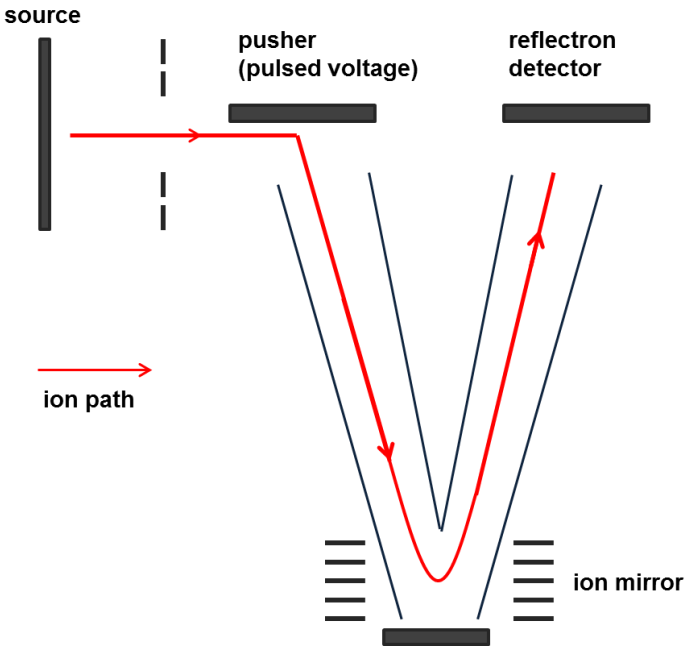

Figure 1.15 *Representation of an orthogonal reflectron time of flight analyser. Ions derived from the source are accelerated into the orthogonal TOF by a pulsed voltage, travelling in a V-shaped trajectory.*

By increasing the length of the analyser path it is possible to increase the mass resolution. In this regard, an additional reflectron TOF can be introduced in the analyser, describing a W-geometry for the ions trajectory (Figure 1.16). It is important to consider that, although the increment of flight path allows a high-resolution, it also increases the chance of ion loss, at the cost of the sensitivity (Fliegel *et al.*, 2006; Greaves and Roboz, 2013; Chernushevich *et al.*, 2017) (Figure 1.16).

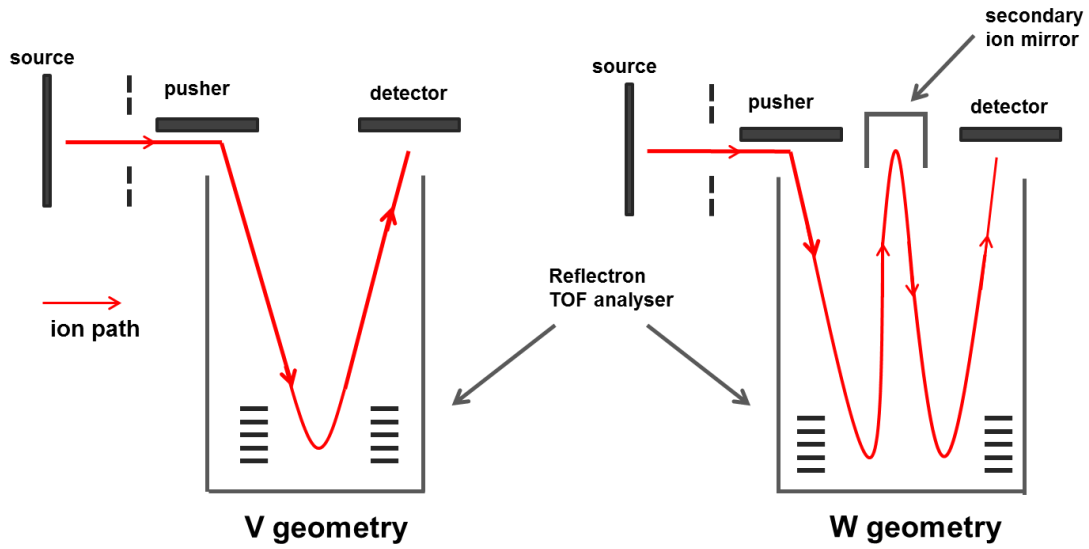

Figure 1.16 *Comparison of an orthogonal reflectron time of flight analyser with V-geometry and W-geometry. In the W-geometry two TOF analysers are combined, this allows the ions to travel within a longer flight path and hence, increases the mass resolution.*

1.4.2 Quadrupole

A quadrupole mass analyser consists of four parallel metal rods arranged in opposite pairs, to which direct current (DC) and alternating radio frequency (RF) voltages are applied. In particular, one pair of rods has an applied potential of (U+Vcos(ωt)) and the other pair a potential of -(U+Vcos(ωt)). The separation of the ions in accordance with their mass to charge ratio (*m/z*) is based on their stability within the oscillating electric field applied to the rods: ions with stable trajectory (*bounded oscillation*) will be able to pass through the rods and reach the detector, whereas ions with an unstable trajectory (*unbounded oscillation*) will strike the rods, neutralising them (Figure 1.17)**.** The quadrupole, as an analyser, can operate in two modes, in "full scan" or in "selected ion monitoring". In the first case, by changing RF and DC voltages, while maintaining the ratio of these two voltages constant, the analyser performs a sequential scan of ions with different mass to charge ratios. In the second case, the quadrupole is fixed at a specific voltage in order to allow only ions with a specific *m/z* to reach the detector. The quadrupole is used in this mode for

tandem mass spectrometry (MS/MS) experiments, allowing selection of a specific ion of interest prior to fragmentation.

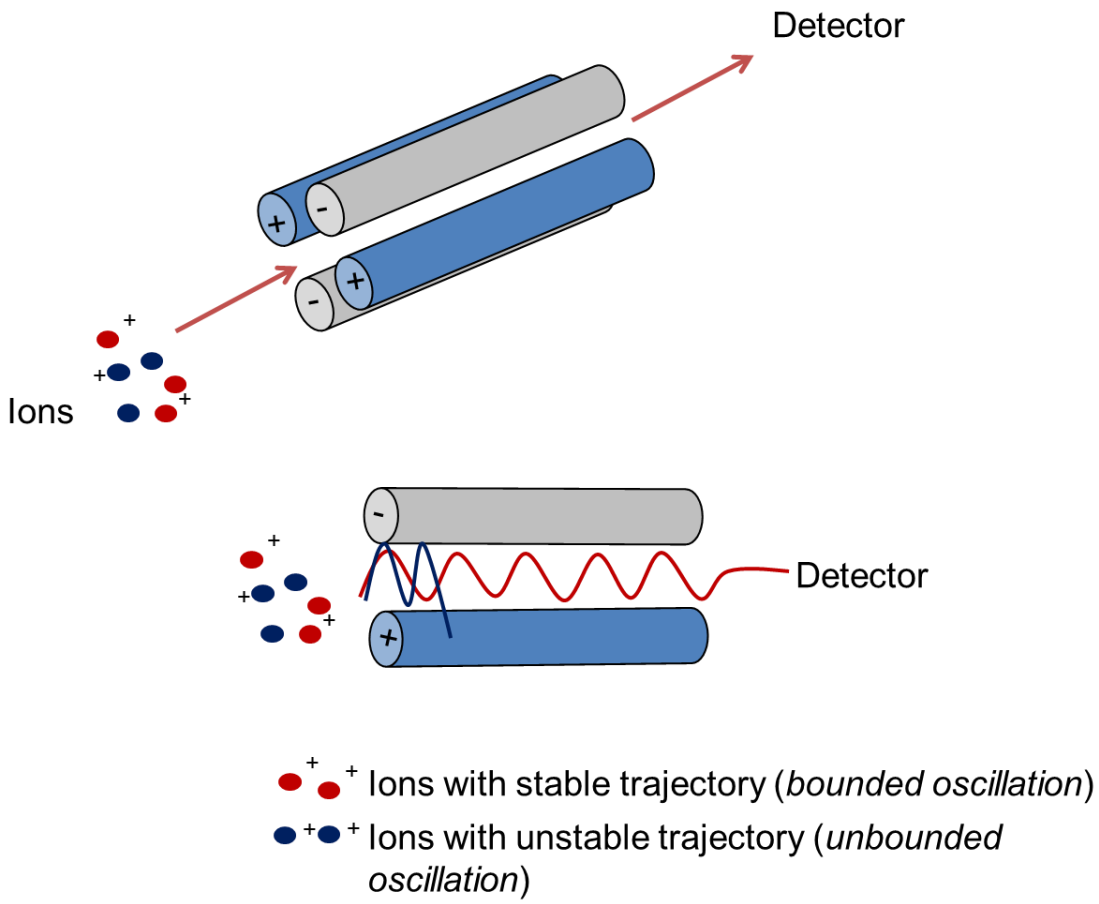

Figure 1.17 *Representation of a quadrupole mass analyser; the red ions with stable trajectory (bounded oscillation) are able to pass through the quadrupole whilst the blue ions with unstable trajectory (unbounded oscillation) collide with the metal rods.*

1.5 Multi-analyser systems

1.5.1 Tandem MS/MS Instruments

1.5.1.1 TOF/TOF

Tandem time-of-flight (TOF/TOF) is a tandem mass spectrometry method that uses two TOF analysers in sequence. In the currently available instruments, the more common configuration is the combination of a linear TOF as a first analyser with a reflectron TOF, as a second analyser (Medzihradszky *et al.*, 2000; Cotter *et al.*, 2005). An electronic gate, called a timed ion selector (TIS) allows an ion of interest, separated from the first TOF, to pass through and enter a collision chamber, where the parent ion will undergo dissociation by induced collision with an unreactive gas (nitrogen or argon) (Figure 1.18).

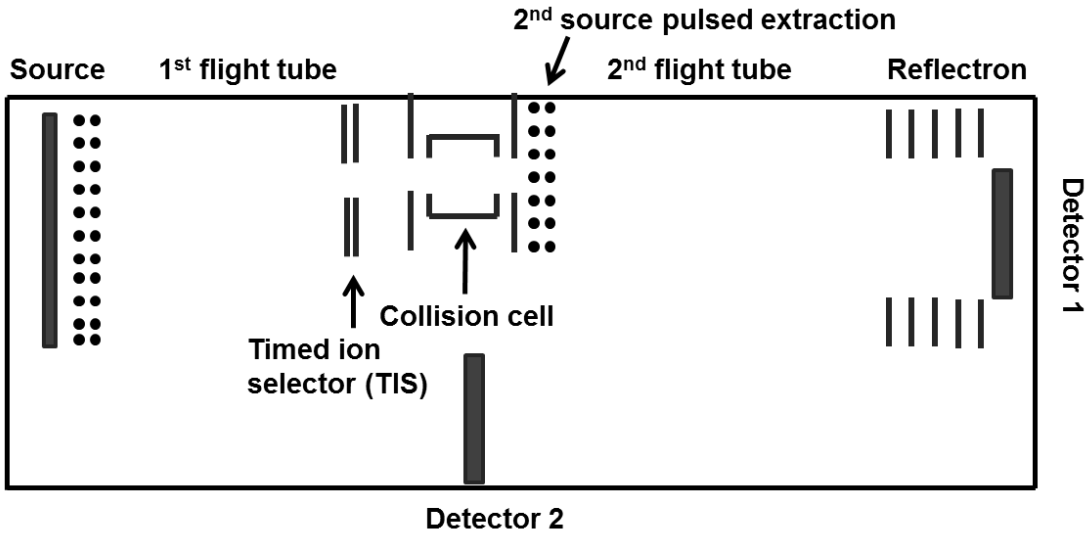

Figure 1.18 *A schematic diagram of a tandem time of flight mass analyser; the precursor ions selected by the TIS enter into the collision cell, where they undergo collisionally induced dissociation. Once generated, the product ions are extracted and reaccelerated into the second TOF* (Cotter *et al.*, 2005).

In this thesis, the tandem TOF instrument used is the Autoflex III manufactured by Bruker Daltonics (Germany), which employs LIFT technology.

In the LIFT configuration, to perform MS/MS experiments ions generated in the source are accelerated to 8 keV and enter the collision chamber. The precursor ion and its product ions, together indicated as an "ion family", have the same velocity and reach the TIS gate at the same time. The TIS gate enables only the "ion family" of interest to pass through and enter the LIFT cell, a free field region whose the potential is raised by 19 keV while the ions are in residence, adding acceleration energy when they are extracted into the second TOF (Cotter *et al.*, 2005).

A schematic representation of a LIFT-TOF/TOF mass spectrometer is illustrated in Figure 1.19.

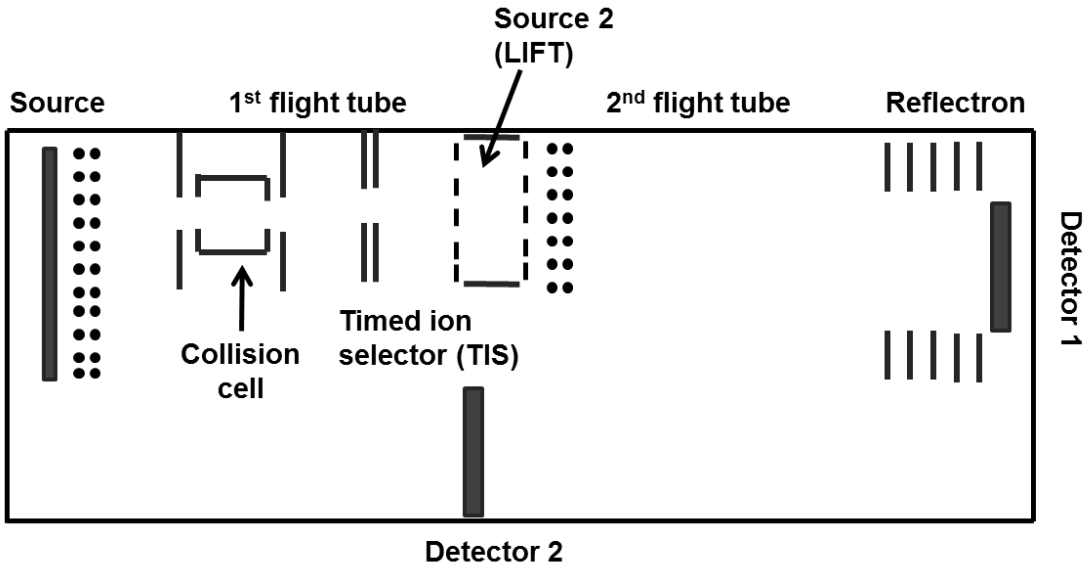

Figure 1.19 *A schematic diagram of a tandem time of flight mass analyser using LIFT technology; the precursor with the product ions are selected by the TIS gate and enter the LIFT cell, from where they are extracted and reaccelerated into the second TOF* (Cotter *et al.*, 2005).

1.5.2 Hybrid mass spectrometers

1.5.2.1 Quadrupole Time-of-Flight (QTOF)

Mass spectrometers that combine different mass analysers are commonly termed “hybrid” mass spectrometers. Quadrupole time of flight (QTOF or QqTOF) instruments are robust and versatile configurations usually combined with ESI and MALDI sources. In the common QTOF instruments, an additional quadrupole Q_0, operated in RF-only mode, is inserted, therefore the instrument consists of three quadrupoles Q_0, Q_1 and Q_2 combined with an orthogonal TOF mass analyser (Chernushevich, Loboda and Thomson, 2001). The first quadrupole Q_0 acts as ion guide rather than a mass analyser, enabling the transmission of all ions within a specific mass range (Greaves and Roboz, 2013).

To obtain full-scan MS data, the three quadrupoles are operated in RF-only mode (i.e. as transmission devices) and all ions are transferred into the TOF analyser for detection. When using a QTOF for obtaining MS/MS data, the first quadrupole Q_0 functions as transmission device, the second Q_1 as a mass filter to select a specific ion of interest, the third Q_2 acts as a collision cell, into which a collision gas (argon or nitrogen) is introduced (Figure 1.20). The product ions then travel into the TOF analyser and are detected (Oberacher and Pitterl, 2009).

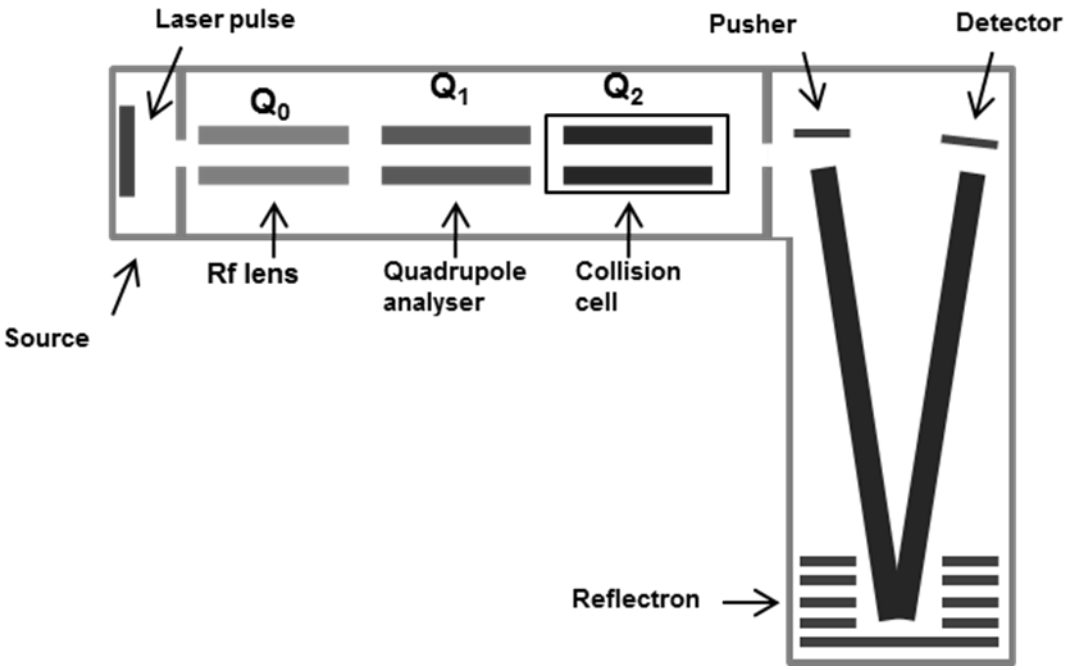

Figure 1.20 *Representation of a hybrid quadrupole time of flight mass analyser.*

In the commercial instrument Synapt G2 HDMS (Waters Corp., UK) (used in this thesis) the first quadrupole, used for transmission, is replaced by a hexapole and the analytical capabilities of the instrument are increased by introducing a 'triwave' region into the QTOF system (Figure 1.21).

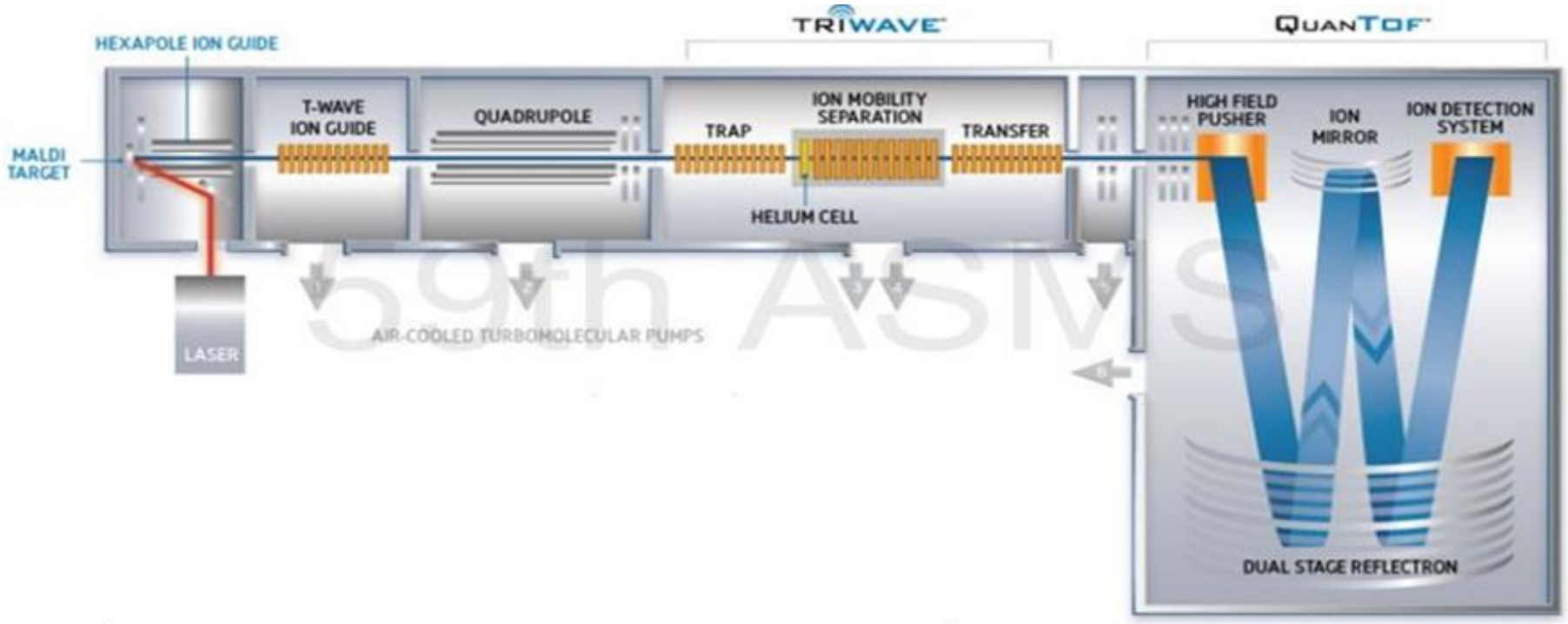

Figure 1.21 *Synapt G2 HDMS mass spectrometer adapted with a MALDI source (Waters Corporation, Manchester, UK).*

The triwave consists of a travelling wave ion mobility separator (TWIMS), preceded and followed by the trap and transfer travelling wave ion guides (TWIG's), respectively. IMS is a powerful technique, which enables the separation of ions based on their size/charge ratios, as well as their shape (cross-sectional area), as they move through an inert gas due to the influence of an electric field (Kanu *et al.*, 2008).

The drift tube of a TWIMS cell is made up of a series of stacked ring ion guides (SRIG), organised so that opposite RF voltages are applied on adjacent rings, forming a confining barrier surrounding the ions. The superimposition of a DC voltage on the RF of adjacent electrodes in a repeating pattern generated a series of potential hills (travelling waves). These enable ions to propel over the top of the travelling waves as they traverse the cell in the presence of the carrier gas buffer (Giles *et al.*, 2004; Pringle *et al.*, 2007). Ions with lower mobility will interact more with gas particles and will roll over the wave more times than higher mobility ions (Figure 1.22).

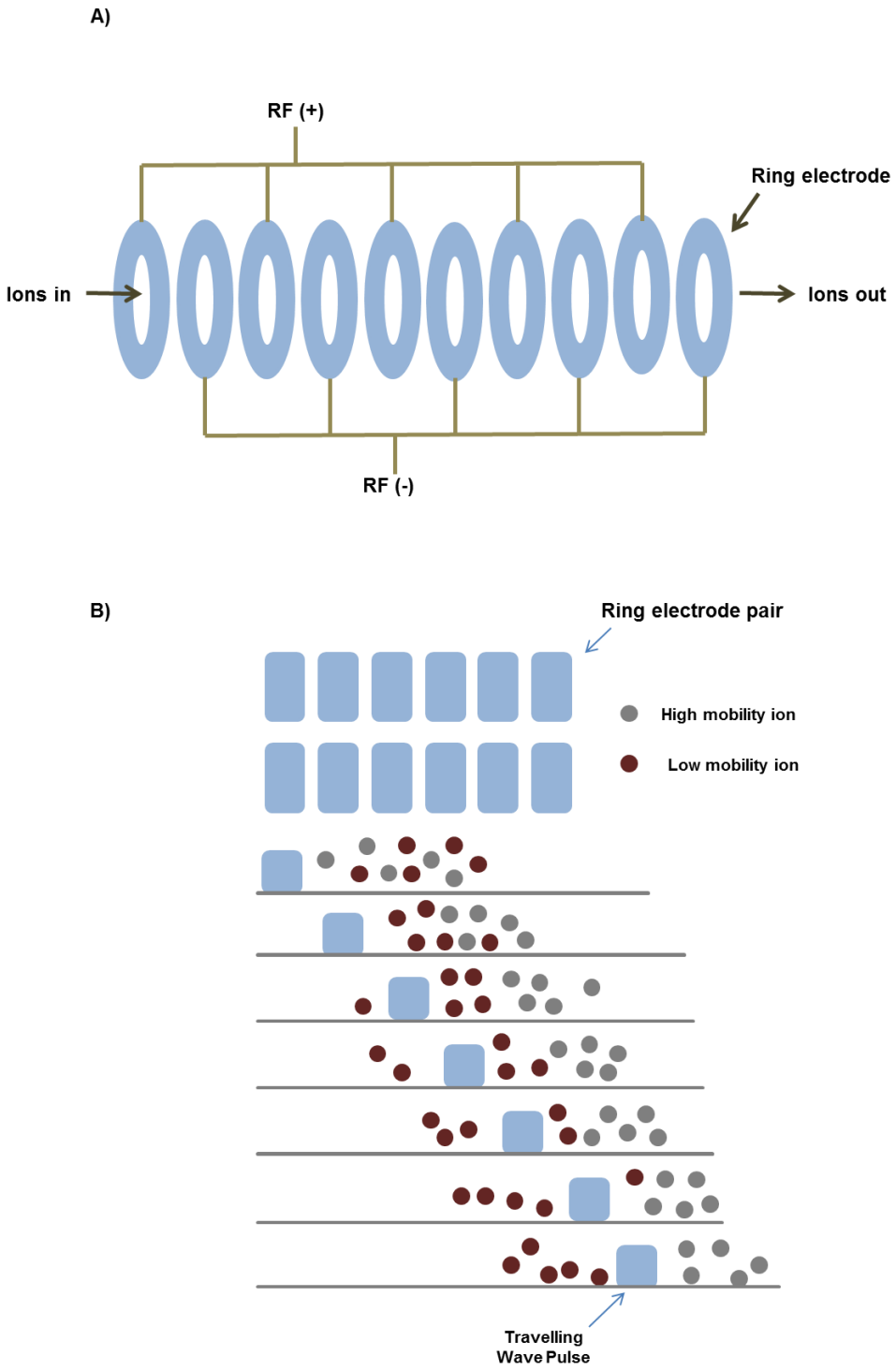

Figure 1.22 *A) Representation of the IMS cell of the Synapt G2 HDMS instrument, showing a series of stacked ring ion guides (SRIG) carrying opposite RF voltages on adjacent rings to form a confining barrier surrounding the ions. B) Representation of the propulsion of ions over the top of the travelling wave pulse in the presence of the carrier gas buffer.*

1.6 Skin structure

The skin is the largest organ of the human body and represents a natural barrier to the environment. It restricts the inward and outward movement of substances, i.e. water and electrolytes, and at the same time, ensures protection against toxic agents, microorganisms, mechanical insults and ultraviolet radiation (Bensouilah and Buck, 2006).

The skin is commonly subdivided in two structural layers: the epidermis and the dermis. The dermis is attached underneath to the hypodermis or subcutaneous layer, containing adipose and areolar connective tissue (Tortora and Nielsen, 2011) (Figure 1.23).

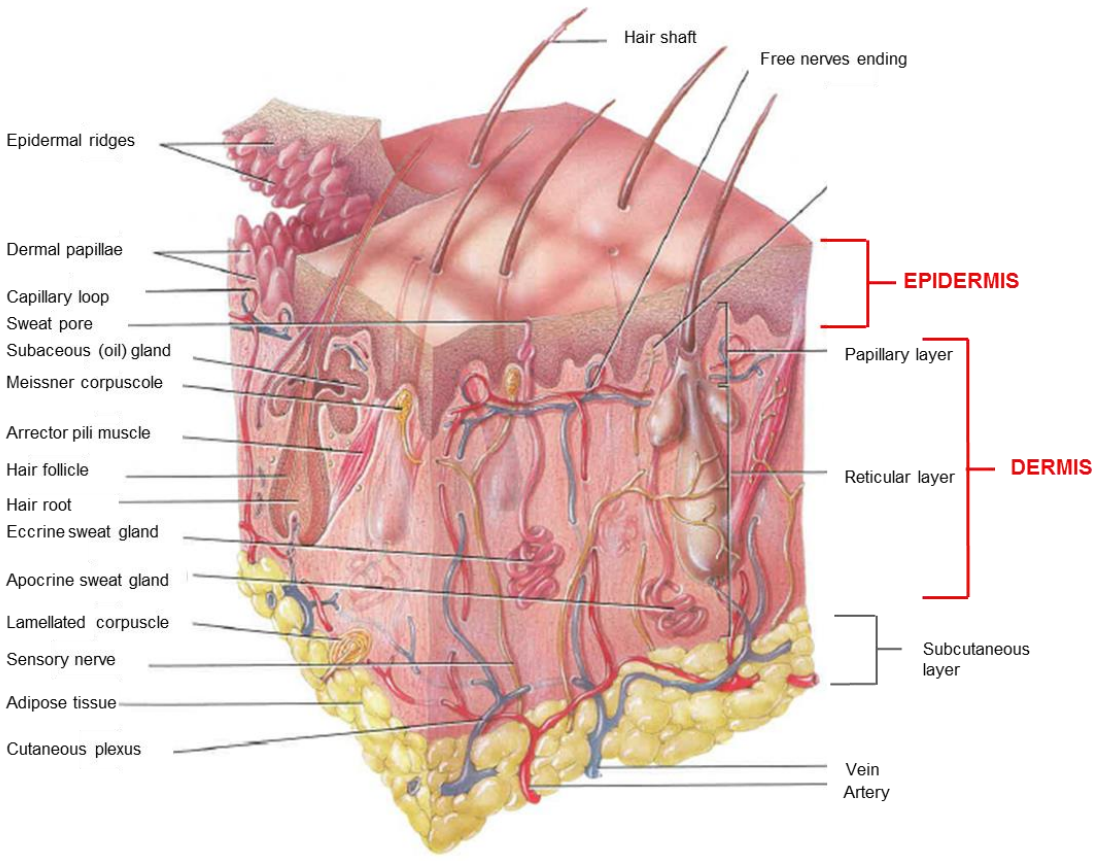

Figure 1.23 *Structure of skin. Image adapted from* (Tortora and Nielsen, 2011).

95% of the epidermis is comprised of keratinocyte cells (Xu, Timares and Elmets, 2013). Keratinocytes are derived from basal cells, which go through a constant process of differentiation and migrate through several suprabasal layers (the spinous layer, granular layer, lucidum layer and corneum layer) losing their nucleus and becoming more and more compacted in size before being finally shed from the surface by the process of desquamation (Sandilands *et al.*, 2009).

The stratum basale consists in a single layer of cuboidal-shaped keratinocyte cells, anchored to the basement membrane by epithelia multiprotein complexes, called hemidesmosomes-junctions. This layer is also called the germinativum layer for the presence of stem cells that undergo mitosis and generate new keratinocytes (Borradori and Sonnenberg, 1999). Melanocytes, Langerhans cells and Merkel cells can also be present (Parsons, 2002; Tortora and Nielsen, 2011).

The spinous layer, also called the prickle-cell layer, is made up of 8-10 layers of keratinocytes, which join together through desmosomes. Among the keratinocytes, in this layer Langerhans cells and melanocytes may also be found (Parsons, 2002; Tortora and Nielsen, 2011).

In the higher layer, the granular layer, the keratinocytes assume a more flattened shape. Here, it is possible to find from three to five layers of keratinocyte cells that start to undergo apoptosis. The cells contain granules of keratohyalin protein; responsible for binding keratin intermediate filaments into keratin (Tortora and Nielsen, 2011; Nafisi and Maibach, 2018).

The lucidum layer contains about five layers of translucent, flat and dead cells that accumulate eleidin, a protein derived from keratohyalin. This layer is commonly present in the skin of the palm, soles and fingertips (Tortora and Nielsen, 2011; Yousef and Sharma, 2017)

The stratum corneum, the outermost layer of the epidermis, represents an essential mechanical barrier responsible for limiting the penetration of external substances as well as limiting water loss. It is made up of 25 to 30 layers of flat corneocytes, the finally differentiated keratinocytes, comprised mostly of keratin. The corneocytes fix one to another through adhesive intercellular structure

called corneodesmosomes, degradation of which seems to be directly correlated to the desquamation process (Ishida-Yamamoto and Igawa, 2015) (Figure 1.24).

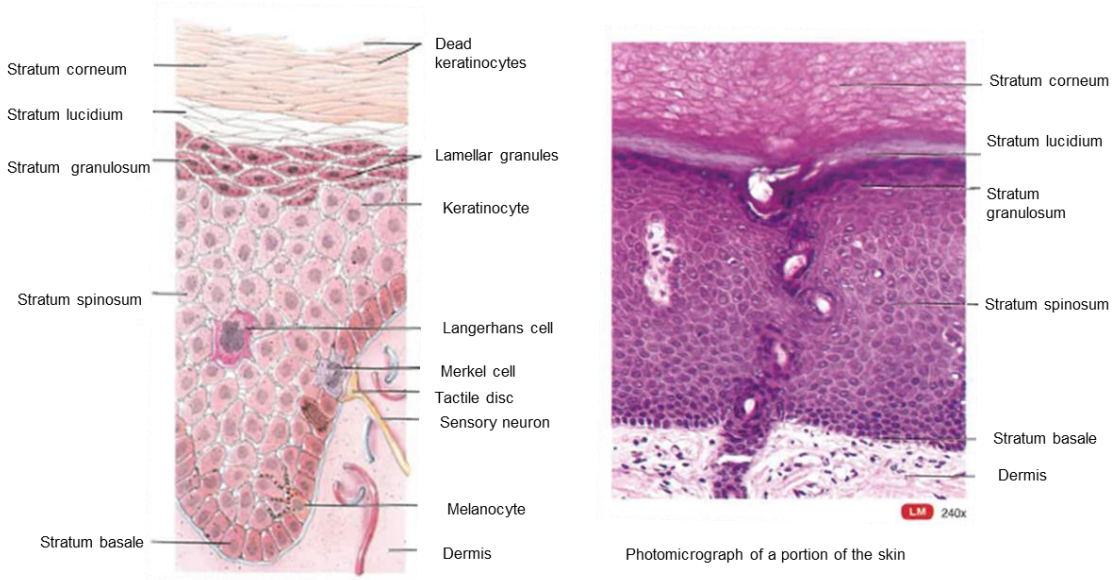

Figure 1.24 *Representation of the structure of the epidermis. Starting from the basal layer, the keratinocytes migrate into layers: spinous, granular, lucidum and corneum. Image adapted from* (Tortora and Nielsen, 2011)*.*

The dermis is composed mainly of connective tissue, blood vessels, hair shafts, sweat glands and nerves; it supports and feeds the epidermis. The main cells present in the dermis are fibroblasts, macrophages and adipocytes. The dermis is divided into two areas: a papillary layer and a reticular layer (Freinkel and Woodley, 2001).

The papillary layer is the uppermost layer of the dermis, consisting mainly of loose connective tissue. From here small extensions of the dermis, called "dermal papillae", protrude inside the epidermis, increasing the surface area between epidermis and dermis (Hardy, 1992). The dermal papillae nourish the avascular epidermis through the capillaries and are directly associated with hair follicles growing. Furthermore, the papillary layer can also include free nerve endings and touch receptors, called Meissner corpuscles (Tortora and Nielsen, 2011; Stocum, 2012; Borojevic, 2013). In contrast to the papillary layer, the

reticular dermis, the bottom layer of the dermis, is constituted primarily by dense irregular connective tissue. It provides elasticity and overall strength to the skin. Furthermore, this layer contains also hair follicles, sebaceous as well as sweat glands (Tortora and Nielsen, 2011).

1.7 Barrier properties in the skin

The stratum corneum (SC) represents the principal skin barrier and this function is essentially due to the lipid composition and organisation within it (Grubauer *et al.*, 1989; Bouwstra *et al.*, 1999; Wertz, 2018). In the SC each corneocyte is surrounded by an envelope of cross-linked proteins with which a layer of lipids (lipid envelope) are covalently bound, forming the cornified envelope structure (Abraham and Downing, 1990; Nemes and Steinert, 1999; Candi, Schmidt and Melino, 2005). Between corneocytes, instead, a matrix of lipids arranged into a multi-lamellae structure is present. This represents around 20% of the SC volume and includes mainly ceramides, cholesterol, cholesterol esters, fatty acids, and a small fraction of cholesterol sulphate (Madison *et al.*, 1987; Bouwstra *et al.*, 2003). In a few regions of the stratum corneum, the intercellular lipid matrix is absent and the interaction of lipid envelopes of adjacent corneocytes can occur, increasing the cohesion of the stratum corneum (Wertz *et al.*, 1989).

Michaels and colleagues first proposed the "brick and mortar" model to describe the structure of the SC (Michaels, Chandrasekaran and Shaw, 1975). With this model, the skin barrier is defined as a two compartment system; corneocytes as the bricks and the tightly packed intercellular lipids as the mortar (Nemes and Steinert, 1999; Norlén, 2001). A schematic representation of the "bricks and mortar" model is offered in Figure 1.25.

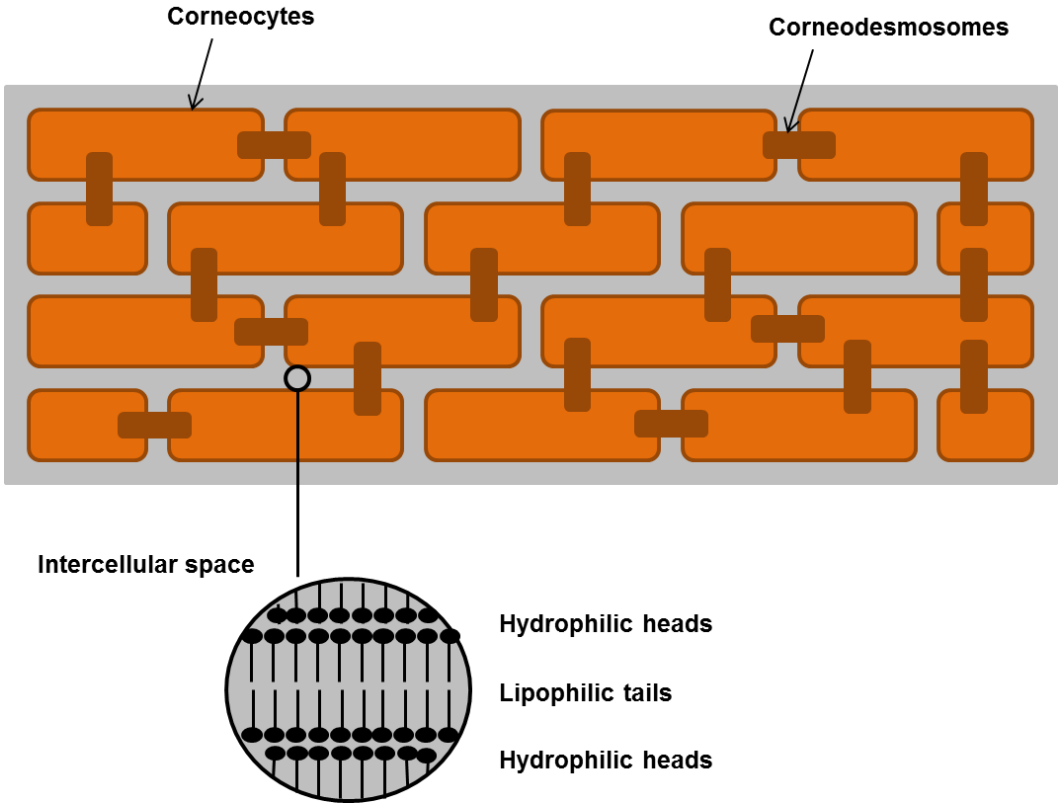

Figure 1.25 *Schematic representation of the "bricks and mortar" model for the stratum corneum.*

1.8 Percutaneous absorption

The stratum corneum represents the principal obstacle for the percutaneous absorption of therapeutic agents, wherever designed for topical or transdermal delivery (Schaefer *et al.*, 1980). With topical drug delivery it is intended that a pharmaceutical agent is applied directly onto the skin surface for a localised action; whereas with transdermal drug delivery it is intended that a pharmaceutical agent enters into the circulation in order to execute its action; hence transdermal formulation must be able to pass through all the layers of the epidermis and dermis (Osborne, 2008; Murthy and Shivakumar, 2010). Percutaneous delivery represents a valid alternative to conventional oral and parenteral delivery; it in fact offers the advantage of bypassing the hepatic "first pass effect", controlling drug delivery over a longer period of time, acting directly on target (e.i. in case of skin pathologies), and increasing patient compliance (Kanikkannan *et al.*, 2000; Brown *et al.*, 2006; Pathan and Setty, 2009).

It has been established that there is a direct correlation between stratum corneum reservoir function (its ability to accumulate topically applied molecules) and percutaneous absorption (Rougier *et al.*, 1983; Teichmann *et al.*, 2005). The absorption through the stratum corneum is a passive diffusion process, which occurs in three possible ways (Haque and Talukder, 2018):

- intercellular diffusion through the lipid matrix;
- intracellular diffusion through both the corneocytes and the lipid matrix;
- transappendageal diffusion along the sweat pores and follicles.

A schematic representation of the main permeation routes across the stratum corneum is shown in Figure 1.26.

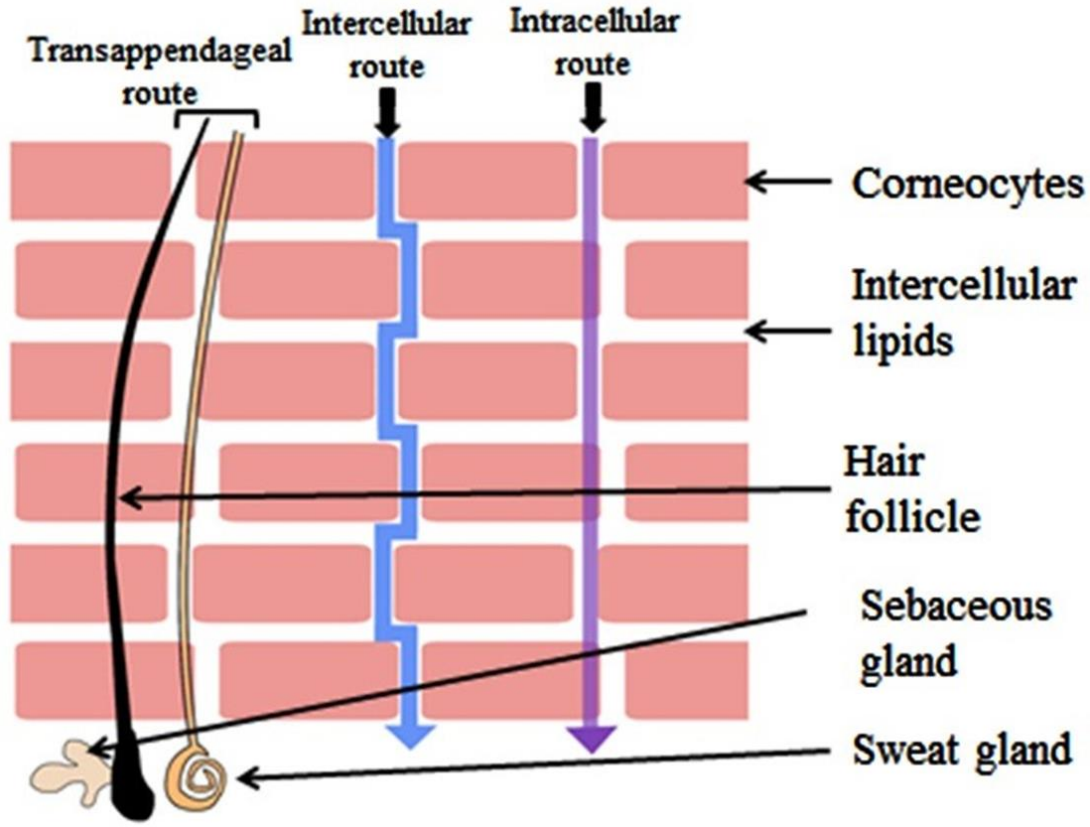

Figure 1.26 *Representation of the pathways responsible for the penetration of substances through the stratum corneum. Figure taken from* (Haque and Talukder, 2018).

The passive diffusion of a drug through the stratum corneum can be described by Fick's first law of diffusion, as shown below (Lane, 2013; Ita, 2015) .

Equation 1.2

$$Jss = \frac{ADKCv}{h}$$

where: *Jss* is the steady-state flux of the drug, *A* is the surface area, *D* is the diffusion coefficient of the drug in the membrane, *K* is the vehicle/membrane coefficient of partition, *Cv* is the drug concentration in the vehicle and *h* is the membrane thickness.

From this equation it is evident that the flux is directly proportional to the gradient of concentration and inversely proportional to the thickness of the stratum corneum. However, it does not consider other factors (biological, biopharmaceutical and physio-chemical) that could influence the percutaneous absorption too, as summarised in Table 1.1 (Leite-Silva *et al.*, 2012).

Drug	• Solubility • Molecular dimension • Ionisation • Concentration
Skin	• Age, sex, race • Stratum corneum integrity • Anatomical site • Individual variability • Stratum corneum hydration • Pathological conditions • Temperature
Vehicle	• Distribution in the stratum corneum • Penetration enhancer • Solubility • Volatility

Table 1.1 *Factors that influence the percutaneous absorption.*

1.8.1 Chemical penetration enhancers (CPEs)

A method commonly employed for enhancing permeation of drugs is based on the inclusion of additives within the formulation. These additives called chemical penetration enhancers (CPEs) increase drug flux by provoking reversible alterations to the skin constituents (Walker and Smith, 1996; Sindhu *et al.*, 2017).

CPEs should satisfy the following properties, (although accomplishing all is unlikely) (Williams and Barry, 2012; Sindhu *et al.*, 2017):

- chemical stability and absence of toxicity;
- pharmacological inactivity;
- compatibility with the drug and excipients;
- absence of irritant and allergenic activity;
- absence of odour and colour;
- cost-effectiveness;
- rapidity in onset and action.

The CPEs can mainly act in three different ways: i) by disrupting SC intercellular lipids ii) by improving the partitioning of drug in the membrane or iii) by interacting with SC proteins (Williams and Barry, 2012; Sindhu *et al.*, 2017). These mechanisms were first summarised in the lipid-protein-partitioning theory, proposed by Barry *et al.* (Barry, 1991).

1.8.1.1 Disruption of stratum corneum lipids

As described in Chapter 1.7, in the SC lipids surround the corneocytes in a high organised multi-lamellae structure. CPEs can interact either with the head groups or the hydrophobic tails of the lipids (Marjukka Suhonen, A. Bouwstra and Urtti, 1999). In the first case, CPEs can break hydrogen-bonding between ceramide head groups and become new H bond acceptor or donator (Jain, Thomas and Panchagnula, 2002; Dragicevic and Maibach, 2015). Amphiphilic compounds, instead, are able to enter between the hydrophobic tails of the bilayer, disrupting the structure and favouring the lateral fluidisation of lipids (Vavrova and Hrabalek, 2005). Some CPEs can act by inducing phase

separation in the lamellae (i.e oleic acid) (Ongpipattanakul *et al.*, 1991) or *via* lipid extraction (i.e dimethylsulfoxide, ethanol) (Bommannan, Potts and Guy, 1990; Anigbogu *et al.*, 1995; Dragicevic and Maibach, 2015). In all cases, a perturbation of the original multi-lamellae order is observed, with a decrease of microviscosity and an increase in diffusion of substances as a consequence (Hadgraft, 1999).

1.8.1.2 Increase of the partitioning of drug

The partitioning of the drug between the SC and the vehicle represents a key role for percutaneous absorption and it is expressed by the coefficient of partition (K) (Rougier *et al.*, 1990). For lipophilic substances with log K > 3, the preferential absorption pathway is the intercellular route, whereas for hydrophilic penetrants with log K < 1, the intracellular route represents the prominent route (N'Da, 2014; Marwah *et al.*, 2016) Some CPEs are able to penetrate into the SC and modify its chemical properties and, hence, its solvent nature. This causes as a result an increase of solubility and partitioning of drug into the SC (Dragicevic and Maibach, 2015).

1.8.1.3 Interaction with stratum corneum proteins

The dense crosslinking of SC proteins is responsible of the insolubility of corneocytes, and, hence, limits drug absorption through the intracellular route (Marjukka Suhonen, A. Bouwstra and Urtti, 1999). The CPEs increase drug permeation by denaturing or modifying SC proteins conformation causing swelling and increase of hydration (Williams and Barry, 2012). An example of CPEs belonged to this category are sulfoxide enhancers, that have been shown to denature keratin from alpha helical to beta sheet (Oertel, 1977).

A common classification of the CPEs is based on their chemical structure, as shown in Table 1.2 (Lane, 2013; Dragicevic and Maibach, 2015).

Chemical class	Enhancers
Alcohols	Short chain alcohols Ethanol Isopropyl alcohol Long chain alcohols Decanol Octanol
Terpens	Cineole D-Limonene
Amides	Azone
Esters	Alkyl esters Ethyl acetate Buthyl acetate Fatty acid esters Isopropyl myristate Isopropyl palmitate
Ether alcohols	Transcutol®
Fatty acids	Lauric acid Oleic acid
Glycols	Dipropylene glycol Propylene glycol
Pyrrolidones	N-methyl-2-pyrrolidone 2-pyrrolidone
Sulfoxides	Dimethyl sulfoxide Decylmethyl sulphoxide

Table 1.2 *Main classification of chemical penetration enhancers*

1.9 Methods for evaluating percutaneous absorption and drug quantitation in skin

The evaluation of quantitation of skin penetration/permeation is of essential importance for the analysis of dermatoxicity and pharmacological activity of topically applied drugs. This analysis can be carried out either *in-vivo* or *in-vitro.* However, considering the issues relating to costs and ethics, *in-vivo* studies are limited and, hence, *in-vitro* techniques are usually more popular.

A comprehensive analysis of the many techniques used for the analysis of drugs in the skin was performed by Moser *et al.* (Moser *et al.*, 2001) and Ruela *et al.* (Ruela *et al.*, 2016). Three approaches - tape-stripping, diffusion cell and autoradiography - are described below.

1.9.1 Tape stripping

Tape stripping represents the traditional method for the analysis of drug concentration throughout the SC (Escobar-Chávez *et al.*, 2008). This technique consists on removing the cells from the SC by applying serial adhesive tapes to the skin surface; from each tape the drug levels and stratum corneum thickness are calculated (Moser *et al.*, 2001) (Figure 1.27).

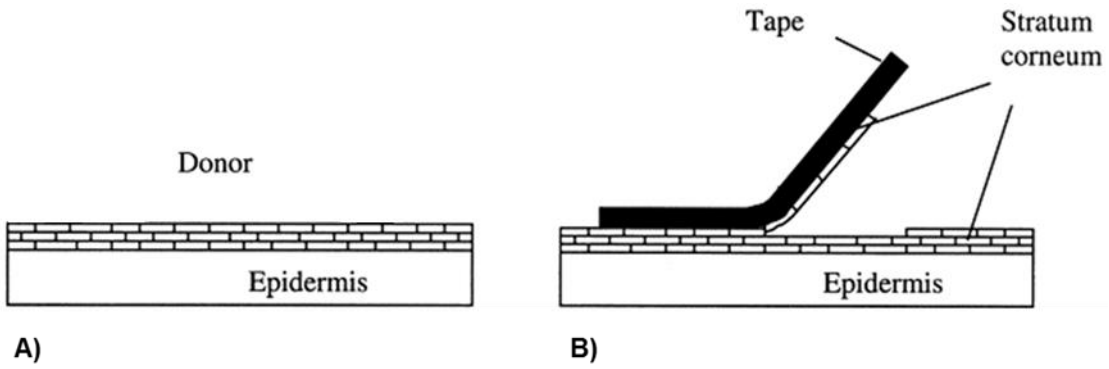

Figure 1.27 *Representation of tape stripping method. After applying formulation at the skin surface of the donor (A), the cells from the stratum corneum are progressively removed by adhesive tapes (B). Image adapted from* (Moser *et al.*, 2001)*.*

This technique is easy to perform, relatively non-invasive and does not require labelled compounds and, hence, it can be performed both *in-vivo* and *in-vitro.* However, it also presents several drawbacks; the amount of the SC removed is not constant on each strip, and decreases as more tapes are used, probably due to a more effective cohesiveness of the SC in the deeper layers (Alikhan and Maibach, 2010). In this regard, the measurement of the SC harvested from each tape strip must be identified e.g. by calculating the weight of the pieces of tape before and after stripping (Bommannan, Potts and Guy, 1990). In addition, the difficulty of removing completely the stratum corneum must be also considered. As reported by van der Molen *et al.* the presence of furrows in the skin can prevent complete cell removal (van der Molen *et al.*, 1997). As a consequence of these issues, a high experimental error from tape stripping can be expected.

1.9.2 Diffusion cell method

A classic diffusion cell experiment is composed of two compartments, a donor and a receptor, separated by a mounted sample (i.e. skin), as illustrated in Figure 1.28.

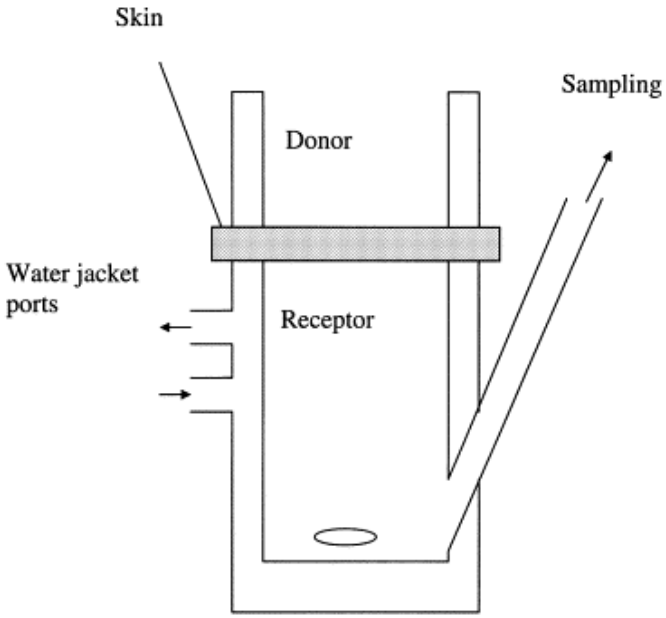

Figure 1.28 *Schematic representation of a diffusion cell, containing a donor and a receptor compartment separated by the skin sample. Image taken from* (Moser *et al.*, 2001)

In the donor compartment the drug formulation is inserted and, then, by measuring periodically the drug concentration in the receptor compartment it is possible to evaluate the permeation rate of the drug through the skin barrier (Touitou, Meidan and Horwitz, 1998). Usually the analysis of drug within the receptor fluid is performed using high performance liquid chromatography (HPLC). In addition, excess analyte on top of the skin as well within the skin layers can be examined for further evaluations, such as total disposition and percentage recovery.

1.9.3 Autoradiography

Autoradiography is a photographic technique able to visualise radiolabelled compounds across the stratum corneum, at both the cellular and sub-cellular level (Caro and van Tubergen, 1962). Its application for transdermal research was first reported by Touitou and co-workers (Fabin and Touitou, 1991; Touitou, Alkabes, *et al.*, 1994; Touitou, Levi-Schaffer, *et al.*, 1994). In the work of Fabin and Touiton quantitative evaluation of drug localised in various levels of skin, using autoradiography was obtained with the aid of imaging software (Fabin and Touitou, 1991).

Autoradiography can also be performed on the whole body, enabling the evaluation of dermal absorption and the involvement of other tissues in the body (Wester and Maibach, 2001; Griem-Krey *et al.*, 2019)**.**

1.10 Models for analysis

Over the years animal samples have been often used as a replacement for human subjects in order to generate representative information, important for the progress of pharmaceutical, toxicological and cosmetic skin research.

However, studies carried out by Netzlaff *et al.* and Bronaugh *et al.* provide evidence that the choice of the animal is key in such studies and that the most appropriate animal will depend on the compound under investigation. They showed that differences in the skin structure of different animals, such as

thickness of the SC, composition of intercellular SC lipids, and density of hair follicles could give rise to changes in the absorption kinetics for different compounds. It is therefore impossible to find a perfect animal model but, most often, porcine skin has been selected as the model of choice (Bronaugh, Stewart and Congdon, 1982; Netzlaff *et al.*, 2006; Lademann *et al.*, 2010). The understanding of whether animal models can actually predict the human *in-vivo* response represents a contentious issue and difficulties in translating results derived from animal models to clinical studies have recently been highlighted by leading pharmaceutical companies (Shanks *et al.*, 2009; Mead *et al.*, 2016). The intrinsic differences between human and other species as well as the common failure to reproduce all of the clinical and histopathological features of individual subtypes can give rise to misleading results (Conn, 2013). In addition, under the 7th Amendement to the EU Cosmetics Directive, the use of animals to test cosmetic ingredients has been banned (EU 2003), therefore the cosmetics industry has been forced to consider alternatives.

1.11 3D skin models

The NC3Rs (National Centre for the Replacement, Reduction and Refinement of Animals in Scientific Research) is an UK national organisation that strives to find alternative models as efficient methods for non-animal testing and research. The principles behind the 3Rs were first described by Russell and Burch in 1959; these include: Replacement, the use of insentient material as an alternative to conscious living animals; Reduction, the use of fewer animals that experience distress; Refinement, the use of methods to reduce or eliminate animal distress (Tannenbaum and Bennett, 2015). In light of these principles, a variety of *in-vitro* three dimensional (3D) reconstructed skin models have been developed (Nakamura *et al.*, 2018).

The possibility of isolating the epidermis from the dermis in human skin and culturing keratinocytes *in-vitro* represents the starting point behind the development of 3D skin models (Medawar, 1941; Rheinwald and Green, 1977). For the development of these models, following isolation of the epidermis, keratinocytes are cultured at an air liquid interface, either on an acellular

support or on a cellular support (dermal component consisting of fibroblasts in a 3D scaffold) (Niehues *et al.*, 2018). The scaffolds most commonly used are collagen and fibrin. The scaffold plays an important role since it recapitulates the *in-vivo* dermal extracellular matrix and allows cells to communicate with each other and form a differentiated epidermis; this process occurs after about two weeks, resembling the structure of the *in-vivo* skin epidermis (Macneil, 2007; Rademacher *et al.*, 2018). Alternatively, keratinocytes can be cultured directly onto a human de-epidermised acellular dermis (DED) (Pruniéras, Régnier and Woodley, 1983; Ponec *et al.*, 1988). However, in the work reported by El-Ghalbzouri and colleagues it was illustrated that the inclusion of fibroblasts positively affected the epidermal morphogenesis and differentiation (El-Ghalbzouri *et al.*, 2002; Tjabringa *et al.*, 2008). In light of these considerations, human skin equivalent models [HSEs] can be divided into two main groups: reconstructed human epidermis [RHEs] - 3D differentiated epidermis cultures derived from human keratinocytes; and full thickness living skin equivalents [LSEs], constituted of both epidermis and dermis.

A schematic representation of the 2 groups of 3D skin models is illustrated below in Figure 1.29.

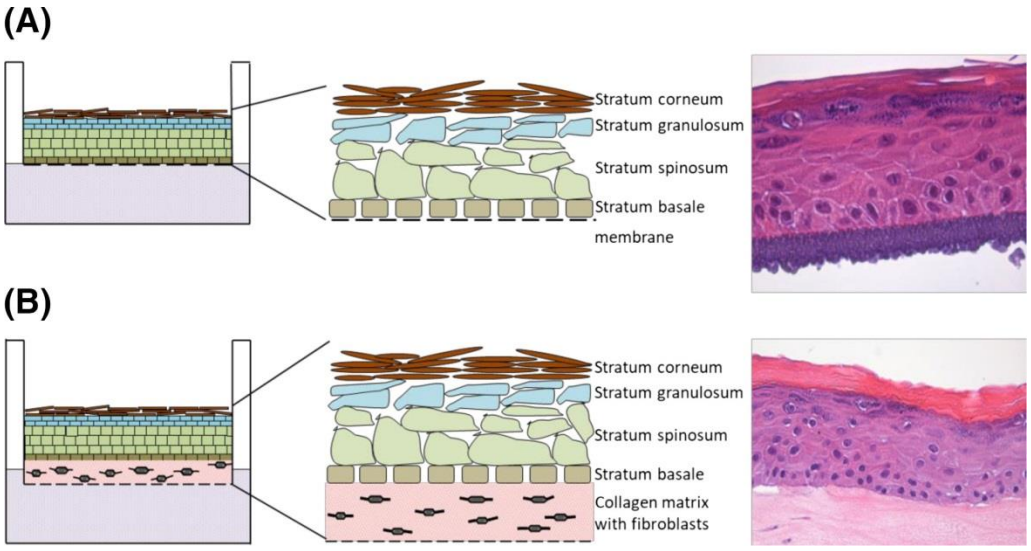

Figure 1.29 *Schematic representation of A) a reconstructed human epidermis [RHE]. Keratinocytes are cultured on the membrane of a cell culture insert; B) living skin equivalent [LSE]. Keratinocytes are cultured on a dermal support, consisting of fibroblasts in a 3D scaffold. Figure taken from* (Rademacher *et al.*, 2018).

To date, a range of commercially available models have become established for toxicological and pharmaceutical studies. These include RHEs, such as EpiSkin (Epskin, Lyon, France) and EpiDerm (Mattek, Ashland, USA) and LSEs, for example EpiDermFT (Mattek, Ashland, USA), T-skin (Episkin, Lyon, France) and Labskin (Innovenn (UK) Ltd, York, UK). A comprehensive review of their use in drug development has been published by Mathes and co-workers (Mathes and Ruffner, 2014; Ruffner, Graf-Hausner and Mathes, 2016). As a result of including the dermal component, the biological complexity increases moving from RHEs to LSEs, and can be further increased by adding within these models cell types such as melanocytes, stem cells or Langerhans cells, or by using novel approaches, such as organ-on-a-chip (Mathes and Ruffner, 2014; Niehues *et al.*, 2018). This last approach offers the possibility to culture different types of cells on a specially designed microchip, in which cells interact with a dynamic micro or nano fluidic flow in order to reproduce the *in-vivo* microenvironment (Wang *et al.*, 2015). The fabrication of the first chip, on which skin cells were directly cultured and differentiated on, was presented by Lee *et al.* (Lee *et al.*, 2017). The chip consisted of two compartments, separated by a porous membrane. On the top compartment, a chamber containing fibroblasts within a mixture of collagen and keratinocytes was present; whereas the bottom compartment contained a chamber for vascular cells and channels for the infusion of culture media with nutrients. Compared to engineered skin equivalents, RHEs and LSEs, skin-on-chip offers the advantage of including vascular structure into the model, as well as reproducing mechanical forces and dynamic flow system, representing a more physiologically appropriate skin model. However, the high cost and technical challenge of this model represent the main drawbacks that hamper its wide spread use (Abaci *et al.*, 2017; van den Broek *et al.*, 2017; Rademacher *et al.*, 2018; Sriram *et al.*, 2018).

The main advantages of 3D over 2D skin models for the testing of topical medication have been described by Teimouri *et al.* (Teimouri, Yeung and Agu, 2018). 3D cell culture models provide a better representation of native skin compared to monolayer 2D cell culture. More representative cell-to-cell and cell-to-extracellular matrix interactions occur in 3D skin models, leading to a better understanding of the *in-vivo* processes. 3D skin models offer an enhancement in quality, since they can be cultured for a longer time before de-differentiation

and decline occurs, making these models more appropriate and flexible for *in-vitro* analysis (Teimouri, Yeung and Agu, 2018).

1.11.1 3D skin models and skin absorption

Over the years tissue engineered HSEs have been established as valid models for *in-vitro* cosmetic and pharmaceutical testing, as well as for the investigation of skin biology mechanisms behind the generation of the epidermis, skin barrier repair/wound healing, skin pathologies and absorption testing (Schäfer-Korting, Mahmoud, *et al.*, 2008; Xie *et al.*, 2010; Ali *et al.*, 2015; De Vuyst *et al.*, 2017; Lewis *et al.*, 2018; Bataillon *et al.*, 2019).

The main aim of developing RHEs is to obtain models able to mimic faithfully the structure and architecture of *in-vivo* skin, such as protein expression and lipid organisation (Zhang and Michniak-Kohn, 2012). In the work reported by Ponec *et al.* tissue architecture, lipid organisation and permeability properties of three RHEs models (EpiDerm, SkinEthic, EpiSkin) were investigated (Ponec *et al.*, 2000). From this study it emerged that the tissue architecture of these 3D models highly mirrored that in native epidermis, whereas the main differences were found in the lipid expression levels. The levels of polar ceramide subclasses were much lower or absent in RHEs models in comparison to *in-vivo* skin, causing a higher permeability. In the work reported by Smeden *et al.* the lipid analysis of HSE models was performed using liquid chromatography-mass spectrometry (LC-MS) (Van Smeden *et al.*, 2014). The results showed that HSEs differed from native skin mainly in the free fatty acid (FFA) chain length and grade of unsaturation. In particular an increase of monounsaturated FFAs were present compared to native skin, in agreement with previous results showed by Thakoersing *et al.* (Thakoersing *et al.*, 2013). The formation of epidermal barrier in RHEs can be improved by the introduction of supplements within the culture media. Several studies have shown that vitamin D, vitamin C, fatty acids and serum growth factor type can decisively influence the final lipid content in the skin (Ponec *et al.*, 1997; Vičanová *et al.*, 1999; Gibbs *et al.*, 2007).

However, a concern that has been expressed in the use of 3D cell culture models for absorption studies relates to the difference in the absorption properties of such models compared to human skin (Schäfer-Korting, Bock, *et al.*, 2008). It was found in a large-scale validation study carried out in Germany that the permeation of chemicals was overestimated when using 3D models (Schäfer-Korting, Bock, *et al.*, 2008). This aspect is mainly due to the deviations in lipid composition and organisation within these models (Bell *et al.*, 1991; Mathes and Ruffner, 2014; Abd *et al.*, 2016).

A discussion of the philosophy of the use of tissue models is appropriate. For acceptance of the use of these models in demonstrating absorption what is required is an acknowledgment that the models are "models", not human skin. In order for the models to be used to predict absorption behaviour in human skin, what is therefore required is that their absorption behaviour be fully characterised for substrates with a range of physio-chemical properties so that conversion/scaling factor can be derived (Russo *et al.*, 2018).

1.11.2 Labskin

In this thesis the skin model system used is a commercial 3D living skin equivalent model, Labskin, produced by Innovenn (York,UK).

Labskin is a well-structured model, containing all of the layers of skin (epidermis, dermis and complete basement membrane). The development of this model consists of the following steps:

1. Dermal equivalent: first, fibroblast cells are placed in a fibrin gel scaffold and left for 6 days within media specifically created for Labskin;
2. Living skin equivalent: after 6 days, keratinocyte cells are deposited on top of the dermal component and left for 2 days within the media (submerged growth). Afterwards, the media on the surface is removed allowing the keratinocyte cells to differentiate into the suprabasal layers at an air-liquid interface. After seven days exposure at the air-liquid interface, the keratinocytes differentiate into the different layers of the epidermis; at this point, the stratum corneum is thin and therefore, the model mimics sensitive skin. At day 12 air-liquid interface, the stratum

corneum becomes thicker thus, mimicking mature skin. The company ships the model at day 12 air liquid interface.

After 12 days at the air-liquid interface, Labskin is viable for an additional 10 - 14 days, representing a valuable model for longer-term skin experiments. In addition, Labskin is the only 3D skin model presently available, able to host microorganisms on the surface and, hence, mimic the microflora of human skin. This potential is due to the properties of surface, which is relatively dry compared to other models and presents protective functions similar to human skin. Considering these aspects, it is understandable that interest in the use of Labskin has increased over the years as a valuable platform for microbial studies of cosmetics and skin products, drug delivery as well as wound care products (https://www.labskin.co.uk/).

In light of all these benefits in addition to the easy availability of the model (no ethical licence required), Labskin was selected as the model of choice for the experiments carried out in this thesis.

1.11.3 MALDI-MSI and skin

This thesis is particularly focused on the quantitative assessment of percutaneous absorption of an antifungal agent, terbinafine hydrochloride, in a 3D LSE model, Labskin, by using MALDI-MSI. In addition, the effect of the penetration enhancer dimethyl isosorbide (DMI) to the delivery vehicle has also been investigated.

1.12 Terbinafine hydrochloride

Terbinafine hydrochloride is an antifungal agent belonging to the allylamine class (Petranyi, Ryder and Stütz, 1984) and it acts by blocking squalene epoxidase (Nowosielski *et al.*, 2011). The hydrochloride form of terbinafine has been included in topical formulations for the treatment of dermatophytoses, pityriasis versicolor, and cutaneous candidiasis (Belal, El-din and Eid, 2013)

(Figure 1.30). Commercial dosage cream contains 1% (w/w) of terbinafine hydrochloride and, in a previous study, this was used as a model formulation for dermatopharmacokinetics (DPK) study of terbinafine hydrochloride through *in-vivo* and *in-vitro* tape-stripping experiments (Saeheng *et al.*, 2013).

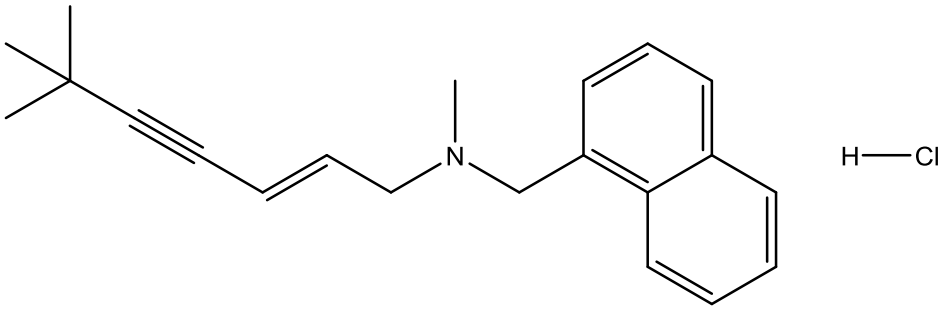

Figure 1.30 *Structure of terbinafine hydrochloride.*

Chapter 2: Optimisation of the detection and imaging of terbinafine hydrochloride in a commercial 3D skin model using MALDI-MSI.

2.1 Introduction

As discussed in Chapter 1.8 drug penetration through the skin represents a crucial process for targeting the active agent directly to the action site in the body, whilst limiting the side effects. The understanding of this process represents a very big scientific challenge that, if addressed, would lead to the significant advancement of novel topical and transdermal system delivery (Depieri *et al.*, 2015; Ruela *et al.*, 2016). Traditional techniques widely accepted for assessing the efficacy of drug formulations for topical and transdermal delivery include tape stripping and diffusion cells, as discussed in Chapter 1.9. However, the major disadvantage of these approaches is represented by the lack of spatial resolution, as they are restricted to the thickness of skin layers.

To increase the spatial resolution, mass spectrometry imaging techniques have been introduced to assess drug penetration directly in biological sections; the imaging techniques employed to date include matrix assisted laser desorption ionisation mass spectrometry imaging (MALDI-MSI) (Prideaux *et al.*, 2007) time-of-flight secondary ion mass spectrometry (TOF-SIMS) (Sjövall *et al.*, 2014), and desorption electrospray ionisation mass spectrometry imaging (DESI-MSI) (D'Alvise *et al.*, 2014; Taudorf *et al.*, 2015). Comprehensive reviews of the application of mass spectrometry imaging techniques for drug distribution studies have been produced by Stoeckli and Prideaux (Prideaux and Stoeckli, 2012) and Swales *et al.* (Swales *et al.*, 2019).

MALDI-MSI is currently the most popular MSI technique being used to visualise the distribution of compounds directly in tissue sections (Jove *et al.*, 2019; Strnad *et al.*, 2019). MALDI-MSI offers large advantages; comprising high throughput, robustness and the ability to map ion distribution of many compounds without requiring the use of labels, such as isotopes or fluorescent tags (Schulz *et al.*, 2019).

Although over the years, several studies have described the application of MALDI-MSI to examine endogenous compounds in skin tissue, such as lipids and proteins (Hart *et al.*, 2011; Enthaler *et al.*, 2012, 2013), few publications have reported its application for the study of drug absorption. In work completed

by Bunch *et al.* MALDI-MSI was used to map the distribution of an antifungal agent, ketoconazole, in porcine epidermal tissue (Bunch, Clench and Richards, 2004). More recent work by Bonnel *et al.* used MALDI-MSI to investigate the distribution profiles of four different drugs in human skin explants (Bonnel *et al.*, 2018).

Because of the poor accessibility of *ex-vivo* human skin due to ethical and functional limitations, 3D *in-vitro* engineered models have been developed as an alternative system for drug penetration testing, as described in Chapter 1.11 (Mathes and Ruffner, 2014; Ruffner, Graf-Hausner and Mathes, 2016). MALDI-MSI of 3D skin models was initiated by the Clench group, who published the first publication on the use of MSI with these models, demonstrating that MALDI-MSI could be used to analyse the drug penetration of imipramine within a commercially available 3D tissue model of the epidermis "Straticell" (Avery *et al.*, 2011). Other studies of a similar type have been reported by Francese *et al.* (Francese *et al.*, 2013) and Mitchell *et al.* (Mitchell *et al.*, 2015, 2016). In the work of Francese *et al.* MALDI-MSI was used to map the distribution of the drug acetretin within a commercial living skin equivalent model, with the purpose of investigating the efficiency of the compound curcumin as a matrix compared to CHCA. MSI data of Labskin 4 hours post-treatment showed the penetration of acetretin into the epidermal layer (Francese *et al.*, 2013). In further development of this work reported by Harvey *et al*., the localisation of the same drug was analysed using MALDI-MSI, after the creation of an LSE exhibiting psoriatic-like properties by treatment of the commercial product with the pro-inflammatory cytokine interleukin-22 (Harvey *et al.*, 2016). In this modified model, the distribution of acetretin was studied at 24 hours and 48 hours post-treatment and the data obtained demonstrated that after 48 hours, it was possible to observe the drug penetration into the dermal region, whereas at 24 hours, it was still localised in the epidermal layer only.

In MALDI-MSI experiments a basic requirement is the presence of a matrix (usually a small organic compound) which enables analyte desorption and ionisation (Hoffmann and Stroobant, 2007). The choice of the correct matrix plays a pivotal role as it can highly influence the desorption/ionisation process, thus contributing to spectral quality, i.e., peak resolution, sensitivity, intensity

and noise (Lemaire *et al.*, 2006). A comprehensive review into MALDI approaches for the analysis of low molecular weight compounds was conducted by Bergman *et al.* (Bergman, Shevchenko and Bergquist, 2014). Most commonly for MALDI positive mode, alpha-cyano-4-hydroxycinnamic acid (α-CHCA), 2,5-dihydroxybenzoic acid (DHB) and sinapinic acid (SA) matrices have been found to be good candidates for direct analysis of both large molecules, i.e. peptides and proteins, and low-weight molecules (endogenous and exogenous). Matrices such as 9-aminoacridine (9-AA) are preferred for the detection of small molecules in negative mode (Baker, Han and Borchers, 2017). Aside from the conventional matrices, novel strategies have been developed to overcome matrix selectivity issues, i.e. including additives to matrix solutions (Billeci and Stults, 1993), combining matrix compounds (binary matrices) (Laugesen and Roepstorff, 2003; Guo and He, 2007) and using ionic matrices (Zhao *et al.*, 2017).

There is not an easy way to determine which matrices will work for a particular analyte, and a "trial and error" approach is often employed. The fastest and most cost-effective way for matrix sample preparation is by manual pipetting of analyte-matrix onto a MALDI sample target. This way could include a variety of possible procedures, i.e. crushed-crystals (Xiang, Beavis and Ens, 1994), sandwich (Kussmann *et al.*, 1997) and dried droplet (Karas and Hillenkamp, 1988), which represents the most common (Chapter 1.3.1.1).

Although the dried droplet method has been widely used for MALDI-MS profiling (MALDI-MSP), it is usually not applicable for MALDI-MS imaging (MALDI-MSI), due to diffusion and segregation effects causing irregular distribution of matrix crystals (Luxembourg *et al.*, 2003).

The crystal size and homogeneity of matrix distribution onto the sample are strongly influenced by the matrix deposition technique, which therefore affects the spatial resolution of images when using MSI. Over the years multiple matrix deposition techniques have been established, such as micro-spotting, airbrushing, inject printing, spraying and sublimation (Aerni, Cornett and Caprioli, 2006).

Several studies have provided evidence that sublimation is able to create smaller matrix crystal size diameters (1 to 3 µm) than those produced by

spraying methods which are typically 5 to 20 µm (Phan *et al.*, 2016). Murphy *et al.* showed the improved quality of imaging of lipids in different tissues analysed by MSI when the matrix was applied by sublimation (Murphy *et al.*, 2011). However, owing to its solvent-free mechanism, a recrystallisation step after sublimation can be necessary to allow better extraction of analyte of interest from the sample and therefore a more intense signal (Yang and Caprioli, 2011). Commonly the recrystallisation step is performed by incubation with solvent vapour (Yang and Caprioli, 2011; Meisenbichler *et al.*, 2019; Morikawa-Ichinose *et al.*, 2019), although the literature has also reported the use of sprayers for solvent application (Ferguson *et al.*, 2013; Lauzon *et al.*, 2015; Dueñas, Carlucci and Lee, 2016).

2.2 Aims of the chapter

In the following chapter we aimed to develop a suitable method to detect an antifungal agent, terbinafine hydrochloride, in a 3D LSE, Labskin, by using MALDI-MSI. Firstly, optimisation work of mass spectrometry analysis to improve the signal of the standard terbinafine hydrochloride (TBF HCl) was performed. Furthermore, in this chapter, two different matrix deposition techniques, automated spraying and sublimation, to image the distribution of terbinafine HCl in Labskin, were examined and compared. Finally, the use of the penetration enhancer dimethyl isosorbide dimethyl ether (DMI) was investigated for assessing percutaneous penetration of the drug by MALDI-MSI.

2.3 Materials and methods

2.3.1 Chemicals and materials

MALDI matrices and instrument calibrants - Alpha cyano-4-hydroxycinnamic acid (α-CHCA), 2,5-dihydroxybenzoic acid (DHB), 9-aminoacridine (9-AA), aniline, acetone, trifluoroacetic acid (TFA), phosphorus red and formic acid (FA) were purchased from Sigma-Aldrich (Gillingham, UK). For tissue staining protocols haematoxylin, eosin, xylene substitute and ethanol (EtOH) were

purchased from Sigma-Aldrich (Gillingham, UK). Pertex mounting medium was obtained from Leica Microsystems (Milton Keynes, UK). Acetonitrile (ACN) and methanol (MeOH) were purchased from Fisher Scientific (Loughborough, UK).

Terbinafine hydrochloride standard and isosorbide dimethyl ether (DMI) were purchased from Sigma-Aldrich (Gillingham, UK). Conductive indium tin oxide (ITO)-coated microscope glass slides were purchased from Sigma-Aldrich (Gillingham, UK).

2.3.2 Tissue preparation

Living skin equivalent models (LSEs) were supplied by Innovenn (York UK). LSEs were delivered after 14 days of development in transport culture medium. At the time of delivery LSEs were transferred into new 12 deep well plates, suspended in fresh Labskin maintenance medium and left to incubate for 24 hours with 5% CO_2, 37°C. Labskin was treated with terbinafine hydrochloride at 1% w/w dissolved either in acetone/olive oil (80:20 v/v) or in 100% DMI. After treatment, LSEs were re-incubated for 24 hours. After incubation, the samples were taken, snap-frozen with liquid nitrogen cooled isopentane (2-5 min) and stored at -80°C. For cryosectioning, LSEs were transferred into the cryostat (Leica 200 UV, Leica Microsystems, Milton Keynes, U.K.) and mounted onto a cork ring using diH_2O at −25°C for 30 min to allow to thermally equilibrate. The tissues were cryosectioned (12 µm), thaw mounted onto ITO glass slides, and stored at −80°C.

2.4 Optimisation of mass spectrometry imaging

2.4.1 Mass spectrometric profiling of terbinafine hydrochloride

Different matrices dissolved in several solvent mixtures were compared for best mass spectrometric analysis of terbinafine hydrochloride. For positive mode the matrices used were: either 5 mg/mL or 10 mg/mL of α-CHCA in ACN/0.5% TFA (7:3, v/v); 5 mg/mL of α-CHCA in ACN/0.2% TFA (1:1, v/v) + equimolar amount

of aniline added to the final volume; 20 mg/mL DHB in either ACN/MeOH (1:1, v/v) or ACN/0.2% TFA (1:1, v/v). The binary matrix was prepared by mixing in ratio 1:1 CHCA solution matrix (20 mg/mL in ACN/5% FA (7:3, v/v)) with DHB solution matrix (20 mg/mL in ACN/0.1%TFA (7:3, v/v)). For negative mode, the matrix used was: 15 mg/mL 9-AA in MeOH/diH_2O (4:1, v/v).

Terbinafine hydrochloride (100 µg/mL unless otherwise stated) was mixed with each matrix solvent composition (ratio 1:1) by using the dried droplet method. Then, three spots (0.5 µL) from each mixture were deposited across the length of the MALDI stainless steel plate and then allowed to dry at room temperature prior to mass spectrometric analysis.

2.4.2 Mass spectrometric imaging of terbinafine in Labskin

2.4.2.1 Matrix deposition

2.4.2.1.1 Spraying

All sample sections were taken from -80^{o}C and freeze-dried under vacuum (0.035 mbar) for 2 hours to avoid delocalisation of the analyte and preserve the integrity of the tissues. The matrix (5 mg/mL α-CHCA in ACN/0.2% TFA (1:1, v/v) with equimolar amount of aniline added to the final volume) was deposited onto the treated tissue section surface using a SunCollect^{TM} automated sprayer (KR Analytical, Sandbach, UK). Eleven layers of matrix were sprayed with a flow rate of 3 µL/min for the first layer and 3.5 µL/min for the following ten layers. The time taken to spray eleven layers of matrix on an area of 432 mm^2 was around 1 hour and the total amount of matrix deposited was around 1 mg per the entire area (432 mm^2), hence 2.31 µg/mm^2.

2.4.2.1.2 Sublimation

α-CHCA (300 mg) was spread evenly at the bottom of the sublimation apparatus (Sigma-Aldrich). ITO-coated glass slides containing treated Labskin tissues were attached to the flat top of the chamber using double-sided tape. The flat top of the chamber was then attached to the bottom using an O-ring

seal and the vacuum was applied. When a stable vacuum of 2.5 x 10^{-2} Torr was achieved, the top was filled with cold water (5°C) and the temperature was set to 180°C. The sublimation process was performed until the optimal amount of α-CHCA (0.2 mg/cm^2) was achieved. To monitor the quantity of matrix deposited, the glass slide with the tissue section was weighed before and after the sublimation process; the amount of matrix (mg) was calculated by the difference and divided by the area of the sublimed slide (mg/cm^2). The time taken to complete this process was around 20 minutes.

2.4.2.1.3 Recrystallisation

For MS/MSI experiments, after sublimation an additional recrystallisation process was performed. A glass Petri dish (100 mm diameter x 15 mm depth) was used to carry out the recrystallisation on sublimated tissues. The glass slide was fixed to the underside of a petri dish lid using standard double-sided tape. The lid was then placed on the rest of the dish and put in the oven for 2 minutes at 180°C. The petri dish was then retrieved from the oven and a solution of 1 mL deionised water and 50 µL trifluoroacetic acid was pipetted onto filter paper placed at the bottom of the petri dish. The petri dish was then sealed with Parafilm (Sigma Aldrich, UK) and placed in the oven for 6 minutes. The dish was then unsealed, and the lid returned to the oven to dry for a further 2 minutes.

2.5 Instrumentation

2.5.1 Mass spectrometry

All experiments were performed using an Autoflex III (Bruker Daltonik GmbH, Germany) equipped with a 200-Hz Smartbeam™ laser. For MALDI-MSP mass spectra were manually acquired in positive and negative mode in reflectron mode at a mass range of 50-1000 *m/z*. Six hundred laser shots were acquired for each spectrum. External mass calibration was achieved using a phosphorus red standard at approximately 200 ppm.

2.5.2 Data processing

MALDI-MSP data were acquired using FlexControl (Bruker Daltonics, Germany), converted to .txt file format using FlexAnalysis (Bruker Daltonics, Germany) and analysed using Mmass v5 open source software (Strohalm et al., 2010).

For MALDI-MSI positive ion mode, mass spectra were acquired at a pixel size of either 30 µm or 10 µm from 100 *m/z* -1000 *m/z*. The laser was focused at the small setting (around 20 µm diameter). Four hundred laser shots were acquired for each pixel and the data were processed using FlexImaging 3.0 software (Bruker Daltonics, Germany).

2.6 Histological analysis

2.6.1 Haematoxylin and eosin staining

LSE sections (12 µm) after MALDI-MSI were stained used Mayer's haematoxylin and eosin solutions. First, any presence of matrix was removed by washing the slides with 100% (v/v) EtOH. Sections were then rehydrated by submerging in 95% (v/v) and 70% (v/v) EtOH washes for 3 min and they were left for 1 min in deionised water before being stained in filtered Meyer's haematoxylin for 10 min. Tissues were washed in running tap water for 3-5 min and dehydrated using 70% (v/v) and 95% (v/v) EtOH solutions then immersed in filtered eosin 100% (v/v) for 1 min. The last dehydration step was performed using 95% (v/v) and 100% (v/v) EtOH solution, each for a period of 3 min. Finally, the slides were submerged in 2 changes of xylene substitute for 5 min each and mounted using Pertex mounting medium.

Optical images were obtained using an Olympus BX60 microscope and analysed with Q-Capture-Pro 8.0 software (QImaging, Surrey, BC, Canada).

2.7 Results and discussion

2.7.1 Comparison of matrices

A wide variety of matrices are currently available for the analysis of low molecular weight analytes. The optimisation of the matrix choice remains a fundamental aspect, since it strongly depends on the analyte under investigation in terms of structure, solubility and physiochemical properties (Reyzer and Caprioli, 2007).

In positive mode, a standard solution of terbinafine hydrochloride (100 µg/mL) was examined using MALDI-MSP with the two most commonly used matrices, CHCA and DHB, at different concentrations and solvent compositions. Alternatively, in negative mode, terbinafine hydrochloride (100 µg/mL) was analysed using 9-AA matrix. With 9-AA matrix no significant signals were obtained; this matrix was therefore not considered further (Figure 2.1). These results were expected due the basic nature of the amine group of terbinafine. All profiling experiments were performed using the dried droplet technique, the most common approach used to prepare MALDI sample spots.

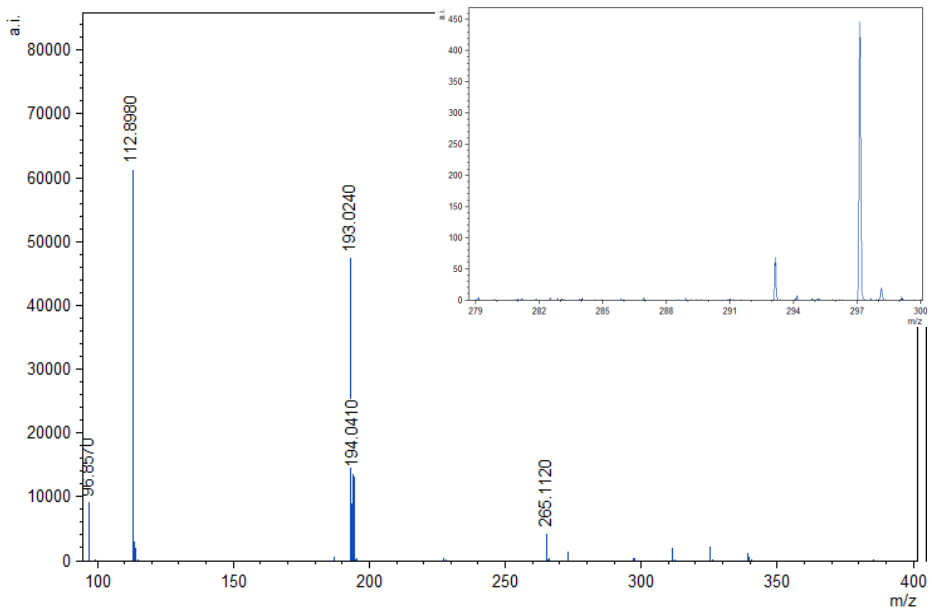

Figure 2.1 *MALDI-MS spectrum acquired in negative mode on the spot TBF (100 µg/mL) mixed with the matrix 9-AA. No evidence of the expected peak [M-H]⁻, m/z 290.19 was observed.*

For positive mode, first, the effect of DHB at the same concentration (20 mg/mL) prepared in either ACN/MeOH (1:1, v/v) or ACN/0.2% TFA (1:1, v/v), were compared. The presence of TFA in the solvent, an excellent proton donator, led to a more efficient ionisation of the analyte and consequently higher signal intensity, as show in the Figure 2.2A. In addition, a lower standard deviation in the latter case was also observed. However, the differences in error bars shown in the Figure 2.2A could be derived from inhomogeneity of matrix-analyte crystals, responsible for spot to spot irreproducibility, as well as from the background noise of the MALDI technique (Krutchinsky and Chait, 2002; Wijetunge *et al.*, 2015) The chemical noise measured at the detector, beside limits the sensitivity of the technique, affects the signal of the acquired spectra, generating a non-uniform background.

Next, the performance of CHCA at two different concentrations; 5 and 10 mg/mL dissolved in ACN/0.5% TFA (7:3, v/v) was investigated. The optimal concentration of matrix was found to be 5 mg/mL; since a lower signal intensity of terbinafine hydrochloride was detected when the higher concentration of CHCA was used (Figure 2.2B). As reported in the proteomic study conducted

by Zhang *et al.*, this aspect may be explained by the fact that an increase in matrix concentration may derive an increase of matrix clusters responsible for the analyte signal suppression (Zhang *et al.*, 2010).

To increase the sensitivity of the terbinafine hydrochloride different approaches have been investigated, either by mixtures of matrix compounds (CHCA-DHB) or by adding liquid aniline to matrix preparation.

The application of CHCA-DHB mixture was previously reported to improve the spot-to-spot reproducibility and signal-to-noise ratio in peptide analysis (Laugesen and Roepstorff, 2003; Schlosser *et al.*, 2005). In more recent work, Shanta *et al.* reported the combination of CHCA-DHB with a mixture of piperidine and TFA for the visualisation and identification of phospholipids in brain tissue by using MALDI-MSI in both positive and negative modes (Shanta *et al.*, 2011).

Another strategy widely employed to increase the sensitivity and improve the ionisation of the analyte of interest involves the use of ionic liquid matrices (ILMs). The most common examples of ILMs consist of a combination of an acid normally used as MALDI matrix with an organic base, i.e pyridine, aniline, tributylamine in equimolar proportions (Meriaux *et al.*, 2010). In particular, the addition of aniline within CHCA matrix solution has been reported as an excellent strategy to detect low molecular mass analytes, thanks to the improvement in the signal-to-noise ratio and absence of interfering peaks generated by conventional CHCA matrix (Calvano, Carulli and Palmisano, 2009).

Analysing these two different approaches, ANI-CHCA was found to be the most favorable for increasing the absolute intensity of terbinafine hydrochloride and reducing the matrix interference in the low *m/z* range on the spectrum (Figure 2.2C).

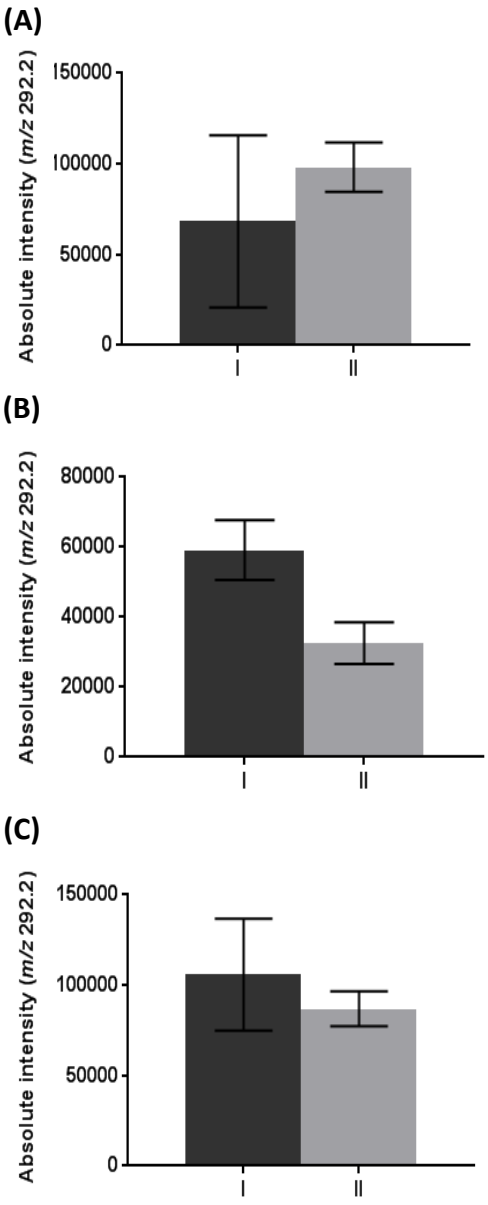

Figure 2.2 *The effect of several matrices on the signal intensity of terbinafine hydrochloride ($[M+H]^+$; m/z 292.2) (n = 9). A) 20 mg/mL DHB dissolved in I) ACN/MeOH (1:1, v/v), II) ACN/0.2% TFA (1:1, v/v). B) CHCA dissolved in ACN/0.5% TFA (7:3, v/v) at concentrations: I) 5 mg/mL and II) 10 mg/mL. C) CHCA dissolved in different solvents at different concentrations: I) 5 mg/mL in ACN/0.2% TFA (1:1, v/v) with equimolar aniline, II) 20 mg/mL in ACN/5% FA (7:3, v/v) mixed in ratio 1:1 with 20 mg/mL DHB in ACN/0.1% TFA (7:3, v/v).*

The final step of the matrix optimisation study was to compare the energy threshold for ion production of terbinafine hydrochloride obtained when mixed with all different matrix compositions (Figure 2.3).

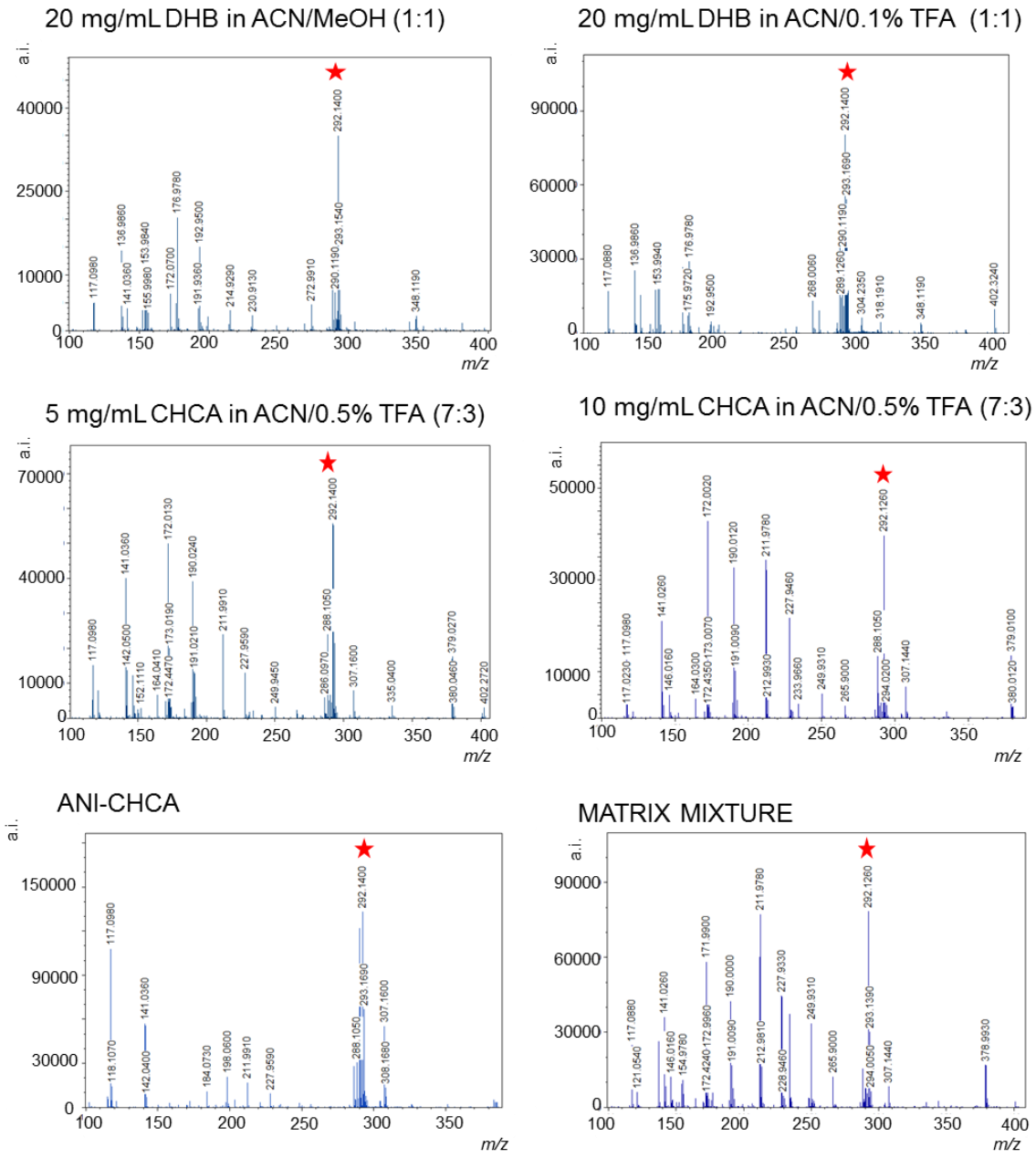

Figure 2.3 *MALDI-MS spectra of terbinafine hydrochloride standard (100 µg/mL) obtained for different matrices. Peaks with a star represent the peak of the terbinafine hydrochloride in positive mode ($[M+H]^+$; m/z 292.2).*

Figure 2.4A shows that the employment of ANI-CHCA matrix resulted in a significant enhancement in spectral quality of terbinafine hydrochloride compared to the other matrices. Furthermore, the superiority of the ionic liquid matrix was highlighted also when the relative intensity of the analyte was investigated (intensity peak of terbinafine HCl/intensity peak of matrix), supporting the ability of the ionic liquid matrix (ANI-CHCA) to suppress matrix ion peaks (Figure 2.4B).

Morphological aspects of matrix crystallisation resulting from sample deposition in different matrices by the dried droplet technique are shown in Figure 2.4C. With manual spotting, the crystallisation tended to be irregular and inhomogeneous, DHB formed needle-shaped crystals pointing to the edge of the rim, whereas CHCA crystals appeared smaller with low density at the center of the rim. A slightly higher homogeneity crystal distribution was obtained with the combination of two matrices (CHCA-DHB), whereas the ANI-CHCA gave a very typical transparent droplet base with crystal clusters across.

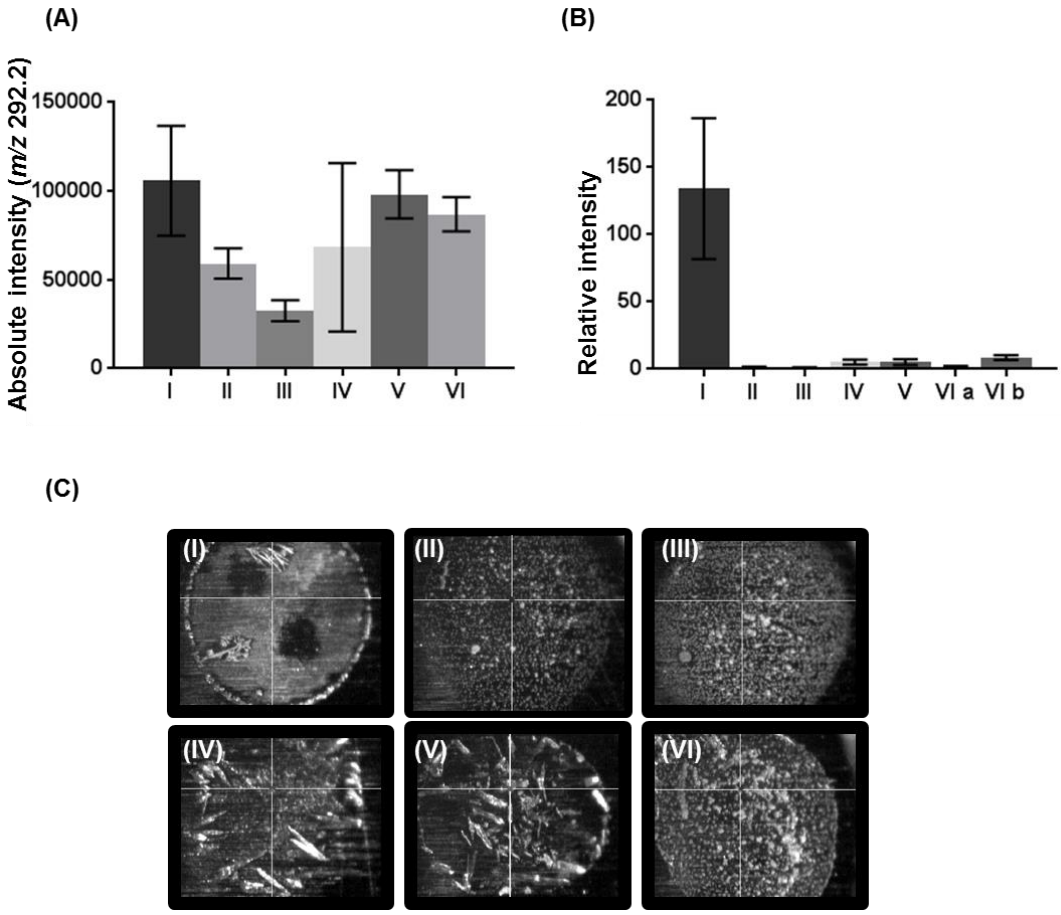

Figure 2.4 *A) Absolute and B) relative intensity of terbinafine hydrochloride peak ($[M+H]^+$; m/z 292.2) with several matrices (n = 9). I) 5 mg/mL CHCA in ACN/0.2% TFA (1:1, v/v) with equimolar aniline, II) 5 mg/mL and III) 10 mg/mL CHCA in ACN/0.5% TFA (7:3, v/v); 20 mg/mL DHB in: IV) ACN/MeOH (1:1, v/v) and* V) *ACN/0.2% TFA (1:1, v/v). VI) 20 mg/mL CHCA in ACN/5% FA (7:3, v/v) mixed in ratio 1:1 with 20 mg/mL DHB in ACN/0.1% TFA (7:3, v/v). For relative intensity, TBF intensity was normalised with the $[CHCA+H]^+$ peak of m/z 190.05, when CHCA was used as matrix, and with the $[DHB+H]^+$ peak of m/z 155, when DHB was used as matrix. When the binary matrix was used, the TBF peak was normalised for both VIa) $[CHCA+H]^+$ peak and VIb) $[DHB+H]^+$ peak. C) Matrix crystal morphologies obtained by the dried droplet deposition method.*

2.7.2 Spraying

As the ionic liquid matrix ANI-CHCA was found to be the optimal matrix to enhance the intensity of the analyte of interest, terbinafine hydrochloride, it was decided to use this matrix for further MALDI-MS imaging investigations. First, the matrix ANI-CHCA was applied onto the Labskin tissue by using a SunCollect automated sprayer, widely used as matrix deposition device (Francese *et al.*, 2013; Barré *et al.*, 2019; Morikawa-Ichinose *et al.*, 2019). The spraying conditions were optimised and, to assess the optimal number of layers, the sample was observed using microscopy when different layers of matrix were applied. It was found that 11 layers of matrix were required to give a good consistency in crystal size and excellent coverage of tissue.

Figure 2.5 shows MALDI-MS images of the distribution of terbinafine parent compound at *m/z* 292.2 in a section of Labskin following treatment with 20 µL of terbinafine (1% (w/w) in emulsion acetone/olive oil (80:20)) for 24 hours. To increase the lateral spatial resolution of the MALDI-MS image, it was decided to reduce the pixel size to 10 µm. This was possible using the Autoflex III (Bruker Daltonic) instrument, which offered the advantage of changing the laser focus diameter down to 10 µm, allowing the generation of high resolution images, without oversampling. From the image it can be seen that the terbinafine signal appeared to be localised solely to the epidermal layer, with no penetration within the dermal region. The absence of the drug in the deeper layer of the skin was as expected considering the high lipophilicity and keratophilicity of the molecule, which leads to its accumulation solely onto the epidermal layer (Pretorius *et al.*, 2008).

From the image it was also possible to detect an undesirable migration/diffusion of the analyte. The analyte delocalisation could represent a major drawback when spray-coating is used; primarily due to the presence of the solvent responsible for tissue wetting during the spraying (Schwartz, Reyzer and Caprioli, 2003; Puolitaival *et al.*, 2008). In addition, other parameters could affect analyte delocalisation, i.e. the pressure with which the matrix solution hits the tissue, nozzle movement and height. Although these parameters could be optimised to minimise analyte delocalisation, the presence of a solvent is

necessary to prepare the matrix solution for this method and hence it cannot be completely eliminated.

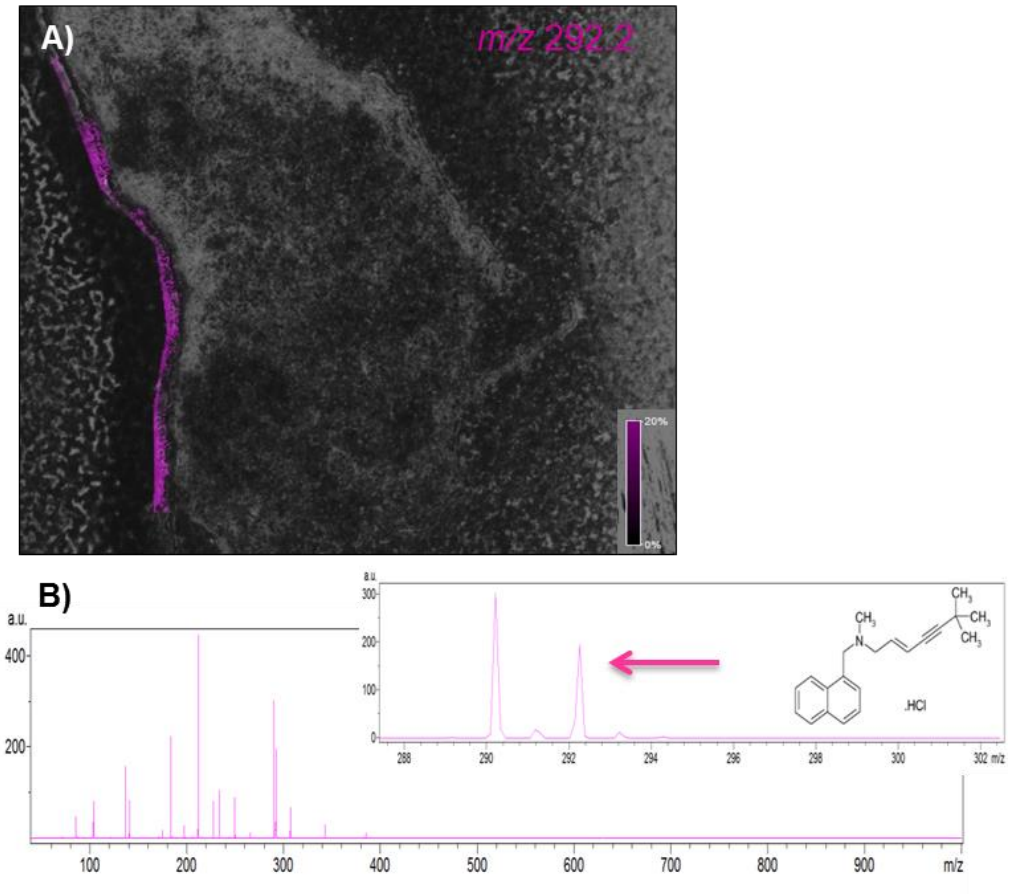

Figure 2.5 *A) MALDI-MS image showing the distribution of terbinafine hydrochloride ($[M+H]^+$; m/z 292.2). (Spatial resolution = 10 µm). B) Overall MALDI-MS spectra, inlay shows zoom at m/z 292.2. Image is generated by using TIC normalisation.*

2.7.3 Sublimation

To increase the spatial resolution, sublimation, a solvent-free matrix deposition technique was examined. Kim *et al.* were the first to describe the use of sublimation/deposition for direct MALDI analysis (Kim, Shin and Yoo, 1998). In the study, the authors highlighted the excellent advantage of employing this technique to deposit both sample and matrix when they were not soluble with each other (Kim, Shin and Yoo, 1998). Over the years, the use of sublimation

for direct sample analysis by MALDI-MS imaging applications has been more widely established (Hankin, Barkley and Murphy, 2007; Caughlin *et al.*, 2017; Bøgeskov Schmidt *et al.*, 2018; Kaya *et al.*, 2018). A wide sublimation study was performed by Thomas *et al.* on 12 different matrices (Thomas *et al.*, 2012). From the study it was found that the sublimation of the matrix 1,5-diaminonaphthalene (DAN) was particularly efficient for high spatial resolution imaging of lipids in both positive and negative ion polarities.

In this work 0.2 mg/cm^2 of organic matrix CHCA alone was applied by sublimation onto a section of Labskin treated with terbinafine (1% (w/w) in acetone/olive oil (80:20)) for 24 hours. In agreement with results obtained using the automatic sprayer system, MS images of Labskin section showed no delivery of the drug into the dermis, but confirmed the localisation of terbinafine hydrochloride at *m/z* 292.2 only in the outmost layer of the skin, the epidermis (Figure 2.6). The localisation of drug was also supported by haematoxylin and eosin staining performed on the same section of Labskin after sublimation (Figure 2.7).

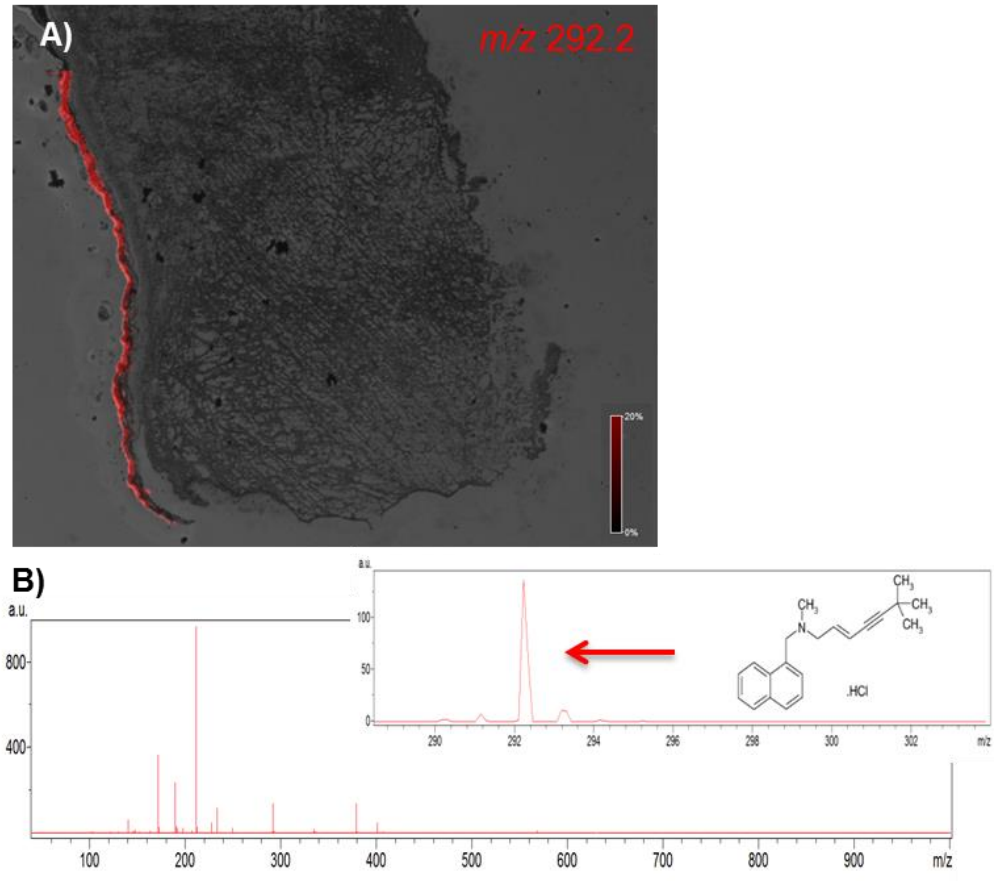

Figure 2.6 *A) MALDI-MS image showing the distribution of terbinafine hydrochloride ($[M+H]^+$; m/z 292.2). (Spatial resolution= 10 µm). B) Overall MALDI-MS spectra, inlay shows zoom at m/z 292.2. Image is generated by using TIC normalisation.*

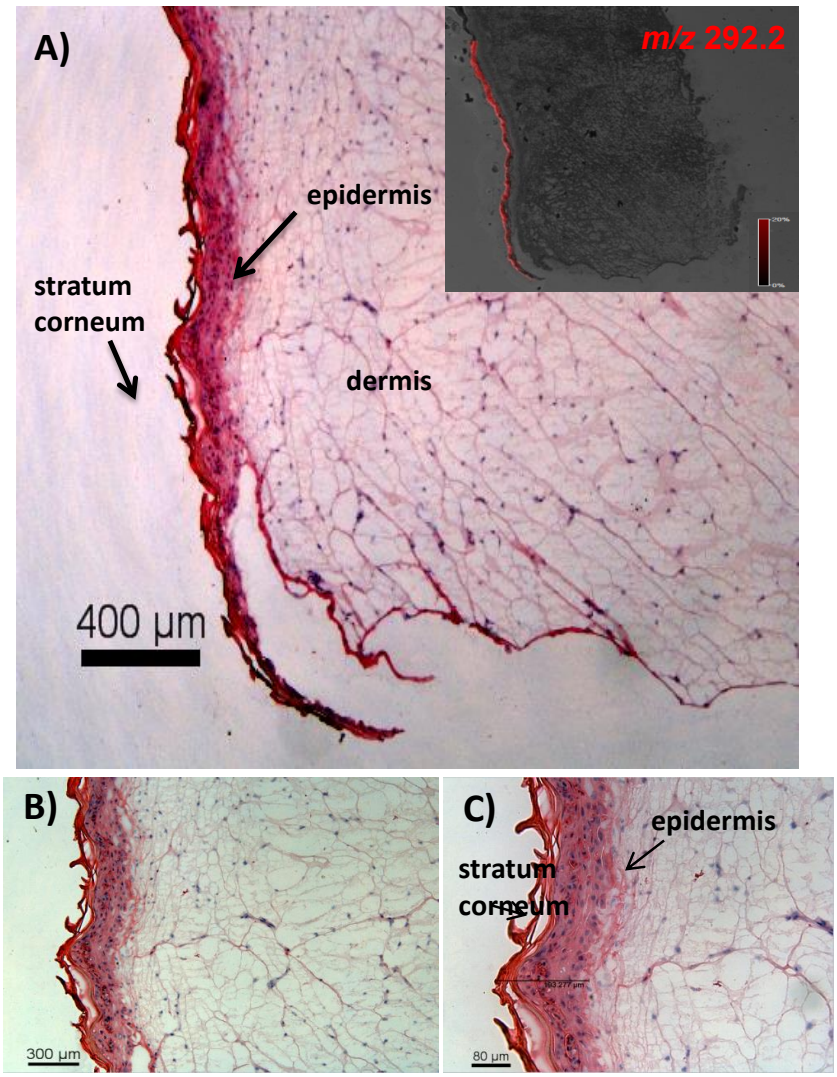

Figure 2.7 *Haematoxylin & eosin stained optical image of the sublimated section after MALDI-MSI A) 4X magnification B) 10X magnification C) 20X magnification.*

After sublimation, a recrystallisation step can be performed on the sample in order to rehydrate it (Bouschen *et al.*, 2010). The necessity to execute this additional step on sublimed samples was considered in order to increase the analyte extraction. The extraction efficiency may be relatively low without a recrystallisation because of absence of solvent in the sublimation (Shimma *et al.*, 2013; Morikawa-Ichinose *et al.*, 2019). The choice of solvent used for rehydration of sample depends on the analyte and matrix used. One water-based solvent, with addition of TFA, was chosen to incorporate the analyte into

the sublimated matrix, following the recrystallisation procedure developed by Yang and Caprioli (Yang and Caprioli, 2011).

The recrystallisation was performed on a sublimated sample treated with terbinafine for 24 hours in the same composition examined previously. MALDI MS/MS imaging was performed on the recrystallised sample while keeping high spatial resolution at 10 µm. Figure 2.8 shows the MALDI-MS/MSI spectrum obtained from the major product ion at *m/z* 141.

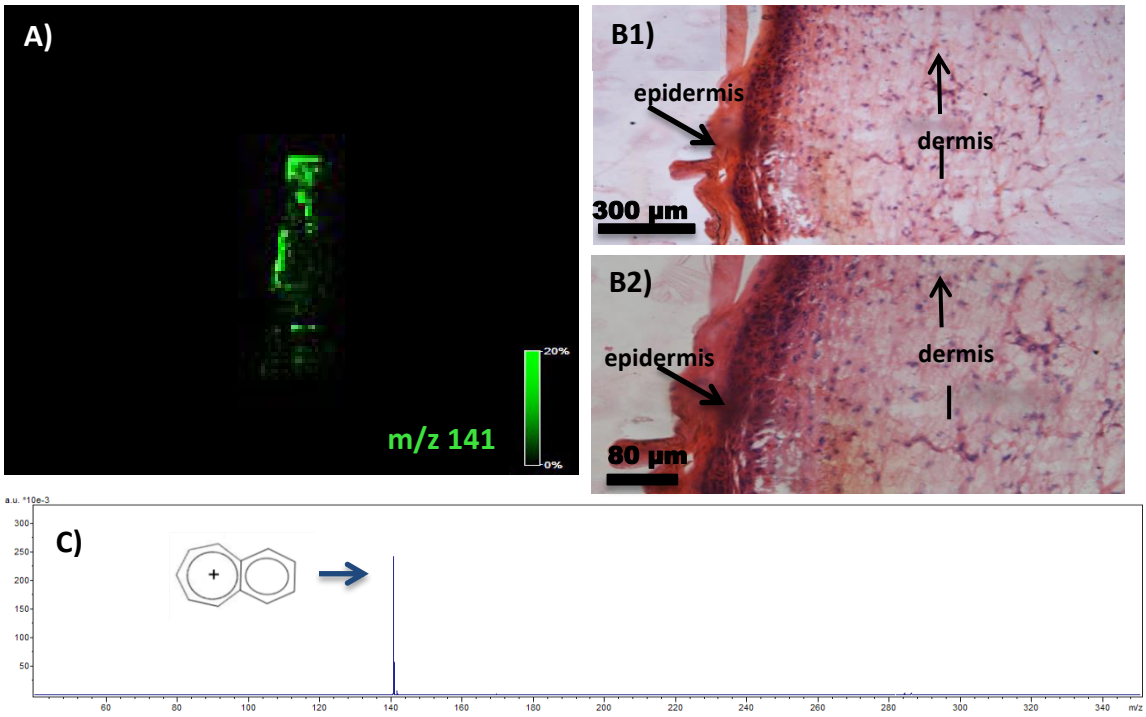

Figure 2.8 *A) MALDI-MS/MSI distribution of terbinafine fragment $[M+H]^+$ at m/z 141 of LSE 24 hours post-treatment B) Haematoxylin & eosin stained optical image of the same section 1) 10X magnification 2) 20X magnification C) MALDI-MS/MSI spectrum showing the major product ion at m/z 141.*

Although the MS/MS data supported the MALDI-MSI data, which showed that the localisation of drug was confined in the epidermal layer, the spatial resolution appeared to be lost with the additional recrystallisation step. This drawback could be due to the fact that the exposure with the vapor may lead to an excessive water condensation on the glass surface, generating a non-

homogenous matrix composition and consequently causing analyte migration from the tissue. Although this aspect could be improved with further optimisation of solvents and time (Yang and Caprioli, 2011; Dueñas, Carlucci and Lee, 2016), by analysing the signal of terbinafine hydrochloride (*m/z* 292.2) in two sections of Labskin, one exposed only to matrix sublimation and the other exposed to matrix sublimation/recrystallisation, an increase of intensity was not detected in the latter (data not shown). However, it is important to note that the analysis was performed on different sections of Labskin and on different days, hence, a direct comparison was not suitable. In this study it was decided to not proceed further with a recrystallisation step after sublimation.

2.8 Comparison of automated sprayer and sublimation methods for terbinafine mass spectrometry imaging

The MALDI-MS images obtained by automated sprayer and sublimation were directly compared. Both images showed a relatively uniform intensity of terbinafine across the outermost layer of skin, the epidermis, although a significant enhancement of the spatial resolution was obtained when the matrix was applied by sublimation (Figure 2.9).

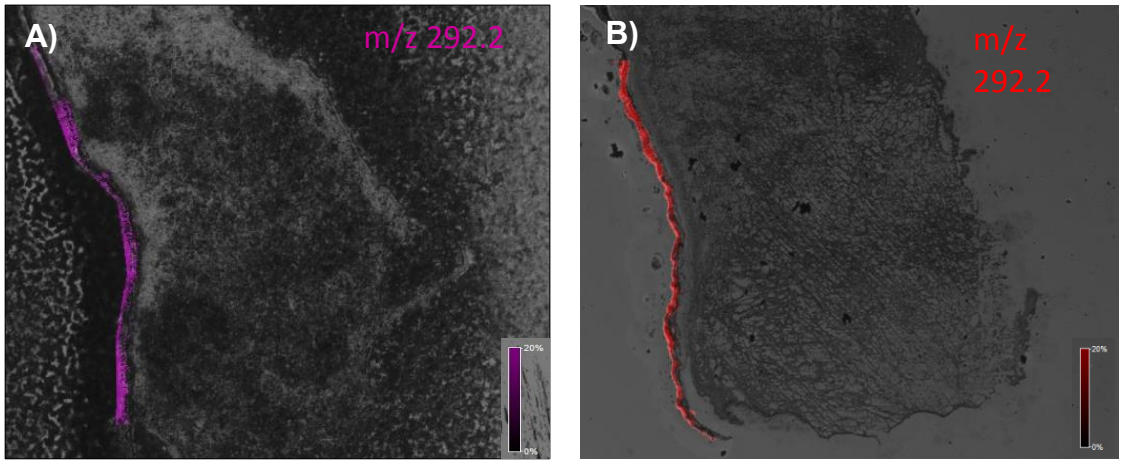

Figure 2.9 *Comparison of MALDI-MS images of terbinafine hydrochloride ($[M+H]^+$; m/z 292.2) by applying CHCA with A) optimised automatic sprayer and B) optimised sublimation method to Labskin section 24 hours post-treatment.*

It is common knowledge that, beside the laser spot size, the quality of the image could be strongly limited by factors including crystal size and uniformity of the matrix. In regards to this, the analysis of the matrix morphology was investigated. The spraying of 11 layers of ANI-CHCA produced a heterogeneous matrix deposition with splits and many incongruities, whereas very small crystal size and high uniformity of matrix was achieved with CHCA applied by sublimation (Figure 2.10). The superiority of a dry-coating approach for the imaging of small molecules was emphasised also by Lauzon *et al.* (Lauzon *et al.*, 2015). Yang and Caprioli also highlighted the benefit of a sublimation approach for achieving high spatial resolution for imaging of large molecules, proteins up to *m/z* 30000 on mouse and rat brain (Yang and Caprioli, 2011).

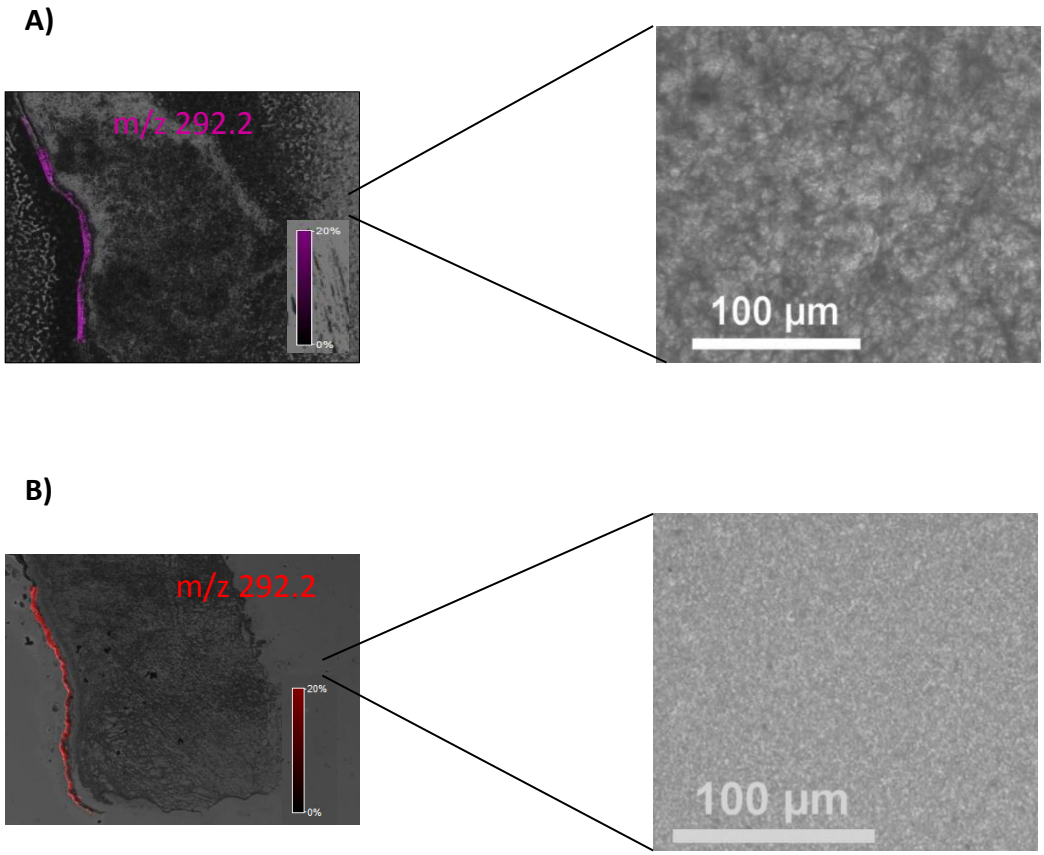

Figure 2.10 *Optical images comparing matrix coverage and crystal morphology for the A) optimized automatic sprayer, and B) optimized sublimation matrix application methods using CHCA as matrix.*

The ion peak patterns generated by the matrix were also investigated. In this regard, regions of interest (ROIs) with equal area (24 pixels) were selected in the tissue-free regions and the signal from CHCA applied by these two different techniques was extracted and compared. The overall spectrum from the sprayed ANI-CHCA showed multiple matrix sodium/potassium-adduct peaks ($[M+K]^+$, *m/z* 228; $[M-Na+K]^+$, *m/z* 250) hardly detectable in the overall spectrum from the sublimed CHCA (Figure 2.11). The reduction of the intensity of CHCA cluster peaks in the spectrum from sublimed CHCA was attributable to the higher purity of matrix and this aspect guaranteed less interference in the spectrum in the low *m/z* range, minimising possible peak interference drawbacks with the terbinafine hydrochloride ion peak.

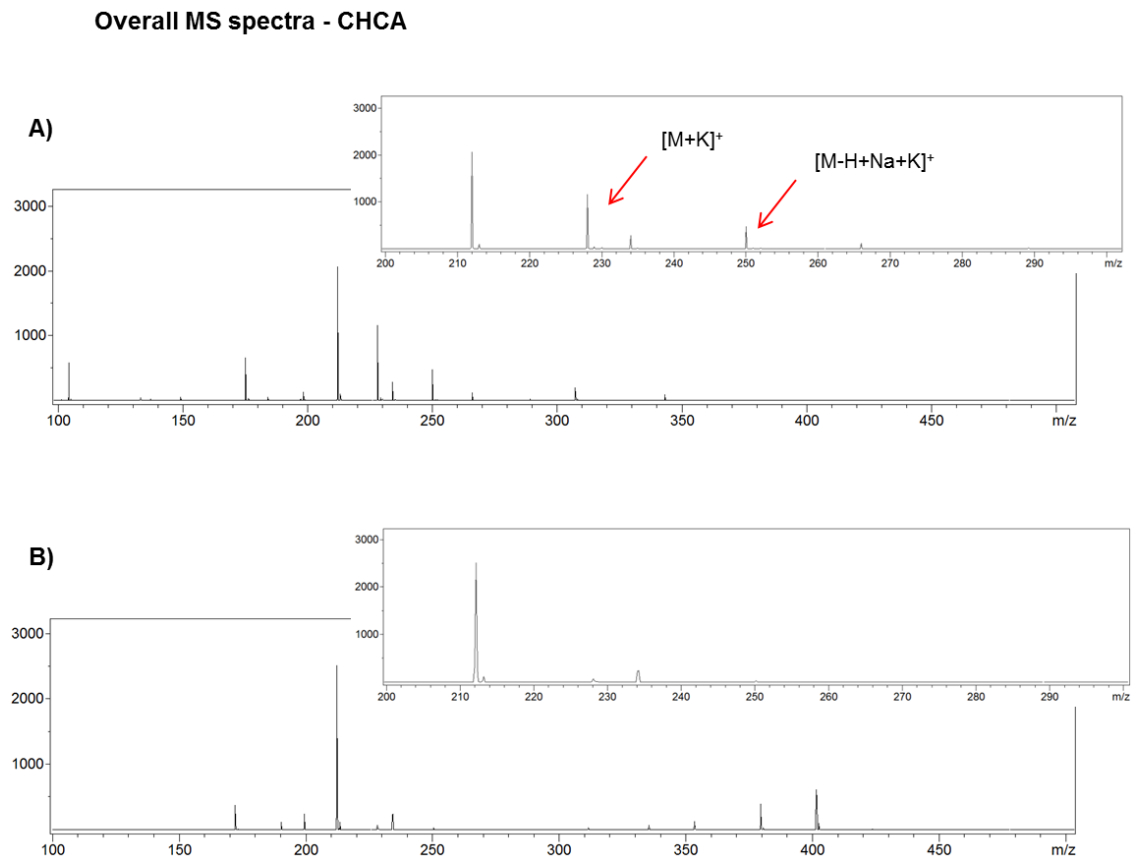

Figure 2.11 *Overall MS spectra of CHCA matrix peaks (with no sample) when applied to ITO glass slide with A) optimised automated spraying and B) optimised sublimation matrix application methods. Spatial resolution = 30 µm. Inlays show the MS spectra zoomed in the lower m/z range (m/z 200-300). TIC normalisation.*

2.9 Optimisation of percutaneous delivery of terbinafine hydrochloride

Once established that the uniform coating of matrix and small crystal sizes achieved by sublimation ensured a better spatial resolution and limited analyte delocalisation compared to the automatic sprayer method, this study proceeded with the optimisation of the terbinafine percutaneous delivery.

As discussed in Chapter 1.8.1, the inclusion of chemical penetration enhancers (CPEs) within a drug formulation could represent a valid strategy to enhance the drug penetration through the stratum corneum (the limiting barrier to drug absorption). In the work reported by Erdal *et al.* (Erdal *et al.*, 2014) three CPEs

(nerolidol, dl-limonene and urea) were investigated. From this study it emerged that the addition of nerolidol in a topical terbinafine formulation increased the delivery of the drug within deeper layers of epidermis, allowing potentially the treatment of deep cutaneous infections (Erdal *et al.*, 2014).

Specifically, in the study presented in this chapter, the assessment of enhanced topical delivery of terbinafine by using DMI based formulation was investigated (Figure 2.12). DMI is a "sustainable" solvent widely included in cosmetic and pharmaceutical formulations (Durand *et al.*, 2009). In this context the term "sustainable" refers to a solvent where the production process includes pollution prevention/control and resource-usage reduction (Glavič and Lukman, 2007). DMI acts as chemical enhancer by improving the partitioning of active agents into the stratum corneum and leading to a greater penetration of them into the epidermis (Zia *et al.*, 1991; Otto *et al.*, 2008).

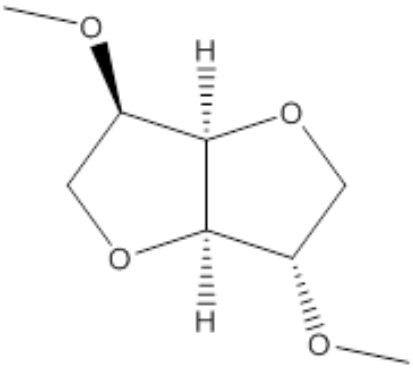

Figure 2.12 *Structure of isosorbide dimethyl ether.*

Figure 2.13 shows MALDI-MSI images of the distribution of the terbinafine parent compound at *m/z* 292.2 in a section of Labskin following treatment with 20 µL of terbinafine (1% (w/w) in 100% DMI) for 24 hours. As can be seen from the figure, the main concentration of terbinafine was focused in the epidermis. Tandem MS/MS imaging experiments carried out on the $[M+H]^+$ signal for terbinafine at *m/z* 292.2 showed the expected major product ion at *m/*z 141 and supported the presence of terbinafine in the epidermis (Figure 2.14). These results find support from previous unpublished studies performed on *ex-vivo* human skin, in which it was shown that the inclusion of DMI within vehicle

enhanced the drug penetration only within the epidermal layer and did not lead to penetration into the dermis (personal communication).

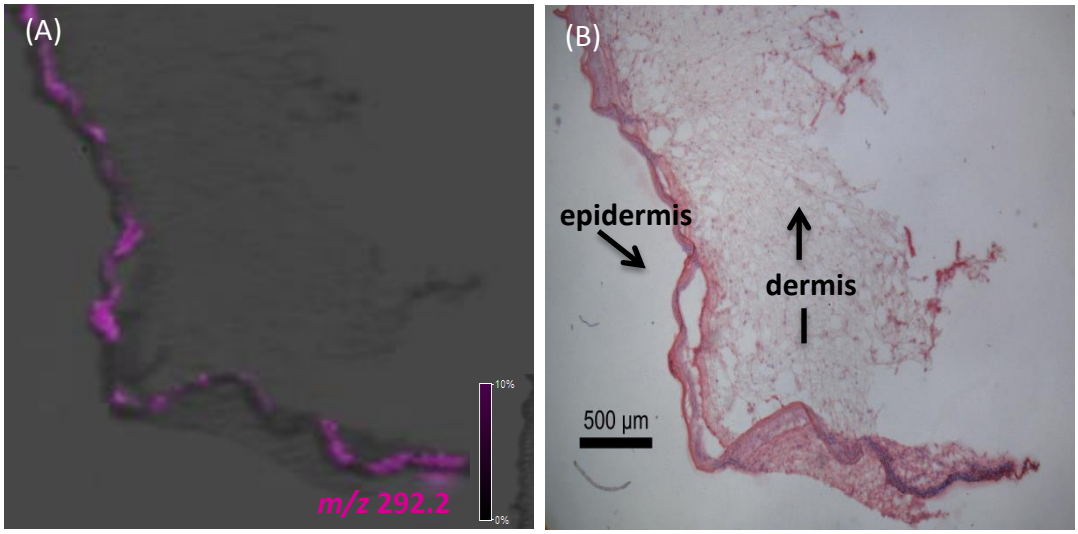

Figure 2.13 ***A)*** *MALDI-MSI distribution of terbinafine* $[M+H]^+$ *at m/z 292.2 of LSE 24 hours post-treatment in 100% DMI. Matrix (CHCA) applied by sublimation. Spatial resolution = 30 µm.* ***B)*** *Haematoxylin & eosin stained optical image of the sublimated section. 4X magnification.*

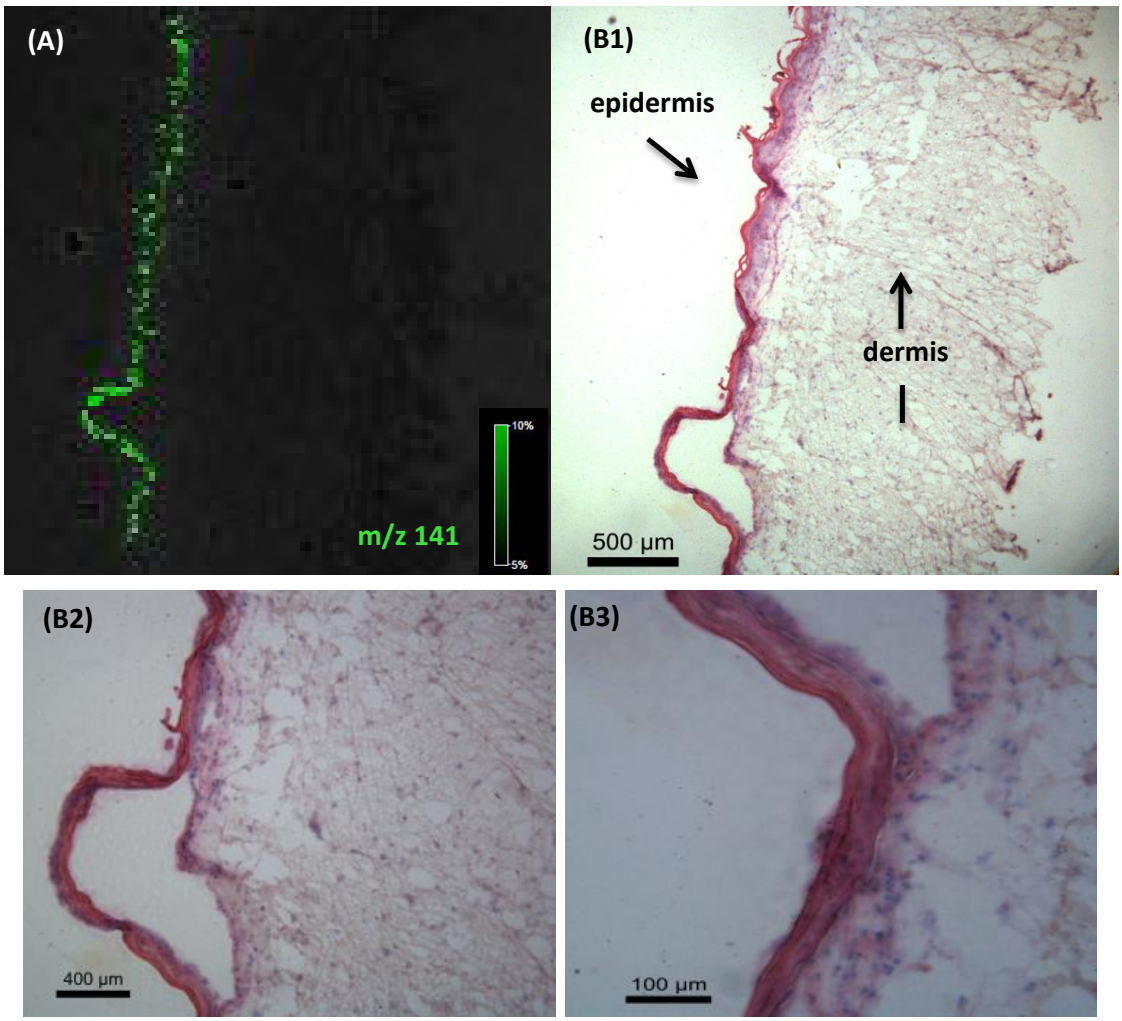

Figure 2.14 *(A) MALDI-MS/MSI distribution of terbinafine fragment $[M+H]^+$ at m/z 141 of LSE 24 hours post-treatment in 100% DMI. Matrix (CHCA) applied by sublimation. Spatial resolution = 10 µm. (B) Haematoxylin & eosin stained optical image of the same section. (B1) 4X magnification. (B2) 10X magnification. (B3) 20X magnification.*

.

2.10 Concluding remarks

In this study, a commercial LSE model was treated with terbinafine hydrochloride dissolved in different solvent mixtures. Additionally, MALDI-MSI was used to identify the localisation of the drug in samples of the LSE. Data was obtained after depositing the matrix onto the sample using two different matrix deposition techniques, spraying and sublimation. Use of the sublimation was shown to give a better spatial resolution of the images obtained from the samples 24 hours post-treatment. This result was due to several factors associated with the sublimation technique: microcrystalline morphology of the matrix deposition, increased purity of deposited matrix, evenness of deposition and less spreading of analyte due to solvent deposition during matrix application.

It was demonstrated that 24 hours post-treatment terbinafine was localised only in the epidermal layers of the LSE, either when the drug was formulated with acetone/olive oil (80:20) or with a known penetration enhancer 100% DMI.

Chapter 3: Optimisation of methodology for quantitation in MALDI-MSI.

3.1 Introduction

The quantitation of drugs in tissues is an essential part of pharmaceutical discovery and development. The determination of the concentration of a drug at the site of action is extremely important for the assessment of its efficacy.

Quantitative whole-body autoradiography (QWBA) and liquid chromatography tandem mass spectrometry (LC-MS/MS) represent traditional techniques widely employed to detect the amount of drugs and metabolites in biological tissues after their administration (Hamm, Bonnel, Legouffe, Pamelard, J.-M. Delbos, *et al.*, 2012).

Quantitative whole body autoradiography (QWBA) is an advancement of whole body autoradiography (WBA), which is an imaging technique able to visualise the *in situ* distribution of radiolabelled molecules throughout tissue sections of laboratory animals, usually rodents (Solon and Kraus, 2001).

In brief, the WBA technique comprises first of the administration of a radiolabelled molecule (typically ^{14}C or ^{3}H) to lab animals and then euthanasia at specified time points. The entire animal carcass is then snap-frozen, embedded in carboxymethylcellulose and cryosectioned to obtain a representative slice (Solon and Kraus, 2001). By exposing tissue sections to a detector capable of measuring radioactivity (x-ray film or phosphor image plate) it is possible to obtain information about the distribution and the relative concentration of radiolabelled material in an animal body. To generate absolute quantitative data, Schweitzer *et al.* (Schweitzer, Fahr and Niederberger, 1987) introduced a robust and simple quantitation method that consisted of spiking a range of radioactive calibration standards within blood samples and embedding them with the animal.

The QWBA technique allows spatial information to be retained and it is highly sensitive and reliable. In addition, the images generated are of high resolution. However, this technique presents several drawbacks that need to be contemplated too. Firstly, it is a technique which can only be used for targeted analysis and it is expensive in terms of instrumentation and synthesis of radiolabels. In addition, the quantitation relies only on the concentration of radioactivity, which could include as well as the parent compound its

metabolites or degradation products. This can lead to misleading results for the amount of parent compound in the section (Solon *et al.*, 2010). For this reason, often liquid chromatography tandem mass spectrometry (LC-MS/MS) is used as a complementary technique to support QWBA data. In the pharmaceutical industry LC-MS/MS has been indicated as technique of choice for the identification and quantitation of drugs and metabolites in biological tissues (Rönquist-Nii and Edlund, 2005). Although this technique offers the enormous advantage that it can give excellent separation of compound mixtures as well as reliable quantitation, it has the disadvantage of losing spatial information from the sample. LC-MS/MS analysis cannot be carried out directly on intact tissue sections, but analytes of interest have to be extracted out of the tissue. This increases the complexity of sample preparation and leads only to an average concentration within the tissue sample being obtained.

In light of these considerations, in the last decade the potential of mass spectrometry imaging (MSI) technology for quantitative studies has been extensively examined. This technology combines the benefit of keeping the spatial information of non-labelled compounds in the tissues with the specificity of mass spectrometry. A comprehensive review into quantitative MSI strategies for biomedical applications was conducted by Ellis *et al.* (Ellis, Bruinen and Heeren, 2014).

The major drawbacks in generating quantitative mass spectrometry imaging (QMSI) data from biological tissue sections concern the ionisation of the analyte of interest. Indeed, the ion intensity of the analyte depends strongly on both the nature of the analyte as well as on the histological microenvironment that is sampled with the analyte. This latter aspect is responsible for what are defined as "matrix" or "ion suppression" effects. In addition the recovery of the analyte from the tissue also needs to be considered (Porta *et al.*, 2015).

In this regard, methods to overcome the limitations and increase the potential of MSI for quantitative analysis are highly sought after and developed. In particular, the imaging techniques most commonly employed to acquire absolute quantitative data include matrix assisted laser desorption ionisation mass spectrometry imaging (MALDI-MSI) (Groseclose and Castellino, 2013), and desorption electrospray ionisation (DESI-MSI) (Vismeh, Waldon and Zhao,

2012; Groseclose and Castellino, 2013; Hansen and Janfelt, 2016). Additionally, a recent study reported by Swales *et al.* described the application of liquid extraction surface analysis mass spectrometry imaging (LESA-MSI) for spatial quantitation of drugs in tissues (Swales *et al.*, 2016).

The generation of calibration curves based on the use of serial dilution of standards represents a pivotal aspect to assess absolute quantitation. A comprehensive review on calibration/standardisation strategies for quantitation of small molecules using MALDI-MSI has been conducted by Rzagalinski and Volmer (Rzagalinski and Volmer, 2017). In order to mimic ion suppression effects within tissue a common approach used is by using mimetic arrays created from tissue homogenates (Groseclose and Castellino, 2013; Jadoul, Longuespée and Noël, 2015) and surrogate material (pseudo-tissue) (Takai, Tanaka and Saji, 2014a) or to spot working standard solutions using a control tissue in two different ways: (1) by spotting a range of standard concentration onto the tissue prior to depositing the matrix or (2) by spotting a range of concentration underneath the tissue prior to positioning the tissue and depositing the matrix.

Lagarrigue *et al.* used spotting onto tissue in order to quantify the amount of pesticide chloredecon within mouse liver sections (Lagarrigue *et al.*, 2014). In this study six replicates were performed and a good linearity coefficient was achieved (R^2 from 0.9807 to 0.9981). In contrast, Pirman *et al.* spotted a range of calibration standards underneath a control brain tissue in order to quantify levels of cocaine by visualisation of the expected major product ion at *m/z* 182 using MALDI-MS/MS imaging (Pirman *et al.*, 2013).

In MALDI-MSI, the nature of analyte ionisation depends strongly on the entity of the analyte as well as the tissue. The same molecule can be subjected to varying ion suppression effects in different tissues or across the same tissue in response to a changeable histological framework as well as to the ionisation competition with compounds within the morphological microenvironment (Hamm, Bonnel, Legouffe, Pamelard, J. M. Delbos, *et al.*, 2012). This aspect in addition to the variation of ion signals due to heterogeneity of matrix deposition represent the major issues that need to be addressed in the development of MALDI-MSI as a method for quantitative mass spectrometry imaging (QMSI).

In order to correct for the issues that could compromise MALDI-MSI spectral quality different normalisation strategies were developed (Fonville *et al.*, 2012). The basic principle of normalisation is to employ a factor against which to correct each mass spectrum. Total ion current (TIC) normalisation represents the most commonly used correction approach. In previous studies, TIC was used to normalise MALDI-MSI spectra acquired from rat brain tissue sections and perform quantitative analysis of both several neurotransmitters and drugs (Goodwin *et al.*, 2011; Shariatgorji *et al.*, 2014) .

Although the TIC normalisation approach has been widely used to eliminate systematic artefacts derived from matrix crystal distribution, this approach may generate misleading conclusions from MALDI-MSI spectra, especially when the intensity of the analyte varies in different regions of the tissue (Deininger *et al.*, 2011).

In order to correct for "matrix" or "ion suppression" effects, largely highlighted in the study carried out by Stoeckli *et al.* (Stoeckli, Staab and Schweitzer, 2007), different normalisation strategies for MALDI-MSI data have been developed and examined.

The normalisation method developed by Hamm *et al.* based on a factor called the tissue extinction coefficient (TEC) aimed to correct for the ion suppression effects of the analyte of interest in a particular organ or region of interest (Hamm, Bonnel, Legouffe, Pamelard, J. M. Delbos, *et al.*, 2012). This technique was adopted to quantify the amount of olanzapine specifically in rat kidney sections as well as quantify the amount of propranolol in multiple organs of a mouse. The method consisted of covering a glass slide and a control tissue section with the analyte mixed with matrix. The average intensity of the analyte extracted from the tissue section was divided by the average intensity of the analyte on the glass slide and, in this way, the tissue extinction coefficient (TEC) was calculated. Then a calibration curve was generated by spotting a range of standards near a dosed tissue; the average intensity of the analyte from the dosed tissue was extracted and multiplied by the TEC and, then, compared to the calibration curve in order to assess the quantity of the drug in the tissue.

Matrix peaks have also been used to normalise the intensity of the analyte of interest and in the literature it is possible to find a large variety of applications of this approach to perform quantitative MALDI imaging of small molecules (Bunch, Clench and Richards, 2004; Takai *et al.*, 2012). In the works reported by Takai *et al.* a DHB matrix peak was employed to normalise the signal intensity of the drug raclopride in multiple organs by using whole-body sections (Takai *et al.*, 2012). Instead, Bunch *et al.* investigated the normalisation to a CHCA sodium adduct peak at *m/z* 212 for the determination of the drug ketoconazole in the skin (Bunch, Clench and Richards, 2004).

Multiple studies have shown how normalisation to an internal standard increases the quantitative capabilities of MSI analysis (Pirman and Yost, 2011; Prentice, Chumbley and Caprioli, 2017). The internal standard is a molecule with chemical and physical characteristics similar to analytes under study. During MSI analysis the internal standard mimics the behaviour of the analyte of interest in terms of ionisation efficiency and compensates for the tissue-dependent ion signal variations of the analyte. This aspect causes an improvement in relative signal ion reproducibility and image quality due to an increase in pixel to pixel precision (Pirman *et al.*, 2013; Chumbley *et al.*, 2016).

The growing interest in the QMSI field has led to the necessity of developing software packages designed for QMSI data. For this purpose, ImaBiotech developed the package software Quantinetix™ (www.imabiotech.com); whereas, more recently, Uppsala University (Sweden) developed msIQuant freeware software available from www.maldi-msi.org. It is a novel and established software designed for visualising and processing quantitative analysis of a large MSI data set, supporting multiple functions and MSI normalisation factors (Källback *et al.*, 2016).

In this study, different methods for generating accurate quantitative data of terbinafine hydrochloride in treated Labskin have been investigated. Different calibration/standardisation approaches have been compared, including: 1) cell films; on-tissue application of standards by 2) spraying and 3) microspotting; and 4) cell plug. In addition, preliminary quantitative data of terbinafine levels in Labskin tissues treated with different formulations have been obtained and the

performance of the penetration enhancer dimethyl isosorbide (DMI) in increasing the drug penetration has been assessed.

3.2 Aims of the chapter

In the following chapter we aimed to develop a robust, sensitive and reproducible methodology for generating accurate quantitative analysis of terbinafine hydrochloride, in Labskin, by using MALDI-MSI. The capability of the penetration enhancer dimethyl isosorbide (DMI) was also investigated.

3.3 Materials and methods

3.3.1 Chemicals and materials

Alpha cyano-4-hydroxycinnamic acid (α-CHCA), phosphorus red, terbinafine hydrochloride standard (TBF HCl, MW 327.89), isosorbide dimethyl ether (DMI), haematoxylin, eosin and xylene substitute were purchased from Sigma-Aldrich (Gillingham, U.K.). X-tra® slides and Pertex mounting medium was obtained from Leica Microsystems (Milton Keynes, U.K.). Industrial methylated spirit (Ims) was purchased from Thermo Fisher Scientific (USA).

Labskin living skin equivalent (LSE) samples were provided by Innovenn (U.K.) Ltd. (York, England).

3.3.2 Tissue preparation

3.3.2.1 Cell culture

Normal human dermal fibroblasts (NHDF) were purchased from PromoCell (Heidelberg, Germany) and cultured in Dulbecco's modified Eagle's medium (DMEM) media (Lonza Ltd, UK) supplemented with 10% foetal bovine serum (FBS) and 1% penicillin and streptomycin (Thermo Scientific, USA).

Immortalised human epidermal keratinocytes (T0345) were obtained from ABM (Richmond, BC, Canada) and cultured in Green's media. Green's media was obtained by mixing under sterile conditions the following: Hams F12 media (Lonza Ltd, UK) (108 mL), DMEM media (330 mL), L-glutamine (5 mL; 200mM), 10% FBS, 1% penicillin and streptomycin, adenine (2 mL, 4.62 x 10^{-2} M), and insulin-transferrin-selenium (ITS-G, 100 X; 2.5 mL), hydrocortisone (80 µL of 2.5 mg/mL), isoproterenol (80 µL of 2.5 mg/mL) and epidermal growth factor (EGF) (25 µL of 1 mg/mL).

All cell lines were maintained in a humidified atmosphere containing 5% CO_2 at 37 ^{o}C. They were cultured until they reached 80% confluence. Once confluent, the cell lines were passaged by trypsinisation, subsequent centrifugation, resuspension in fresh medium and seeded in new flasks.

3.3.2.2 Living skin equivalent samples

Living skin equivalent (LSE) samples were obtained and cultured as described in Chapter 2.3.2. For these experiments, Labskin was treated with 20 µL of terbinafine hydrochloride at 1% (w/w) dissolved either in 100% DMI or in an emulsion made up of water/olive oil (80:20 v/v) with 10% and 50% DMI; and incubated for 24 hours. For the blank tissue, used for generating on-tissue calibration array, Labskin was left untreated and incubated for 24 hours. For the vehicle control tissue, instead, Labskin was treated with 20 µL of vehicle water/olive oil (80:20) alone and incubated for 24 hours. After incubation, the samples were taken, snap-frozen with liquid nitrogen cooled isopentane (2−5 min) and stored at −80 °C. For cryosectioning, LSEs were transferred into the cryostat (Leica 200 UV, Leica Microsystems, Milton Keynes, U.K.), mounted onto cork ring using diH_2O at −25 °C for 30 min to allow to thermally equilibrate. The 12 µm tissue sections were cryosectioned, thaw mounted onto poly-L-lysine glass slides, and stored at −80 °C. Before standards and matrix application the samples were freeze-dried under vacuum (0.035 mbar) for 2 hours to avoid delocalisation of the analyte and preserve the integrity of the tissues.

3.3.3 Strategies for generating standard curves

3.3.3.1 Cell films

Working standards were made to 1, 10, 50, 100 and 500 ng/µL of TBF HCl in MeOH/H_2O (50:50) and deposited onto a “film” of keratinocyte and fibroblast cells cultured on a poly-L-lysine glass slide. Before culturing the cells, the glass slide was prepared and cleaned. A wax pen was used to draw on the slide a square constituting of hydrophobic barriers, inside of which the cells could be cultured. The slide was then sterilised by submerging in Ims 70% for 10 sec, and then it was washed with phosphate buffered saline (PBS) twice for 10 sec and Green's media for 10 sec. At this point the cells were prepared; keratinocyte (T0345) and fibroblast cells (NHDF) were cultured as described in Section 3.3.2.1. Once confluent, they were trypsinised and counted; 45000 keratinocytes and 15000 fibroblasts were mixed in order to mimic the same ratio composition present in the Labskin tissue (3:1) and then, 300 µL of the mixture was deposited onto the slide. The slide with cells was maintained in a humidified atmosphere containing 5% CO_2 at 37 ^oC overnight in order to allow the cells to settle onto the slide. The day after the excess media was tapped off and the slide was washed twice in PBS and the cells were fixed in formalin 10% for 30 min at room temperature. The glass containing the cell film was kept in PBS at + 4 ^oC until performing MALDI-MSI experiments. For MALDI-MSI analysis, the slide containing the cell film was washed with 0.1 M ammonium bicarbonate solution in order to remove the excess PBS and kept freeze-dried under vacuum (0.035 mbar) for 2 hours. The working solutions of TBF HCl (from 1 to 500 ng/µL) were deposited onto different areas of cell film using the SunCollect^{TM} automated sprayer (KR Analytical, Sandbach, UK). The standards were sprayed in a series of four layers using a flow rate of 4 µL/min.

3.3.3.2 On-tissue application of standards

For quantitative MALDI-MSI experiments the second approach investigated was based on generating a calibration curve by applying a dilution series of terbinafine hydrochloride standard onto blank tissue sections. Working standards were made to 0.1, 1, 100, 500, 1000, 1500, 2000, 3000 and 4000 ng/µL of TBF HCl in MeOH/H_2O (50:50). Calibration standards were applied onto the epidermis area of 12 µm thick of blank tissue sections using both spraying and microspotting.

3.3.3.3 Spraying

Terbinafine hydrochloride standards (0.1-4000 ng/ µL in MeOH/H_2O (50:50)) were deposited onto blank Labskin sections using the SunCollect^{TM} automated sprayer (KR Analytical, Sandbach, UK). A tissue section was used for each drug concentration. The standards were sprayed in a series of two layers and with a flow rate of 5 µL/min.

3.3.3.4 Microspotting

Terbinafine hydrochloride standards (0.1-4000 ng/µL in MeOH/H_2O (50:50)) were applied onto the epidermis area of 12 µm thick section of blank Labskin tissue using an acoustic robotic spotter (Portrait 630, Labcyte Inc., Sunnyvale, CA). For application of the standards the number of cycles for each spot was set to 20 for a total volume of 3.4 nL of each deposited solution. Five extra spots were applied outside the tissue to give a “drying time” between each cycle.

3.3.3.5 Cell plug

Working standards were made to 3, 300, 1500, 3000, 9000, 15000, 21000 and 42000 ng/µL of TBF HCl in MeOH/H_2O (50:50). 20 µL of these standards were mixed with 40 µL of non-homogenised keratinocytes cells. The resulting suspension was pipetted into a gelatin block in order to generate a calibration array. The gelatin block was made by pouring 20% gelatin (w/v) into an ice cube mould, which was set in the fridge at +4 ºC for 4 hours before being frozen overnight in -80 ºC. Before the loading process, the top of the block was cryosectioned in order to obtain an even surface and 10 holes were drilled into the frozen gelatin at a drill diameter of 2.5 mm and depth of 10 mm. The holes were filled with the suspensions made up of non-homogenised cells mixed with drug standards in a ratio 2:1 v/v. In order to generate non-homogenised keratinocytes, T0345 cells were cultured in 2D conditions as explained in Section 3.3.2.1. Once confluent the cells were trypsinised and counted; to fill the 10 holes to generate a full cell plug array ≥ 11,000,000 cells were necessary. The cells were centrifuged, the supernatant was removed, and the residue of media was washed out using 0.1 M ammonium bicarbonate without perturbing the pellet. The cells were then mixed with drug standards (2:1 v/v), the suspension loaded into the gelatin holes and kept at -80 ºC. Mixtures with cells resulted in dilution of the drug standards by a factor of 3, thus the final concentration of drug standards in the calibration array was 1, 100, 500, 1000, 3000, 5000, 7000, 14000 ng/µL. Before MALDI-MSI analysis the cell plug was cryosectioned at a -30 ºC using Leica Cryostat (Leica 200 UV, Leica Microsystems, Milton Keynes, U.K.) to obtain a section of 12 µm.

3.4 Matrix deposition

3.4.1 Sublimation

The matrix CHCA was applied by the sublimation technique as described in Chapter 2.4.2.1.2.

3.5 Instrumentation

3.5.1 Mass spectrometry

All imaging experiments were performed using a Waters MALDI HDMS Synapt G2 mass spectrometer (Waters Corporation, Manchester, U.K.) equipped with a neodynium:yttrium aluminum garnet (Nd:YAG) laser operated at 1 kHz. The instrument calibration was performed using phosphorus red. MALDI-MS images were acquired in positive mode, in full scan “sensitivity” mode at a range of *m/z* 100−1500, (resolution 10 000 FWHM) at pixel size of 60 µm × 60 µm, and with laser energy set to 250 arbitrary units. The ion mobility function of the instrument was not enabled. It was only possible to convert MSI raw files to imzML format by disabling the ion mobility function, which is the format supported by msIQuant software.

3.5.2 Data processing

MALDI-MSI data were processed using the HDI 1.4 (Waters Corporation, U.K.) software tool. Using this software, MSI raw data files were converted to imzML format and imported into msIQuant software. With msIQuant software, region of interest (ROIs) were selected and peak intensities from them were extracted in order to perform quantitative investigation.

Statistical analysis was performed using StatDirect software (StatsDirect, Cheshire, U.K.).

3.6 Histological analysis

3.6.1 Haematoxylin and eosin staining

Haematoxylin and eosin staining on the cell films was performed as reported in Chapter 2.6.1.

3.7 Results and discussion

3.7.1 Strategies for generating calibration curves

3.7.1.1 Cell films

The first method investigated consisted of generating a "cell array slide" made by spraying standards of terbinafine hydrochloride onto a microscope glass slide on which keratinocyte and fibroblast cells were cultured.

The culture of cells directly on microscope slides is a technique widely used in cell biology since it offers the high advantage of performing studies on a small, accessible culture area, where the cells are fixed after being treated or manipulated (Koh, 2013).

In the following work, the purpose of using this technique was to culture the main cells that constitute Labskin, keratinocytes and fibroblasts, onto slides in order to produce a "cell films" model able to mimic the histological framework of Labskin. This would, consequently, reproduce the "ion suppression effects" arising after a serial dilution of standards are sprayed onto it.

Figure 3.1 shows the microscope view of keratinocyte and fibroblast cells cultured onto a poly-lysine glass slide in the same ratio composition present in the Labskin tissue (3:1).

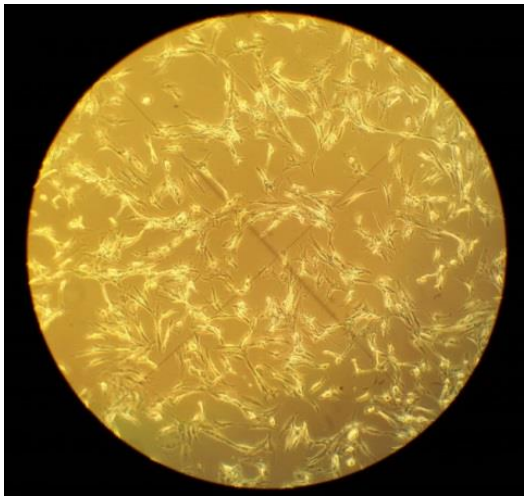

Figure 3.1 *Keratinocyte and fibroblast co-culture (ratio 3:1) on a poly-lysine glass slide viewed through light microscopy.*

To perform QMSI investigations a serial dilution of standards (from 1 ng/µL to 500 ng/µL) were sprayed onto different areas of the “cell films” by using the SunCollect^{TM} automated sprayer.

Figure 3.2 shows the MALDI-MS image of the TBF HCl in source generated fragment ion at *m/z* 141, which is derived from the parent compound $[M+H]^+$ *m/z* 292.2, recorded at 60 µm pixel size following the spraying of the drug dilution series.

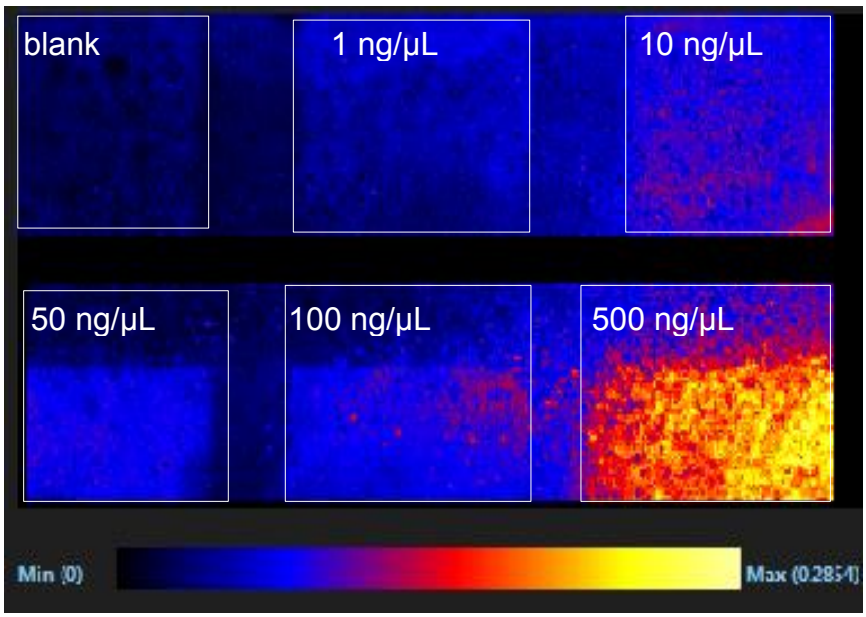

Figure 3.2 *MALDI-MS image showing the TBF HCl in source generated fragment ion (m/z 141), derived from the spraying of the drug dilution range onto different areas of a "cell films" model, made up of keratinocyte and fibroblast cells. Resolution image = 60 µm.*

Three regions of interest (ROIs) were selected for each drug concentration and processed using msIQuant software (Figure 3.3A).

A calibration curve was also obtained by plotting the average intensity of the TBF HCl ion at *m/z* 141 (TIC normalisation) versus the concentration of terbinafine hydrochloride expressed in ng/mm^2 (Appendix I). The calibration curve observed in Figure 3.3B showed a coefficient of linearity R^2 of 0.9618; the limit of detection (LOD) and limit of quantitation (LOQ) was found to be 30.96 ng/mm^2 and 93.82 ng/mm^2, respectively. The LOD and LOQ represent the analyte concentration giving a signal equal to the blank signal (only solvent without drug) plus 3.3 and 10 times (respectively) the standard deviation obtained from the replicate measurements of the blank. From the calibration curve, it is possible to estimate LOD and LOQ using the formulas LOD= 3.3s/b and LOQ= 10s/b, where s is the standard deviation of the blank and b is the slope of the curve.

A)

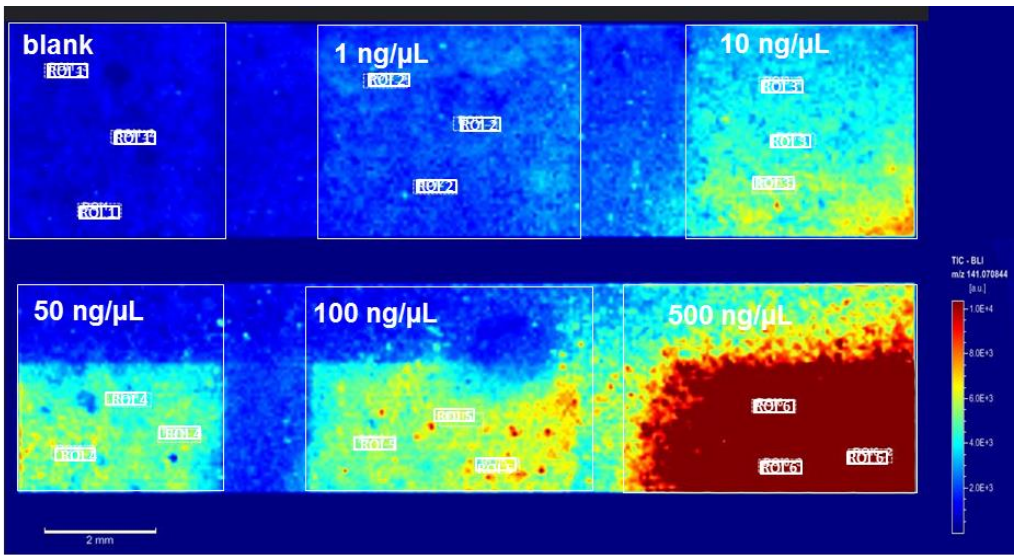

B)

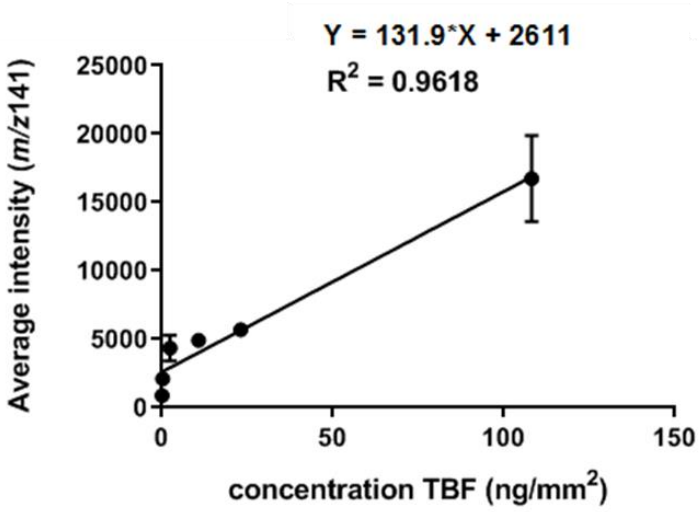

Figure 3.3 *A) MALDI-MS image showing the TBF HCl in source generated fragment ion (m/z 141), derived from the spraying of the drug dilution range onto different areas of a "cell films" model. By using msIQuant software three ROIs were selected for each standard concentration and the peak intensity was extracted. B) A calibration curve obtained for terbinafine dilution ranges onto "cell films" model is presented.*

A good calibration curve was achieved (R^2 = 0.9618) from the pilot experiment. This methodology offered the advantage of being simple and relatively cost-effective, but it also presented several drawbacks. Firstly, it was not possible to obtain full homogenous coverage of the entire slide with cells. This aspect is due to the fact that keratinocytes, which represent the highest portion of cells

seeded onto the slide, prefer to grow in patches, leading to cell empty areas throughout the slide. The distribution of cells onto the slide was visualised using MALDI-MSI by plotting an endogenous lipid marker at *m/z* 184, attributed to the phosphocholine head group of phosphatidylcholines (PC), the most abundant lipids present in cell membranes (Hossen *et al.*, 2015). As shown in Figure 3.4A, the cells did not appear homogenously distributed throughout the slide, but they were found to be more confluent in certain areas than others; this aspect was also confirmed by H&E staining (Figure 3.4B).

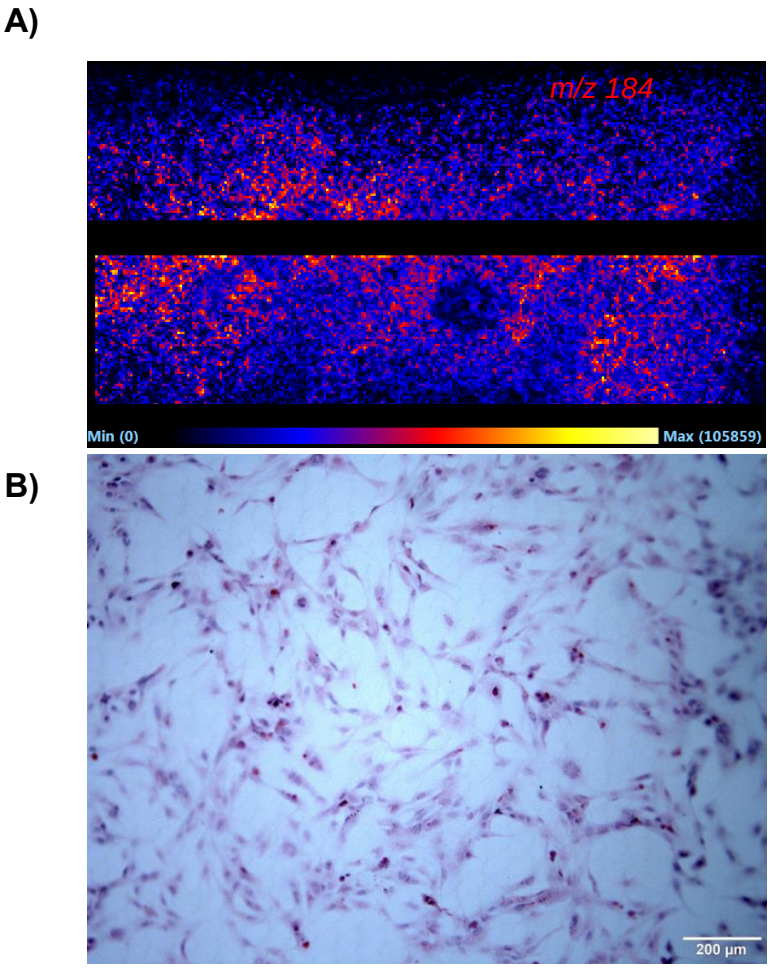

Figure 3.4 *A) MALDI-MS image of the phosphocholine head group of the PC at m/z 184, used as histological marker to visualise the cells distribution onto the slide. B) Haematoxylin and eosin staining of "cell films" slide after MALDI-MSI (20X magnification).*

Additionally, there was a difficulty with controlling the cell films compactness onto the slide; the patches of cells could generate aggregates exhibiting different thicknesses. In the work conducted by Sugiura *et al.* the impact of section thickness on MALDI-MSI analysis was emphasised, reporting that thinner sections improved peak intensity and signal-to-noise ratio (Sugiura, Shimma and Setou, 2006).

It is understandable that the lack of cells in some areas of the slide in addition with variable cell films thickness could affect the intensity of terbinafine standards, which would then no longer mimic matrix ion suppression effects of compound from the sample. This aspect could lead to the production of misleading results and the generation of an unreproducible calibration curve.

Another disadvantage that could occur using this methodology was represented by the overlapping of standard solutions during the spraying. Although parameters, such as pressure, flow rate, distance of spray head to slide and speed of spray, were set to obtain a highly focused beam of small spray drops for each standard concentration, a risk of possible overlap was still possible due to the limited area in which each standard solution needed to be applied. As shown in Figure 3.5 the higher intensity of terbinafine peak at *m/z* 141 in the regions sprayed with 10 ng/µL and 100 ng/µL could be caused by the spread of the highest concentrated solution of terbinafine hydrochloride (500 ng/µL), which was sprayed last.

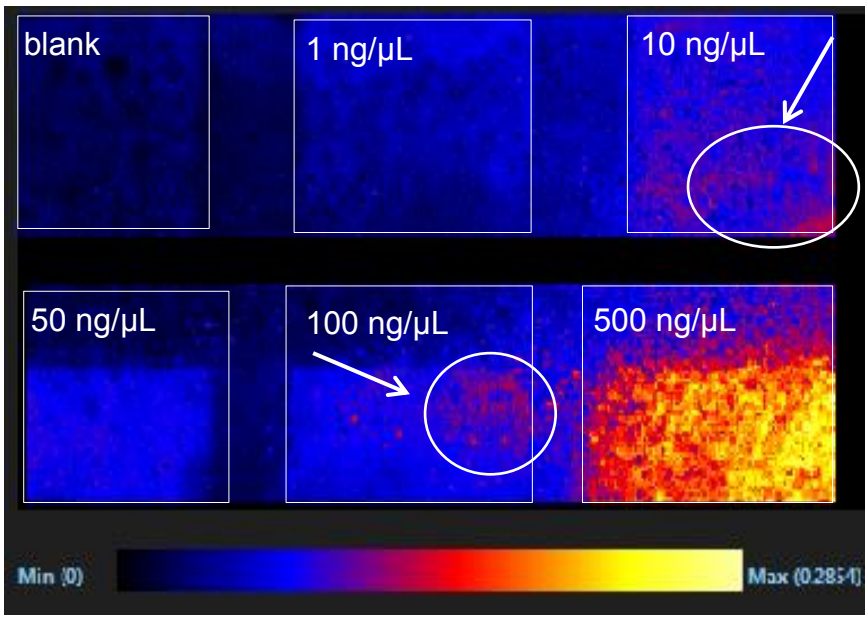

Figure 3.5 *MALDI-MS image showing the TBF HCl in source generated fragment ion (m/z 141), derived from the spraying of the drug dilution range onto different areas of a "cell films" model. The inserts show a higher intensity of TBF HCl that could derive from the spread of the neighbour solution (500 ng/µL).*

In light of all these considerations, it was decided that "cell films" model would not produce a suitable method for generating an accurate and precise QMSI analysis of terbinafine hydochloride in Labskin and other methodologies were explored.

3.7.1.2 Application of standards onto tissue

The second method investigated was based on the application of standards onto blank tissue sections by using two different techniques, spraying and microspotting.

3.7.1.2.1 Application of standards by automated spraying

The application of analytical standards by spraying was previously investigated for quantitative MALDI-MSI of cocaine on user hair samples. Using this

technique, a dilution range of cocaine standards were applied onto blank hair sections and a calibration line was generated (Flinders *et al.*, 2017).

In this study, instead, it was decided to use blank sections of Labskin (12 µm) sprayed with a serial dilution of terbinafine hydrochloride (0.1-4000 ng/µL in MeOH/H_2O (50:50)). To overcome the inconvenience of possible standard spray overlapping encountered with the "cell films" method, each standard was sprayed onto a separate serial section of Labskin. Between three and four Labskin sections were thaw mounted onto each glass slide after cryosectioning. After spraying of standards, the application of matrix by sublimation was performed for each glass slide at different times; for the imaging experiment, the areas of the glass slides containing the sprayed sections were cut, combined together onto the MALDI plate and imaged in the same run.

Figure 3.6 shows the MALDI-MS image of the TBF HCl source generated fragment ion at *m/z* 141 in ten blank sections of Labskin recorded at 60 µm pixel size following the spraying of drug dilution series.

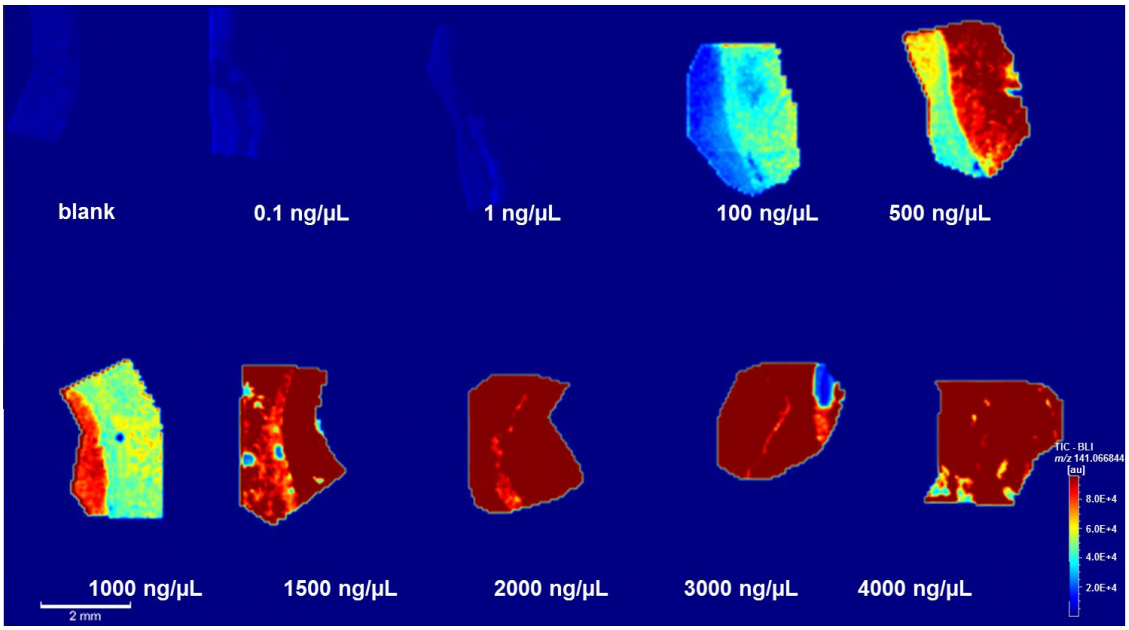

Figure 3.6 *MALDI-MS image showing the TBF HCl source generated fragment ion (m/z 141), following the spraying of the drug dilution range onto blank Labskin sections. Resolution image= 60 µm. TIC normalisation.*

However, from qualitative investigation of the distribution of terbinafine hydrochloride in dosed tissue sections (discussed in Chapter 2) it was found that the presence of drug was restricted only into the epidermal layer of the skin without penetration into the dermis. Based on these observations, it was decided to calibrate the response specifically for calibrant signals arising from the epidermis to achieve "matrix matched standards".

To distinguish the epidermis and stratum corneum from the dermis, two peaks from endogenous species at *m/z* 184 and *m/z* 264 were used, respectively attributed to a fragment ion of phosphocholine-type lipids, which was more apparent in the tightly packed cells of the epidermis and a ceramide fragment peak, primarily expressed in the stratum corneum. By superimposing the MALDI images of the peaks at *m/z* 184 and *m/z* 264, it was possible to visualise mostly the epidermis of the blank tissue sections (Figure 3.7A). However, different scale bar values were selected to make possible the visualisation of the endogenous lipid marker phosphocholine (*m/z* 184) in all blank sections (which can be noted from the colour scales near the images).

Once identified the epidermis of the sprayed sections, ROIs were drawn only on at this level by using msIQuant software and an average intensity for the signals of each concentration of TBF HCl was extracted (Figure 3.7B).

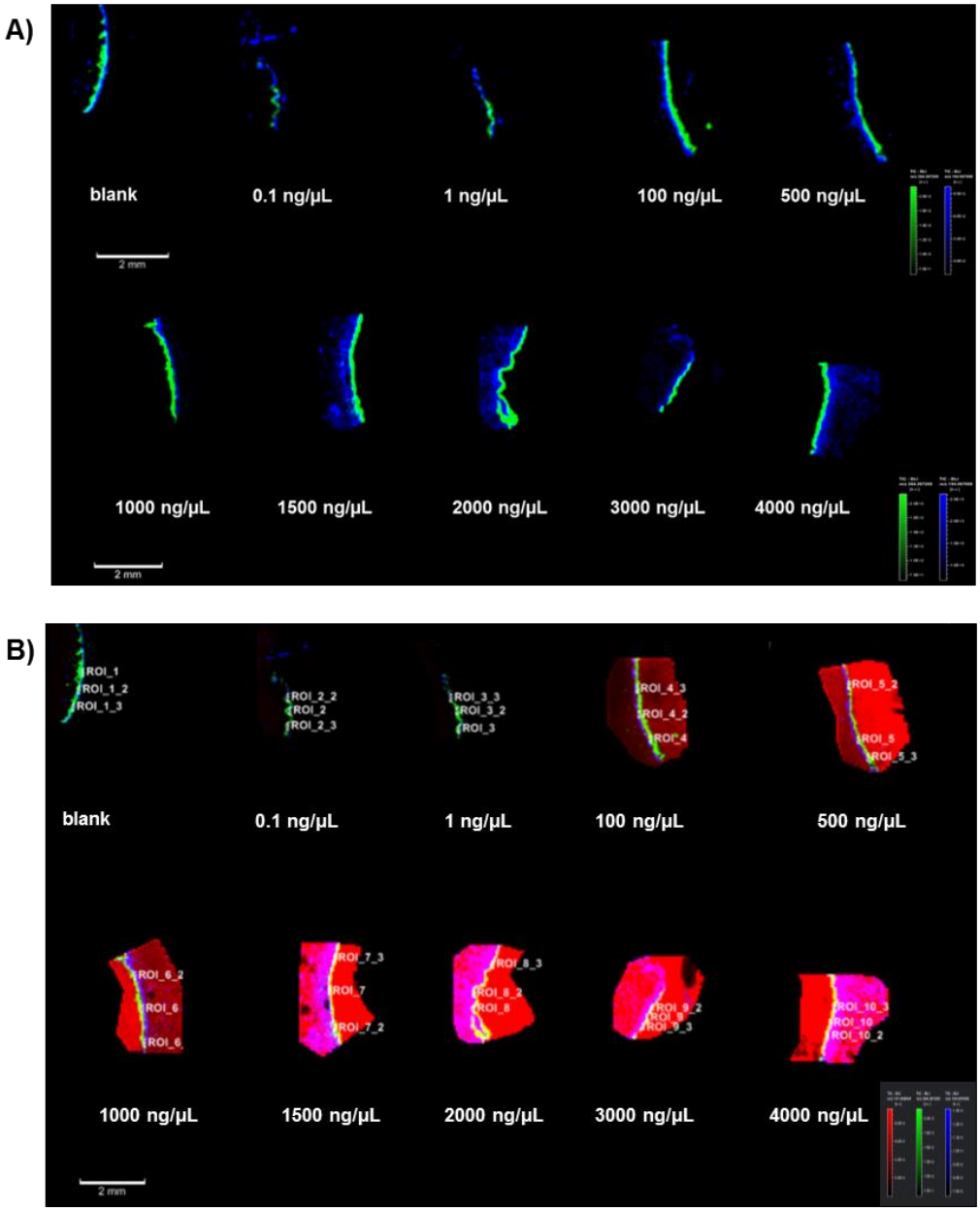

Figure 3.7 *A) MALDI-MSI of phosphocholine head group in blue (m/z 184) superimposed with ceramide fragment peak in green (m/z 264). By exploiting endogenous lipids it was possible to distinguish epidermis and stratum corneum from the dermis. B) MALDI-MSI of the TBF HCl source generated fragment ion in red (m/z 141) superimposed with phosphocholine head group in blue (m/z 184) and ceramide fragment peak in green (m/z 264). Three ROIs for each drug concentration were drawn solely to the epidermal layer and the signal for TBF HCl in source fragment peak was extracted by using msIQuant software. TIC normalisation.*

The calibration curve was obtained by plotting the average intensity of *m/z* 141 (TIC normalisation) versus the concentration of terbinafine hydrochloride expressed in ng/mm^2 (Appendix I). The calibration curve observed in Figure 3.8 showed a coefficient of linearity R^2 of 0.7767. The limit of detection (LOD) and limit of quantitation (LOQ) were 329.51 ng/mm^2 and 998.52 ng/mm^2, respectively.

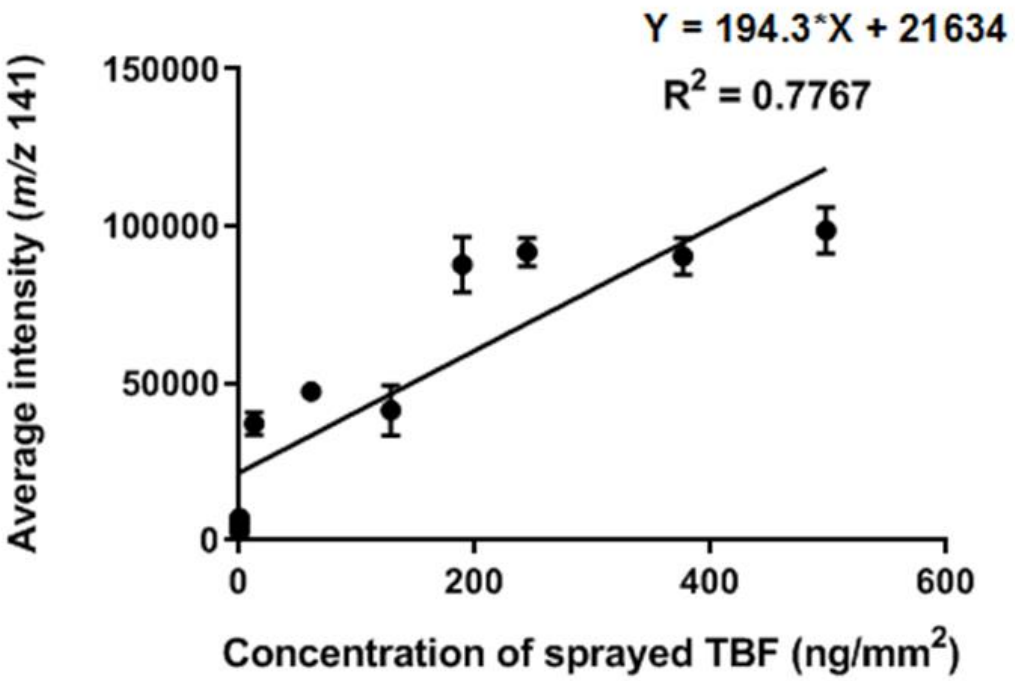

Figure 3.8 *Calibration curve generated plotting the average intensity of m/z 141, derived from standards sprayed onto blank Labskin sections, versus the concentration of terbinafine hydrochloride expressed in ng/mm^2. TIC normalisation.*

The advantage of this technique was that the standard intensity was extracted solely from histology and MSI guided well-defined epidermal layer of blank sections, allowing to mimic cell type ionisation response of the analyte from the dosed tissue sections. In addition, the blank sections were cryosectioned keeping the same thickness of the dosed tissue sections and thus differences in terms of analyte peak intensity section thickness-dependent should not occur.

However, the main disadvantages of this technique were that it was time consuming and not cost-effective. Multiple sections of blank tissue were necessary to obtain a calibration array, making their analysis using MALDI-MSI time consuming. Although for all sections the data acquisition conditions were identical, the matrix application could not be performed at the same time, leading to possible differences in terms of matrix thickness influencing the results. In addition, before spraying each standard solution, washing of the capillary was required in order to remove the "carry-over" from the previous calibrant solution within it. The washing step was performed by flushing acetonitrile through the capillary for 30 min; making the spraying of all standard solutions very time consuming. In light of these considerations, it was decided to proceed to investigate alternative QMSI techniques.

3.7.1.2.2 Application of standards by microspotting

The next approach investigated for generating robust and reproducible calibration curves was based on microspotting analytical standards onto a blank section of Labskin.

For this purpose, the use of an acoustic picoliter droplet ejector, employed previously as a MALDI matrix deposition device (Aerni, Cornett and Caprioli, 2006), was used to spot 3.4 nL of working standard (from 0.1 ng/µL to 4000 ng/µL) in MeOH/H_2O (1:1) onto the epidermis of a blank section of Labskin to create a calibration array.

Figure 3.9 shows MALDI-MSI image of the terbinafine hydrochloride in source generated fragment ion at *m/z* 141 in a blank section of Labskin recorded at 60 µm pixel size following the microspotting of drug dilution series. As shown, the application of working standards of terbinafine hydrochloride by using this methodology allowed a uniform distribution across the epidermis with minimal lateral diffusion. Assuming the high reproducibility of the spots size generated with the acoustic spotter, the appearance of increased spot area in Figure 3.9 was attributed solely to an increment of drug concentration. Evidence of the reproducibility of the spot size using the acoustic spotter is reported in Chapter 4.7.1.

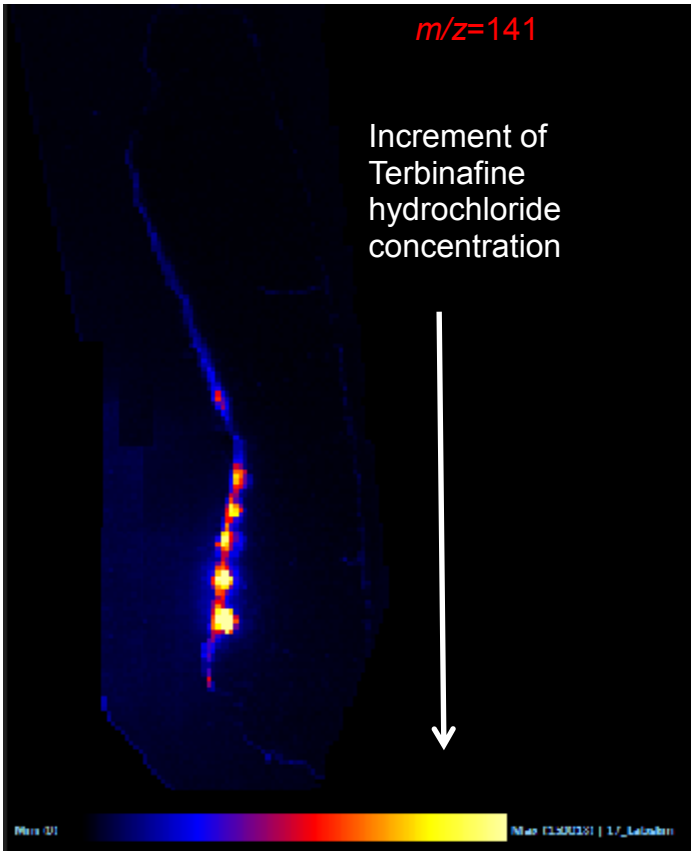

Figure 3.9 *MALDI-MS image showing the TBF HCl source generated fragment ion (m/z 141), following the microspotting of the drug dilution range directly on the epidermis of a blank section of Labskin. Resolution image = 60 µm.*

As previously described, by exploiting endogenous markers, the epidermis and the stratum corneum of the microspotted blank section was visualised and, thus, region of interests (ROIs) were selected for each drug concentration solely in the epidermis area by using msIQuant software.

Figure 3.10 shows the MALDI-MS image of terbinafine hydrochloride in source fragment peak (*m/z* 141) superimposed with phosphocholine head group in blue (*m/z* 184) and ceramide fragment peak in green (*m/z* 264.2).

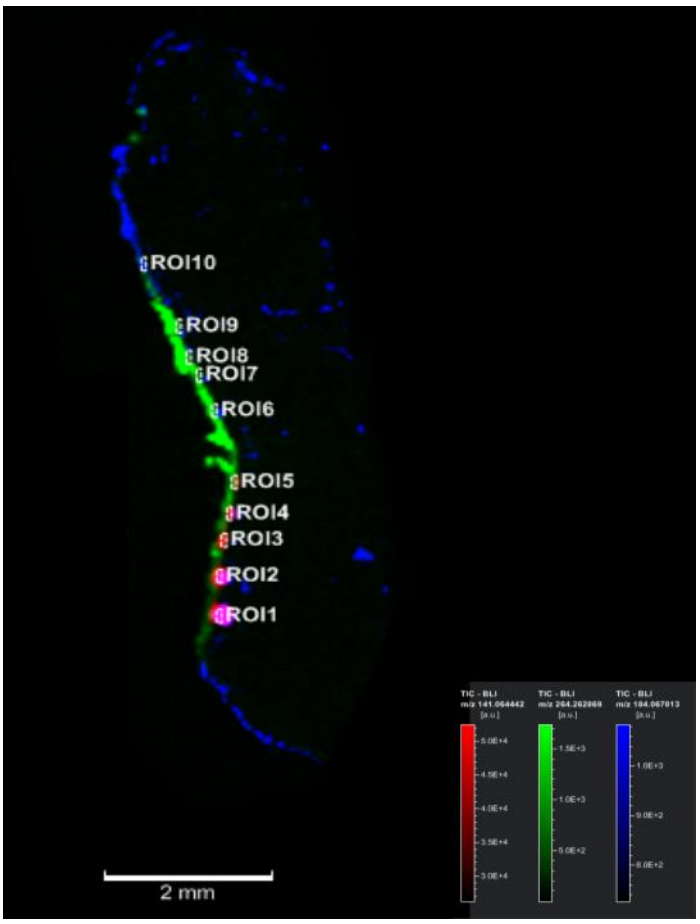

Figure 3.10 *MALDI-MSI of the terbinafine hydrochloride source generated fragment ion in red (m/z 141) superimposed with phosphocholine head group in blue (m/z 184) and ceramide fragment peak in green (m/z 264). TIC normalisation.*

The average intensity of each ROI (TIC normalisation) was extracted and plotted against the respective standards expressed in ng/mm^2 (Appendix I). The calibration curve observed in Figure 3.11 showed a coefficient of linearity R^2 of 0.9617. The LOD and LOQ were found to be 36.11 ng/mm^2 and 109.44 ng/mm^2, respectively.

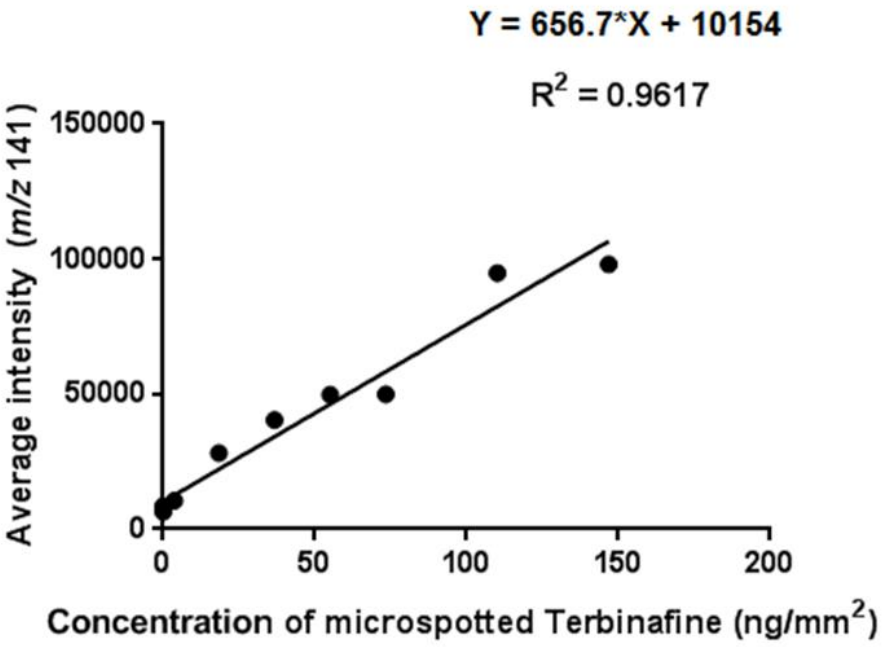

Figure 3.11 *Calibration curve generated plotting the average intensity of m/z 141, derived from standards microspotted onto a blank Labskin section, versus the concentration of terbinafine hydrochloride expressed in ng/mm^2. TIC normalisation.*

The major advantage of the application of standards using the acoustic spotter was the possibility to apply sub-microliter volumes of standard solutions (3.4 nL) directly onto a small and well-defined epidermal area of a blank Labskin section with the same thickness of dosed sections, leading to mimic cell type-based ionisation response of the analyte from the treated tissue sections. In addition, this technique was relatively fast and time effective as only one section was necessary to generate a calibration curve. Unlike the sprayed sections, use of the microspotted section was beneficial as it could be placed directly next to treated sections and analysed under the same condition in terms of data acquisition and sample preparation.

3.7.1.3 Cell plug

The last approach investigated involved the construction of a calibration array by spiking a known amount of terbinafine hydrochloride standard mixed into a non-homogenised “cell plug” of keratinocytes T0345. It was decided to use only keratinocytes since they are the dominant cell type within the epidermis of skin, which is the region of interest for the evaluation of tissue-based matrix effects. Moreover, it was thought that the incorporation of analytical standards with cells would have corrected not only the ion suppression effects, but also the extraction efficiency effects, leading to a more reliable calibration approach for QMSI analysis.

Once prepared, the gelatine block including the cell plug array was presented as shown in Figure 3.12**.**

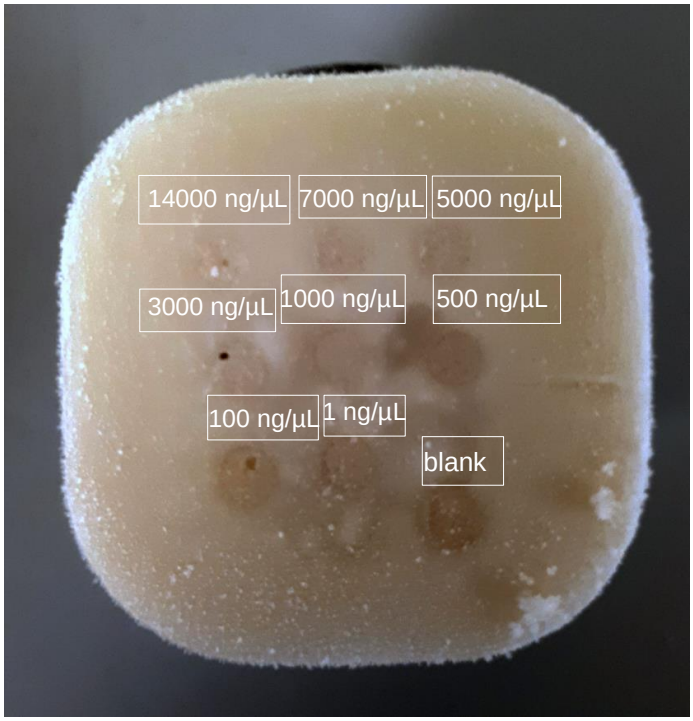

Figure 3.12 *Optical image showing the cell plug array.*

Cell plug design was thought to represent a remarkable alternative to previously employed techniques, such as homogenates and surrogate tissue models. Considering the small thickness of the epidermal layer (the region of interest), a

large number of blank Labskin tissues would have been necessary for the generation of a serial homogenate dilution, resulting in an extremely expensive and laborious process. It might be thought that the use of a surrogate tissue could offer a solution to this problem. In the work reported by Takai *et al.* blank liver homogenates spiked with a serial dilution of raclopride were used to generate a calibration curve from which the concentration of the drug could be extrapolated not only in liver but also in brain, lung, and kidney tissue sections with MALDI-MSI (Takai, Tanaka and Saji, 2014b), However, the use of a surrogate tissue should rely on the assumption that the extraction of the drug of interest from different organs is similar to that occurring from the surrogate model. A criticism of this assumption was discussed in the work by Hansen *et al.* (Hansen and Janfelt, 2016). The authors analysed the extraction efficiency of the drug amitriptyline spiked at the same concentration into different homogenised (liver, brain, kidney, lung and heart) by using DESI-MSI. The results showed a statistical decrease of the signal when the drug was extracted from brain and lung tissue, potentially due to the protein binding effect. It is understandable that a different extraction efficiency would compromise the reliability of quantitative results. However, independently from the issue relating to the protein binding effect, a broader concept of tissue-specific influence on analyte ionisation has been widely examined in literature; and this seems to strengthen the inadequacy of using surrogate models to generate QMSI (Stoeckli, Staab and Schweitzer, 2007; Hamm, Bonnel, Legouffe, Pamelard, J.-M. Delbos, *et al.*, 2012). In line with these considerations, as discussed previously, cell plugs were generated by using only intact keratinocytes, the principal cells compositing the epidermis. It was believed that the use of intact cells, differently from homogenates, offered the advantage of avoiding the release of intercellular debris that could lead to a higher suppression of the analyte signal. In addition, assuming that the drug diffused within the cells, it was hypothesised that cell plug may represent a better model for resembling the ionisation efficiency/extraction of the analyte from dosed tissues.

To reproduce the thickness of treated Labskin sections, the cell plug was cryosectioned at 12 µm. During the sectioning process, the cryostat cut the gelatin block smoothly, but as soon as the knife reached the cells, however

these were torn off the section completely. At the end of the process, a slide of gelatine block without cells within the holes was produced.

Fisher *et al.* described a protocol for cryosectioning tissues and highlighted the possible problems that could occur during the process. In particular, the difficulty of cutting a tissue may be attributed to a blunt knife; this happens especially in the presence of support media used to embed the tissue (Fischer *et al.*, 2008).

In this regard, to troubleshoot the problem of cryosectioning the cell plug array, different approaches were tried, including replacing the blade as well as changing the temperature of the chamber and the angle of crysection, but no improvement in results was achieved.

Another possible problem affecting the cryosection could be due to the nature of a tissue that makes it difficult to cut, such as in the case of watery or fatty tissue (Fischer *et al.*, 2008). In the case of cell plug array the keratinocyte cells were mixed with solutions (50% MeOH) of standard and the poor sectioning could be because of the presence of this liquid mixed with cells which would compromise their consistency. However, removing liquid from the sample was not possible, since it was necessary to dissolve the drug in order to produce the calibration array.

Since it was not possible to produce a calibration array, it was decided not to investigate the cell plug technique further. Beside the cryosection problems, it offered other challenges. Firstly, the entire method was extremely time consuming requiring the culture of at least 11,000,000 cells to obtain one calibration array. In addition, to reach such high amount of cells, multiple passages of cell culture were required; for this reason, immortalised primary keratinocyte cells were employed, which are very delicate and expensive, making the technique much less cost-effective than the cell films and on-tissue approaches previously investigated.

Although prior to use, high expectations were put on the cell plug design, it turned out that this method was extremely complicated, long and not practical for quantitation in Labskin samples.

3.7.2 Quantitative analysis of terbinafine in Labskin

The optimal methodology for performing QMSI analysis should be able to generate an accurate and precise calibration curve, which enables absolute quantitation. In addition, the technique should be advantageous in terms of time and cost as well as easy to perform.

Among all procedures examined previously, the application of analytical standards on top of a blank Labskin section by microspotting appeared to be the most promising technique. In Figure 3.13 the main aspects of the different methods used for absolute quantitation via MALDI-MSI are compared.

	Cell films	Application of standards by		Cell plug
		spraying	microspotting	
THICKNESS REPRODUCIBILITY	✗	✓	✓	✓
MATRIX EFFECT	✗	✓	✓	✗
COST EFFECTIVE	✓	✗	✓	✗
TIME EFFECTIVE	✓	✗	✓	✗

Figure 3.13 *Comparison of several methods explored for performing absolute QMSI analysis. The cell plug routine was not able to reproduce matrix matching since the cryosection of cell plug array was not obtained. The cell films technique was not able to reproduce accurately matrix ion suppression effects, since the cells were distributed throughout the slide with different density and thickness, leading to the formation of cell empty areas.*

By using an acoustic spotter it was possible to obtain a uniform distribution of a serial dilution of terbinafine hydrochloride directly across the epidermal layer of a blank section with minimal lateral diffusion. This aspect offered the enormous advantage of generating a calibration array directly onto a very thin and well-defined epidermal region of Labskin matching the ionisation efficiency of analyte present in the dosed sample. In addition, by using this technique, aspects such as Labskin thickness reproducibility, effectiveness in time and cost were

sufficient and a good linearity in the calibration curve (as indicated by the R^2 value) was obtained (Figure 3.14).

Based on all these considerations, the microspotting of standards in combination with matrix sublimation and recently developed software for quantitative mass spectrometry imaging was employed to obtain preliminary data of the levels of terbinafine hydrochloride in the epidermal region of a full thickness living skin equivalent model. In this study, issues in the use of sublimation over spraying as matrix deposition technique were observed. As previously described (Chapter 2.7.3), being a solvent-free method, sublimation can affect the analyte-matrix interaction and hence the method sensitivity. This is the main reason why this technique found mainly application in MSI of lipids, which are extracted even with solvent-free methods (Hankin, Barkley and Murphy, 2007; Kaletaş *et al.*, 2009). However, in the study reported in this chapter, the main advantage of the sublimation technique in allowing the increase of spatial resolution was selected over the sensitivity. In fact, as well as the sensitivity, for QMSI experiments, the possibility of precisely monitoring the analyte distribution in the sample is a critical factor, since analyte delocalisation could generate variation in analyte ionisation, generating misleading ion intensity values. In line with these theories, an interest of also using sublimation for the detection of small molecules had increased. Jirásko et *al.* (Jirásko *et al.*, 2014) decided to use sublimation technique to study the distribution of atorvastatin and its metabolites in rat tissues by using MALDI-Orbitrap-MS. In this study 13 matrices for small molecules in both polarities were investigated by sublimation and DHB in MALDI-positive mode and DAN in MALDI negative mode represented the best matrices. In the work reported by Goodwin *et al.*, based on the same principles as sublimation, a solvent-free dry CHCA matrix coating was employed to perform quantitative investigation of 4-bromophenyl-1,4- diazabicyclo(3.2.2)nonane-4-carboxylate in rat brain tissues (Goodwin *et al.*, 2010).

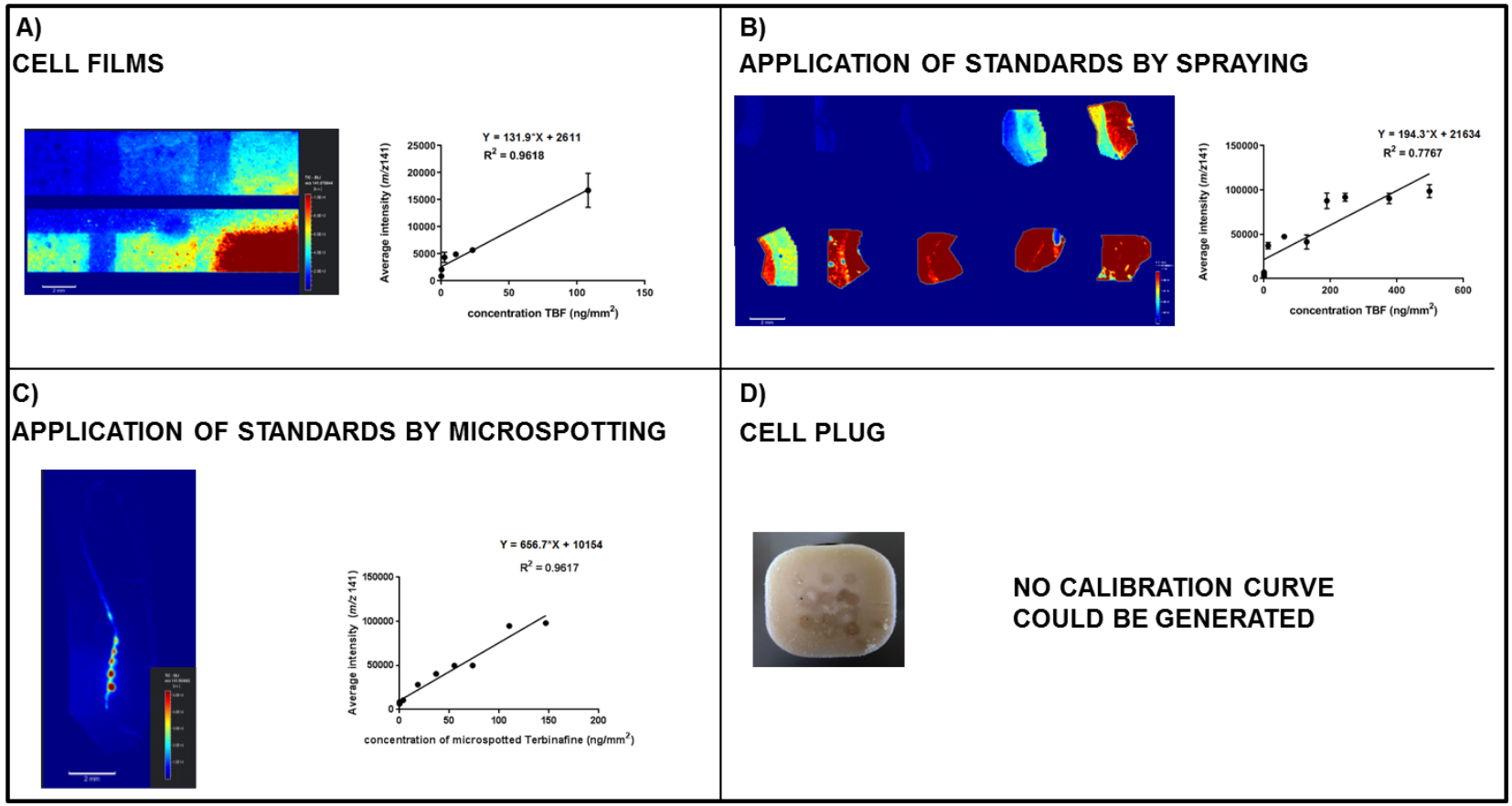

Figure 3.14 *Calibration curves generated using different routines: A) cell films; B) application of standards by spraying; C) application of standards by microspotting; D) cell plug.*

In order to perform QMSI analysis, a blank section of Labskin microspotted with working standard solutions was imaged alongside two sections of Labskin treated with 20 µL of terbinafine 1% (w/w) in 100% isosorbide dimethyl ether (DMI) for 24 hours. The image was performed using Water Synapt G2 without the ion mobility function enabled (Figure 3.15).

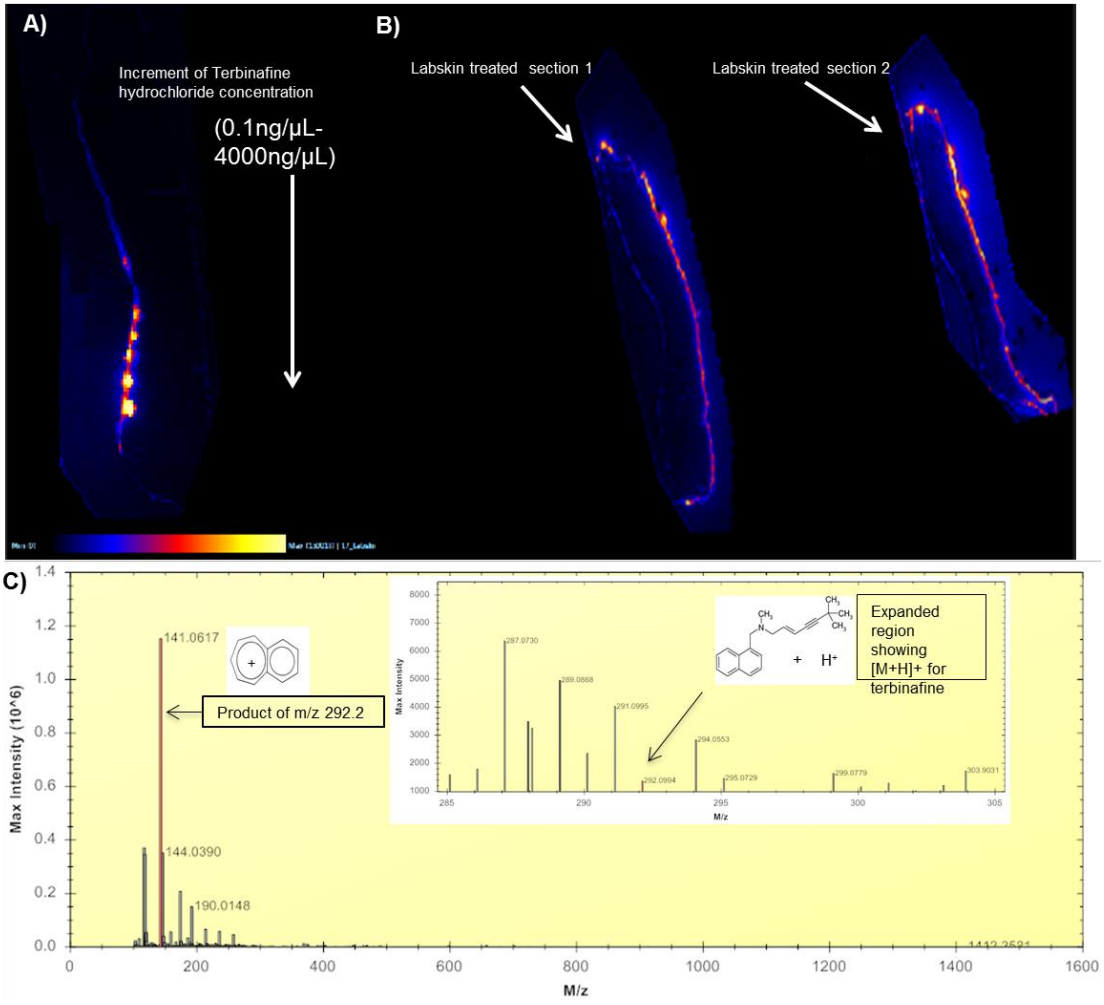

Figure 3.15 *MALDI-MS image at 60 µm X 60 µm spatial resolution of the TBF HCl source generated fragment ion ($[C_{11}H_9]^+$; m/z 141) A) microspotted directly on the epidermal layer of blank tissue section and B) present in two Labskin sections treated with terbinafine 1% (w/w) in 100% DMI for 24 hours. C) Average MALDI-MSI spectra showing the peak of the terbinafine hydrochloride fragment ion at m/z 141.*

As previously discussed, regions of interest (ROIs) were selected for each drug concentration solely to the epidermis area (identified by using endogenous lipid markers) of the blank tissue section, the intensity of drug from each ROI was extracted and the calibration curve was generated by using msIQuant software. The coefficient of linearity (R^2) was 0.9617 and the LOD was found to be 36.11 ng/mm^2 or 3.01 mg/g tissue, whereas the LOQ was found to be 109.44 ng/mm^2 or 9.12 mg/g tissue (Figure 3.16A-B). It is important to highlight that for every image to be quantified, an individual set of calibration points was imaged alongside the treated tissue sections.

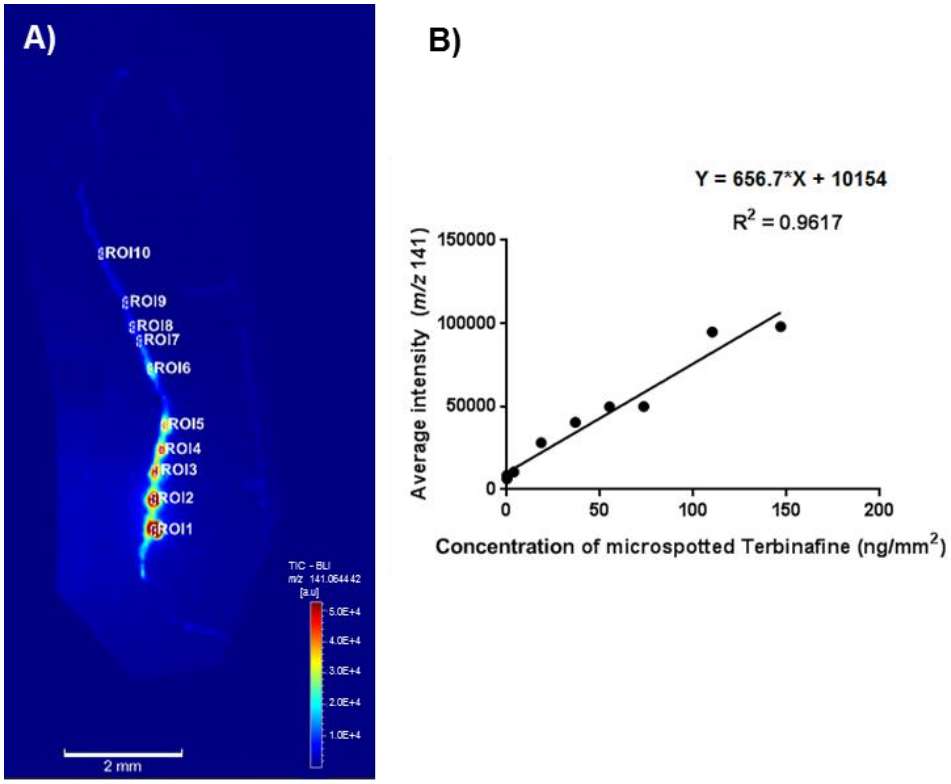

Figure 3.16 *MALDI-MS image at 60 µm X 60 µm spatial resolution of the TBF HCl source generated fragment ion ($[C_{11}H_9]^+$; m/z 141) A) microspotted directly on the epidermal layer of blank tissue section and B) calibration curve generated plotting the average intensity of m/z 141 (TIC normalisation) versus the concentration expresses in ng/mm^2.*

By resolving the equation, the amount of drug in the treated Labskin sections was obtained in ng/mm^2. To calculate the quantitative concentration of

terbinafine hydrochloride in milligrams per grams of tissue, first, the amount in grams of tissue in 1 mm^2 was calculated. The volume of tissue in 1 mm^2 was calculated multiplying the area (1 mm^2) by the thickness of the section (0.012 mm). Then, the volume (0.012 mm^3) was multiplied by the density of Labskin (assumed to be 1 mg/mm^3) and the amount of tissue (g) in 1 mm^2 was obtained (0.000012 g). By dividing in turn, the concentration of terbinafine from each ROI selected on treated sections (ng/mm^2) to the gram of tissue in 1 mm^2, the concentration of the drug was converted in milligrams per gram of tissue. The values derived from ROIs were averaged and the mean concentration of terbinafine hydrochloride was calculated.

From these initial experiments the levels of drug were found to be 3.41 ± 0.62 mg/g tissue within section 1 and 4.2 ± 0.81 mg/g tissue within section 2. The levels of terbinafine detected in both sections were above the LOD, but below the formal LOQ (Figure 3.17).

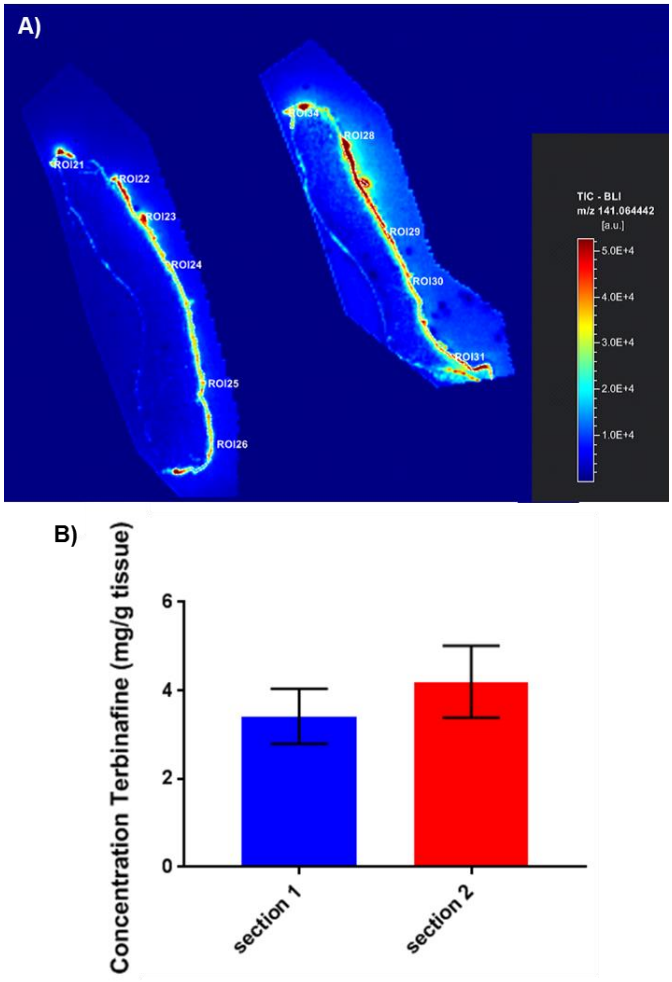

Figure 3.17 *MALDI-MS image of the terbinafine hydrochloride in source generated fragment ion ($[C_{11}H_9]^+$; m/z 141) in A) two Labskin sections treated with terbinafine 1% (w/w) at 100% DMI for 24 hours. Several ROIs were drawn around the epidermis of each section, the peak intensity of m/z 141 was extracted (TIC normalisation) from each ROI and compared to the calibration curve. B) Graph showing the QMSI levels of terbinafine from the sections of Labskin.*

The data shown gave preliminary results for the levels of TBF HCl in Labskin tissue treated with a DMI based formulation. However, to perform investigation on the effects of the penetration enhancer DMI on levels of terbinafine in the epidermal layer of tissue, other formulations containing different percentages of DMI require examination.

3.7.3 Effect of the penetration enhancer DMI on levels of terbinafine in the epidermal layers of Labskin

To assess the potential of the penetration enhancer DMI to increase drug permeability into the upper epidermal layer of Labskin, Labskin tissue was treated with formulations containing levels of DMI similar to those present within commercially available formulations.

A technical publication reported by Grant Industries Inc. indicates that there are no commercial drug formulations consisting of 100% DMI, but the recommended levels of DMI in skin care products usually ranges from 5% to 50% in aqueous systems and from 40% to 90% in non-aqueous systems (https://www.univar.com/US/Industries/~/media/PDFs/US%20Corp%20Region%20PDFs/PC/Naturals/Gransolve%20DMI%20from%20Univar%20Application%20Guide.ashx) .

In light of these considerations, experiments were conducted in which Labskin was treated with water based formulations containing either 10% or 50% DMI.

In addition, for quantitative analysis the presence of a section derived from a negative control tissue (treated only with vehicle without drug) within the image set is necessary to confirm that the drug detection is specific and not a background peak interfering.

For this reason, in this experiment a section of Labskin treated with vehicle water/olive oil (80:20) alone was also included.

The vehicle and the treated sections were imaged alongside a blank Labskin section microspotted with a dilution range of terbinafine hydrochloride, from which a calibration curve could be generated by using msIQuant software.

Figure 3.18 shows the MALDI-MS image of the distribution of the in source generated terbinafine fragment ion at *m/z* 141 on (A) a blank tissue section microspotted with working standards (B) vehicle control section and two Labskin sections treated with terbinafine 1% (w/w) in water/olive oil (80:20) with either (C) 10% or (D) 50% isosorbide dimethyl ether (DMI) for 24 hours.

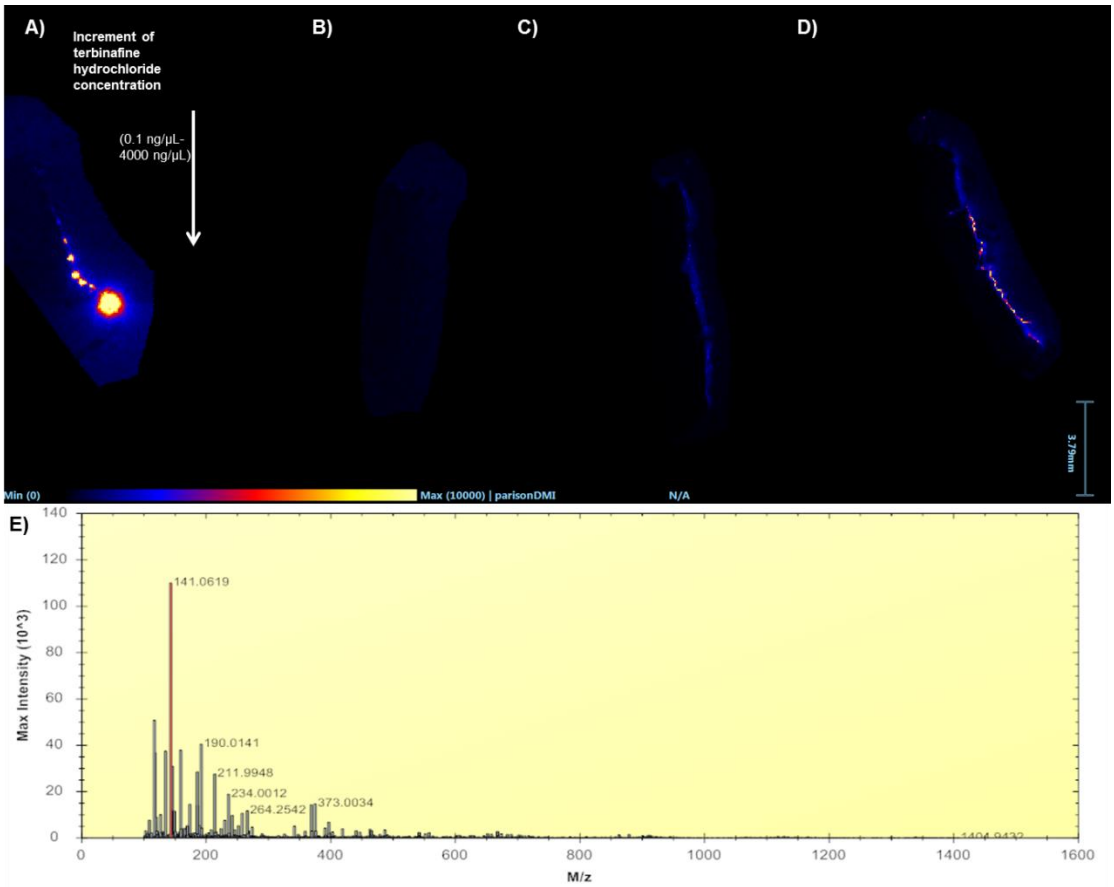

Figure 3.18 *MALDI-MS image at 60 µm × 60 µm spatial resolution of the terbinafine hydrochloride fragment ion ($[C_{11}H_9]^+$; m/z 141) on (A) microspotted section, (B) vehicle control treated with emulsion water/olive oil (80:20) alone, two Labskin sections treated with terbinafine 1% (w/w) in water/olive oil (80:20) with either (C) 10% or (D) 50% isosorbide dimethyl ether (DMI) for 24 hours. E) Average MALDI-MSI spectra showing the peak of the terbinafine hydrochloride fragment ion at m/z 141.*

In this case, the values for the construction of the calibration curve were reduced to a smaller range spanning the expected values, in order to prevent distortion of the standard array due to presence of high concentrations. The

problem relating the distortion of the calibration curve in MALDI-MSI was previously experienced by Pirman *et al.* (Pirman *et al.*, 2013); and such behaviour was suggested to be correlated to matrix-to-analyte ratio changes as the analyte concentration increased. However, in a recent work conducted by Sammour *et al.* the phenomenoum of non-linearity in MALDI-MSI was addressed differently (Abu Sammour *et al.*, 2019). In this study the authors highlighted the difficulty of obtaining a linear calibration curve despite the effort of optimising the matrix-to-analyte ratios and, hence they introduced a novel nonlinear regression model to fit the data generated by MALDI-MSI. It was suggested that, by using this novel model, more accurate and reliable quantitative information of the uptake and distribution of the drug imitanib into gastrointestinal stromal tumor tissue was guaranteed. To support the superiority of this model, the comparison of the residual standard error (RSE) of the calibration generated by both linear and nonlinear regressions with MALDI-MSI was also performed. The results showed a much better fit when the generalised nonlinear calibration was used and, in addition, the quantitative data based on this model well compared the data obtained by UPLC-ESI-QTOF-MS.

In the work reported here, it was instead decided to fit the data in a linear calibration curve; and in this regard, it was necessary to compromise to a limited concentration range. The coefficient of linearity (R^2) was 0.9941 and the LOD was found to be 11.40 ng/mm^2 or 0.95 mg/g tissue, whereas the LOQ was found to be 34.56 ng/mm^2 or 2.88 mg/g tissue (Figure 3.19).

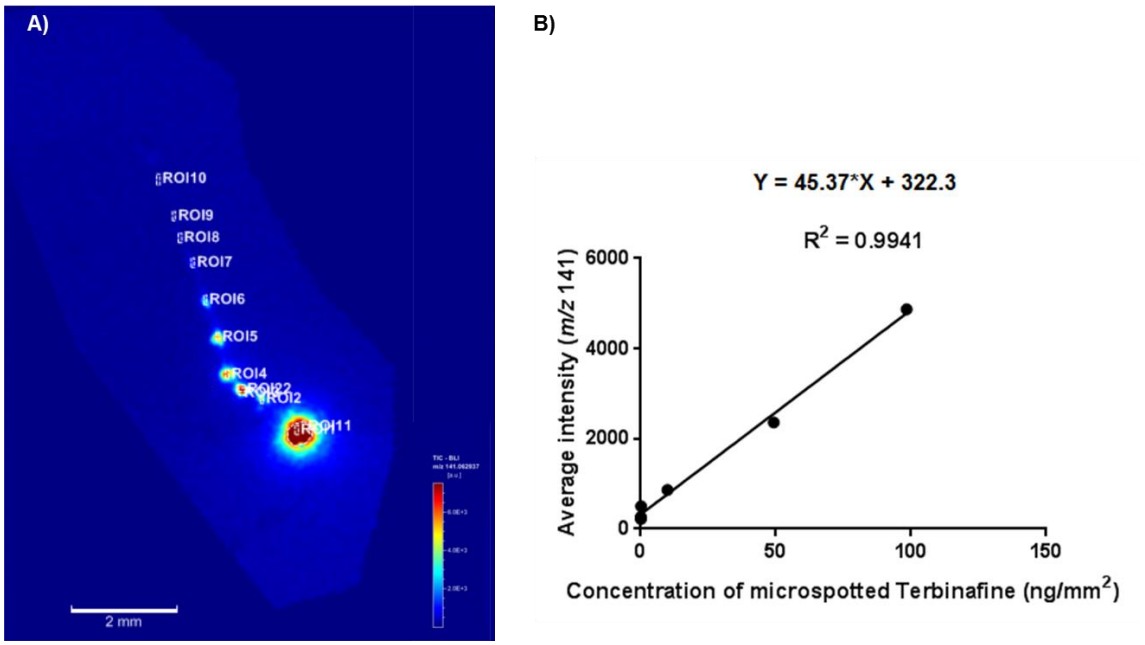

Figure 3.19 *MALDI-MS image at 60 µm X 60 µm spatial resolution of the terbinafine hydrochloride source generated fragment ion ($[C_{11}H_9]^+$; m/z 141)* ***A)*** *microspotted directly on the epidermal layer of blank tissue section and* ***B)*** *calibration curve generated plotting the average intensity of m/z 141 (TIC normalisation) versus the concentration expresses in ng/mm^2.*

In order to calculate the levels of terbinafine in the treated sections ROIs were drawn around the epidermis of the vehicle and treated Labskin sections. The intensity of the peak at *m/z* 141 was extracted and compared to the calibration curve using msIQuant software. In the vehicle control section, the levels of terbinafine were not detectable, at 10% DMI the levels were found to be 0.24 ± 0.12 mg/g tissue (below the formal LOD), at 50% DMI the levels of drug were found to be 1.47 ± 0.74 mg/g tissue (above the LOD, but below the formal LOQ).

A statistical unpaired t test was performed on the data from both tissues treated with terbinafine with either 10% DMI or 50% DMI. The concentration of the drug resulting statistically increased in the tissue when the percentage of DMI increased in the formulation (two sided P= 0.0201) (Figure 3.20).

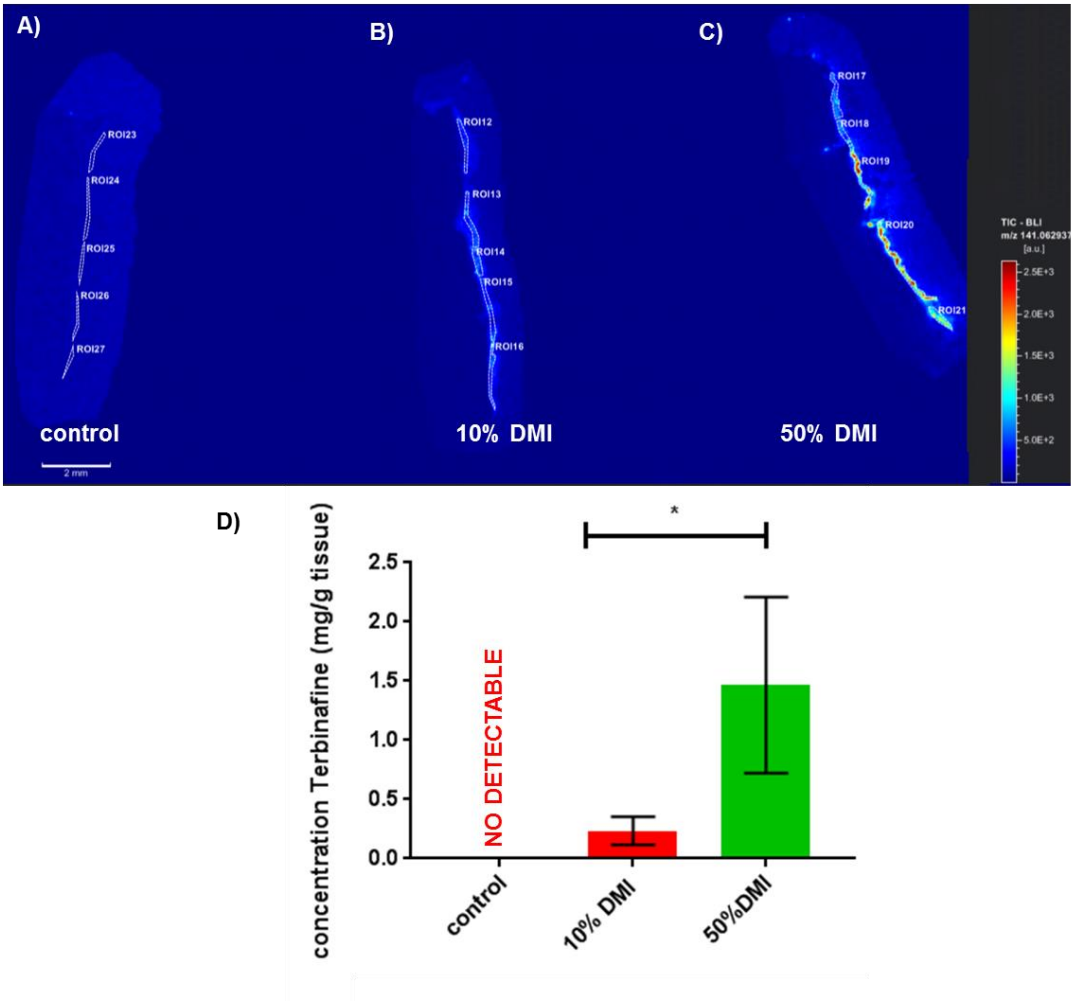

Figure 3.20 *MALDI-MS image of the terbinafine hydrochloride source generated fragment ion ($[C_{11}H_9]^+$; m/z 141) in A) vehicle control section and two Labskin sections treated with terbinafine 1% (w/w) at B) 10% or C) 50% DMI for 24 hours. Five ROIs were drawn around the epidermis of each section, the peak intensity of m/z 141 was extracted (TIC normalisation) from each ROI and compared to the calibration curve. D) Graph showing the QMSI levels of terbinafine from the sections of Labskin. The error bars illustrate the standard deviation of the levels of drug in five different epidermal regions of each section. The concentration of the drug resulted statistically increased in the tissue when the percentage of DMI increased in the formulation (two sided P= 0.0201).*

The data reported here has demonstrated the capability of the penetration enhancer DMI to increase terbinafine penetration into the upper epidermis of a living skin equivalent model.

Although the microspotting technique has shown to be able to generate a robust calibration curve and provide the detection of terbinafine levels in the tissue, an optimisation step of this method is required in order to increase its quantitative potential.

One approach could concern the normalisation strategy to adopt. Over the past year, the normalisation to a stable isotope internal standard has been shown to increase the quantitative capabilities of MSI analysis (Pirman and Yost, 2011; Prentice, Chumbley and Caprioli, 2017). In this study, in the absence of an internal standard, the MSI data were normalised to total ion current (TIC). Although this approach has been widely used in the past, it may generate misleading conclusions from MALDI-MSI spectra, especially when the intensity of the analyte changes in different regions of the tissue (Deininger *et al.*, 2011). For this reason, in order to increase the quantitative potential of the technique, the data needs to be assessed by using an internal standard molecule and, in addition, they need to be validated by using complementary reliable techniques, such as LC-MS/MS.

In addition, to assess the reproducibility of the microspotting technique multiple technical replicates are necessary.

3.8 Concluding remarks

In this study, different calibration strategies have been investigated to assess the most valid and robust technique for the generation of accurate quantitative analysis by using MALDI-MSI.

The methods reported here include cell films, on-tissue application of standards by either spraying or microspotting and cell plug.

The use of an acoustic spotter for generating QMSI analysis turned out to be the most favourable approach for the determination of the amount of an active pharmaceutical ingredient, terbinafine hydrochloride, in a living skin equivalent model. This technique offered the enormous advantage of being practical, relatively fast and cost-effective; only one blank section was required to

generate a calibration array, allowing dosed tissue sections to be placed next by and imaged at the same time to perform quantitative investigations.

In addition, in this study, a quantitative assessment of the effect of the addition of the penetration enhancer (dimethyl isosorbide (DMI)) added to the delivery vehicle at different percentages was also assessed. Preliminary QMSI data demonstrated an increase of concentration of terbinafine into the upper epidermis of Labskin in response to an increase of percentage of DMI in the delivery vehicle.

However, the data obtained in this study requires assessment with an internal standard and validation using a complementary technique, such as LC-MS/MS.

Chapter 4: Quantitative investigation of terbinafine hydrochloride absorption into a living skin equivalent model by using MALDI-MSI.

4.1 Introduction

In Chapter 3 the main aspects hampering the use of MALDI-MSI for quantitative analysis have been discussed. The major limitations for performing QMSI are represented by the inhomogeneous distribution of the matrix and variation in ion suppression of the analyte of interest that could occur intra or inter tissue sample (Wang *et al.*, 2016).

The necessity for homogeneity of matrix coverage in MALDI-MSI has been debated in Chapter 2. Use of sublimation was shown to be an excellent methodology for the production of high-resolution images of the drug in the tissue Labskin, and for this reason, it has been chosen for qualitative as well as quantitative investigations.

In Chapter 3 several strategies were compared for quantifying the amount of an antifungal agent, terbinafine hydrochloride, in the defined epidermal layer of a 3D skin model, Labskin. It is important to note that the effect of the tissue composition on signal response in MSI has large implications when skin is the target organ for quantitative experiments. The layers of the skin comprise distinct cell types and hence each skin layer would be expected to give a slightly different response for the same amount of analyte. This implies that mimetic arrays created from skin homogenates would not be a suitable methodology for calibration in this instance. Instead, the use of acoustic microspotting (Aerni, Cornett and Caprioli, 2006) of analytical standards specifically onto the epidermal layer as a way of calibrating QMSI experiments resulted in being the optimum approach over all the different calibration/standardisation approaches investigated.

Over the past years, the employment of an internal standard has been demonstrated to increase the quantitative capabilities of MSI analysis (Pirman and Yost, 2011; Prentice, Chumbley and Caprioli, 2017). The choice of an appropriate internal standard represents a crucial aspect for a successful MALDI quantitative investigation (Wilkinson *et al.*, 1997). The internal standard must be a molecule with chemical and physical characteristics similar to the analyte under study as well as similar fragmentation pathway. Sleno and Volmer investigated the fundamental properties that a molecule should match

with the analyte to be selected as a suitable internal standard. In particular, affinity between the in-solution ionisation properties of the analyte and its internal standard, such as log D, pka, molecular weight and solubility, was emphasised (Sleno and Volmer, 2005).

During MSI analysis the internal standard mimics the behaviour of the analyte of interest in terms of ionisation efficiency and compensates for the tissue-dependent ion signal variations of the analyte. This aspect causes an improvement of relative signal ion reproducibility and image quality due to an increase of pixel to pixel precision (Pirman *et al.*, 2013; Chumbley *et al.*, 2016). For this reason, most commonly, a stable-isotope labelled (SIL) version of the analyte represents the first choice.

The study reported by Pirman *et al.* introduced the employment of a stable isotope labelled internal standard in the MSI workflow. In this work, the authors used a deuterated version of acetyl-l-carnitine (AC) in order to assess the endogenous concentration of AC in piglet brain tissue (Pirman, Heeren and Yost, 2013). It was reported that the use of a deuterated labelled internal standard against which to normalise the analyte peak helped to correct for both signal variations and tissue specific ion suppression.

However, in the absence of a labelled version of the analyte due to impractical synthesis, cost and time problems, structural analogues represent a valid alternative (Prideaux *et al.*, 2011; Takai, Tanaka and Saji, 2014a). In a recent study, Rao *et al.* developed a method to quantify the drug octreotide, a synthetic somatostatin analogue, in mouse tissues (Rao *et al.*, 2017). In this study, due to the impossibility of using labelled internal standards, multiple somatostatin analogues (native somatostatin-14, lanreotide, vapreotide) were investigated and it was found that lanreotide was the best candidate for its excellent stability.

Whichever internal standard is decided to use, either a stable labelled or a structural analogue, it is essential that it is applied uniformly and is detected in the same MS scan as the analyte of interest, in order to guarantee reliable signal intensity correction in MSI (Pirman, Heeren and Yost, 2013). Different approaches for applying a constant concentration of internal standard uniformly to the tissue have been investigated. Most commonly, an automatic spray-coating device is used to deposit an internal standard either premixed with

MALDI matrix (Källback *et al.*, 2012; Lagarrigue *et al.*, 2014; Poetzsch *et al.*, 2014) or prior to matrix deposition (Clemis *et al.*, 2012; Buck *et al.*, 2015; Sun *et al.*, 2016) onto the tissue. An alternative approach was employed in the work reported by Chumbley *et al.*, in a quantitative study of rifampicin in liver tissues. Here the internal standard was applied using an acoustic spotter investigating four different strategies (Chumbley *et al.*, 2016). These included: 1) application of the internal standard on top of the tissue prior to matrix deposition; 2) application of the internal standard under the tissue section; 3) application of ½ internal standard under the tissue and ½ onto the tissue (sandwich method); 4) application of matrix and internal standard simultaneously as a mixture. The effect of each method on the QMSI analysis of the drug in the tissue was analysed and it was reported that only the method involving the application of the internal standard on top of the tissue prior to matrix deposition offered quantitative data comparable to those obtained with LC-MS/MS performed on extracted tissue.

In the study reported in this chapter further improvement and validation of the microspotting technique (described in Chapter 3) to obtain absolute quantitation of the amount of terbinafine hydrochloride in the epidermal layer of Labskin has been performed. Here, a deuterated version of terbinafine hydrochloride has been employed as an internal standard and the improvement of the quantitation capabilities of mass spectrometry imaging has been examined. QMSI data have been compared to data obtained from LC-MS/MS measurements of homogenates of isolated epidermal tissue.

4.2 Aims of the chapter

In the following chapter we aimed to determine absolute quantitation of terbinafine hydrochloride in the epidermal region of a full thickness living skin equivalent model. Validation of the data using LC-MS/MS technique was also performed.

4.3 Materials and methods

4.3.1 Chemicals and materials

Alpha cyano-4-hydroxycinnamic acid (α-CHCA), acetonitrile (ACN), phosphorus red, terbinafine hydrochloride standard (TBF HCl, MW 327.89), isosorbide dimethyl ether (DMI), haematoxylin, eosin, xylene substitute, ethanol (EtOH) and formic acid ≥ 96% (FA) were purchased from Sigma-Aldrich (Gillingham, UK).

Pertex mounting medium was obtained from Leica Microsystems (Milton Keynes, UK). LC-grade methanol (MeOH) and LC-grade acetonitrile (ACN) were purchased from Fisher Scientific (Loughborough, UK). 18 MΩ water was obtained from an ELGA water purification system (Buckinghamshire, UK). The internal standard terbinafine-d_7 hydrochloride (TBF-d_7 HCl, MW 334.93) was obtained by Clearsynth (Maharashtra, India). Gentian violet 1% was purchased from De La Cruz Laboratories Inc. (Califiornia, USA).

Labskin living skin equivalent (LSE) samples were provided by Innovenn (UK) Ltd (York, England).

4.3.2 Living skin equivalent samples

Living skin equivalent (LSE) samples were obtained and cultured as described in Chapter 2.3.2. For the experiment, three LSE samples were treated with 20 µL of terbinafine hydrochloride (1% w/w) dissolved in an emulsion made up of water/olive oil (80:20 v/v) with either 10% or 50% DMI and incubated for 24 hours. For the vehicle control group, three LSEs samples were treated with 20 µL of the emulsion water/olive oil (80:20 v/v) alone and incubated for 24 hours.

After incubation, the samples were taken and washed with LC-grade MeOH to remove excess formulation and, then, snap-frozen with liquid nitrogen cooled isopentane (2–5 min) and stored at −80 °C.

For cryosectioning, LSEs were transferred into the cryostat (Leica 200 UV, Leica Microsystems, Milton Keynes, U.K.), mounted onto cork ring using diH_2O

at −25 °C for 30 min to allow thermal equilibration. The 12 µm tissue sections were cryosectioned, thaw mounted onto poly-lysine glass slides, and stored at −80 °C. Before matrix application and imaging the samples were freeze-dried under vacuum (0.035 mbar) for 2 hours to avoid delocalisation of the analyte and preserve the integrity of the tissues.

4.3.3 Preparation of standard curves

For MALDI-MSI experiments, working standards were made to 0.01, 0.1, 1, 10, 100, 500, 1000, and 1500 ng/µL of TBF HCl with 100 ng/µL of the internal standard TBF-d_7 HCl in MeOH/H_2O (50:50). Calibration standards were applied onto the epidermis area of 12 µm thick sections of blank tissue sections using an acoustic robotic spotter (Portrait 630, Labcyte Inc., Sunnyvale, CA).

Nine microspots of internal standard TBF-d_7 HCl (100 ng/µL in MeOH/H_2O (50:50)) were deposited onto the epidermis of a vehicle control Labskin section treated with water/olive oil (80:20) alone and two Labskin samples treated with terbinafine hydrochloride 1% w/w in water/olive oil (80:20) with either 10% or 50% DMI.

For application of the standards and internal standard, the number of cycles for each spot was set to 20 for a total volume of 3.4 nL of each deposited solution. Five extra spots were applied outside the tissue to give a “drying time” between each cycle.

For LC–MS/MS, calibration standards were made to 0.001, 0.01, 0.05, 0.1, 0.5, 1, 10 ng/µL of terbinafine hydrochloride with 0.1 ng/µL of internal standard terbinafine-d_7 hydrochloride in acetonitrile + 0.1% formic acid/ultrapure water + 0.1% formic acid (80:20).

4.4 Matrix deposition

4.4.1 Sublimation

The matrix CHCA was applied by a sublimation technique as described in Chapter 2.4.2.1.2

4.5 Instrumentation

4.5.1 MALDI mass spectrometry

All tissues were imaged using a Waters MALDI HDMS Synapt™ G2 mass spectrometer (Waters Corporation, Manchester, UK) equipped with a neodynium: yttrium aluminium garnet (Nd:YAG) laser operated at 1 KHz. The instrument calibration was performed using phosphorous red. MALDI-MS images were acquired in positive mode, in full scan “sensitivity” mode at a range of *m/z* 100-1500, (resolution 10,000 FWHM) at spatial resolution of 60 µm x 60 µm, and with laser energy set to 250 arbitrary units. The ion mobility function of the instrument was not enabled.

4.5.2 LC-MS/MS

All LC–MS/MS experiments were performed using a Xevo G2-XS QTof (Waters Coorporation, Manchester, U.K.) with ionisation mode ESI+ with analyser in sensitive mode. The LC conditions were made of an ACQUITY UPLC HSS T3 C18 1.7 µm, 2.1 × 100 mm (p/n 186003539) column. The mobile phase consisted of ultrapure water (solvent A) and acetonitrile (solvent B) containing both 0.1% formic acid. The flow rate and the injection volume were 0.2 mL/min and 2 µL, respectively. The gradient eluition was performed as follows: 0.0–2.0 min (A, 95%; B, 5%), 2.0–12.0 min (A, 5%; B, 95%), 12.0–30.0 min (A, 5%; B, 95%), 30.0–40.0 min (A, 95%; B, 5%), 40.0–44.0 min (A, 95%; B, 5%).

The experimental instrument parameters used were capillary voltage, 3.0 kV; cone voltage, 35.0 V; source temperature, 140 °C; desolvation temperature,

250 °C; desolvation gas, 1000 L/h; and cone gas, 50 L/h. Argon was utilized as a collision gas and the collision energy was set at 19 eV.

A multiple reaction monitoring (MRM) method was used to detect the product ion of terbinafine (292.3 → 141.1 *m*/*z*) and the product ion of terbinafine-d_7 (IS) (299 → 148 *m*/*z*). The retention time was ∼10.6 min.

4.5.3 Skin extraction

The vehicle control and treated Labskin tissues were placed for 2 min in 1X PBS pre-heated at 60°C; then, the epidermis was separated from the dermis by using a forceps, transferred to tubes and weighted.

The tissue homogenisation and drug extraction were performed by a small modification of previously published work carried out by Sachdeva *et al* (Sachdeva *et al.*, 2010). The modification made was that after the second extraction, the back extraction was not performed; instead, the organic layer containing the extracted drug was evaporated under nitrogen and, then reconstituted in 1.8 mL of ACN/H_2O (80:20) + 0.1% FA. The solution was filtered through a 0.22 µm filter and 0.2 mL of internal standard TBF-d_7 HCl (0.1 ng/µL in ACN/H_2O (80:20) + 0.1% FA) was added to the solutions prior to analysis.

4.5.4 Data processing

MALDI-MSI data were processed using the HDI 1.4 (Waters Corporation, UK) software tool. Using this software, MSI raw data files were converted to imzML format and imported into msIQuant software for quantitative investigations.

For LC-MS/MS data, the chromatograms peaks for terbinafine hydrochloride and terbinafine-d_7 hydrochloride were integrated and processed using Mass Lynx (Waters Corporation, UK) software tool.

Statistical analysis was performed using the StatDirectsoftware (StatsDirect, Cheshire, UK). F test and T test were used to evaluate the statistical

significance in terms of precision and accuracy, respectively, between the values obtained by MALDI-MSI and LC/MS/MS techniques.

Three replicate measurements (n = 3) were used and the level of significance was set to 5%.

Outlier point identifications were performed using Prism software. The method selected was Grubbs' test for outliers (α = 0.05).

4.6 Histological analysis

4.6.1 Haematoxylin and eosin staining

Haematoxylin and eosin staining on LSE sections was performed as reported in Chapter 2.6.1.

Optical images were obtained using a Cytation 5 imaging reader and analysed with Gen5 software (BioTek, Swindon, UK).

4.7 Results and discussion

4.7.1 Reproducibility of droplet size of the Portrait 630

Manually spotting of calibrants onto control tissues has constituted one of the major approaches for generating calibration arrays in previous QMSI experiments (Nilsson *et al.*, 2010; Källback *et al.*, 2012; Lagarrigue *et al.*, 2014; Barré *et al.*, 2016). Although widely practiced, this technique is not without limitations. One of the major drawbacks of manual pipetting is the difficulty in depositing sub-microliter volumes of solutions. This makes it difficult to localise standards to small defined regions of tissue. Furthermore, manually applied spots are susceptible to variations in size and, hence, the amount of standards in the spots is difficult to control.

In this study we decided to measure and compare the perimeter and area of the droplet spots generated by the Portrait 630 in order to assess the reproducibility and accuracy of this device. In order to perform the experiment, a solution of 0.1% of gentian violet in MeOH/H_2O (1:1) was used as a spot size marker and 9 microspots of the solution were deposited onto the epidermal layer of a 12 µm thick blank Labskin section. In each spot the number of cycles was set to 20, with a total deposited volume of 3.4 nL per spot. The experiment was performed twice and, after spotting, the sections were imaged with a Cytation 5 imaging reader equipped with Gen5 software, while the perimeter and area of each spot on recorded images was measured by using ImageJ software (https://imagej.nih.gov/ij/).

As shown in Figure 4.1A the presence of the dye in the solution allowed easy visualisation of the spots onto the tissue. The average perimeter of spots for two Labskin sections was found to be 0.5 ± 0.041 mm and 0.53 ± 0.035 mm, respectively, while the average area was found to be 0.019 ± 0.003 mm^2 and 0.021 ± 0.028 mm^2, respectively. The relative standard deviations of the measurements were as follow: 14.35% (area) and 8.21% (perimeter) from section 1; 13.5% (area) and 6.62% (perimeter) from section 2 (Figure 4.1B-C).

These data demonstrate the high reproducibility in the size of the dye spots intra and inter sections when the Portrait spotter was used. The area and

perimeter values detected from the spots in two sections of Labskin tissue were not statistically different. The use of the Portrait 630 acoustic spotter to generate microspots with constant size and minimal lateral diffusion allowed better control of the concentration of analyte and also avoided the possibility of cross contamination that could occur for direct contact of the pipette with the substrate.

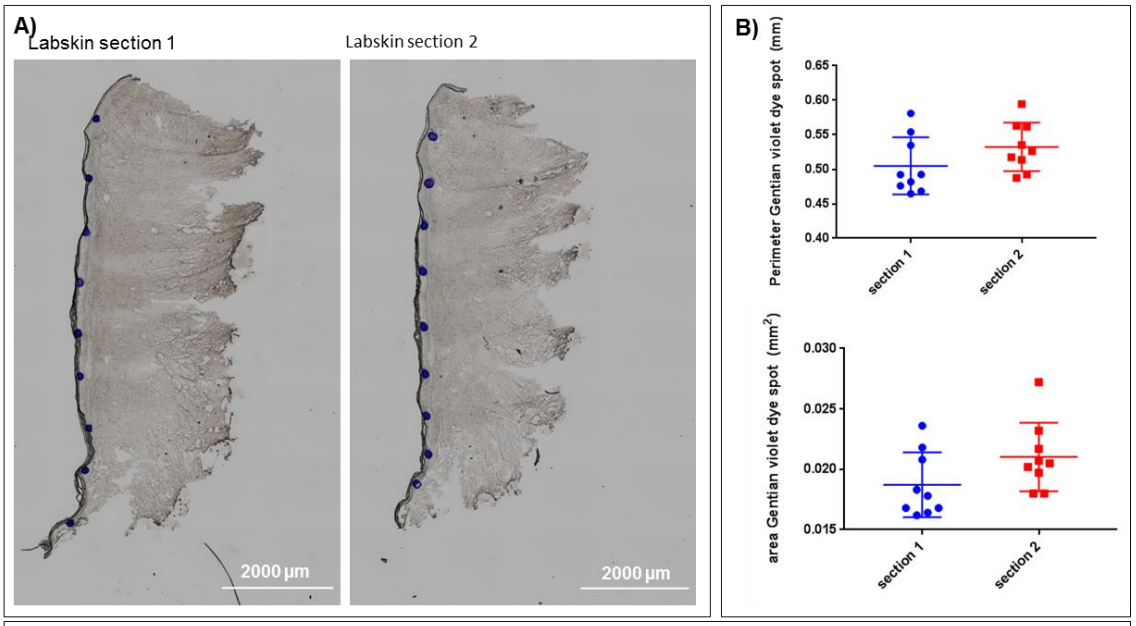

C)

	section 1		section 2	
	area (mm^2)	perimeter (mm)	area (mm^2)	perimeter (mm)
AVERAGE	0.019	0.5	0.021	0.53
ST.DEV	0.003	0.041	0.0028	0.035
%RSD	14.35	8.21	13.5	6.62

Figure 4.1 A) *Optical image of 9 spots of gentian violet dye solution across the epidermis of two blank Labskin sections performed using the Portrait 630.* ***B)*** *Graphs showing the results of spot size measurements with the error bars displaying the standard deviation of 9 spots for each Labskin section.* ***C)*** *Table displaying the arithmetic mean, standard deviation and relative standard deviation (RSD%) of either area or perimeter measurements from gentian violet spots in two sections of Labskin samples. Consistency between the size of spots intra and inter tissues was evidenced. No statistically significant difference was found between the spot parameters from two sections.*

4.7.2 Method used for quantitation

Figure 4.2A-C shows MALDI-MSI images of the distribution of the terbinafine fragment ion at *m/z* 141 in three sections of Labskin recorded at 60 µm pixel size following treatment with (A) 20 µL of emulsion water/olive oil (80:20) alone (vehicle control) and 20 µL of terbinafine 1% (w/w) in water/olive oil (80:20) with (B) 10% or (C) 50% isosorbide dimethyl ether (DMI) for 24 hours. It can be seen that the terbinafine signal appears to be localised to the epidermis and that there is an increase in its intensity with increasing amount of DMI, in agreement with the results shown in Chapter 3.

In addition, from the spectra a unique signal belonging to DMI ($[M+H]^+$ *m/z* 175.1) could not be identified, as an isobaric background peak was present in all of samples, including those without DMI. To obtain more details about the possible presence of DMI, it could be interesting to perform the experiment by using an ion mobility function or ultra-high mass resolution.

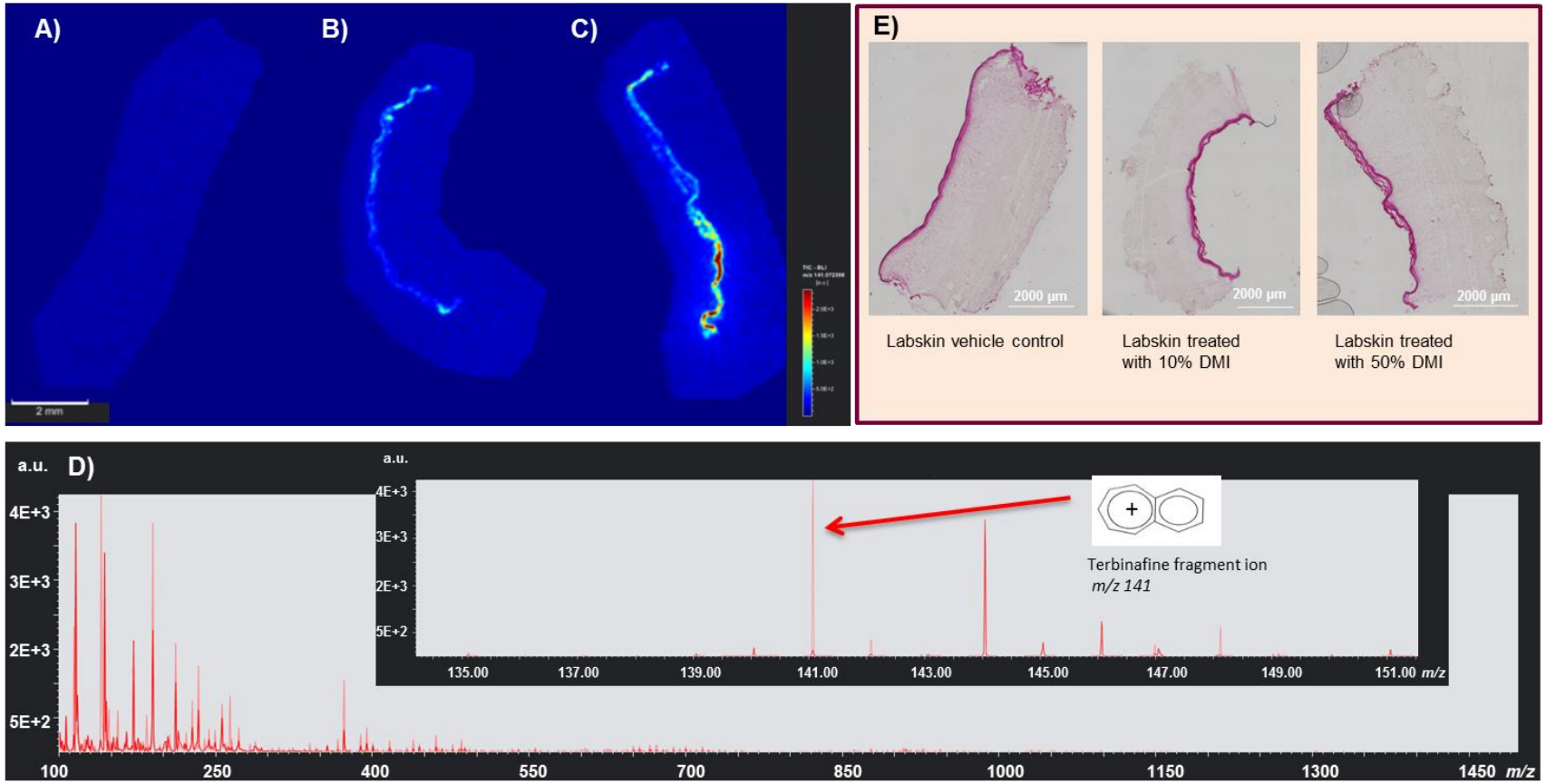

Figure 4.2 *MALDI-MSI at 60 µm × 60 µm spatial resolution of the terbinafine hydrochloride fragment ion ($[C_{11}H_9]^+$; m/z 141) on (A) vehicle control section and two Labskin sections treated with terbinafine 1% (w/w) in water/olive oil (80:20) with either (B) 10% or (C) 50% isosorbide dimethyl ether (DMI) for 24 hours. (D) Average MALDI-MSI spectra showing the peak of the terbinafine hydrochloride fragment ion at m/z 141. (E) Haematoxylin & eosin stained optical image of the sublimated sections after MALDI-MSI (4X magnification).*

In order to quantify the amount of terbinafine in the epidermis from such images it is necessary to calibrate the response specifically for signals arising from the epidermis to achieve "matrix matched standards". Previous studies have shown that the epidermis of Labskin consists of a very thin differentiated layer with an average thickness of 32 µm (Mitchell *et al.*, 2015; Harvey *et al.*, 2016). As discussed previously, this makes preparing standards by tissue spotting challenging. Therefore in this work, the use of an acoustic picoliter droplet ejector, used previously as a MALDI matrix deposition device (Aerni, Cornett and Caprioli, 2006) was used to spot 3.4 nL of the working standards (from 0.01 ng/µL to 1500 ng/µL) in MeOH/H_2O (1:1) onto the epidermis of a blank section of Labskin to create a calibration array. Internal standard terbinafine-d_7 hydrochloride (100 ng/µL) was included into standard solutions prior to spotting. The application of analytical and internal standards onto an untreated section of Labskin by microspotting allowed a uniform distribution across the epidermis with minimal lateral diffusion (Figure 4.3A-B). In this study, it was considered beneficial to apply the internal standard onto the tissue by microspotting in order to preserve the localisation of the calibration analyte, whereas it was found to migrate when the solution of terbinafine-d_7 hydrochloride was sprayed homogenously onto the tissue (data not shown).

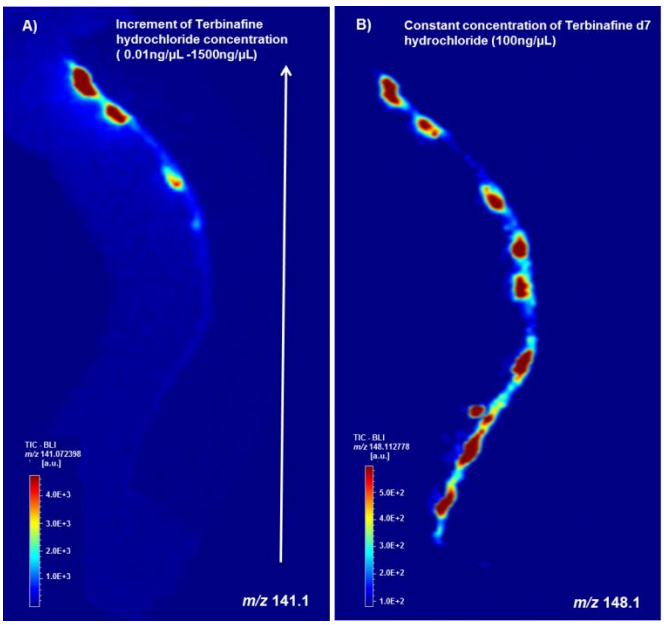

Figure 4.3 *MALDI-MSI at 60 µm X 60 µm spatial resolution of A) the dilution range of terbinafine fragment ion ($[C_{11}H_9]$+; m/z 141) mixed with B) a constant concentration of terbinafine-d_7 hydrochloride fragment ion ($[C_{11}D_7H_2]^+$; fragment ion; m/z 148) microspotted directly on the epidermis of an untreated section of Labskin. Volume of each spot = 3.4 nL.*

Additionally 9 spots of internal standard (100 ng/µL) were applied to the epidermal region of each treated sample for analysis (again using the acoustic picoliter droplet ejector). In this work, it was decided to use a deuterated analogue of terbinafine hydrochloride with seven deuterium ions on naphtalene group in order to distinguish the fragment of the internal standard from the fragment of analyte in the mass spectrum, leading to an increase of selectivity.

Figure 4.4A-D shows the MS image of the distribution of the *m/z* 148 fragment ion of terbinafine-d_7 on (A) untreated sample along with the calibration array, (B) vehicle control skin sample treated with 20 µL of the emulsion water/olive oil (80:20) alone and skin samples treated with terbinafine 1% (w/w) in water/olive oil (80:20) with either (C) 10% or (D) 50% isosorbide dimethyl ether (DMI) for 24 hours. The distribution of the internal standard can be clearly seen for each spot on each section and hence these data are suitable for the definition of the area of spots created by the acoustic picoliter droplet ejector.

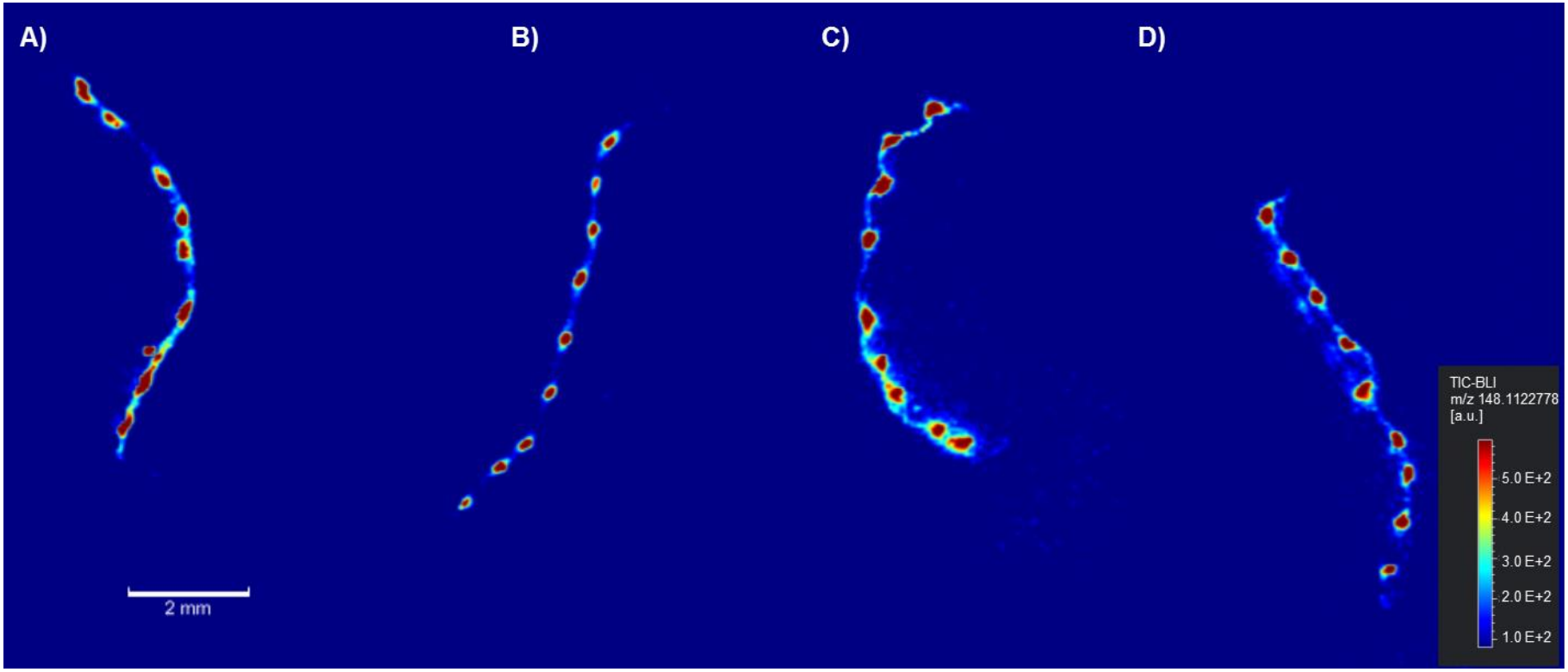

Figure 4.4 *MALDI-MSI at 60 µm × 60 µm spatial resolution of the terbinafine-d_7 hydrochloride source generated fragment ion ($[C_{11}D_7H_2]^+$; m/z 148) microspotted directly on the epidermal layer of (A) untreated sample along with the calibration array, (B) vehicle control section and two Labskin sections treated with terbinafine 1% (w/w) in water/olive oil (80:20) with either (C) 10% or (D) 50% isosorbide dimethyl ether (DMI) for 24 hours.*

The msIQuant software (Källback *et al.*, 2016) allows a number of methods for the definition of regions of interest (ROI) and extraction of peak intensities from them for quantitative analyses. Here the methodology used was to exploit signals from endogenous species to define the epidermis and stratum corneum of the tissue section (*m/z* 184, the phosphocholine ion signal, to define the tightly packed cells of the epidermis and *m/z* 264, the ceramide fragment ion, to define the stratum corneum). Then using the software an average intensity for the signals of the terbinafine and the terbinafine-d_7 of a ROI located to solely the epidermis for each spot could be extracted (Figure 4.5A-B).

The generation of the calibration curve (n = 3) was obtained by plotting either the average intensity of *m/z* 141 (Figure 4.5C) or the average intensity ratio of *m/z* 141/148 (Figure 4.5D) versus the concentration of terbinafine expressed in ng/mm^2. In agreement with previous studies, we found that the normalisation of the analyte signal to its deuterated analogue caused a significant improvement in the calibration curve linearity with a correlation coefficient (R^2) from 0.9968 to 0.9992 upon normalisation. The limits of detection (LOD) and quantitation (LOQ) were calculated; from these calibration data the LOD was found to be 1.30 ng/mm^2 or 0.11 mg/g tissue, whereas, LOQ was found to be 3.93 ng/mm^2 or 0.33 mg/g tissue. By expressing the LOD and LOQ in mg/g tissue it is assumed that the droplets containing the analyte standards diffuse over the entire thickness (12 µm) of the blank Labskin section. Furthermore, in this study the values of LOD resulted to be higher than that typically found in literature, expressed in terms of µg/g tissue (Lagarrigue *et al.*, 2014; Hansen and Janfelt, 2016). However, it is thought that multiple factors could influence this increase value of LOD, such as the ionisation efficiency of the analyte, the tissue-specific ion suppression, the sensitivity of the analyser as well as the background noise derived from matrix ionisation and matrix clusters that have a critical impact on LOD and LOQ.

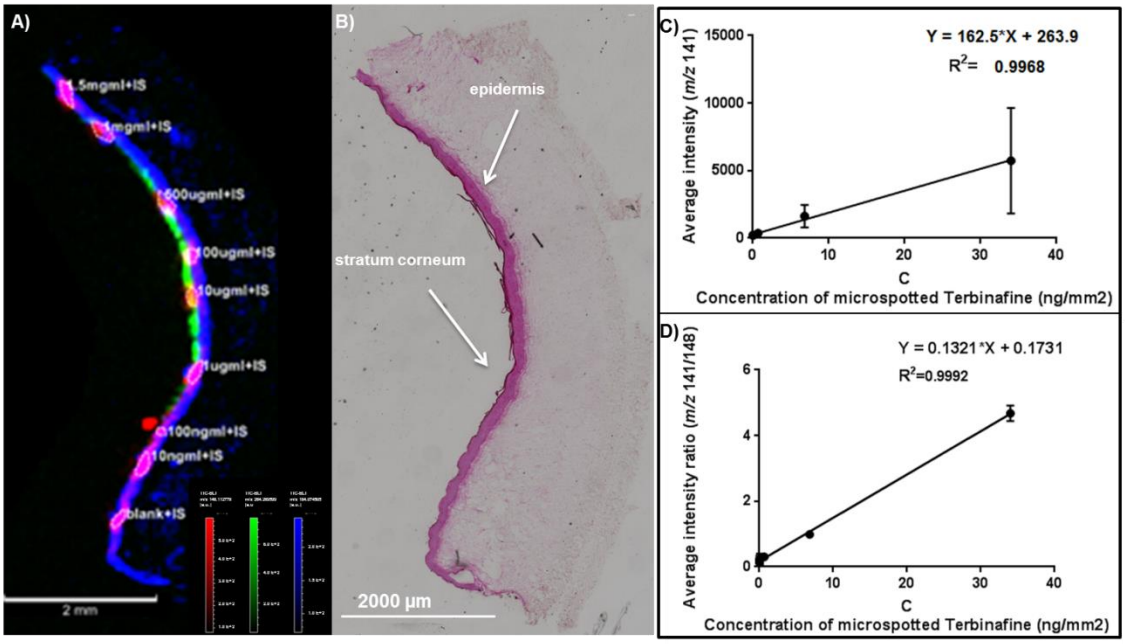

Figure 4.5 *(A) MALDI-MSI of the terbinafine-d_7 source generated fragment ion in red (m/z 148) superimposed with phosphocholine head group in blue (m/z 184) and ceramide fragment peak in green (m/z 264). (B) Haematoxylin & eosin stained optical image of the sublimated section after MALDI-MSI (4X magnification). Calibration curve (n = 3) generated using (C) the average intensity of m/z 141 (no normalisation) and (D) the ratio average intensity of m/z 141/148. Normalisation to the internal standard m/z 148 improved the linearity of the calibration curve.*

Considering the thin layer of the epidermis, for MALDI-MSI experiments ideally a pixel size smaller than 60 µm would have increased the spatial resolution in the imaging experiments. However, the Synapt instrument, unlike the Bruker Autoflex III instrument, does not offer the user the possibility of changing the laser focus diameter, which is set during installation. This aspect compromises the possibility of using the smallest pixel size for high resolution images without excessive oversampling and loss of signal occurring. In addition, considering the number of sections (4) which were imaged in each QMSI experiment, a smaller pixel size would have also resulted in a significant increase of both the throughput time as well as instrument contamination during the analysis. In light

of these considerations, 60 µm pixel size was chosen, although the possibility of a set-up with a smaller pixel size would be highly advantageous for future work.

4.7.3 Quantitation of the drug within the tissue

Using the method described above the concentration of terbinafine in the epidermis of (a) vehicle control Labskin and Labskin treated with 20 µL of terbinafine 1% (w/w) in water/olive oil (80:20) with either (b) 10% or (C) 50% isosorbide dimethyl ether (DMI) for 24 hours was determined. In order to perform the experiment, a total of nine microspots with a known concentration of terbinafine-d_7 hydrochloride (100 ng/µL) was deposited onto the epidermal layer of the vehicle control and treated Labskin samples. ROIs for each microspot of the TBF-d_7 fragment ion (*m/z* 148) were drawn in correspondence of the epidermal layer. Even in this case, the localisation of the microspots of the terbinafine-d_7 fragment ion onto the epidermis and stratum corneum was visualised by superimposing the internal standard fragment ion signal (*m/z* 148) with the phosphocholine ion signal (*m/z* 184) and the ceramide fragment ion signal (*m/z* 264). Using msIQuant software, the average intensity of the terbinafine fragment ion on each ROI was extracted and normalised to the average intensity of the terbinafine-d_7 fragment ion (*m/z* 141/148). Then, the average intensity ratio (*m/z* 141/148) from each spot was compared to the calibration curve, as shown in Figure 4.6A-C.

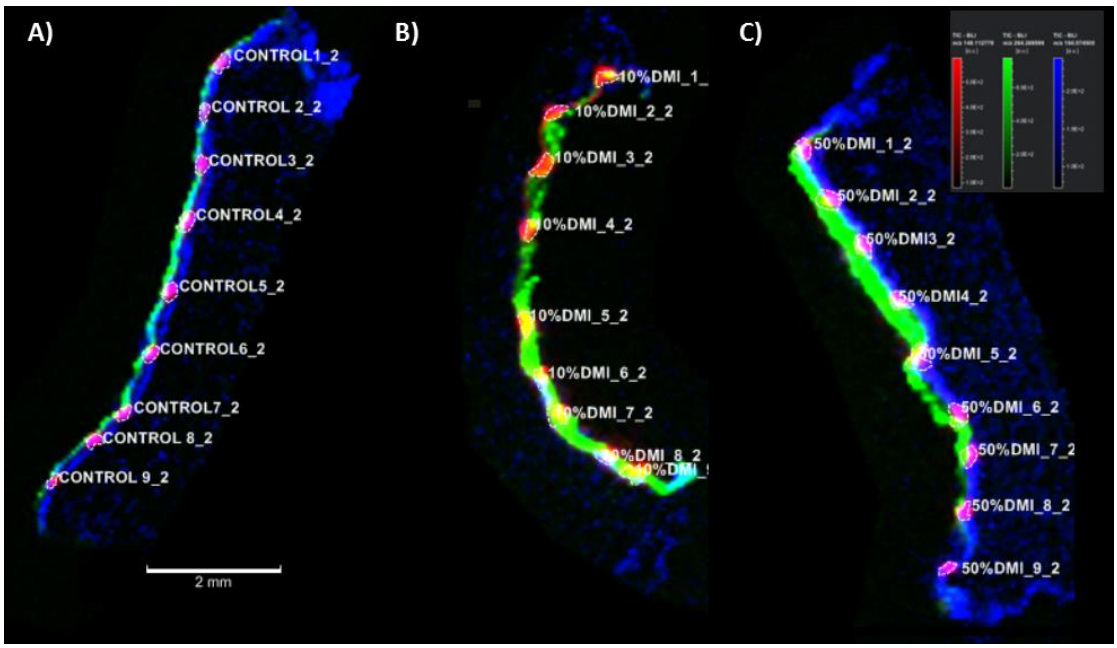

Figure 4.6 *MALDI-MSI of the terbinafine-d_7 fragment ion in red (m/z 148) superimposed with phosphocholine head group in blue (m/z 184) and ceramide fragment peak in green (m/z 264) in (A) vehicle control section and two Labskin sections treated with terbinafine 1% (w/w) at (B) 10% or (C) 50% DMI for 24 hours. The intensity of the analyte normalised to the internal standard was extracted from each ROI and compared to the calibration curve.*

By resolving the calibration equation, the amount of drug from each spot was obtained in ng/mm^2. As described in Chapter 3, to calculate the quantitative concentration of terbinafine hydrochloride in milligrams per gram of tissue, first, the amount in grams of tissue in 1 mm^2 was detected. The volume of tissue in 1mm^2 was calculated multiplying the area (1 mm^2) by the thickness of the section (0.012 mm). Then, the volume (0.012 mm^3) was multiplied by the density of Labskin (1 mg/mm^3) to obtain the value of grams of tissue in 1 mm^2. By dividing in turn the concentration of terbinafine from each spot (ng/mm^2) to the grams of tissue in 1 mm^2, the concentration of terbinafine was converted in milligrams per gram of tissue. The concentration values derived from the spots applied onto each Labskin tissue was averaged and the main concentration of terbinafine hydrochloride in each Labskin tissue was calculated.

In initial experiments the apparent levels of the drug were found to be 0.15 ± 0.11 mg/g tissue in vehicle control, 0.35 ± 0.047 mg/g tissue within Labskin

treated with terbinafine at 10% DMI, and, 0.84 ± 0.14 mg/g tissue within Labskin treated with terbinafine at 50% DMI.

On investigation it was found that the internal standard solution used contained a small amount of the unlabelled drug. Figure 4.7 shows the distribution of the average intensity ratio of the unlabelled drug (*m/z* 141) normalised to its internal standard (*m/z* 148) extracted from each microspot of the terbinafine-d_7 hydrochloride solution deposited onto the epidermal layer of three control Labskin sections at different times. It was noticed that the intensity average ratio increased over time, due to an increase of the unlabelled counterpart of the internal standard in the solution.

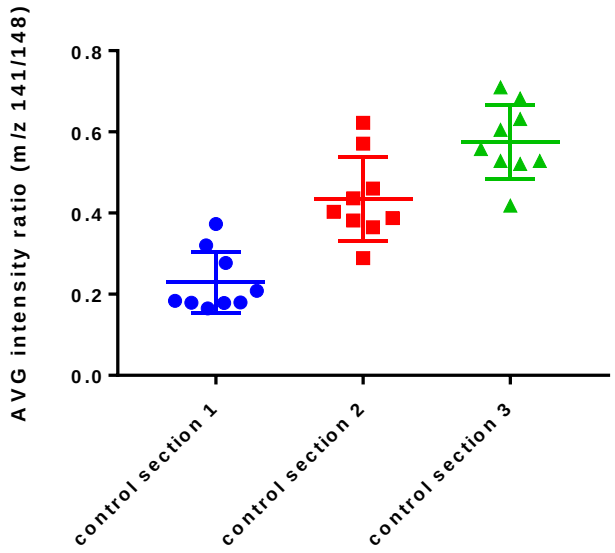

Figure 4.7 *Distribution of the intensity ratio of terbinafine to its internal standard (m/z 141/148) extracted from each microspot of the internal standard solution (terbinafine-d_7 hydrochloride (100 ng/µl) in MeOH/H_2O (1:1)) deposited onto the epidermis of three control Labskin sections over time.*

It is interesting to note that, considering the structure of the terbinafine d_7 (Figure 4.8), the deuterium-hydrogen exchange happened on unusual sites, that not easily undergo to hydrogen-deuterium exchangeability (Englander *et al.*, 1996).

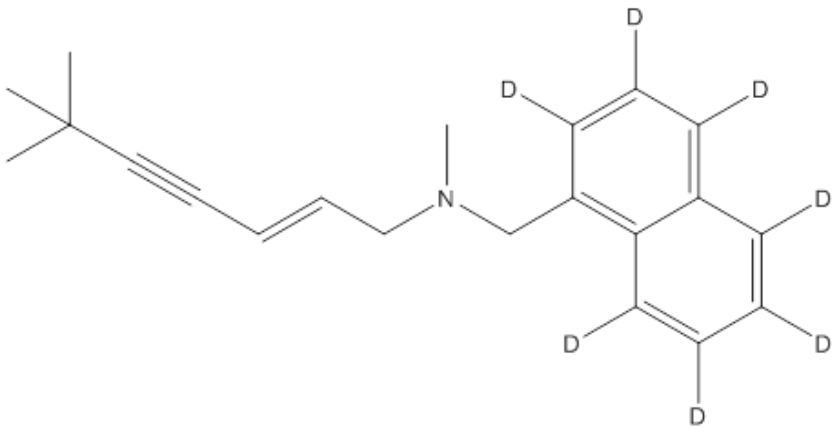

Figure 4.8 *Structure of Terbinafine-d_7.*

However, the problem related to deuterium-hydrogen exchange in deuterated compounds was previously described by Chavez *et al.* (Chavez-Eng, Constanzer and Matuszewski, 2002) and can lead to an overestimation of the concentration of unlabelled analyte. A number of ways were investigated to correct for this problem. Since the degradation of the internal standard in solution increased over time, the concentration of the analyte in the treated tissues could be affected in different percentage in each QMSI experiment. For this reason, it was decided that the optimum approach was to subtract the amount of terbinafine detected in the vehicle control from the amount of terbinafine detected in the treated tissues for each QMSI experiment.

After this correction, at 10% DMI the concentration of TBF was found to be 0.20 ± 0.072 mg/g of tissue (below the formal limit of quantitation), and at 50% the level was found to be 0.69 ± 0.23 mg/g tissue (Figure 4.9A-B).

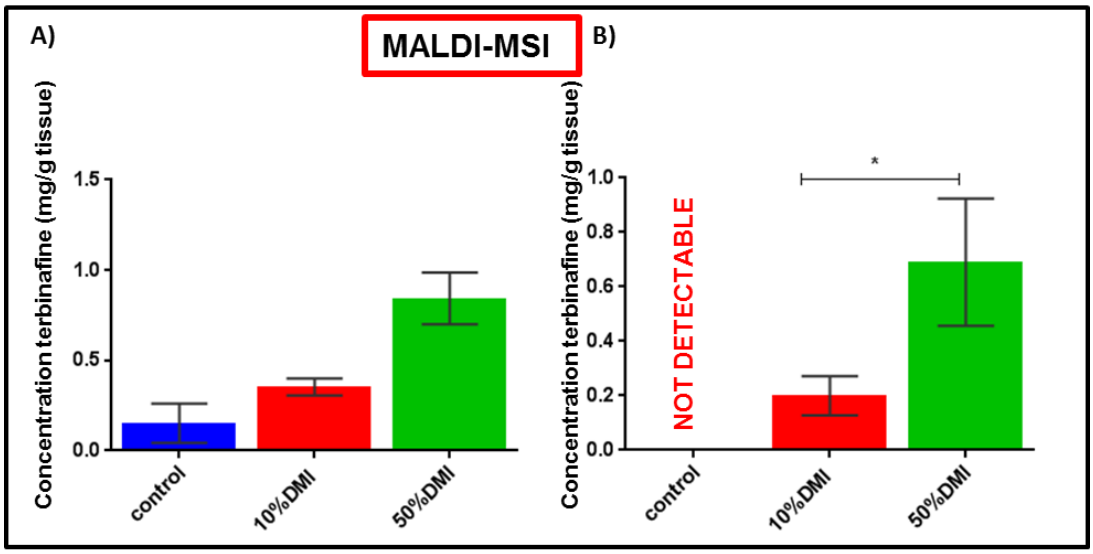

Figure 4.9 *A) Graph showing the initial QMSI levels of terbinafine from the sections of Labskin. B) Graph showing the final levels of terbinafine from the sections of Labskin after correction for the degradation of the internal standard.*

After experiencing the degradation of the internal standard that occurred in solution, it was decided to investigate also the possible degradation of the internal standard on tissue. This experiment is described in the supplementary information (Appendix II).

In order to validate the MALDI-MSI data LC-MS/MS experiments were performed using the methodology described by Sachdeva *et al.* (Sachdeva *et al.*, 2010). LC-MS/MS is a high sensitivity technique, widely used in previous studies for quantitation of terbinafine hydrochloride (Brignol *et al.*, 2000; Dotsikas *et al.*, 2007). Although it is common knowledge that LC-MS/MS provides reliable quantitation, analysis using this technique cannot be carried out directly on the intact surface skin, but analytes of interest have to be extracted out of the tissue, increasing the complexity of sample preparation, time of analysis and loosing spatial information. In addition, another drawback of using LC-MS/MS is represented by the amount of tissue necessary for homogenisation (from 0.5 mg to 50 mg) compared to the small amount of tissue that can be analysed using MALDI-MSI (0.010-0.012 mg).

Furthermore, also in chromatographic analysis the purpose of using internal standards is to increase the quantitative performance of the technique. In this case, the internal standard is meant to correct mainly for random and systematic error of the detection, in LC-MS/MS principally (Wieling, 2002; Stokvis, Rosing and Beijnen, 2005).

In this study, LC-MS/MS experiment was repeated three times per each tissue of Labskin. The calibration curve was generated by plotting the concentration of terbinafine hydrochloride versus the response ratio. The response ratio was calculated by dividing the peak area of the analyte by the peak area of the internal standard.

The calibration curve observed in Figure 4.10A showed a coefficient of linearity R^2 of 0.9989. The limit of detection (LOD) and quantitation (LOQ) were assessed at 0.42 µg/mL and 1.27 µg/mL, respectively. In the vehicle control sample, the levels of terbinafine were below the limit of detection, whereas, at 10% DMI and 50% DMI the levels were above the LOQ and they were found to be 0.28 ± 0.04 mg/g tissue and 0.66 ± 0.057 mg/g tissue, respectively (Figure 4.10B).

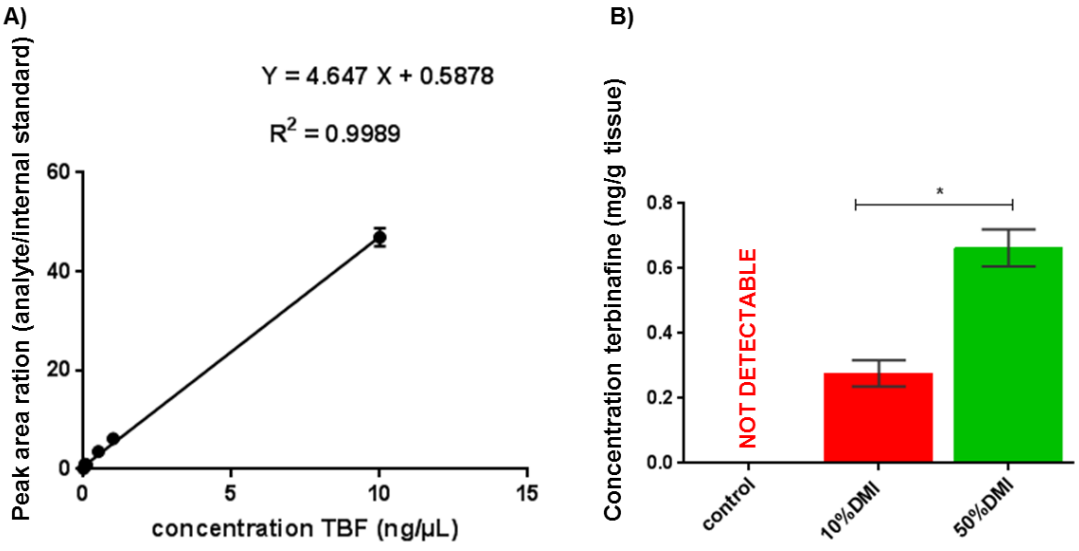

Figure 4.10 *A) Calibration curve (n = 3) generated using the peak area ratio (analyte/internal standard) B) Graph showing the final levels of terbinafine obtained from LC-MS/MS measurements of homogenates of isolated epidermal tissue.*

A statistical unpaired T test was performed on the data from both tissues treated with terbinafine with either 10% DMI or 50% DMI. The concentration of the drug resulted statistically increased in the tissue when the percentage of DMI increased in the formulation in both QMSI (two sided P = 0.0256) and LC-MS/MS (two sided P = 0.0007) (Figure 4.11A-B). Furthermore, in order to compare the values obtained by QMSI and LC-MS/MS, F test and paired T test between the methods were performed. With the F test, the variances between the values of terbinafine at 10% DMI and 50% DMI were found to be not statistically different between the methods (at 10% DMI; two sided P = 0.478; at 50% DMI, two sided P = 0.1116). When the paired T test was performed, also the means between the values of terbinafine at 10% DMI and 50% DMI were found to be not statistically different between the methods (at 10% DMI, two sided P = 0.0726; at 50% DMI, two sided P = 0.8361) (Figure 4.11C).

These data have demonstrated the development of a QMSI method for the determination of the amount of an active pharmaceutical ingredient in skin. In addition the capability of the penetration enhancer DMI to increasing the drug penetration in the upper epidermis of living skin equivalent has been demonstrated.

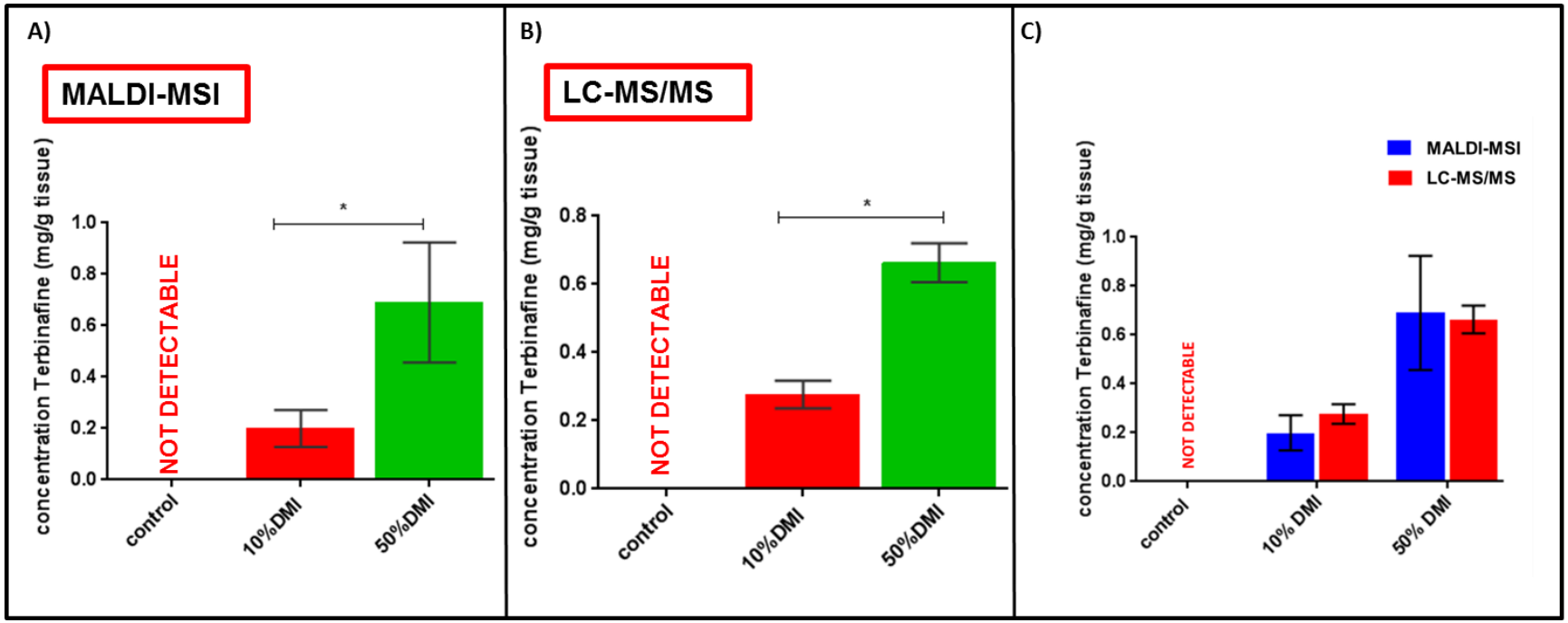

Figure 4.11 *A) Graph showing the final levels of terbinafine from the sections of Labskin by using MALDI-MSI. B) Graph showing the final levels of terbinafine from LC-MS/MS measurements of homogenates of isolated epidermal tissue. C) Graph showing comparison between the results obtained from MALDI-MSI and LC−MS/MS, the error bars illustrate the standard deviation of three repeats for each method. No significant differences between the two methods were found.*

4.8 Concluding remarks

In this chapter, a novel approach for quantitative mass spectrometry imaging (QMSI) of terbinafine hydrochloride in the epidermal region of a full thickness living skin equivalent model has been presented. The use of an acoustic spotter turned out to be ideal for applying precise and uniform analytical and internal standards onto a thin and well-defined epidermal layer of the Labskin tissue, leading to mimic cell-type based ionisation response of the analyte from the treated tissue sections. The combination of microspotting technique and matrix sublimation allowed preservation of the spatial distribution of the analyte and achieving better mass spectral quality and reproducibility.

The study presented here also provided an innovative method to assess the performance of the penetration enhancer DMI added to the delivery vehicle. QMSI data demonstrated an increase in concentration of terbinafine into the upper epidermis of Labskin in response to an increase of percentage of DMI in the delivery vehicle. QMSI data were satisfactory in showing no statistically significant differences from LC–MS/MS measurements of homogenates of isolated epidermal tissue, leading accuracy and precision between the methods to be the same.

Chapter 5: An "on-tissue" derivatisation approach for improving sensitivity and detection of hydrocortisone by MALDI-MSI.

(This data was obtained during a placement period spent in Croda US laboratories and the work was carried out in collaboration with Brian Malys).

5.1 Introduction

In Chapter 4, a novel approach for the quantitation of terbinafine hydrochloride by using MALDI-MSI was illustrated. Terbinafine is a molecule easily detected using mass spectrometry due to the straightforward protonation of its amine group. However, when an analyte of interest contains functional groups with low protonation/deprotonation efficiency, detection by MS is compromised. A chemical derivatisation approach is often employed to overcome this drawback.

Derivatisation offers the potential advantage of increasing analyte signal intensity by introducing groups with permanent charges or with high ionisation efficiency (Zaikin and Halket, 2006). Another advantage of this approach is that the molecular mass of the targeted analyte can be increased, resulting in analyte peaks shifted to a higher mass region. This aspect is particularly beneficial when low molecular mass compounds are analysed by MALDI-MS, since the derivatisation can help to avoid matrix-related background interference present in the lower mass range, which can be an issue with low mass resolution instruments (Tholey *et al.*, 2002). A comprehensive review on the main reactions available for derivatisation of functional groups analysed by mass spectrometry techniques was recently conducted by Huang *et al*. (Huang *et al.*, 2019).

Over the years, on-tissue derivatisation strategies have been reported for increasing the sensitivity and specificity of MSI analysis of exogenous and endogenous compounds, while preserving spatial localisation (Prideaux *et al.*, 2007; Flinders *et al.*, 2015; Esteve *et al.*, 2016; Schulz *et al.*, 2019). On-tissue derivatisation approaches have also been used to improve identification of proteins from tissue sections by MALDI-MSI (Franck *et al.*, 2009).

An interesting aspect of derivatisation for the purpose of MALDI analysis is that often the tags used, in addition to derivatising the analyte, promote its co-crystallisation with the matrix. Furthermore, reagents able to absorb at UV/IR wavelengths can be used for direct analysis without the aid of common MALDI matrices (Huang *et al.*, 2019). In this capacity the reagents are considered as "reactive matrices" since they induce both derivatisation and ionisation of molecules. 2,4-dinitrophenylhydrazine (DNPH) is an example of a reactive

matrix commonly used for the derivatisation of carbonyl containing compounds (Brombacher, Owen and Volmer, 2003; Teuber *et al.*, 2012; Flinders *et al.*, 2015). The typical derivatisation reactions of carbonyl compounds rely on the formation of oximes, by reaction with hydroxylamines, and hydrazones, by reaction with hydrazine derivatives (Zaikin and Halket, 2006). The formation of Schiff's bases, semicarbazones, and thiosemicarbazones has also been reported (Zaikin and Halket, 2009).

Currently, multiple derivatisation agents are commercially available and their selection depends strongly on the targeted analyte. However, all of the chemical tags should satisfy several desirable characteristics: 1) they have to contain a charge or an "easily" ionisable group; 2) they have to contain an appropriate reactive group; and 3) they have to be available to purchase or, at least, their synthesis should be cost-effective (Cartwright *et al.*, 2005; Zaikin and Halket, 2006; Flinders *et al.*, 2015).

In this study the attention was moved from MALDI-MSI analysis of an "easily" detectable molecule, terbinafine hydrochloride, to the analysis of a molecule with low ionisation efficiency, hydrocortisone. Hydrocortisone is a steroid medicine widely used in dermatologic therapy due to its potent anti-inflammatory and antiproliferative activities (Hengge *et al.*, 2006). The application of mass spectrometry techniques for analysis and measurements of steroid hormones represents an important aspect for clinical research, public health assessments and patient care (Cook-Botelho, Bachmann and French, 2017). However, steroid hormones are characterised by a chemical structure with multiple carbonyl groups, which make difficult their detection by mass spectrometry. To date, in literature there has been multiple studies reported that employ chemical derivatisation strategies for steroid hormones to improve the sensitivity of mass spectrometry analysis (Díaz-Cruz *et al.*, 2003; Xu *et al.*, 2007; Rangiah *et al.*, 2011).

In this chapter an in-solution and on-tissue derivatisation approach have been investigated to enhance the detection of hydrocotisone in *ex-vivo* skin by using MALDI-MSI.

5.2 Aims of the chapter

The aim of this chapter was to improve the detection of hydrocortisone in *ex-vivo* skin tissue by MALDI-MSI using a hydrazine-based derivatisation approach investigation.

5.3 Materials and methods

5.3.1 Chemicals and materials

2,5-dihydroxybenzoic acid (DHB), phosphorus red, methanol (MeOH), trifluoroacetic acid (TFA), Girard's reagent T (GirT), hydrocortisone (HC) and conductive indium tin oxide (ITO)-coated microscope glass slides were purchased from Sigma-Aldrich.

5.3.2 *Ex-vivo* skin samples

Ex-vivo human skin (obtained under licence from the New York Firefighters Skin Bank) was treated for 48 hours with 800 µL of hydrocortisone at concentration 0.1% (w/w) dissolved in ethanol/water solution (15:85) using Franz-type diffusion cells (Seo, Kim and Kim, 2016). (This tissue already treated was kindly provided by Croda Inc. (Delaware) and these experiments were conducted in Croda's US Laboratories in Delaware USA).

The tissue was transferred into the Leica Cryostat (Leica CM3050 S) and 12 µm tissue sections were cryosectioned, thaw mounted onto ITO glass slides, and stored at −80 °C.

5.3.3 In-solution derivatisation

The in-solution derivatisation was performed by mixing 100 µL of hydrocortisone standard (200 µg/mL in MeOH 70%) with 100 µL of GirT (5 mg/mL in MeOH

with 0.2% TFA); the final concentration of HC was 0.28 mM. The reaction was left at room temperature for 30 minutes.

5.3.4 Mass spectrometric profiling

Standard hydrocortisone (100 µg/mL in MeOH 70%; the final concentration of HC was 0.28 mM) and derivatised hydrocortisone with Girard's reagent T (GirT-HC) (prepared as previously described), were mixed with DHB matrix (10 mg/mL in 70% MeOH with 0.2% TFA) in ratio 1:1 by using the dried droplet method. Then, three spots (0.5 µL) from each mixture were deposited across the length of the MALDI stainless steel plate and then allowed to dry at room temperature prior to mass spectrometric analysis.

5.3.5 On-tissue derivatisation

On-tissue derivatisation was performed following the protocol by Barré *et al.* (Barré *et al.*, 2016). Briefly, 18 layers of GirT (5 mg/mL in MeOH with 0.2% TFA) were sprayed onto 12 µm thick *ex-vivo* skin sections by using a SunCollect^{TM} automated sprayer (SunChrom, USA). The flow rate was set at 10 µL/min for the first layer, at 15 µL/min for the second layer and at 20 µL/min for the remaining layers. Prior to matrix deposition, the tissue sections were placed in a pipette tip box containing 60 mL of 50% MeOH with 0.2% TFA and incubated at 40 °C for 150 min.

5.3.6 Matrix deposition

After spraying the derivatisation reagent, the matrix (10 mg/mL DHB in 70% MeOH with 0.2% TFA) was deposited onto the tissue sections surface using the SunCollect^{TM} automated sprayer (SunChrom, USA). 29 layers of matrix were sprayed with a flow rate of 10 µL/min for the first layer, 15 µL/min for the second layer and 20 µL/min for the following 27 layers.

5.3.7 Instrumentation

5.3.7.1 MALDI mass spectrometry profiling (MALDI-MSP)

The MALDI-MSP spectra were manually acquired in positive mode using an Autoflex III (Bruker Daltonik GmbH, Germancy) equipped with a 200-Hz Smartbeam^{TM} laser. The mass range was set at 100-1000 *m/z* and six hundred laser shots were acquired for each spectrum. External mass calibration was achieved using a phosphorus red standard at approximately 200 ppm.

5.3.7.2 MALDI mass spectrometry imaging (MALDI-MSI)

For MALDI-MSI, the experiments were performed using an Autoflex Speed equipped with Smartbeam^{TM} II laser (Bruker Daltonik GmbH). MALDI-MS images were acquired in positive mode at a range of *m/z* 100-700. The spatial resolution was set to 50 µm.

5.3.7.3 Data processing

MALDI-MSP data were acquired using FlexControl (Bruker Daltonics, Germany), converted to .txt file format using FlexAnalysis (Bruker Daltonics, Germany) and analysed using Mmass v5 open source software (Strohalm *et al.*, 2010)

For MALDI-MSI, the data were processed using FlexImaging 4.1 software (Bruker Daltonics, GMbH) and were normalised to the total ion current (TIC).

5.4 Results and discussion

5.4.1 MALDI-MS profiling

To illustrate the low ionisation efficiency of the targeted analyte, a standard solution of hydrocortisone (100 µg/mL) was first examined by MALDI-MS profiling using DHB matrix. As shown in Figure 5.1 a low signal intensity of the protonated peak of HC $[M+H]^+$ at *m/z* 363 was observed. The MALDI-MS spectrum displayed, instead, an abundance of matrix related peaks, including the $[M+H_2O+H]^+$ peak at *m/z* 137; the $[M]^+$ peak at *m/z* 154; $[M+H]^+$ peak at *m/z* 155; the $[M+Na]^+$ peak at *m/z* 273; and the $[2M-2H_2O+H]^+$ peak at *m/z* 273. The peaks at *m/z* 304 and at *m/z* 332 could derive from the stainless steel MALDI plate, as described by Yang *et al.* (Yang *et al.*, 2010).

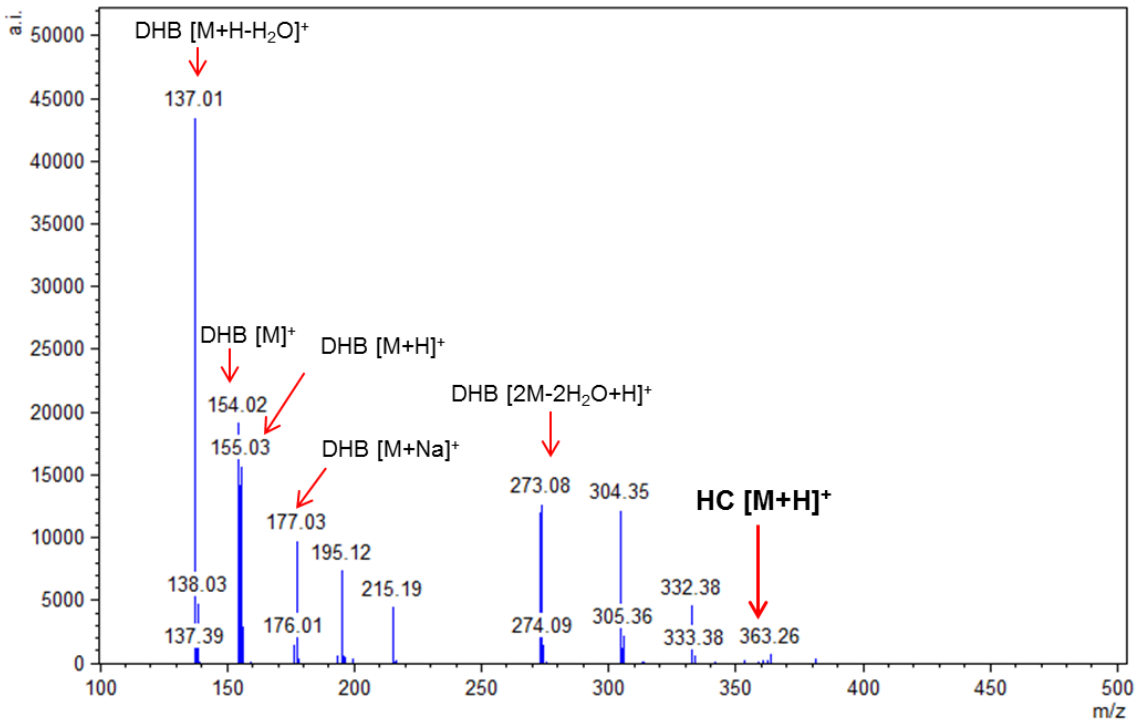

Figure 5.1 *MALDI-MS spectrum of hydrocortisone standard (100 µg/mL) in positive mode using DHB as matrix. The protonated HC peak $[M+H]^+$ at m/z 363 was detected at low intensity.*

5.4.2 In-solution chemical derivatisation

Because of its hydrophobic properties, the detection of hydrocortisone by MALDI-MS was highly challenging and, for this reason, a chemical derivatisation approach was tested. The target for the reaction was the carbonyl group and the Girard's reagent T (GirT) was chosen as reagent for the derivatisation. GirT is a hydrazine derivative that reacts with carbonyl compounds to form hydrazones. Figure 5.2 illustrates the reaction scheme of GirT with HC.

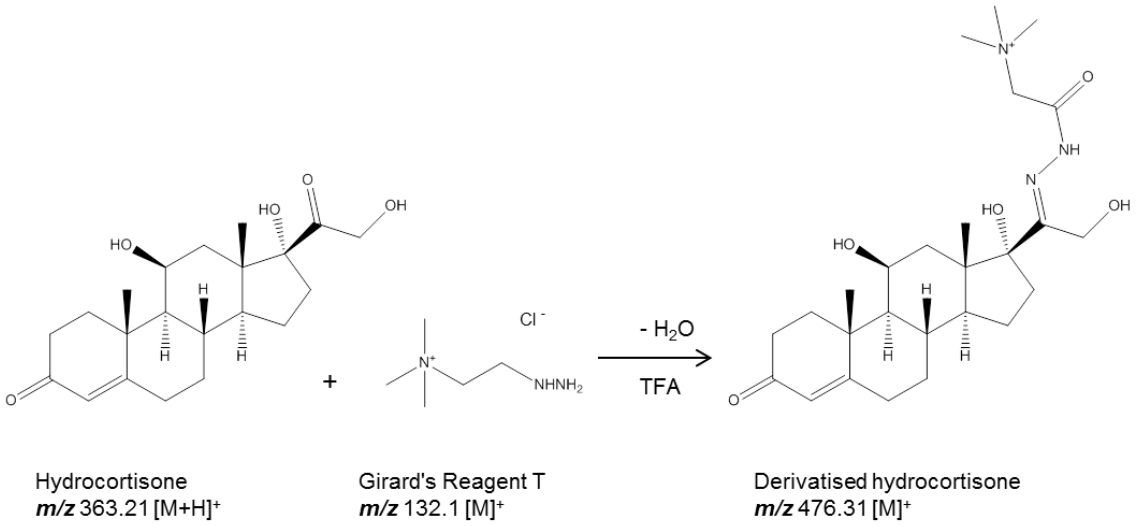

Figure 5.2 *Reaction scheme for GirT reagent reaction with HC*

The permanent positive charge of this reagent leads to a highly abundant $[M]^+$ ion for the derivatised product, detected in mass spectra (Griffiths *et al.*, 2003). Generally, the GirT reaction with carbonyl functionalities takes place in organic solvents in the presence of an acidic catalyst at high temperatures (Naven and Harvey, 1996; Cobice *et al.*, 2016). In this study, the reaction was performed at room temperature for 30 minutes.

Figure 5.3 shows the spectrum of hydrocortisone following the in-solution derivatisation reaction with GirT analysed with DHB as matrix. The MALDI-MS spectrum displayed the hydrazone derivative ($[M]^+$) peak at *m/z* 476 and the un-reacted Girard's reagent T ($[M]^+$) at *m/z* 132, which represented the highest peak.

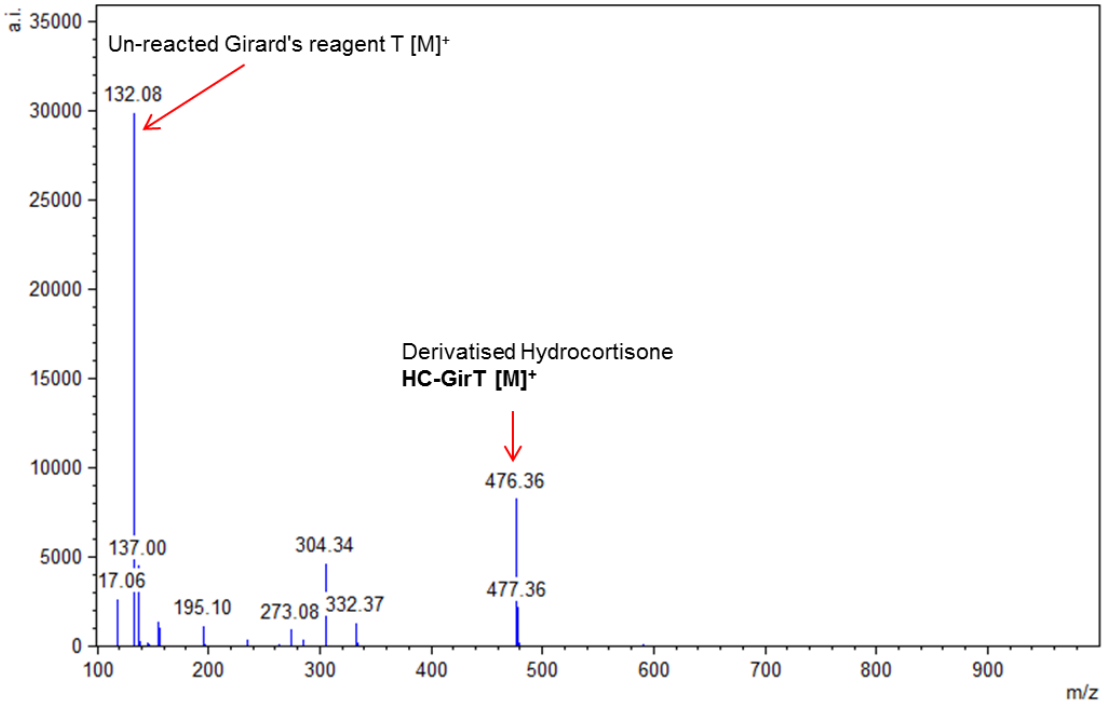

Figure 5.3 *MALDI-MS spectrum displaying hydrocortisone following the in-solution derivatisation reaction with GirT. The spectrum shows the derivatised hydrocortisone* $[M]^+$ *at m/z 476 and the un-reacted GirT* $[M]^+$ *at m/z 132.*

Although HC contains two carbonyl functionalities only the derivatisation of one carbonyl group was detected potentially due to the steric accessibility. As shown in Figure 5.4A-B the derivatisation reaction successfully increased the sensitivity and detection of the derivatised hydrazone ion (*m/z* 476) by approximately 11 fold compared to the un-derivatised HC (*m/z* 363) using MALDI-MS. The greatly increased signal intensity for GirT-HC was also confirmed when the relative intensity was investigated (intensity peak of targeted analyte/intensity peak of matrix) (Figure 5.3C).

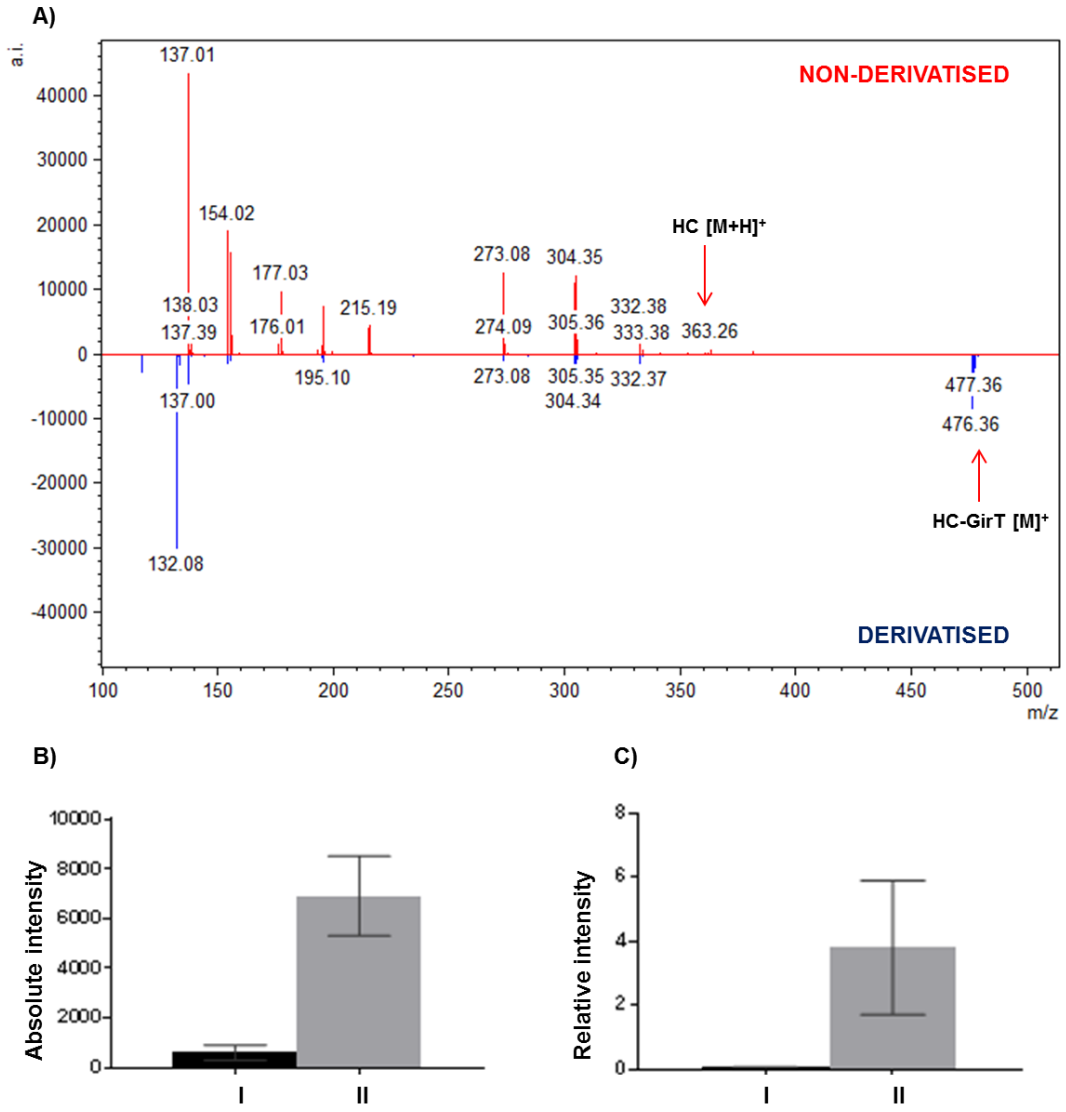

Figure 5.4 *A) Comparison of positive ion MALDI MS spectra of hydrocortisone (HC) standard (without derivatisation) and derivatised hydrocortisone with Girard's reagent T (GirT-HC). Graph showing absolute B) and relative intensity C) of HC (I) and GirT-HC (II). For relative intensity, the peaks of HC ($[M+H]^+$; m/z 363) and GirT-HC ($[M]^+$; m/z 476) were normalised with the $[DHB+H]^+$ peak at m/z 155. The error bars illustrate the standard deviation of nine spectra per analyte.*

5.4.3 On-tissue chemical derivatisation

Once the derivatisation reaction had shown successful results in solution, the GirT reagent was used for on-tissue derivatisation experiments to facilitate the

detection of hydrocortisone in *ex-vivo* skin samples by using MALDI-MS imaging. Previous MALDI-MS imaging experiments reported the use of GirT derivatisation to improve the detection of endogenous androgens in mouse testis (Cobice *et al.*, 2016), and corticosterone in rat adrenal and mouse brain sections (Cobice *et al.*, 2013). In a more recent work, instead, Barré *et al.* used GirT derivatisation to localise and quantify the levels of triamcinolone acetonide in cartilaginous tissue by using MALDI-MSI (Barré *et al.*, 2016). It is understandable that for a molecule with poor ionisation efficiency, detection in tissue is increasingly difficult, since its ionisation will also be affected by ion suppression effects from the presence of other compounds in the tissue.

Figure 5.5A-B shows MALDI-MSI of the distribution of the un-reacted Girard's reagent T (GirT $[M]^+$; *m/z* 132) and the derivatised hydrocortisone (GirT-HC $[M]^+$; *m/z* 476) recorded at 50 µm pixel size following a derivatisation reaction on 2 of 6 sections of *ex-vivo* skin treated with hydrocortisone 0.1% (w/w) for 48 hours. A defuse signal was observed for the un-reacted Girard's reagent T, whereas a very clear signal for the derivatised HC appeared localised only onto the epidermal layer of the skin.

The on-tissue derivatisation approach was successful therefore in increasing the sensitivity of the drug in an imaging experiment, when otherwise it could not be detected (data not shown).

A)

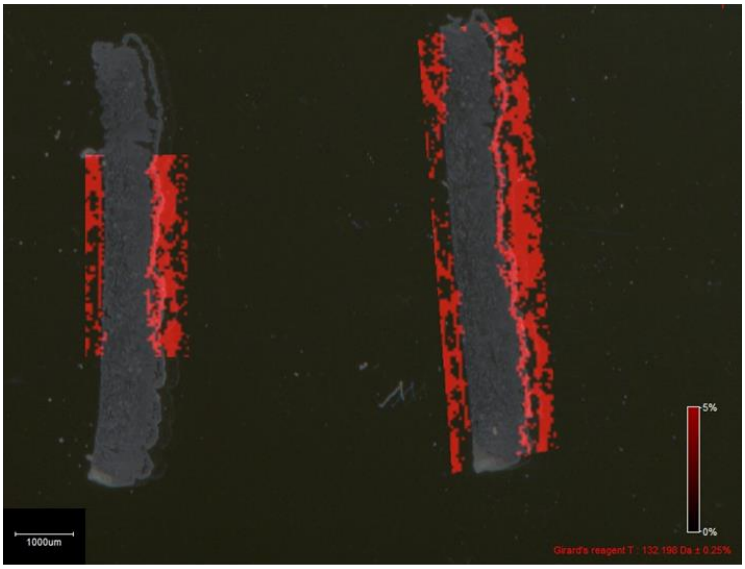

B)

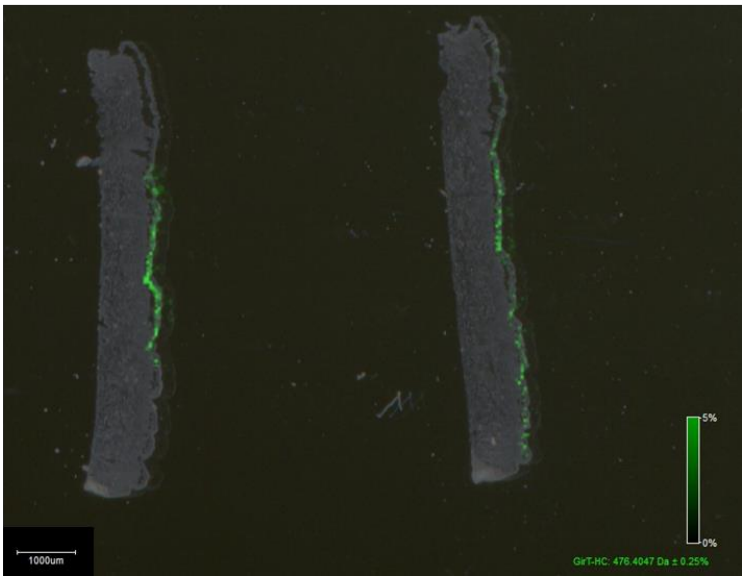

Figure 5.5 *MALDI-MS images displaying the localisation of A) the un-reacted Girard's reagent T ($[M]^+$; m/z 132) and B) the derivatised hydrocortisone (HC-GirT, $[M]^+$; m/z 476). Spatial resolution = 50 µm; TIC normalisation.*

5.5 Concluding remarks

In this chapter, an in-solution and on-tissue derivatisation approach for the detection of hydrocortisone (HC) in *ex-vivo* skin tissue were tested.

The derivatisation reaction using the Girard reagent T, a hydrazine based reagent, led to greatly increased sensitivity and detection of the respective hydrazone derivative ($[M]^+$) over the non-derivatised HC. To our knowledge, this is the first study to report the localisation of hydrocortisone in *ex-vivo* skin samples by using MALDI-MSI. This represents a notable advantage over the traditional techniques since the spatial information is preserved. The localisation of hydrocortisone-derivative was found to be only in the epidermal layer of *ex-vivo* skin tissue after 48 hours of treatment. Future experiments are necessary to optimise the derivatisation method to generate a further increase of the derivatised analyte. These include changing the temperature and time of derivatisation reaction as well as selection of an optimal matrix for analysis.

Chapter 6: Investigation of xenobiotic metabolising enzymes in Labskin using MALDI-MSI.

6.1 Introduction

In Chapter 1 the role of skin as a protective barrier to the environment and valuable site for drug administration was comprehensively investigated. Although skin biology has been widely studied over the years, the current state of knowledge regarding metabolic activity of this organ is still poor (van Eijl *et al.*, 2012; Oesch *et al.*, 2014; Manevski *et al.*, 2015). Understanding of the metabolic activity of skin is extremely important in order to assess the pharmacological as well as toxic effects of exposure to xenobiotic compounds, such as environmental chemicals, cosmetics and pharmaceuticals. In this regard, a pivotal role is represented by xenobiotic-metabolising enzymes (XMEs) and information about their expression in the skin is crucial.

The European Legislation, Directive 76/768 ECC prohibited the use of animal models for the toxicity testing of cosmetics and cosmetic ingredients; leading to an increased interest in the use of reconstructed 3D skin models (EU, 2003). In addition, given the difficulties in reliably obtaining human skin for metabolism studies (and sufficient skin for a representative study given issues including race, gender, age, and genetic polymorphisms) there has been interest in the use of 3D models in this area. In the United Kingdom, the NC3Rs (National Centre for the Replacement, Refinement, and Reduction of Animals in Research) instigated in 2016 a challenge to researchers “To establish, both qualitatively (which metabolites are produced) and quantitatively (concentration of the metabolites produced), the extent to which skin metabolism determines xenobiotic availability in human skin” (https://crackit.org.uk/challenge-20-metaboderm).

In this regard, a growing interest in using 3D skin models to investigate the metabolic activity of human skin has spread rapidly (Sugibayashi *et al.*, 2004; Wiegand, Hewitt and Merk, 2014). A detailed review comparing the xenobiotic-metabolising enzymes in human skin and reconstructed skin models was recently published by Oesch *et al.* (Oesch, Fabian and Landsiedel, 2018).

Contradicting the earlier published work in the field (Ahmad and Mukhtar, 2004; Baron *et al.*, 2008), more recent studies have reported a low expression of cytochrome P450 (CYP) enzymes in human skin and stated that they have an

insignificant role in the metabolism of substances. In the work described by van Eijl *et al.* a detailed proteomic study was performed to investigate phase 1 and phase 2 enzymes in whole *ex-vivo* human skin (10 donors) and in 4 *in-vitro* epidermal models (Epiderm, Episkin, RHE, and HaCat cells) (van Eijl *et al.*, 2012). Results from this study indicated that low levels of CYP enzymes were detected in the skin and the main metabolic activity of the skin was due to the presence of other enzyme families. The enzymes detected belonged to the families of: alcohol dehydrogenases, aldehyde dehydrogenases oxidases, e.g. amine oxidase, carbonyl reductases, epoxidases and carboxylesterase hydrolyses (from phase 1 enzymes) and several isoforms of glutathione S transferase (from phase 2 enzymes). Similarly, Hewitt *et al.* (Hewitt *et al.*, 2013) and Wiegand et *al.* (Wiegand, Hewitt and Merk, 2014) also reported no or a low expression of CYP enzymes in *ex-vivo* human skin and *in-vitro* skin models. In all of these studies *in-vitro* skin models highly mirrored the enzymatic profiles of whole *ex-vivo* skin, indicating that these are a valuable alternative to human or animal skin for experimentation in this area.

Working towards this aim, mass spectrometry imaging (MSI) has been employed to localise the presence of metabolising enzymes in full thickness *ex-vivo* human skin and a commercial skin model. In order to achieve this, the Clench group developed "substrate-based mass spectrometry imaging" (SBMSI) (Newton *et al.*, 2017). In the work reported by Newton *et al.* the surface of the skin or model was treated with a known substrate for a specific metabolising enzyme, left to incubate for 48 hours before a section through the skin model was examined by MALDI-MSI. Results indicated a presence of esterase activity in a full thickness skin model using methylparabens as a probe (Abbas *et al.*, 2010).

There are several reports in the literature which highlight the expression of esterases in skin, with predominant levels in the epidermal layer and hair follicles (Müller *et al.*, 2003). In the work reported by Tokudome *et al.* the levels of carboxylesterase activity in human epidermal cultured skin models (LabCyte EPI-MODEL and EPI-DERM) were deemed comparable to those detected in human and rat epidermis (Tokudome, Katayanagi and Hashimoto, 2015).

Carboxylesterases act by adding water to an ester group leading to the release of a carboxylic acid and an alcohol, increasing in this way the polarity of the molecule and facilitating its elimination (Laizure *et al.*, 2013). Two main carboxylesterase isozymes have been found in humans: carboxylesterase 1 (CES1) and carboxylesterase 2 (CES2). The activity of these strongly depends on the substrate structure: esters with a large acyl group and a small alcohol group are preferentially hydrolysed by CES1, whereas esters with a small acyl group and a large alcohol group are preferentially hydrolysed by CES2 (Taketani *et al.*, 2007).

In the following chapter, two CES1 substrates, methylparaben and methylphenidate, have been chosen in order to investigate the esterase activity in a commerical living skin equivalent model, Labskin (Innovenn Ltd York UK), by using MALDI-MSI following the SBMSI approach. A chemical derivatisation approach was additionally performed in order to increase the sensitivity of both methylparaben and its metabolite 4-hydroxybenzoic acid and allow their detection by MALDI mass spectrometry. As described in Chapter 5, molecules containing functional groups with low protonation efficiency are challenging to analyse by mass spectrometry tools and a chemical derivatisation strategy is often employed as solution to overcome this drawback. Furthermore, LC-MS/MS analysis on extracts of epidermis and dermis derived from substrate-treated Labskin was performed for comparison with the MALDI-MSI data.

6.2 Aims of the chapter

The aim of this chapter was to investigate the metabolic esterase activity of Labskin using MALDI-MSI by employing the approach of “substrate-based mass spectrometry imaging” (SBMSI).

6.3 Materials and methods

6.3.1 Chemical and materials

Alpha cyano-4-hydroxycinnamic acid (α-CHCA), N-(1-naphthyl) ethylenediamine dihydrochloride (NEDC), trifluoroacetic acid (TFA), phosphorus red, methylphenidate hydrochloride (MPH HCl), ritalinic acid (RA), methylparaben (MP), 4-hydroxybenzoic acid (4-HBA) and isosorbide dimethyl ether (DMI), ethanol (EtOH), formic acid ≥ 96% (FA), 2-fluoro-1-methylpyridinium p-toluenesulfonate (FMPTS), and triethylamine (TEA) were purchased from Sigma Aldrich (Gillingham, UK). Acetonitrile (ACN) and methanol (MeOH) were purchased from Fisher Scientific (Loughborough, UK).

6.3.2 Living skin equivalent samples

Living skin equivalent (LSE) samples were obtained and cultured as described in Chapter 2.3.2. For the experiment, three LSE samples were treated with 20 µL of methylphenidate hydrochloride (0.5% w/w) dissolved in an emulsion made up of water/olive oil (80:20 v/v) with 10% DMI; three LSE samples were treated with 20 µL of methylparaben (0.5% w/w) dissolved in acetone/olive oil (80:20) with 10% DMI. The samples were incubated for 24 hours. After incubation, the samples were taken and washed with LC-grade MeOH to remove the excess formulation and, then snap-frozen with liquid nitrogen cooled isopentane (2-5 min) and stored at - 80 °C.

For cryosectioning, LSEs were transferred into the cryostat (Leica 200 UV, Leica Microsystems, Milton Keynes, U.K.), mounted onto a cork ring using diH_2O at −25 °C for 30 min to allow thermal equilibration. Tissue sections were

cryosectioned at 12 µm, thaw mounted onto poly-lysine coated glass slides, and stored at −80 °C.

6.3.3 In-solution derivatisation

The in-solution derivatisation was performed on the hydroxyl group of MP and 4-HBA by following previously published work carried out by Beasley *et al.* (Beasley, Francese and Bassindale, 2016). 40 µL of FMPTS (10 mg/mL in acetonitrile) and 10 µL of triethylamine were mixed by vortexing. Then, 20 µL of MP and 4-HBA solution, both at concentration of 350 µg/mL in MeOH/H_2O (1:1, v/v)) was added. The reactions were left for 5 min at room temperature. The final concentration of MP and 4-HBA was 0.66 mM and 0.72 mM, respectively.

6.3.4 Mass spectrometric profiling

Standard methylparaben (MP), methylphenidate (MPH), 4-hydroxybenzoic acid (4-HBA), ritalinic acid (RA) prepared at 100 µg/mL in MeOH/H_2O (1:1, v/v)), as well as derivatised MP and 4-HBA with FMPTS reagent (prepared as previously described), were analysed by using MALDI-MS profiling. For positive mode the matrix used was 5 mg/mL of α-CHCA in ACN/0.5%TFA (7:3, v/v), whereas for negative mode the matrix used was 7 mg/mL of NEDC in MeOH/H_2O (7:3, v/v).

Each standard and derivatised compound (FMPTS-MP and FMPTS-4-HBA) were mixed with matrix solution (ratio 1:1) by using the dried droplet method.

Then, three spots (0.5 µL) from each mixture were deposited across the length of the MALDI stainless steel plate and then allowed to dry at room temperature prior to mass spectrometric analysis.

6.4 Instrumentation

6.4.1 MALDI mass spectrometry profiling (MALDI-MSP)

The MALDI-MSP spectra were manually acquired in both positive and negative mode using a Waters MALDI HDMS Synapt^{TM} G2 operated with a 1 KHz Nd:YAG laser (Waters Corporation, Manchester, UK) and an Autoflex III (Bruker Daltonik GmbH, Germancy) equipped with a 200-Hz Smartbeam^{TM} laser.

The mass range was set at 100-1500 m/z and external mass calibration was achieved using a phosphorus red standard at approximately 200 ppm.

6.4.2 MALDI mass spectrometry imaging (MALDI-MSI)

All tissues were imaged using the Synapt™ G2. MALDI-MS images were acquired in positive mode, in full scan “sensitivity” mode at a range of m/z 100-1500, (resolution 10,000 FWHM) at spatial resolution of 60 µm x 60 µm, and with laser energy set to 250 arbitrary units. The ion mobility function of the instrument was not enabled.

6.4.3 LC-MS/MS

All LC–MS/MS experiments were performed using a Xevo G2-XS QTof (Waters Coorporation, Manchester, U.K.) set to ionization mode ESI+ with analyzer in sensitive mode. The mobile phase composition, the gradient elution, as well as the flow rate and the injection volume were set as described in Chapter 4.6.2.

The experimental instrument parameters used were capillary voltage, 3.0 kV; cone voltage, 30.0 V; source temperature, 150 ºC; desolvation temperature, 500 ºC; desolvation gas, 1000 L/h; and cone gas, 150 L/h. Argon was utilised as a collision gas and the collision energy was set at 15 eV.

A multiple reaction monitoring (MRM) method was used to monitor the following transitions for methylphenidate (m/z 234.2 → 84) and for ritalinic acid (m/z 220.1 →84). The retention time for methylphenidate was ~ 7.88 mins, whereas for ritalinic acid it was ~ 7.34 mins

6.4.4 Skin extraction

The extraction of CES1 substrates and metabolites from Labskin was performed as reported in Chapter 4.5.3.

6.4.5 Data processing

MALDI-MSP spectra on the Bruker Autoflex III were acquired using FlexControl (Bruker Daltonics, Germany) and converted to .txt file format using FlexAnalysis (Bruker Daltonics, Germany).

MALDI-MSP spectra on the Waters Synapt G2 were acquired and converted to .txt file format using MassLynx™ software (Waters Corporation, UK).

The spectra exported as .txt files were analysed using Mmass v5 open source software (Strohalm *et al.*, 2010).

6.5 Results and discussion

6.5.1 MALDI-MS profiling of carboxylesterase 1 probes and metabolites

6.5.1.1 Methylparabens/4-hydroxybenzoic acid

Methylparaben belongs to the parabens class and it is widely included as preservative in food and cosmetic formulations (Tahan *et al.*, 2016). It is metabolised by CES1 enzyme to 4-hydroxybenzoic acid, as shown in Figure 6.1.

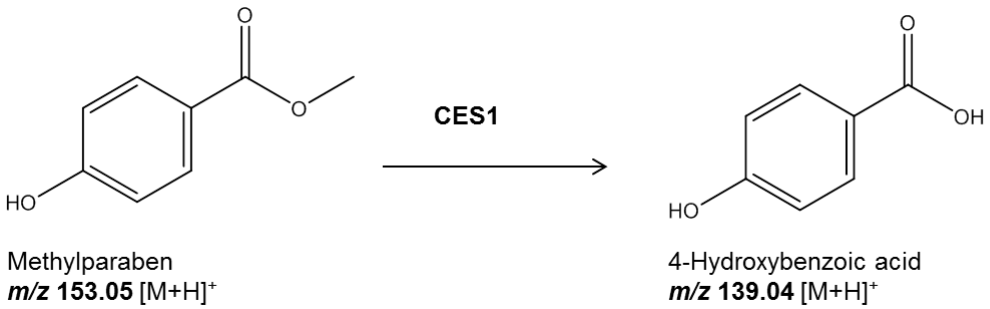

Figure 6.1 *Metabolism of methylparaben.*

Prior to investigating the metabolic activity in Labskin tissue, standards of methylparaben and its metabolite 4-hydroxybenzoic acid (100 µg/mL) were first analysed by MALDI-MS profiling using CHCA as matrix. As shown in Figure 6.2 from MALDI MSP spectra no protonated peaks were detected for both analytes (methylparabens $[M+H]^+$, *m/z* 153.05; 4-hydroxybenzoic acid $[M+H]^+$, *m/z* 139.04).

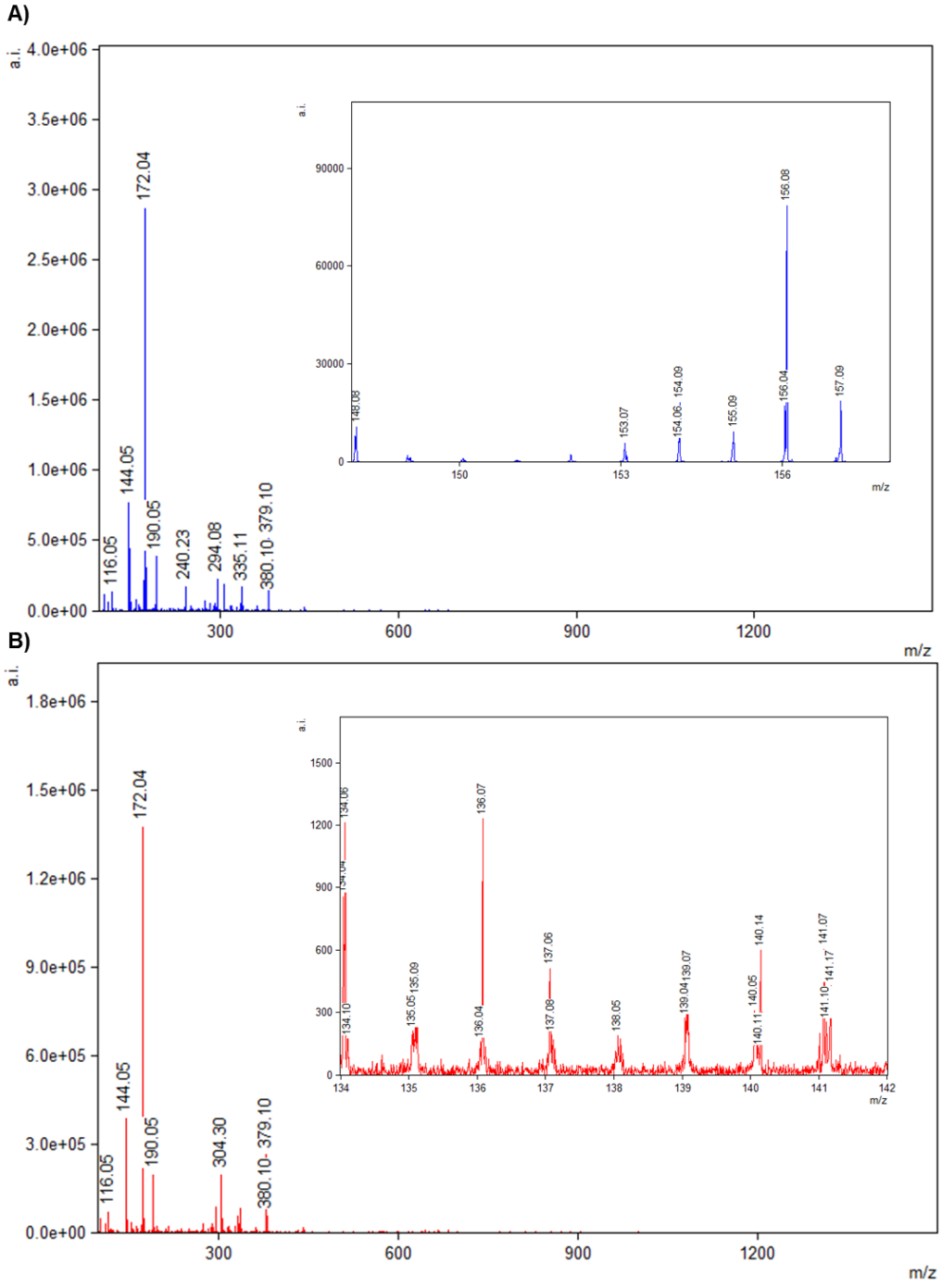

Figure 6.2 *MALDI-MS spectrum acquired in positive mode on A) the spot of methylparaben (100 µg/mL) and B) 4-hydroxybenzoic acid mixed with the matrix α-CHCA. There was no evidence of the expected protonated peaks* $[M+H]^+$ *at m/z 153.05 and at m/z 139.04 for methylparabens and 4-hydroxybenzoic acid, respectively.*

The difficulty of detecting MP and 4-HBA analytes in positive mode was due to the low protonation efficiency of their functional groups: hydroxyl and carboxyl acid groups. Compounds containing hydroxyl groups bonded to an aliphatic structure (alcohols) are neutral molecules, and hence, they are not easily ionised in either positive or negative mode; instead, compounds containing the hydroxyl group bonded to a phenyl group (phenols) are slightly acidic and, hence, they are more likely to ionise in negative mode (Quirke, Adams and Van Berkel, 1994; Bajpai *et al.*, 2005). Similarly, compounds containing carboxylic groups have been previously shown to be more suited to ionisation in negative mode (Shroff and Muck, 2007). In this regard, MP and the metabolite 4-HBA (100 µg/mL) standards were also analysed with negative polarity by using NEDC as matrix. The signals of the deprotonated peak of MP (*m/z* 151.04) and 4-HBA (*m/z* 137.02) were detected exclusively when the MALDI-MSP spectra were acquired by using an Autoflex III mass spectrometer (Bruker Daltonik GmbH, Germany) (Appendix III Figure 1-Figure 2). This finding is due to the fact that a Smartbeam laser, unlike conventional Nd:YAG lasers is more suitable to work with a wider range of matrices; hence, it is more likely to perform better analysis in negative mode (Holle *et al.*, 2006). The Smartbeam laser in the Bruker is a Nd:YAG laser and, as the Nd:YAG laser present in the Synapt, the laser wavelengh in both instruments is of 355 nm; however, the better performance of the Smartbeam laser for several MALDI matrices is due to the laser beam profile. The Nd:YAG laser (in Synapt) is characterised by a very focused Gaussian profile whereas, Smartbeam laser (in Bruker) presents a structured beam profile, similar to that of N_2 laser. In the work reported by Holle *et al.* the influence of the laser beam profile, more than the wavelength, on the MALDI performance was highlighted; and, a comprehensive description of the modulation of the Nd:YAG in the Bruker was offered (Holle *et al.*, 2006). As consequence of this modulation, the Smartbeam laser "mimics" the beam profile, and hence the distribution of the intensity over the target surface, of the N_2 laser.

Besides NEDC matrix, in this study it could have been interesting to investigate a larger number of negative mode matrices in order to assess the potential detection of MP and 4-HBA also with Synapt. However, considering the high performance of Nd:YAG laser in Synapt instrument with CHCA matrix in positive

mode, a derivatisation strategy, fast and cost-effective, seemed to be a valid alternative over the matrix optimisation step, that could have been extensive and time consuming.

6.5.1.1.1 In-solution derivatisation

To increase the sensitivity of the methylparaben and 4-hydroxybenzoic acid in positive mode a derivatisation approach was investigated. The hydroxyl group was chosen as target group for the derivatisation, since it was a common functional group for both compounds. 2-fluoro-1-methylpirydinium p-tolunesulfonate (FMPTS) was selected as derivatisation reagent, which reacts with hydroxyl groups, in the presence of the basic catalyst triethylamine to form the corresponding N-methylpyridinium ether derivative, as shown in Figure 6.3.

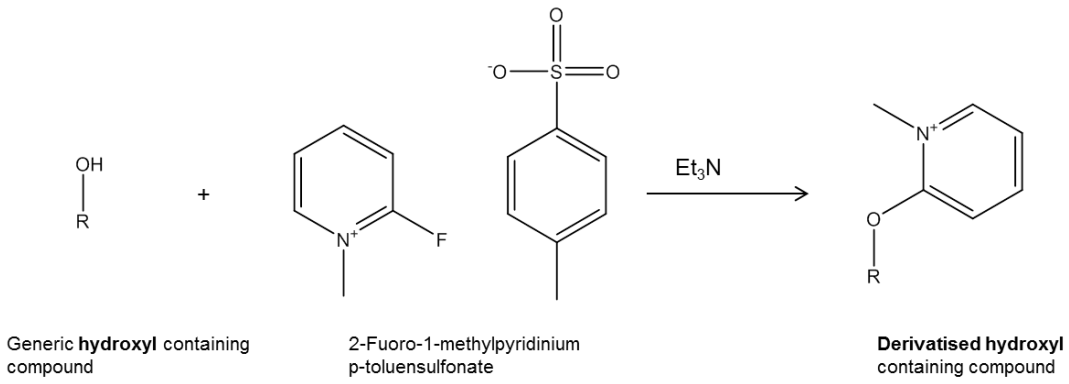

Figure 6.3 *Reaction scheme for 2-fluoro-1-methylpyridinium p-toluensulfonate (FMPTS) with a generic hydroxyl containing compound.*

In previous studies FMPTS has been reported to increase the detection of hydroxyl containing compounds, due to its positive permanent charge, by using LC-MS (Dunphy *et al.*, 2001; Thieme, Sachs and Thevis, 2008), LC-MS/MS (Faqehi *et al.*, 2016; Baghdady and Schug, 2018) and MALDI-MS profiling (Hailat and Helleur, 2014). Furthermore, by using this reagent the derivatisation reaction could be performed rapidly at room temperature, making it extremely straightforward.

As shown in Figure 6.4 the in-solution derivatisation approach using FMPTS resulted in an increase in sensitivity for the MP and 4-HBA peaks, which were detected in the derivative forms $[M]^+$, FMPTS-MP (*m/z* 244.10) and FMPTS-4-HBA (*m/z* 230.08).

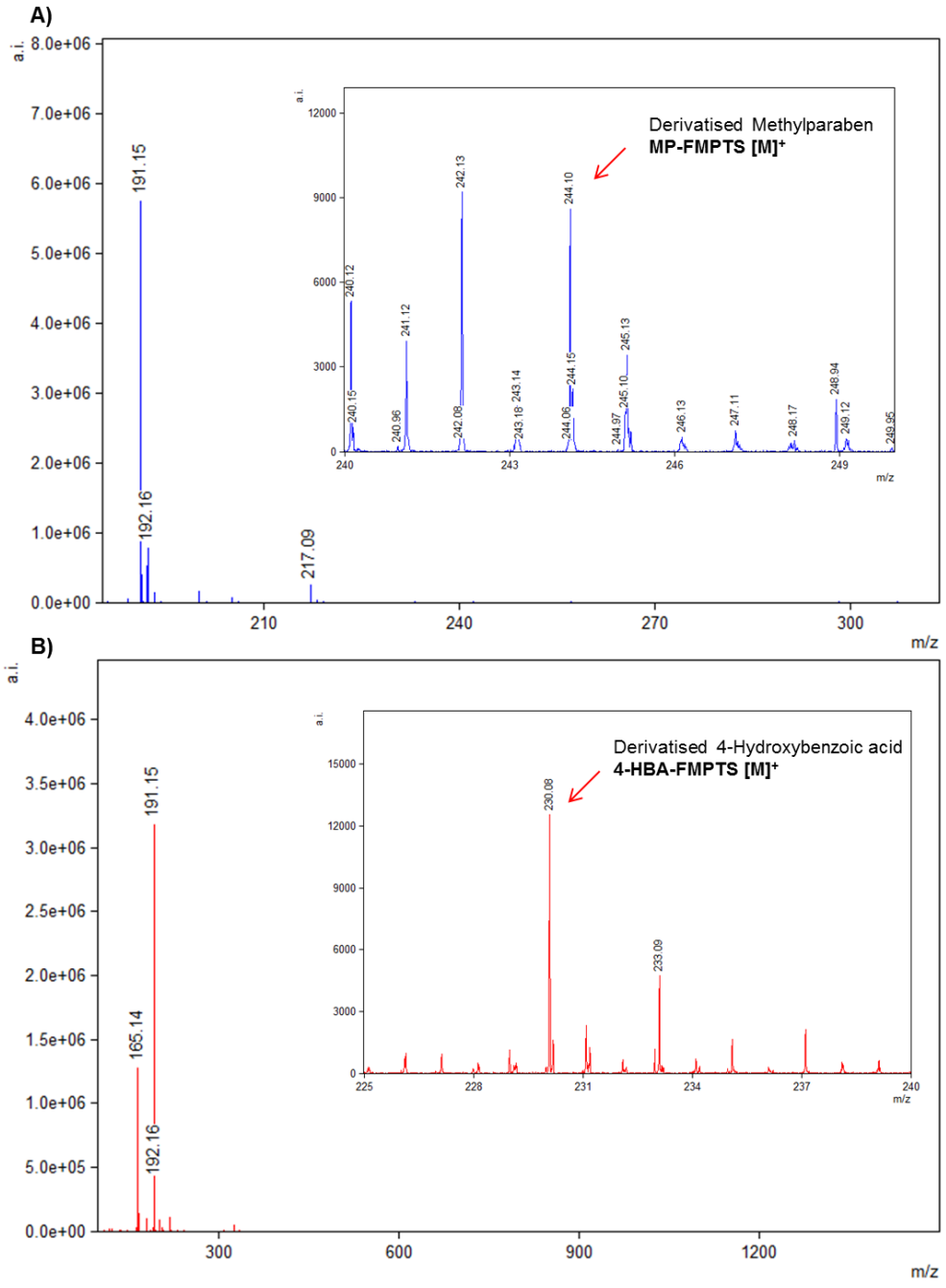

Figure 6.4 *MALDI-MS spectra showing MP and 4-HBA following the in solution derivatisation reaction with FMPTS. The spectra show the derivatised MP* $[M]^+$ *at m/z 244.10 (A) and the derivatised 4-HBA at m/z 230.08 (B).*

6.5.1.2 Methylphenidate/ritalinic acid

Another substrate chosen to investigate metabolic activity in the skin was methylphenidate. Methylphenidate is a central nervous system stimulant, used as medication for the treatment of attention-deficit/hyperactivity disorder (ADHD); it is commercially available in oral formulations in the forms of tablets, chewable tablets and liquid (Challman and Lipsky, 2000; Guzman, 2019). Although it is not possible to find a methylphenidate based topical formulation, in this study it was decided to treat Labskin with this substrate to analyse the expression of carboxylesterase enzymes in the skin. Like methylparabens, methylphenidate is metabolised by CES1 enzyme activity and its major metabolite is represented by ritalinic acid (Figure 6.5).

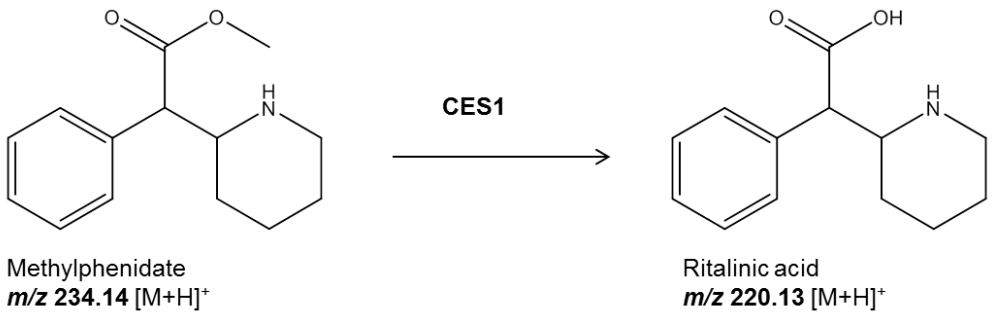

Figure 6.5 *Metabolism of methylphenidate.*

Standard solutions of methylphenidate (100 µg/mL) and its metabolite ritalinic acid (100 µg/mL) were analysed by MALDI-MS profiling using CHCA as matrix. MALDI-MS spectra showed the protonated peak of methylphenidate at *m/z* 234.14 and ritalinic acid at *m/z* 220.13 (Figure 6.6). The easy detection of these compounds by MALDI-MS can be attributed to the protonation efficiency of the amine group on the piperidine moiety. Although ritalinic acid contains two functional groups (amine and carboxylic acid) only the peak arising from monoprotonation was detected $[M+H]^+$. As discussed previously this aspect is due to the low protonation affinity of carboxylic groups in positive mode, which, instead, ionise preferably in negative mode.

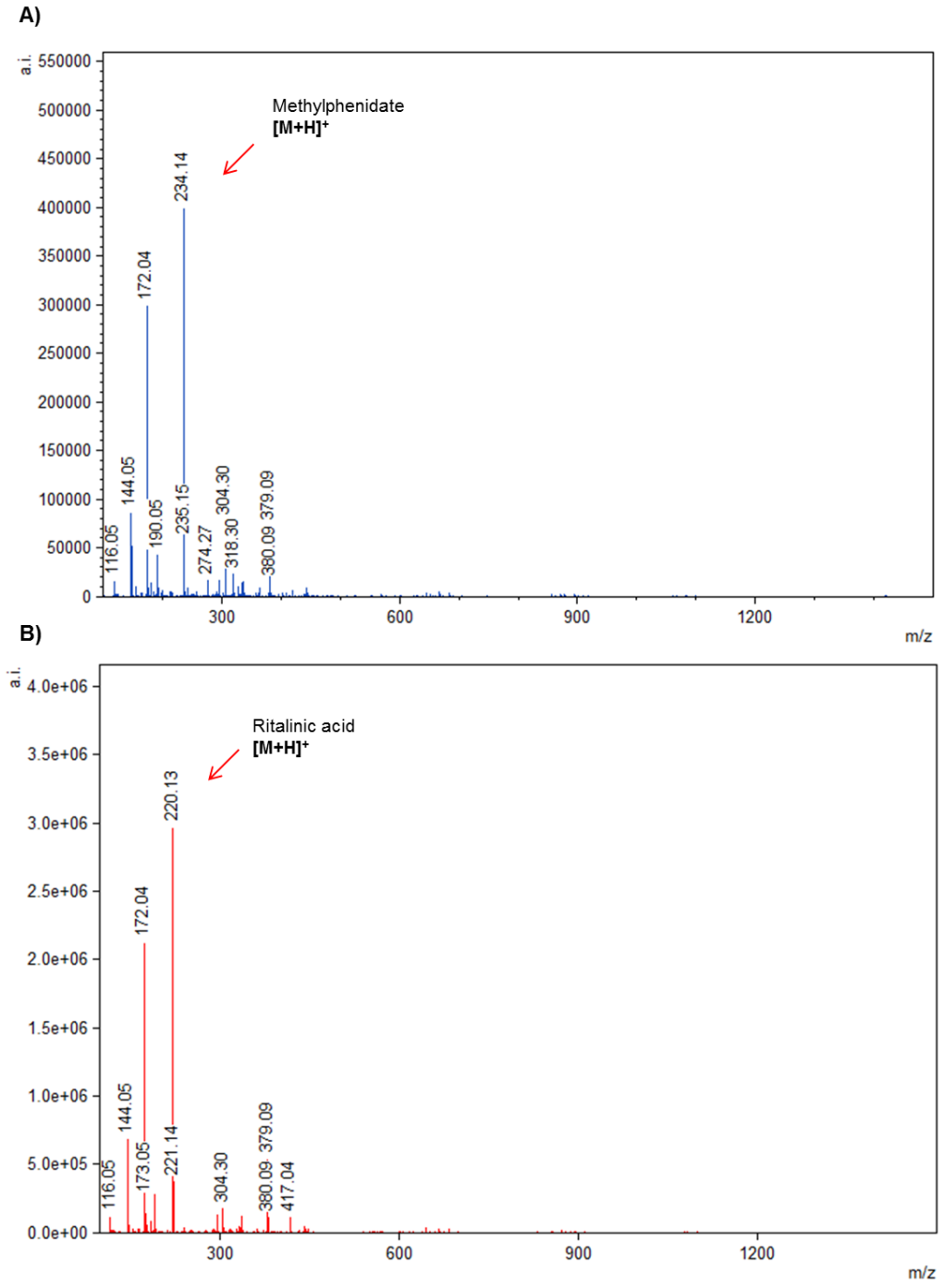

Figure 6.6 *MALDI-MS spectrum acquired in positive mode on a) the spot of methylphenidate (100 µg/mL) and B) ritalinic acid mixed with the matrix α-CHCA. MALDI-MSP spectra showed expected protonated peaks* $[M+H]^+$ *at m/z 234 and at m/z 220 for methylphenidate and ritalinic acid, respectively.*

6.5.2 Analysis of skin metabolism by MALDI-MSI

Following MALDI-MSP, MALDI-MSI experiments were performed to examine the carboxylesterase activity in Labskin by using the "substrate-based mass spectrometry imaging" (SBMSI) approach. For this purpose, Labskin tissue was treated with 0.5% w/w of CES1 substrates (methylparaben and methylphenidate) for 24 hours.

As previously discussed, an in-solution derivatisation with FMPTS was essential to increase the detection of methylparaben and its metabolite 4-hydroxybenzoic acid by using MALDI-MSP. In the work reported by Beasley *et al.* an in-situ derivatisation using FMPTS was exploited to detect cannabinoids in hair samples by MALDI-MSI (Beasley, Francese and Bassindale, 2016). For this experiment, the authors airbrushed FMPTS onto hairs derived from cannabis users and nonusers before spraying CHCA matrix. Six different cannabinoids, previously undetectable, were detected in hair samples by using this approach.

Following the same principle, in this study, an on-tissue derivatisation approach onto Labskin treated with methylparaben for 24 hours was attempted. The FMPTS reagent was manually sprayed onto treated Labskin sections and CHCA matrix was applied by sublimation. However, no successful images were achieved (data not shown). Lack of signal was most likely because an insufficient matrix coverage of derivatised Labskin sections was obtained with the sublimation method and hence further sample optimisation is required.

Experiments were then focused on the metabolic analysis by using methylphenidate substrate. A Labskin section treated with methylphenidate 0.5% (w/w) in water/olive oil (80:20) for 24 hours was imaged alongside a blank Labskin section (without treatment). The epidermal layer in the Labskin was identified by selecting an endogenous peak at *m/z* 186.91 (Figure 6.7A).

Figure 6.7B-C shows MALDI-MSI images of the distribution of methylphenidate ion at *m/z* 234 and ritalinic acid ion at *m/z* 220 in both blank and treated Labskin sections recorded at 60 µm spatial resolution. Standard methylphenidate and ritalinic acid (1 mg/mL) were spotted alongside the Labskin sections as references. It can be seen that the metabolite ritalinic acid signal appeared to

be localised in the outer layer of skin, epidermis. This suggests that the CES1 enzymes are potentially located in the epidermal layer of Labskin.

Additional work now needs to be performed in order to assess the levels of CES1 detected in Labskin and their comparability with those present in human skin.

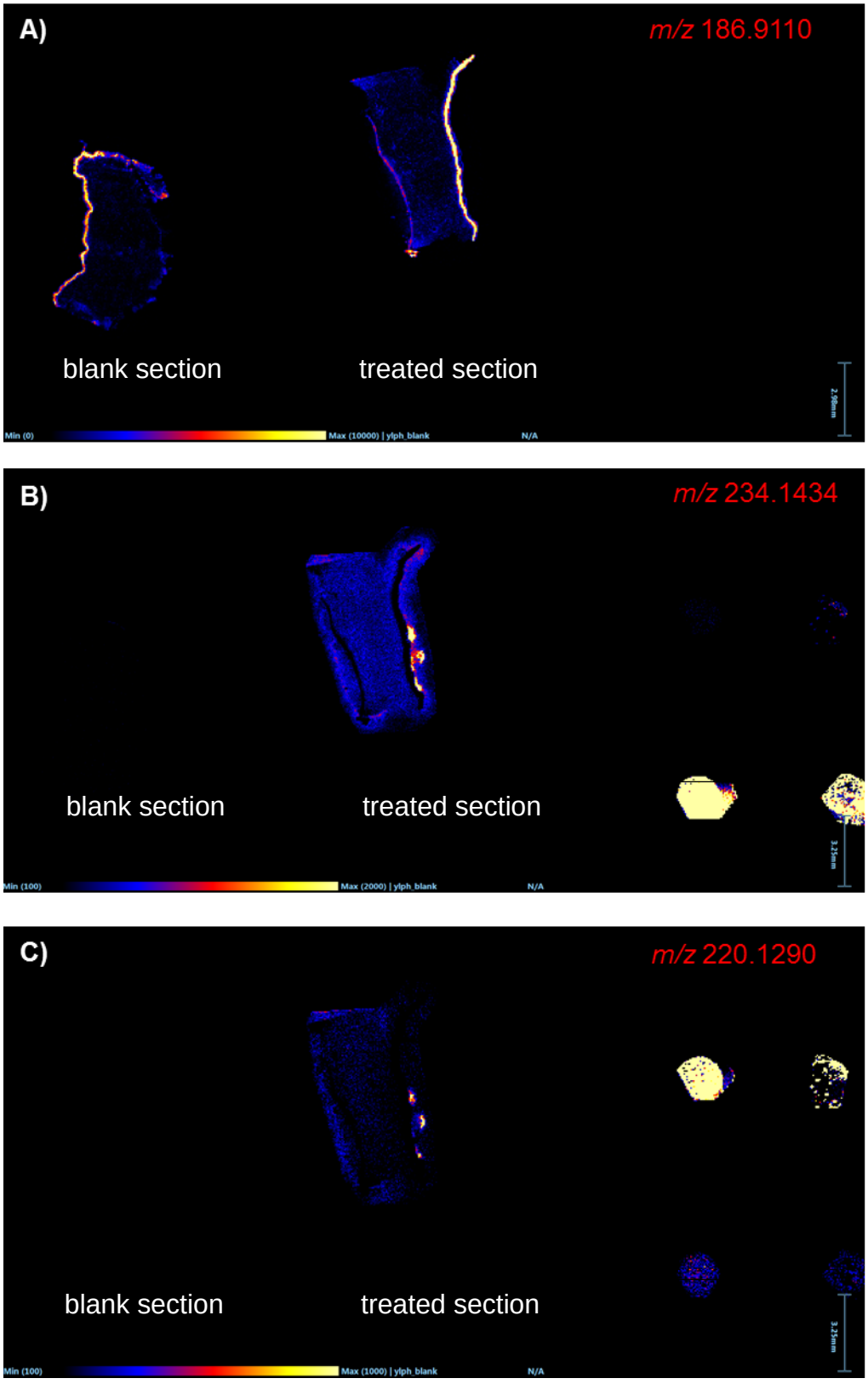

Figure 6.7 *MALDI-MSI on blank Labskin section and a section of Labskin treated with methylphenidate (0.5% w/w) for 24 hours showing the distribution of A) an endogenous peak at m/z 186 for the detection of epidermal layer; B) methylphenidate peak at m/z 234; C) ritalinic acid peak at m/z 220.*

6.5.3 LC-MS/MS

LC-MS/MS was used to enhance the sensitivity and selectively for the simultaneous determination of methylphenidate (MPH) and ritalinic acid (RA) in epidermal and dermal tissue extracts. Previous studies have reported the use of LC-MS/MS for the detection of MPH and RA in hair (Jang *et al.*, 2019) and urine samples (Danaceau, Freeto and Calton, 2018).

Figure 6.8 shows a representative MRM chromatogram of MPH and RA standards (10 ng/mL) obtained by selecting the transition of 234.2 → 84 for MPH (A) and 220.1 → 84 for RA (B). The retention time for MPH and RA was ~ 7.88 min and 7.34 min, respectively.

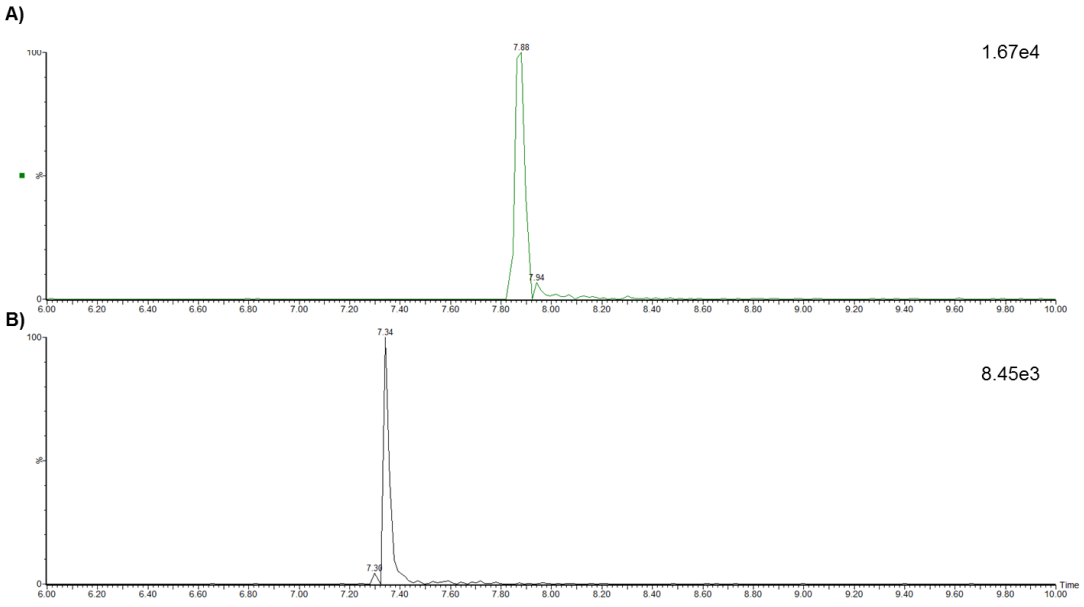

Figure 6.8 *Extracted ion chromatogram (XIC) for A) 10 ng/mL of methylphenidate and B) 10 ng/mL of ritalinic acid.*

It is important to note that higher concentrations of methylphenidate standard appeared to contain a percentage of ritalinic acid, probably as a degradation product. Furthermore, an insistent interfering MPH peak was observed in the following chromatograms (reagent blanks and ritalinic acid standards), due to the problem of an extended carry-over. Analyte carry-over is one of the most common drawbacks for LC-MS/MS during method development (Weng and

Hall, 2002). It mainly depends on the analyte contamination which can be selectively retained in the column as well as in the system. To troubleshoot this problem multiple investigations are necessary, such as changing the composition and the elution type of the mobile phase; using a strong needle washing solvent, increasing the number of blanks from one run to another; reducing the contact surface between analyte and needle.

In this case, as shown in Figure 6.9A to obtain a reagent blank chromatogram entirely free of MPH and RA an intense flushing of the column for several hours with acetonitrile was necessary. Figure 6.9 shows representative chromatograms of B) epidermis and C) dermis extracts derived from Labskin treated with MPH 0.5% (w/w) for 24 hours.

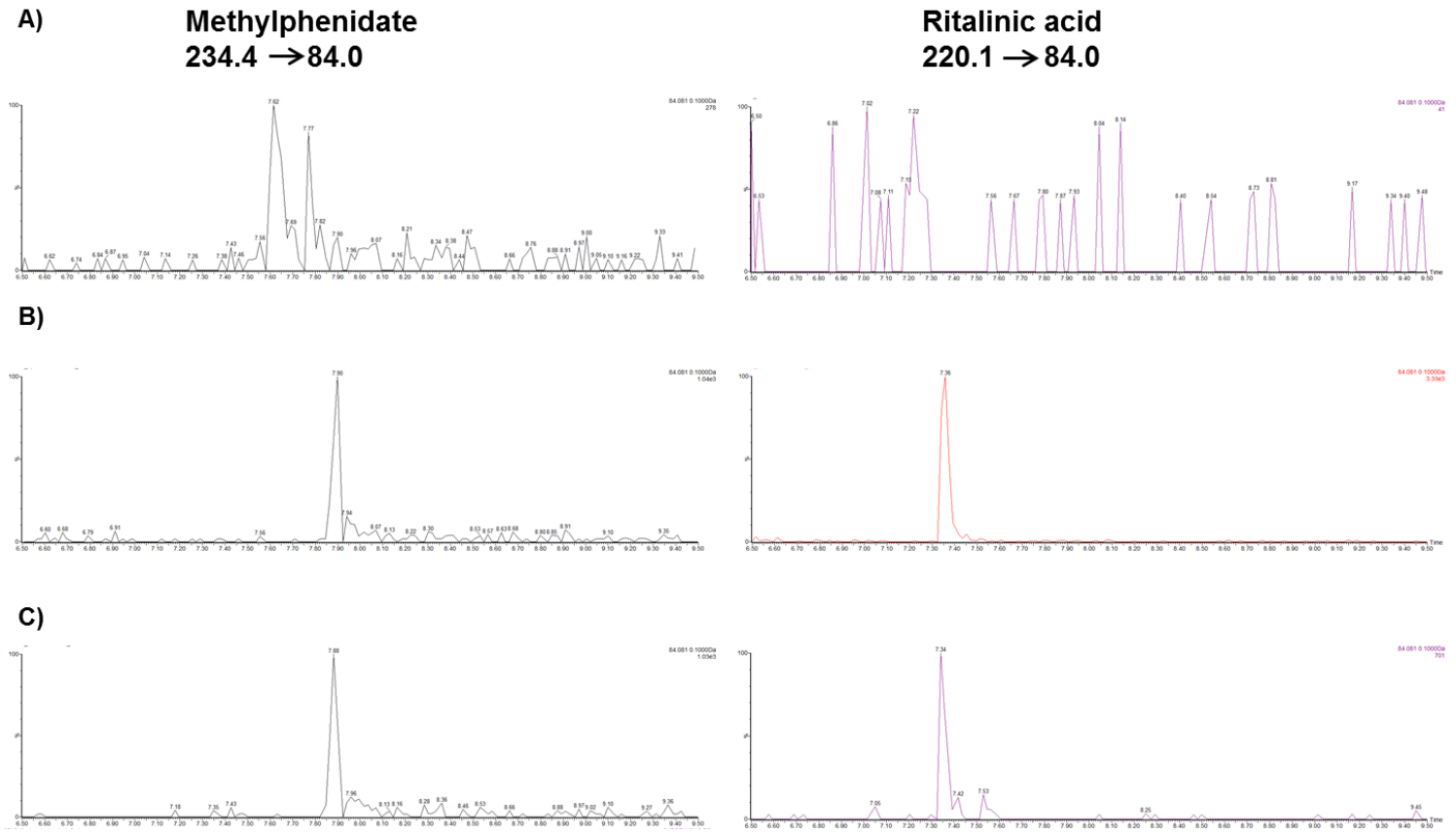

Figure 6.9 *Representative MRM ion chromatograms of methylphenidate (MPH) and ritalinic acid (RA) in reagent blank (A), epidermis (B) and dermis (C) extracts derived from Labskin treated with MPH (0.5% w/w) for 24 hours*

The MPH peak was detected at low intensity in the extracts of both epidermis and dermis of treated Labskin. However, it was not possible to associate completely this peak to the presence of MPH in the tissue; this is because a small interfering MPH peak was also detected in extracts of dermis derived from untreated Labskin (blank matrix) (data not shown).

In contrast to the MPH peak, a slightly more intense and clear signal for ritalinic acid was detected only in extracts derived from the epidermis of treated Labskin. Even in this case, this finding seemed to suggest that the presence of CES1 and, hence, the majority of MPH metabolism occurred in the epidermal region of skin, supporting MALDI-MSI data.

6.6 Concluding remarks

In this chapter, a commercial living skin equivalent model, Labskin, was used to investigate the localisation of carboxylesterase 1 (CES1) activity by MALDI-MSI. Substrate based mass spectrometry imaging (SB-MSI) was chosen as the technique to perform the experiments, which included the treatment of Labskin tissue with 2 substrates enzymes, methylparaben and methylphenidate.

A derivatisation strategy using FMPTS reagent was assessed in order to detect MP and its metabolite 4-HBA by mass spectrometry. An in-solution derivatisation with FMPTS resulted in a significant increase in signal of MP and 4-HBA analytes, which were detected in the derivatised form $[M]^+$ in MALDI-MDP spectra. In contrast, an on-tissue derivatisation approach involving the application of FMPTS reagent onto Labskin sections treated with MP for 24 hours, did not show successful results, leading to the inopportunity of using this substrate for metabolic analysis before more optimisation of the technique is performed.

In this regard, MALDI-MSI was performed on Labskin sections treated with the alternative substrate MPH, which with its metabolite RA was easily detected by mass spectrometry. The localisation of carboxylesterase 1 was detected mainly in the epidermal layer of the tissue. This data was compared with LC-MS/MS

analysis, which displayed a peak belonging to MPH metabolite (ritalinic acid) only on the extract of isolated epidermis derived from treated Labskin tissue.

Additional future work is necessary to investigate reproducibility of the results. These include: optimising sample preparation steps for both MALDI and LC-MS/MS analysis; increasing the number of technical and biological repeats; and increasing the number of CES1 substrates tested. Furthermore, a comparison of the metabolic enzyme distribution found in Labskin to those found in human skin is required in order to assess the pharmacokinetic similarities between these two models.

Chapter 7: Conclusion and future work

Conclusion

3D *in-vitro* tissue models of human skin represent a valid alternative to monolayer 2D cell culture, *ex-vivo* human and animal skin models, and, at the present time, their application finds a place in many skin research fields (Schäfer-Korting, Mahmoud, *et al.*, 2008; Xie *et al.*, 2010; Ali *et al.*, 2015; De Vuyst *et al.*, 2017; Lewis *et al.*, 2018; Bataillon *et al.*, 2019). 3D *in-vitro* skin models offer several advantages; they have a higher resemblance to the *in-vivo* human skin microenvironment compared to monolayer 2D cell culture, they guarantee a higher quality of preservation compared to *ex-vivo* skin, as they are still living systems they are easy to obtain without requiring an individual ethical licence, and they represent a valid replacement to animal testing in line with the principle of the UK organisation 3Rs (Replacement, Reduction and Refinement). For years *ex-vivo* and animal skin models have represented the gold standards for skin research but not without problems. The major issues related to *ex-vivo* skin are the short viability period (< 24h), donor variability (race, gender, age) and genetic polymorphism, making a standardised assay complicated (Rodrigues Neves and Gibbs, 2018). Similarly, when using animal models, inter-species differences (animal versus human), such as thickness of the stratum corneum (SC), composition of intercellular SC lipids, density of hair follicles, could generate misleading results (Bronaugh, Stewart and Congdon, 1982; Netzlaff *et al.*, 2006). Considering all of these factors in addition to ethical problems relating to the use of *ex-vivo* and animal skin models, there are great benefits to transitioning to 3D *in vitro* skin equivalents.

However, it is important to consider that differences between 3D skin models and native skin inevitably are present, due to the simplified structure of the models. For this reason, currently, technology and progress are focused on improving 3D skin models in order to increase their similarity to human skin.

The work presented in this thesis demonstrates the success of the combination of MALDI mass spectrometry imaging (MSI) with a full thickness living skin equivalent model, Labskin, for a label-free investigation of either drug absorption or drug biotransformation in skin.

The development of quantitative methodologies for the detection of an antifungal agent, terbinafine hydrochloride, in Labskin, by MALDI-MSI has been reported, and the performance of the penetration enhancer (dimethyl isosorbide (DMI)) added to the delivery vehicle has also been assessed. Furthermore, approaches to improve the detection of pharmaceutical agents with low protonation/deprotonation efficiency and preliminary analysis of the metabolic activity of Labskin was also described.

In the study reported in this thesis only technical replicates were carried out, and, in future work, it would be interesting to perform biological repeats in order to assess the reproducibility of the model. In fact, although Labskin has already been studied extensively, more validation studies are necessary to test the robustness of the model and its ability to represent human skin.

7.1 MALDI-MSP method optimisation

In MALDI analysis the choice of the matrix represents a fundamental factor since it strongly influences the desorption/ionisation process and the spectral quality (Lemaire *et al.*, 2006). In Chapter 2 a "trial and error" approach was employed both in positive and in negative mode in order to determine the ideal matrix able to enhance the signal of the standard terbinafine hydrochloride. With negative polarity no signal was detected, whereas in positive mode a variety of matrix compositions, including also binary matrices and liquid matrices were investigated. The spectral quality of terbinafine hydrochloride was enhanced when the liquid ionic matrix aniline-CHCA was employed; both when the absolute and relative intensity of the analyte under investigation was considered. However, there are a variety of matrices and solutions which were not tested in this work, and further investigations into a more ideal matrix could be appropriate to enhance further analyte signal by MALDI-MSP.

7.2 MALDI-MSI method optimisation

In Chapter 2, to detect the localisation of terbinafine hydrochloride in Labskin by using MALDI-MSI, two different matrix deposition techniques, automated

spraying and sublimation, were investigated. The localisation of drug after 24 hours treatment was found to be solely in the epidermal layer of skin using both approaches. However, the sublimation method ensured a more uniform coating of matrix and smaller crystals as well as a better spatial resolution and limited analyte delocalisation compared to spraying technique. The permeation of terbinafine hydrochloride solely in the epidermal layer of Labskin was also visualised with MALDI-MSI when the chemical enhancer (dimethyl isosorbide (DMI)) was included in the formulation used for the treatment of Labskin for 24 hours. In future work, it would be useful also to optimise a recrystallisation step after sublimation as well as test an acoustic droplet ejector, as matrix deposition technique, alongside spraying and sublimation, to investigate an increase of analyte signal, while preserving the analyte localisation.

7.3 Quantitative mass spectrometry imaging (QMSI)

Although MALDI-MSI has been widely used for qualitative analysis, its application for quantitative analysis represents one of the major critical challenges in the field. The possibility of identifying and quantifying pharmaceutical agents in specific locations within skin by MALDI-MSI represents a potential advantage over traditional quantitative techniques.

All of QMSI analysis were performed by using a Water Synapt G2 instrument. The main reason for the decision to use the Synapt instrument instead of the Bruker instrument (Chapter 2) was related to the possibility of processing MSI data with msIQuant software, specific for MSI quantitative analysis. To import the data into msIQuant software it was necessary to convert MSI raw data files to imzML format; this conversion was enabled by only the software tool present in the Synapt (HDI 1.4. software), but was absent in the Bruker software (FlexImaging 3.0), limiting, hence, its application.

In the work presented in Chapter 3 different approaches to generate robust and sensitive quantitative mass spectrometry imaging (QMSI) data were developed. The first method included the application by automatic sprayer of a serial dilution of standards onto keratinocytes and fibroblasts, co-cultured directly onto a glass slide. The second method included the application of a serial dilution of

terbinafine standards onto untreated sections of Labskin using an automated sprayer. The third method included the microspotting of serial dilution of standards solely onto the epidermis of an untreated Labskin section by using an automated acoustic spotter Portrait 630. The last method included the construction of a cell plug, consisting of the spiking of serial dilution of standards within intact keratinocyte cells embedded in frozen gelatin. MsIQuant software, recently developed for quantitative mass spectrometry imaging, was used to create calibration curves from MSI data. However, the impossibility of generating the calibration curve with the cell plug method made it impracticable for QMSI investigations and it was not considered further. Among the other methods, the application of analytical standards on top of an untreated Labskin section by microspotting was the most favourable technique, since it offered the enormous advantage of generating a linear calibration curve, being practical, relatively fast and cost-effective; only one blank section was required to generate a calibration array, allowing treated tissue sections to be located next to sample sections and imaged at the same time to perform quantitative investigations. From preliminary quantitative analysis an increase of concentration of terbinafine into the upper epidermis of Labskin in response to an increase of percentage of DMI in the delivery vehicle was shown.

The further work presented in Chapter 4 emphasised the success of including an internal standard (deuterated terbinafine) in the analysis to enhance the quantitative capabilities of MSI. QMSI data was also validated with a traditional and widely accepted quantitative LC-MS/MS method; no statistical difference in the levels of drug detected in Labskin by the two techniques was detected. However, in the work reported in Chapter 4 problems related the degradation of the deuterated internal standard were experienced and future work in this area to investigate a more suitable internal standard as well as the optimal conditions in which to conserve the internal standard could be useful in order to avoid degradation.

7.4 Derivatisation

Pharmaceutical compounds containing functional groups with low protonation/deprotonation efficiency are challenging to investigate with mass spectrometry techniques. In Chapter 5 the problems relating to the low sensitivity and detection of hydrocortisone hydrochloride in *ex-vivo* skin samples after treatment were raised. In Chapter 5 the success of a chemical derivatisation approach to overcome this problem was presented. The target for the reaction was the carbonyl group of the hydrocortisone and Girard's reagent T (GirT), a hydrazine based agent, was chosen as reagent for the derivatisation. An increase of signal of the derivative hydrocortisone was obtained using both an in-solution and on-tissue derivatisation approach; the on-tissue derivatisation allowed visualisation of the localisation of the derivatised drug in the epidermal layer of *ex-vivo* skin tissue, when otherwise it could not be detected. More experiments are necessary to optimise the derivatisation method to examine a further increase of the derivatised analyte using MALDI-MSI. These include investigating different derivatisation agents, changing the temperature and time of derivatisation reaction as well as choosing the optimal matrix for analysis.

7.5 Metabolic activity in Labskin

As well as investigating drug absorption in the skin, it is important to investigate drug biotransformation in order to assess the pharmaceutical as well as toxic effects of pharmaceuticals. In Chapter 6, the metabolic esterase activity of Labskin using MALDI-MSI was assessed by employing the approach of "substrate-based mass spectrometry imaging" (SBMSI). This approach included the treatment of Labskin tissue with 2 substrates carboxylesterase 1 enzyme, methylparaben (MP) and methylphenidate hydrochloride (MPH). Methylparaben and its metabolite 4-hydroxybenzoic acid (4-HBA) could not be detected in MALDI-MSP spectra in positive mode, due to the low protonation efficiency of the hydroxyl and carboxyl acid groups. As reported in Chapter 5, to enhance the signal a derivatisation approach was investigated using the hydroxyl group as target, since it was present in both analytes (MP and 4-HBA) and 2-fluro-1-methypyridinum p-tolunesulfonate (FMPTS) was selected as a derivatisation

agent to give the corresponding N-methylpyridinium ether derivatives. The in-solution derivatisation showed a significant increase in the signal of MP and 4-HBA derivatives, whereas an on-tissue derivatisation was not successful. Further work is necessary to optimise the on-tissue derivatisation of MP and, attempt to observe the metabolite 4-HBA; this includes investigating the amount of derivatisation reagent to use for the reaction, the deposition technique, as well as time and reaction conditions. Attention in future work could be also be focused on investigating different reagents selective for the hydroxyl functional group.

On the other hand, it was possible to investigate the metabolic activity of skin using methylphenidate (MPH) and its metabolite ritalinic acid (RA) due to the presence of the easily ionisable amine group in the molecules. Using MALDI-MSI the localisation of probe (MPH) and metabolite (RA) was detected only on the epidermal layer of Labskin, suggesting an enzymatic activity of carboxylesterase 1 at this level. The results were compared with LC-MS/MS analysis performed on the extract of isolated epidermis and dermis of treated Labskin. LC-MS/MS data supported MALDI-MSI findings, displaying a peak belonging to RA only on the extract of isolated epidermis of Labskin. However, more technical and biological repeats are necessary to validate the reliability and the reproducibility of the experiment. More probes of carboxylesterase 1 can be investigated to validate the results. In addition an optimisation step is required for both MALDI-MSI and LC-MS/MS techniques to enhance the signal intensity, and; finally, a comparison of the metabolic enzyme distribution found in Labskin to those found in human skin is required in order to assess the pharmacokinetic similarities between these two models.

Appendix I

Table of contents

1) Cell films

Standard (ng/µL)	Time for total spraying (sec)	Total volume sprayed (µL)	Amount of Terbinafine (ng) per total area	Area sprayed (mm^2)	Amount of Terbinafine per mm^2 (ng/mm^2)
0	232.21	15.48	0	68.87	0
1	152.26	10.15	10.15	43	0.24
10	168.36	11.22	112.24	46.89	2.39
50	164.16	10.94	547.2	51.22	10.68
100	168.08	11.21	1120.53	48.65	23.03
500	204.28	13.62	6809.33	63	108.09

Table displaying the results of the concentration of terbinafine hydrochloride (ng) per mm^2. Firstly, the time requested for spraying two layers of each standard solution was tracked. The flow rate was set at 4 µL/min for spraying all standard solutions. By knowing the flow rate and the total time employed for spraying, the total volume (µL) applied was calculated for each standard solution. The area sprayed was calculated for each standard solution by multiplying the coordinates selected for the spraying (x and y). The amount of terbinafine (ng) within the volume sprayed was divided by the area sprayed for each standard solution and the amount of drug in ng/mm^2 was calculated.

2) On-tissue application of standards by spraying

Standard (ng/µL)	Time for total spraying (sec)	Total volume sprayed (µL)	Amount of Terbinafine (ng) per total area	Area sprayed (mm^2)	Amount of Terbinafine per mm^2 (ng/mm^2)
0	436	36.3	0	292.5	0
0.1	634	52.83	5.28	432	0.012
1	398	33.17	33.17	272.18	0.12
100	364	30.33	3033.03	241.2	12.58
500	512	42.67	21333.33	351	60.78
1000	170	14.17	14166.67	110.21	128.55
1500	276	23	34500	182.30	189.24
2000	244	20.33	40666.67	166.46	244.30
3000	366	30.5	91500	243.07	376.43
4000	336	28	112000	225	497.78

Table displaying the results of the concentration of terbinafine hydrochloride (ng) per mm^2. Firstly, the time requested for spraying two layers of each standard solution was tracked. The flow rate was set at 5 µL/min for spraying all standard solutions. By knowing the flow rate and the total time employed for spraying, the total volume (µL) applied was calculated for each standard solution. The area sprayed was calculated for each standard solution by multiplying the coordinates selected for the spraying (x and y). The amount of terbinafine (ng) within the volume sprayed was divided by the area sprayed for each standard solution and the amount of drug in ng/mm^2 was calculated.

3) On-tissue application of standards by microspotting

Concentration TBF (ng/µL)	Concentration TBF (ng) in spot volume (3.4 nL)	Concentration TBF (ng) per mm^2
0	0	0
0.1	0.00034	0.003671
1	0.0034	0.036705
100	0.34	3.670517
500	1.7	18.35259
1000	3.4	36.70517
1500	5.1	55.05776
2000	6.8	73.41034
3000	10.2	110.1155
4000	13.6	146.8207

Table displaying the results of the concentration of terbinafine hydrochloride (ng) per mm^2. Firstly, the amount of drug in each spot (3.4 nL) was calculated. To determine the spot size, ROI of the terbinafine fragment ion (*m/z* 141) was drawn around the spot at highest concentration (4000 ng/µL) and the area (mm^2) was extracted by using msIQuant. The area of the spot was 0.09263 mm^2. Assuming the droplet size spot of the Portrait 630 is reproducible, the concentration of terbinafine from each spot was divided by the spot area (0.09263 mm^2) and the concentration of drug was found in ng/mm^2.

Appendix II

Degradation of the Internal Standard on Tissue

In Chapter 4 the degradation of the internal standard terbinafine-d_7 hydrochloride in solution has been reported. In this Appendix data from an investigation of the rate of degradation of the internal standard terbinafine-d_7 hydrochloride on tissue is reported.

Materials

Alpha cyano-4-hydroxycinnamic acid (α-CHCA), phosphorus red, terbinafine hydrochloride standard (TBF HCl, MW 327.89) were purchased from Sigma-Aldrich (Gillingham, UK). The internal standard terbinafine-d_7 hydrochloride (TBF-d_7 HCl, MW 334.93) was obtained by Clearsynth (Maharashtra, India).

Labskin living skin equivalent (LSE) samples were provided by Innovenn (UK) Ltd (York, England).

Methods

For this experiment, 9 microspots of a solution of terbinafine hydrochloride (100 ng/µL) with terbinafine-d_7 hydrochloride (100 ng/µL) in MeOH/H_2O (50:50) were deposited on the dermis of 6 sections (12 µm thick) of blank Labskin using an acoustic robotic spotter (Portrait 630, Labcyte Inc., Sunnyvale, CA). The number of cycles for each spot was set to 20 for a total volume of 3.4 nL. Five extra spots were applied outside the tissue to give a "drying time" between each cycle. The microspotting of all sections was performed at the same time.

The organic matrix CHCA was applied onto all six blank sections by sublimation as described in Chapter 2.4.2.1.2 and the sections were kept in the fridge at + 4 ^oC.

Instrumentation

The sections were imaged using a Waters MALDI HDMS Synapt G2 mass spectrometer (Waters Coorporation, Manchester, U.K.) equipped with a neodynium: yttrium aluminium garnet (Nd:YAG) laser operated at 1 KHz, as reported in Chapter 4.6.1. Although all sections were prepared at the same time, they were imaged on different days in order to assess the degradation of the internal standard on the tissue over time. The ion mobility function of the instrument was not enabled in order to use the msIQuant software.

Results

By plotting the terbinafine-d_7 hydrochloride source generated fragment ion peak ($[C_{11}D_7H_2]^+$; *m/z* 148) it was possible to visualise each spot applied onto the dermis of blank Labskin sections. MsIQuant software was used to define regions of interest (ROIs) with equal area (4 pixels) for each spot and from them the average intensity for the signal of the terbinafine (*m/z* 141) and the terbinafine-d_7 was extracted (Appendix Figure 1).

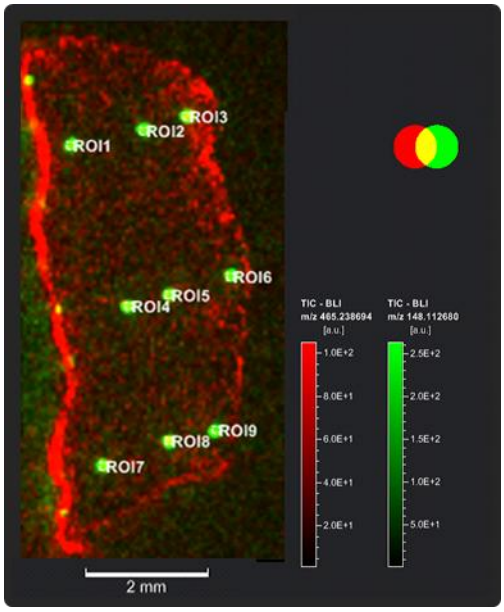

Appendix II Figure 1. *MALDI-MSI at 60 µm X 60 µm spatial resolution of a constant concentration of terbinafine-d_7 hydrochloride fragment ion in green ($[C_{11}D_7H_2]^+$; fragment ion; m/z 148) microspotted directly on the dermis of an untreated section of Labskin. Volume of each spot = 3.4 nL.*

To assess the degradation of the internal standard on tissue, the average intensity ratio of the unlabelled drug (*m/z* 141) to its internal standard (*m/z* 148) was extracted from each microspot deposited onto the dermis of six Labskin sections and compared (Appendix Figure 2).

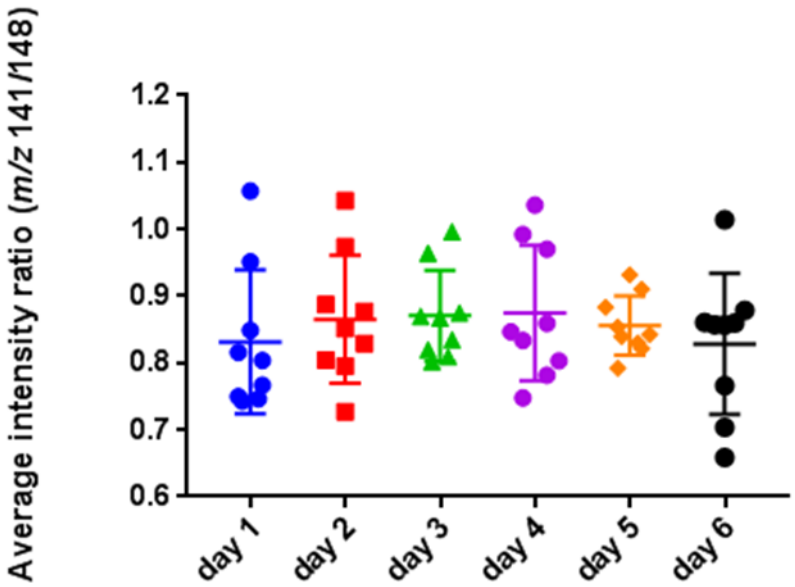

Appendix II Figure 2. *Distribution of the intensity ratio of terbinafine to its internal standard (m/z 141/148) extracted from each microspot of the solution (terbinafine (100 ng/µL) mixed with terbinafine-d_7 (100 ng/µL) in MeOH/H_2O (1:1)) deposited onto the dermis of six control Labskin sections. The sections were microspotted at the same time and imaged on different days.*

When the internal standard was kept onto the tissue over time, an increased amount of the unlabelled drug, due to hydrogen-deuterium exchange effect, was not observed. This was demonstrated by the comparison of the average intensity ratio (*m/z* 141/148) that was found to be similar in all sections. These results were in contrast with the data reported in Chapter 4, in which a significant loss of the deuterium from the internal standard kept in an aqueous solution over time was reported.

The difference in the degree of internal standard degradation, in solution and on tissue, could be attributed to the different environment in which the internal

standard is kept. As reported by Chavez-Eng *et al.* the presence of water containing solvents favours the deuterium-hydrogen exchange. The authors reported the loss of deuterium from the internal standard of rofecoxib ($^{13}CD_3$-rofecoxib) dissolved in acetonitrile (ACN) due to the trace of water usually present in ACN solvent (Chavez-Eng, Constanzer and Matuszewski, 2002).

In this case, it is thought that the increased stability of the internal standard located on the tissue over time is due to a reduction of the solvent component.

Conclusions

In this Appendix the evaluation of an isotope exchange on tissue has been investigated. The results presented here showed the absence of a deuterium-hydrogen exchange occurring from the internal standard terbinafine-d_7 hydrochloride on tissue over time. The stability of the internal standard on tissue could be explained by the absence of the solvent that is reported to increase the efficiency of deuterium-hydrogen exchange process.

Appendix III

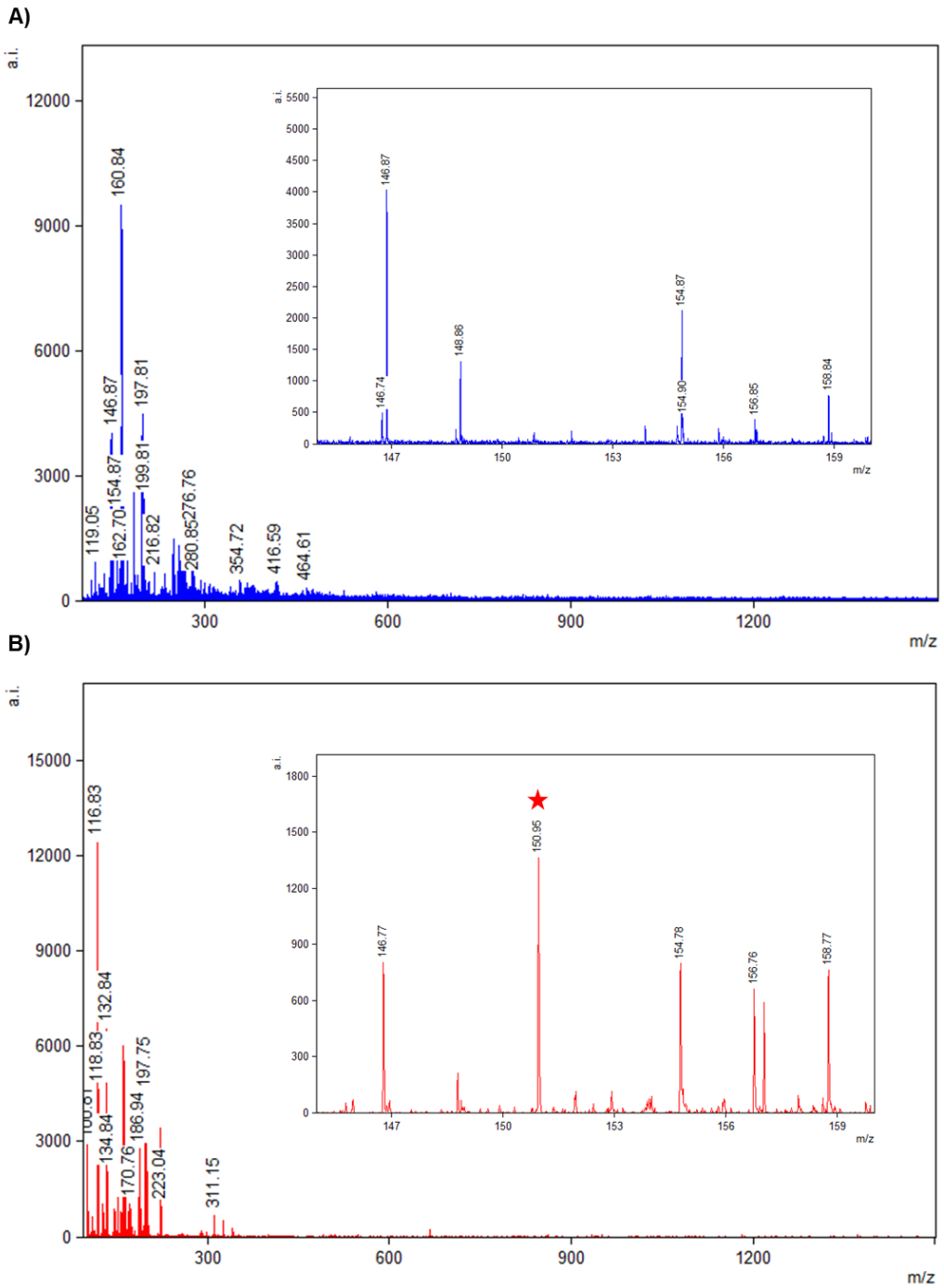

Appendix III Figure 1. *MALDI-MSP spectra acquired in negative mode of methylparaben standard (100 µg/mL) mixed with the matrix NEDC. The methylparaben peak [M-H]$^-$ at m/z 151.04 was not detected using the Synapt G2 mass spectrometer instrument (A), whereas it was detected (indicated with a star) at low intensity when the Bruker mass spectrometer was used (B).*

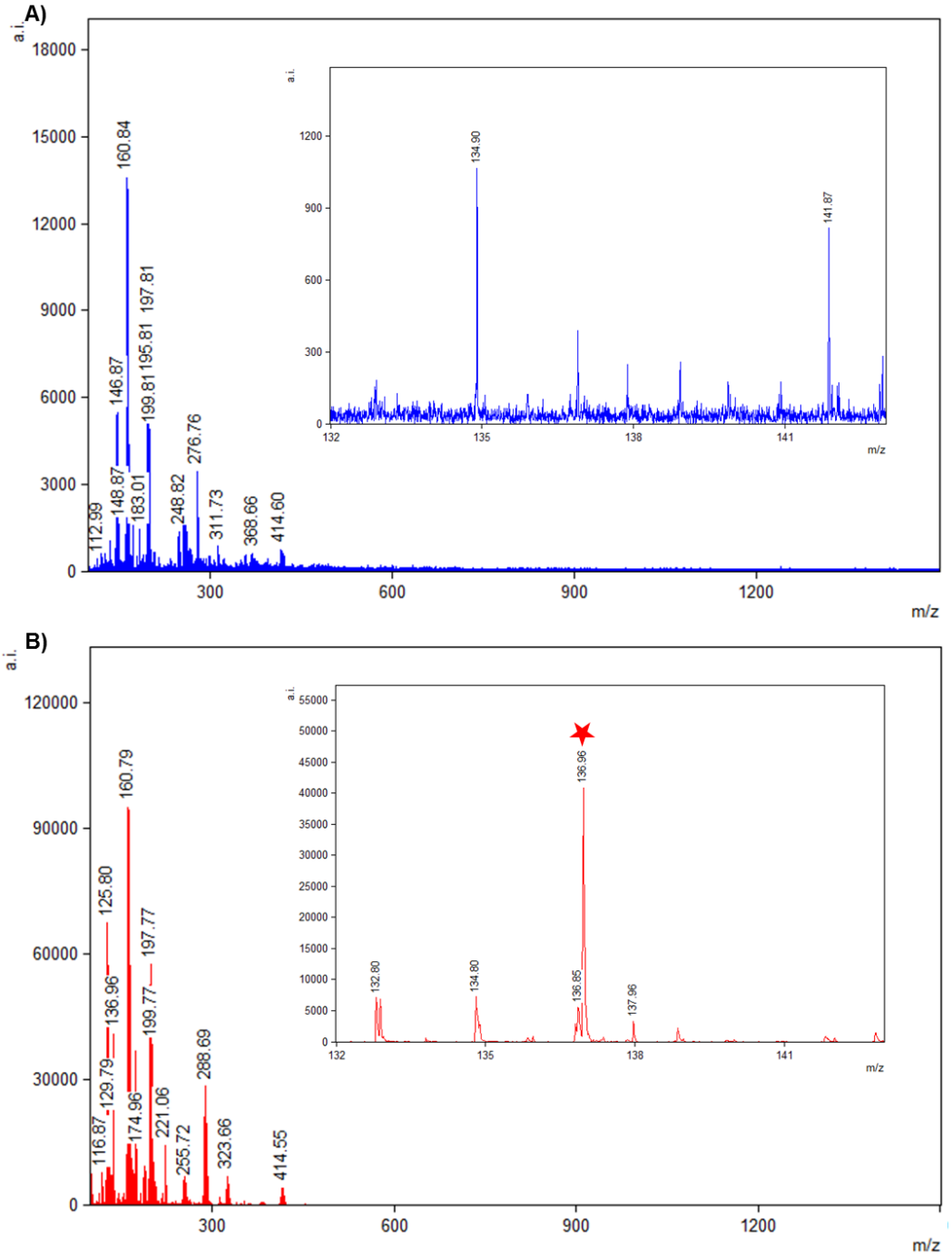

Appendix III Figure 2. *MALDI-MS spectra acquired in negative mode of 4-hydroxybenzoic acid standard (100 µg/mL) mixed with the matrix NEDC. The 4-hydroxybenzoic acid peak [M-H]⁻ at m/z 137.02 was not detected using the Synapt G2 mass spectrometer instrument (A), whereas it was detected (indicated with a star) at high intensity when the Bruker mass spectrometer was used (B).*

Appendix IV

Scientific Publications

Russo, C., Lewis, E. E. L., *et al.* (2018) ‘Mass Spectrometry Imaging of 3D Tissue Models.’, *Proteomics*, 1700462, p. e1700462. doi: 10.1002/pmic.201700462.

Russo, C., Brickelbank, N., *et al.* (2018) ‘Quantitative Investigation of Terbinafine Hydrochloride Absorption into a Living Skin Equivalent Model by MALDI-MSI’, *Analytical Chemistry*. American Chemical Society, 90(16), pp. 10031–10038. doi: 10.1021/acs.analchem.8b02648.

Conference Presentations

Oral presentations

Method development for quantitative investigation of Terbinafine hydrochloride in a 3D skin model by MALDI-MSI. *38th BMSS Annual Meeting, Manchester, UK, 2017.*

Method development for quantitative investigation of Terbinafine hydrochloride in a 3D skin model by MALDI-MSI. *Drug Metabolism Discussion Group, Cambridge, UK, 2017.*

Tissue specific Regions Of Interests (ROIs).How to generate them? / How to act when internal standard contain unlabeled counterpart?. *ASMS Imaging MS Workshop. 66th ASMS Conference on Mass Spectrometry and Allied Topics, San Diego, CA, USA, 2017.*

Poster presentations

Optimisation of imaging the distribution of terbinafine hydrochloride in a 3D skin model. *BMSS Mass Spectrometry Imaging Symposium, Sheffield, 2016* **(1st Poster Prize).**

Optimisation of Matrix Condition for the Analysis of the Antifungal Agent (Terbinafine hydrochloride) in a Living Skin Equivalent Model. *64th ASMS Conference on Mass Spectrometry and Allied Topics, San Antonio, TX, USA, 2016.*

Optimisation of imaging the distribution of terbinafine hydrochloride in a 3D skin model. *37th BMSS Annual Meeting, Eastbourne, UK, 2016.*

Optimisation of imaging the distribution of Terbinafine hydrochloride in a 3D skin model. *OurCon IV: Imaging Mass Spectrometry Conference, Ustron, Poland, 2016.*

Method development for quantitative investigation of Terbinafine hydrochloride in a 3D skin model by MALDI-MSI. *65th ASMS Conference on Mass Spectrometry and Allied Topics, Indianapolis, IN, USA, 2017.*

Quantitative Determination of Terbinafine Hydrochloride in a 3D Skin Model by MALDI-MSI. *OurCon V: Imaging Mass Spectrometry Conference, Doorn, The Netherlands, 2017.*

Quantitative Determination of Terbinafine Hydrochloride in a 3D Skin Model by MALDI-MSI. *BMRC/MERI Christmas poster event, Sheffield Hallam University, Sheffield, UK, 2017* **(1st Poster Prize).**

Detection of drug absorption in living skin equivalent models by using MALDI-MSI. *BMSS Mass Spectrometry Imaging Symposium, Sheffield Hallam University, Sheffield, UK, 2018* **(1st Poster Prize).**

Detection of drug absorption in living skin equivalent models by using MALDI-MSI. *66th ASMS Conference on Mass Spectrometry and Allied Topics, San Diego, CA, USA, 2018.*

A quantitative method for the detection of drug absorption in living skin equivalent models using MALDI-MSI. *38th BMSS Annual Meeting, Cambridge, UK, 2018.*

Chapter 8: Bibliography

Abaci, H. E. *et al.* (2017) 'Next generation human skin constructs as advanced tools for drug development', *Experimental Biology and Medicine*, 242(17), pp. 1657–1668. doi: 10.1177/1535370217712690.

Abbas, S. *et al.* (2010) 'Metabolism of Parabens (4-Hydroxybenzoic Acid Esters) by Hepatic Esterases and UDP-Glucuronosyltransferases in Man', *Drug Metabolism and Pharmacokinetics*, 25(6), pp. 568–577. doi: https://doi.org/10.2133/dmpk.DMPK-10-RG-013.

Abd, E. *et al.* (2016) 'Skin models for the testing of transdermal drugs', *Clinical Pharmacology: Advances and Applications*, 8, pp. 163–176. doi: 10.2147/CPAA.S64788.

Abraham, W. and Downing, D. T. (1990) 'Interaction between corneocytes and stratum corneum lipid liposomes in vitro', *Biochimica et Biophysica Acta (BBA) - Biomembranes*, 1021(2), pp. 119–125. doi: https://doi.org/10.1016/0005-2736(90)90023-H.

Abu Sammour, D. *et al.* (2019) 'Quantitative Mass Spectrometry Imaging Reveals Mutation Status-independent Lack of Imatinib in Liver Metastases of Gastrointestinal Stromal Tumors', *Scientific Reports*, 9(1), pp. 1–9. doi: 10.1038/s41598-019-47089-5.

Aerni, H.-R., Cornett, D. S. and Caprioli, R. M. (2006) 'Automated acoustic matrix deposition for MALDI sample preparation', *Analytical Chemistry*, 78(3), pp. 827–34. doi: 10.1021/ac051534r.

Ahadi, E. and Konermann, L. (2012) 'Modeling the Behavior of Coarse-Grained Polymer Chains in Charged Water Droplets: Implications for the Mechanism of Electrospray Ionization', *The Journal of Physical Chemistry B*, 116(1), pp. 104–112. doi: 10.1021/jp209344z.

Ahmad, N. and Mukhtar, H. (2004) 'Cytochrome P450: A Target for Drug Development for Skin Diseases', *Journal of Investigative Dermatology*, 123(3), pp. 417–425. doi: 10.1111/j.0022-202X.2004.23307.x.

Ali, N. *et al.* (2015) ‘Skin equivalents: Skin from reconstructions as models to study skin development and diseases’, *British Journal of Dermatology*, 173(2), pp. 391–403. doi: 10.1111/bjd.13886.

Alikhan, A. and Maibach, H. I. (2010) ‘Biology of Stratum Corneum: Tape Stripping and Protein Quantification’, in Farage, M. A., Miller, K. W., and Maibach, H. I. (eds) *Textbook of Aging skin*. Berlin, Germany: Springer, pp. 401–407. doi: 10.1007/978-3-540-89656-2_40.

Amstalden van Hove, E. R., Smith, D. F. and Heeren, R. M. A. (2010) ‘A concise review of mass spectrometry imaging’, *Journal of Chromatography A*, 1217(25), pp. 3946–3954. doi: 10.1016/j.chroma.2010.01.033.

Anderson, D. M. G. *et al.* (2010) ‘Examination of the translocation of sulfonylurea herbicides in sunflower plants by matrix-assisted laser desorption/ionisation mass spectrometry imaging’, *Rapid Communications in Mass Spectrometry*, 24(22), pp. 3309–3319. doi: 10.1002/rcm.4767.

Anigbogu, A. N. C. *et al.* (1995) ‘Fourier transform Raman spectroscopy of interactions between the penetration enhancer dimethyl sulfoxide and human stratrum corneum’, *International Journal of Pharmaceutics*, 125(2), pp. 265-282. doi: https://doi.org/10.1016/0378-5173(95)00141-5.

Avery, J. L. *et al.* (2011) ‘Matrix-assisted laser desorption mass spectrometry imaging for the examination of imipramine absorption by Straticell-RHE-EPI/001 an artificial model of the human epidermis’, *Xenobiotica*, 41(8), pp. 735–742. doi: 10.3109/00498254.2011.573015.

Baghdady, Y. Z. and Schug, K. A. (2018) ‘A novel diagnostic in situ derivatization kit for the simultaneous determination of 14 biomarkers of exposure to benzene, toluene, ethyl benzene and xylenes in human urine by isotope dilution liquid chromatography tandem mass spectrometry and kit optimiza’, *Analytica Chimica Acta*, 1036, pp. 195–203. doi: https://doi.org/10.1016/j.aca.2018.06.064.

Bajpai, L. *et al.* (2005) ‘Mass spectral fragmentation of the intravenous anesthetic propofol and structurally related phenols’, *Journal of the American Society for Mass Spectrometry*, 16(6), pp. 814–824. doi:

10.1016/j.jasms.2005.02.009.

Baker, T. C., Han, J. and Borchers, C. H. (2017) 'Recent advancements in matrix-assisted laser desorption/ionization mass spectrometry imaging', *Current Opinion in Biotechnology*, 43, pp. 62–69. doi: 10.1016/J.COPBIO.2016.09.003.

Baron, J. *et al.* (2008) 'Expression and Function of Cytochrome P450-Dependent Enzymes in Human Skin Cells', *Current Medicinal Chemistry*, 15(22), pp. 2258–2264. doi: 10.2174/092986708785747535.

Barré, F. *et al.* (2019) 'Faster raster matrix-assisted laser desorption/ionization mass spectrometry imaging of lipids at high lateral resolution', *International Journal of Mass Spectrometry*, 437, pp. 38–48. doi: 10.1016/j.ijms.2018.09.015.

Barré, F. P. Y. *et al.* (2016) 'Derivatization Strategies for the Detection of Triamcinolone Acetonide in Cartilage by Using Matrix-Assisted Laser Desorption/Ionization Mass Spectrometry Imaging', *Analytical Chemistry*, 88(24), pp. 12051–12059. doi: 10.1021/acs.analchem.6b02491.

Barry, B. W. (1991) 'Lipid-Protein-Partitioning theory of skin penetration enhancement', *Journal of Controlled Release*, 15(3), pp. 237–248. doi: https://doi.org/10.1016/0168-3659(91)90115-T.

Bataillon, M. *et al.* (2019) 'Characterization of a new reconstructed full thickness skin model, t-skin^{TM}, and its application for investigations of anti-aging compounds', *International Journal of Molecular Sciences*, 20(9). doi: 10.3390/ijms20092240.

Beasley, E., Francese, S. and Bassindale, T. (2016) 'Detection and Mapping of Cannabinoids in Single Hair Samples through Rapid Derivatization and Matrix-Assisted Laser Desorption Ionization Mass Spectrometry', *Analytical Chemistry*, 88(20), pp. 10328–10334. doi: 10.1021/acs.analchem.6b03551.

Belal, F., El-din, M. K. S. and Eid, M. I. (2013) 'Spectrofluorimetric Determination of Terbinafine Hydrochloride and Linezolid in their Dosage Forms and Human Plasma', *Journal of Fluorescence*, 23(5), pp. 1077–1087. doi: 10.1007/s10895-013-1237-3.

Bell, E. *et al.* (1991) 'The living skin equivalent: Its manufacture, its organotypic

properties and its responses to irritants', *Toxicology in Vitro*, 5(5), pp. 591–596. doi: https://doi.org/10.1016/0887-2333(91)90099-Y.

Bensouilah, J. and Buck, P. (2006) *Aromadermatology: Aromatherapy in the Treatment and Care of Common Skin Conditions*. Abingdon, UK: Radcliffe Publishing.

Bergman, N., Shevchenko, D. and Bergquist, J. (2014) 'Approaches for the analysis of low molecular weight compounds with laser desorption/ionization techniques and mass spectrometry', *Analytical and Bioanalytical Chemistry*, 406(1), pp. 49–61. doi: 10.1007/s00216-013-7471-3.

Billeci, T. M. and Stults, J. T. (1993) 'Tryptic Mapping of Recombinant Proteins by Matrix-Assisted Laser Desorption/Ionization Mass Spectrometry', *Analytical Chemistry*, 65(13), pp. 1709–1716. doi: 10.1021/ac00061a013.

Bøgeskov Schmidt, F. *et al.* (2018) 'Mass Spectrometry Based Imaging of Labile Glucosides in Plants', *Frontiers in Plant Science*, 9(892). doi: 10.3389/fpls.2018.00892.

Bommannan, D., Potts, R. O. and Guy, R. H. (1990) 'Examination of stratum corneum barrier function in vivo by infrared spectroscopy', *Journal of Investigative Dermatology*, 95(4), pp. 403–408. doi: 10.1111/1523-1747.ep12555503.

Bonnel, D. *et al.* (2018) 'MALDI imaging facilitates new topical drug development process by determining quantitative skin distribution profiles', *Analytical and Bioanalytical Chemistry*, 410(11), pp. 2815–2828. doi: 10.1007/s00216-018-0964-3.

Borojevic, R. (2013) 'Resident Stem Cell in Skin', in dos Santos Goldenberg, R. C. and Campos de Carvalho, A. C. (eds) *Resident Stem Cells and Regenerative Therapy*. Oxford, UK: Academic Press, pp. 89–103. doi: https://doi.org/10.1016/B978-0-12-416012-5.00005-0.

Borradori, L. and Sonnenberg, A. (1999) 'Structure and function of hemidesmosomes: More than simple adhesion complexes', *Journal of Investigative Dermatology*, 112(4), pp. 411–418. doi: 10.1046/j.1523-1747.1999.00546.x.

Bouschen, W. *et al.* (2010) ‘Matrix vapor deposition/recrystallization and dedicated spray preparation for high-resolution scanning microprobe matrix-assisted laser desorption/ionization imaging mass spectrometry (SMALDI-MS) of tissue and single cells’, *Rapid Communications in Mass Spectrometry*, 24(3), pp. 355–364. doi: 10.1002/rcm.4401.

Bouwstra, J. A. *et al.* (1999) ‘The role of ceramide composition in the lipid organisation of the skin barrier’, *Biochimica et Biophysica Acta - Biomembranes*, 1419(2), pp. 127–136. doi: 10.1016/S0005-2736(99)00057-7.

Bouwstra, J. A. *et al.* (2003) ‘Structure of the skin barrier and its modulation by vesicular formulations.’, *Progress in Lipid Research*, 42(1), pp. 1–36. Available at: http://www.ncbi.nlm.nih.gov/pubmed/12467638.

Brignol, N. *et al.* (2000) ‘Quantitative analysis of terbinafine (Lamisil®) in human and minipig plasma by liquid chromatography tandem mass spectrometry’, *Rapid Communications in Mass Spectrometry*, 14(3), pp. 141–149.

van den Broek, L. J. *et al.* (2017) ‘Progress and Future Prospectives in Skin-on-Chip Development with Emphasis on the use of Different Cell Types and Technical Challenges’, *Stem Cell Reviews and Reports*, 13(3), pp. 418–429. doi: 10.1007/s12015-017-9737-1.

Brombacher, S., Owen, S. J. and Volmer, D. A. (2003) ‘Automated coupling of capillary-HPLC to matrix-assisted laser desorption/ionization mass spectrometry for the analysis of small molecules utilizing a reactive matrix’, *Analytical and Bioanalytical Chemistry*, 376(6), pp. 773–779. doi: 10.1007/s00216-003-2024-9.

Bronaugh, R. L., Stewart, R. F. and Congdon, E. R. (1982) ‘Methods for in vitro percutaneous absorption studies II. Animal models for human skin’, *Toxicology and Applied Pharmacology*, 62(3), pp. 481–488. doi: 10.1016/0041-008X(82)90149-1.

Brown, M. B. *et al.* (2006) ‘Dermal and Transdermal Drug Delivery Systems: Current and Future Prospects’, *Drug Delivery*, 13(3), pp. 175–187. doi: 10.1080/10717540500455975.

Buck, A. *et al.* (2015) ‘Distribution and quantification of irinotecan and its active

metabolite SN-38 in colon cancer murine model systems using MALDI MSI', *Analytical and Bioanalytical Chemistry*, 407(8), pp. 2107–2116. doi: 10.1007/s00216-014-8237-2.

Bunch, J., Clench, M. R. and Richards, D. S. (2004) 'Determination of pharmaceutical compounds in skin by imaging matrix-assisted laser desorption/ionisation mass spectrometry', *Rapid Communications in Mass Spectrometry*, 18(24), pp. 3051–3060. doi: 10.1002/rcm.1725.

Calvano, C. D., Carulli, S. and Palmisano, F. (2009) 'Aniline/ α -cyano-4-hydroxycinnamic acid is a highly versatile ionic liquid for matrix-assisted laser desorption/ionization mass spectrometry', *Rapid Communications in Mass Spectrometry*, 23(11), pp. 1659–1668. doi: 10.1002/rcm.4053.

Candi, E., Schmidt, R. and Melino, G. (2005) 'The cornified envelope: A model of cell death in the skin', *Nature Reviews Molecular Cell Biology*, 6(4), pp. 328–340. doi: 10.1038/nrm1619.

Caprioli, R. M., Farmer, T. B. and Gile, J. (1997) 'Molecular Imaging of Biological Samples: Localization of Peptides and Proteins Using MALDI-TOF MS', *Analytical Chemistry*, 69(23), pp. 4751–4760. doi: 10.1021/ac970888i.

Caro, L. G. and van Tubergen, R. P. (1962) 'High-resolution autoradiography. I. Methods.', *The Journal of Cell Biology*, 15(2), pp. 173–188. doi: 10.1083/jcb.15.2.173.

Cartwright, A. J. *et al.* (2005) 'Derivatisation of carboxylic acid groups in pharmaceuticals for enhanced detection using liquid chromatography with electrospray ionisation tandem mass spectrometry', *Rapid Communications in Mass Spectrometry*, 19(8), pp. 1058–1062. doi: 10.1002/rcm.1883.

Caughlin, S. *et al.* (2017) 'Sublimation of DAN matrix for the detection and visualization of gangliosides in rat brain tissue for MALDI imaging mass spectrometry', *Journal of Visualized Experiments*, 121(e55254). doi: 10.3791/55254.

Challman, T. D. and Lipsky, J. J. (2000) 'Methylphenidate: Its Pharmacology and Uses', *Mayo Clinic Proceedings*, 75(7), pp. 711–721. doi: 10.4065/75.7.711.

Chavez-Eng, C. M., Constanzer, M. L. and Matuszewski, B. K. (2002) 'High-performance liquid chromatographic-tandem mass spectrometric evaluation and determination of stable isotope labeled analogs of rofecoxib in human plasma samples from oral bioavailability studies', *Journal of Chromatography B*, 767(1), pp. 117–129. doi: 10.1016/S0378-4347(01)00552-7.

Chernushevich, I. *et al.* (2017) 'A W-Geometry Ortho-TOF MS with High Resolution and Up to 100% Duty Cycle for MS/MS', *Journal of The American Society for Mass Spectrometry*, 28(10), pp. 2143–2150. doi: 10.1007/s13361-017-1742-8.

Chernushevich, I. V, Loboda, A. V and Thomson, B. A. (2001) 'An introduction to quadrupole–time-of-flight mass spectrometry', *Journal of Mass Spectrometry*, 36(8), pp. 849–865. doi: 10.1002/jms.207.

Chu, K. Y. *et al.* (2014) 'Thermal Proton Transfer Reactions in Ultraviolet Matrix-Assisted Laser Desorption/Ionization', *Journal of The American Society for Mass Spectrometry*, 25(3), pp. 310–318. doi: 10.1007/s13361-013-0792-9.

Chumbley, C. W. *et al.* (2016) 'Absolute Quantitative MALDI Imaging Mass Spectrometry: A Case of Rifampicin in Liver Tissues', *Analytical Chemistry*, 88(4), pp. 2392–2398. doi: 10.1021/acs.analchem.5b04409.

Clemis, E. J. *et al.* (2012) 'Quantitation of spatially-localized proteins in tissue samples using MALDI-MRM imaging', *Analytical Chemistry*, 84(8), pp. 3514–3522. doi: 10.1021/ac202875d.

Cobice, D. F. *et al.* (2013) 'Mass spectrometry imaging for dissecting steroid intracrinology within target tissues', *Analytical Chemistry*, 85(23), pp. 11576–11584. doi: 10.1021/ac402777k.

Cobice, D. F. *et al.* (2016) 'Spatial Localization and Quantitation of Androgens in Mouse Testis by Mass Spectrometry Imaging', *Analytical Chemistry*, 88(21), pp. 10362–10367. doi: 10.1021/acs.analchem.6b02242.

Conn, P. M. (2013) *Animal models for the study of human disease*. 1st edition. London, UK: Elsevier.

Cook-Botelho, J. C., Bachmann, L. M. and French, D. (2017) 'Chapter 10 -

Steroid hormones', in Nair, H. and Clarke, W. (eds) *Mass Spectrometry for the Clinical Laboratory*. London, UK: Academic Press, pp. 205–230. doi: https://doi.org/10.1016/B978-0-12-800871-3.00010-9.

Cotter, R. J. *et al.* (2005) 'Tandem Time-of-Flight (TOF/TOF) Mass Spectrometry and Proteomics', *Journal of the Mass Spectrometry Society of Japan*, 53(1), pp. 7–17. Available at: https://www.ncbi.nlm.nih.gov/pubmed/20717501.

D'Alvise, J. *et al.* (2014) 'Detection of follicular transport of lidocaine and metabolism in adipose tissue in pig ear skin by DESI mass spectrometry imaging', *Analytical and Bioanalytical Chemistry*, 406(15), pp. 3735–3742. doi: 10.1007/s00216-014-7802-z.

Dai, Y., Whittal, R. M. and Li, L. (1996) 'Confocal Fluorescence Microscopic Imaging for Investigating the Analyte Distribution in MALDI Matrices', *Analytical Chemistry*, 68(15), pp. 2494–2500. doi: 10.1021/ac960238z.

Danaceau, J. P., Freeto, S. and Calton, L. J. (2018) 'A Comprehensive Method for the Analysis of Pain Management Drugs and Drugs of Abuse Incorporating Simplified , Rapid Mixed-Mode SPE with UPLC-MS / MS for Clinical Research', Waters Application Note, pp. 1–15. Available at: https://www.waters.com/webassets/cms/library/docs/720006187en.pdf.

Deininger, S. *et al.* (2011) 'Normalization in MALDI-TOF imaging datasets of proteins : practical considerations', *Analytical and Bioanalytical Chemistry,* 401(1), pp. 167–181. doi: 10.1007/s00216-011-4929-z.

Depieri, L. V. *et al.* (2015) 'Advances in the bioanalytical study of drug delivery across the skin.', *Therapeutic delivery*, 6(5), pp. 571–94. doi: 10.4155/tde.15.20.

Díaz-Cruz, M. S. *et al.* (2003) 'Determination of estrogens and progestogens by mass spectrometric techniques (GC/MS, LC/MS and LC/MS/MS)', *Journal of Mass Spectrometry*, 38(9), pp. 917–923. doi: 10.1002/jms.529.

Dole, M. *et al.* (1968) 'Molecular beams of macroions', *The Journal of Chemical Physics*, 49(5), pp. 2240–2249. doi: 10.1063/1.1670391.

Dotsikas, Y. *et al.* (2007) 'An improved high-throughput liquid chromatographic /

tandem mass spectrometric method for terbinafine quantification in human plasma , using automated liquid – liquid extraction based on 96-well format plates', *Biomedical Chromatography*, 21, pp. 201–208. doi: 10.1002/bmc.

Dragicevic, N. and Maibach, H. I. (eds) (2015) *Percutaneous Penetration Enhancers Chemical Methods in Penetration Enhancement.* 1st edition. Berlin, Germany: Springer. doi: 10.1007/978-3-662-47039-8.

Dueñas, M. E., Carlucci, L. and Lee, Y. J. (2016) 'Matrix Recrystallization for MALDI-MS Imaging of Maize Lipids at High-Spatial Resolution', *Journal of the American Society for Mass Spectrometry*, 27(9), pp. 1575–1578. doi: 10.1007/s13361-016-1422-0.

Dunphy, J. C. *et al.* (2001) 'Derivatization LC/MS for the Simultaneous Determination of Fatty Alcohol and Alcohol Ethoxylate Surfactants in Water and Wastewater Samples', *Environmental Science & Technology*, 35(6), pp. 1223–1230. doi: 10.1021/es001491q.

Durand, M. *et al.* (2009) 'Solubilizing and hydrotropic properties of isosorbide monoalkyl-and dimethyl-ethers', *Journal of Surfactants and Detergents*, 12(4), pp. 371–378. doi: 10.1007/s11743-009-1128-4.

van Eijl, S. *et al.* (2012) 'Elucidation of Xenobiotic Metabolism Pathways in Human Skin and Human Skin Models by Proteomic Profiling', *PLoS ONE*, 7(7), p. e41721. doi: 10.1371/journal.pone.0041721.

El-Ghalbzouri, A. *et al.* (2002) 'Effect of fibroblasts on epidermal regeneration', *British Journal of Dermatology*, 147(2), pp. 230–243. doi: 10.1046/j.1365-2133.2002.04871.x.

Ellis, S. R., Bruinen, A. L. and Heeren, R. M. A. (2014) 'A critical evaluation of the current state-of-the-art in quantitative imaging mass spectrometry', *Analytical and Bioanalytical Chemistry*, 406(5), pp. 1275–1289. doi: 10.1007/s00216-013-7478-9.

Englander, S. W. *et al.* (1996) 'Mechanisms and uses of hydrogen exchange', *Current Opinion in Structural Biology*, 6(1), pp. 18–23. doi: 10.1016/S0959-440X(96)80090-X.

Enthaler, B. *et al.* (2012) ‘Improved sample preparation for MALDI–MSI of endogenous compounds in skin tissue sections and mapping of exogenous active compounds subsequent to ex-vivo skin penetration’, *Analytical and Bioanalytical Chemistry*, 402(3), pp. 1159–1167. doi: 10.1007/s00216-011-5562-6.

Enthaler, B. *et al.* (2013) ‘MALDI imaging in human skin tissue sections: focus on various matrices and enzymes’, *Analytical and Bioanalytical Chemistry*, 405(4), pp. 1159–1170. doi: 10.1007/s00216-012-6508-3.

Erdal, M. S. *et al.* (2014) ‘Impacts of chemical enhancers on skin permeation and deposition of terbinafine’, *Pharmaceutical Development and Technology*, 19(5), pp. 565–570. doi: 10.3109/10837450.2013.813538.

Escobar-Chávez, J. J. *et al.* (2008) ‘The tape-stripping technique as a method for drug quantification in skin’, *Journal of Pharmacy and Pharmaceutical Sciences*, 11(1), pp. 104–130. doi: 10.18433/J3201Z.

Esteve, C. *et al.* (2016) ‘Mass spectrometry imaging of amino neurotransmitters: a comparison of derivatization methods and application in mouse brain tissue’, *Metabolomics*, 12(2), pp. 1–9. doi: 10.1007/s11306-015-0926-0.

EU (2003) ‘Directive 2003/15/EC of the European Parliament and of the Council of 27 February 2003 amending Council Directive 76/768/EEC on the approximation of the laws of the Member States relating to cosmetic products’, *Official Journal of the European Union*, L066, pp. 26–35.

Fabin, B. and Touitou, E. (1991) ‘Localization of lipophilic molecules penetrating rat skin in vivo by quantitative autoradiography’, *International Journal of Pharmaceutics*, 74(1), pp. 59–65. doi: https://doi.org/10.1016/0378-5173(91)90408-G.

Faqehi, A. M. M. *et al.* (2016) ‘Derivatization of estrogens enhances specificity and sensitivity of analysis of human plasma and serum by liquid chromatography tandem mass spectrometry’, *Talanta*, 151, pp. 148–156. doi: https://doi.org/10.1016/j.talanta.2015.12.062.

Ferguson, L. S. *et al.* (2013) ‘Efficiency of the dry-wet method for the MALDI-MSI analysis of latent fingermarks’, *Journal of Mass Spectrometry*, 48(6), pp.

677–684. doi: 10.1002/jms.3216.

Fernandez de la Mora, J. (2000) ‘Electrospray ionization of large multiply charged species proceeds via Dole’s charged residue mechanism’, *Analytica Chimica Acta*, 406(1), pp. 93–104. doi: https://doi.org/10.1016/S0003-2670(99)00601-7.

Fischer, A. H. *et al.* (2008) ‘Cryosectioning Tissues’, *Cold Spring Harbor Protocols*, 3(8). doi: 10.1101/pdb.prot4991.

Fliegel, D. *et al.* (2006) ‘Evaluation of a pulsed glow discharge time-of-flight mass spectrometer as a detector for gas chromatography and the influence of the glow discharge source parameters on the information volume in chemical speciation analysis’, *Analytical and Bioanalytical Chemistry*, 386(1), pp. 169–179. doi: 10.1007/s00216-006-0515-1.

Flinders, B. *et al.* (2015) ‘The use of hydrazine-based derivatization reagents for improved sensitivity and detection of carbonyl containing compounds using MALDI-MSI’, *Analytical and Bioanalytical Chemistry*, 407(8), pp. 2085–2094. doi: 10.1007/s00216-014-8223-8.

Flinders, B. *et al.* (2017) ‘Optimization of Sample Preparation and Instrumental Parameters for the Rapid Analysis of Drugs of Abuse in Hair samples by MALDI-MS/MS Imaging’, *Journal of The American Society for Mass Spectrometry*, 28(11), pp. 2462–2468. doi: 10.1007/s13361-017-1766-0.

Fonville, J. M. *et al.* (2012) ‘Robust data processing and normalization strategy for MALDI mass spectrometric imaging’, *Analytical Chemistry*, 84(3), p. 1310. doi: 10.1021/ac201767g.

Francese, S. *et al.* (2013) ‘Curcumin: A multipurpose matrix for MALDI mass spectrometry imaging applications’, *Analytical Chemistry*, 85(10), pp. 5240–5248. doi: 10.1021/ac4007396.

Francese, S. and Clench, M. (2010) ‘MALDI Mass Spectrometry Imaging, a New Frontier in Biostructural Techniques: Applications in Biomedicine’, in Shah, H. N. and Gharbia, S. E. (eds) *Mass Spectrometry for Microbial Proteomics*. Chichester, UK: John Wiley & Sons, Ltd, pp. 91–116. doi: 10.1002/9780470665497.ch5.

Franck, J. *et al.* (2009) ‘On-tissue N-terminal peptide derivatizations for enhancing protein identification in MALDI mass spectrometric imaging strategies’, *Analytical Chemistry*, 81(20), pp. 8305–8317. doi: 10.1021/ac901043n.

Freinkel, R. K. and Woodley, D. (eds) (2001) *The biology of the skin*. 1st edition. Casterton Hall, Carnforth Lancs, UK: The Parthenon Publishing Group.

Fujita, T. and Fujino, T. (2013) ‘Settlement of the Sweet-spot Problem of MALDI Crystals Using Cyclodextrin-supported Matrix’, *Chemistry Letters*, 42(4), pp. 350–351. doi: 10.1246/cl.121232.

Gessel, M. M., Norris, J. L. and Caprioli, R. M. (2014) ‘MALDI imaging mass spectrometry: Spatial molecular analysis to enable a new age of discovery’, *Journal of Proteomics*, 107, pp. 71–82. doi: 10.1016/j.jprot.2014.03.021.

Gibbs, S. *et al.* (2007) ‘Xenobiotic Metabolism in Human Skin and 3D Human Skin Reconstructs: A Review’, *Current Drug Metabolism*, 8(8), pp. 758–772. doi: 10.2174/138920007782798225.

Giles, K. *et al.* (2004) ‘Applications of a travelling wave-based radio-frequency-only stacked ring ion guide’, *Rapid Communications in Mass Spectrometry*, 18(20), pp. 2401–2414. doi: 10.1002/rcm.1641.

Glavič, P. and Lukman, R. (2007) ‘Review of sustainability terms and their definitions’, *Journal of Cleaner Production*, 15(18), pp. 1875–1885. doi: 10.1016/j.jclepro.2006.12.006.

Goodwin, R. J. A. *et al.* (2010) ‘Use of a solvent-free dry matrix coating for quantitative matrix-assisted laser desorption ionization imaging of 4-bromophenyl-1,4-diazabicyclo(3.2.2)nonane-4-carboxylate in rat brain and quantitative analysis of the drug from laser microdissected tissue’, *Analytical Chemistry*, 82(9), pp. 3868–3873. doi: 10.1021/ac100398y.

Goodwin, R. J. A. *et al.* (2011) ‘Qualitative and Quantitative MALDI Imaging of the Positron Emission Tomography Ligands Raclopride (a D2 Dopamine Antagonist) and SCH 23390 (a D1 Dopamine Antagonist) in Rat Brain Tissue Sections Using a Solvent-Free Dry Matrix Application Method’, *Analytical Chemistry*, 83(24), pp. 9694–9701. doi: 10.1021/ac202630t.

Greaves, J. and Roboz, J. (2013) *Mass Spectrometry for the Novice*. 1st edition. Boca Raton: CRC Press.

Griem-Krey, N. *et al.* (2019) 'Autoradiography as a Simple and Powerful Method for Visualization and Characterization of Pharmacological Targets', *Journal of Visualized Experiments : JoVE*, (145). doi: 10.3791/58879.

Griffiths, W. J. *et al.* (2003) 'Derivatisation for the characterisation of neutral oxosteroids by electrospray and matrix-assisted laser desorption/ionisation tandem mass spectrometry: The Girard P derivative', *Rapid Communications in Mass Spectrometry*, 17(9), pp. 924–935. doi: 10.1002/rcm.1002.

Groseclose, M. R. and Castellino, S. (2013) 'A Mimetic Tissue Model for the Quantification of Drug Distributions by MALDI Imaging Mass Spectrometry', *Analytical Chemistry*, 85(21), pp. 10099–10106. doi: 10.1021/ac400892z.

Grubauer, G. *et al.* (1989) 'Lipid content and lipid type as determinants of the epidermal permeability barrier.', *Journal of Lipid Research*, 30(1), pp. 89–96. Available at: http://www.ncbi.nlm.nih.gov/pubmed/2918253.

Guo, Z. and He, L. (2007) 'A binary matrix for background suppression in MALDI-MS of small molecules', *Analytical and Bioanalytical Chemistry*, 387(5), pp. 1939–1944. doi: 10.1007/s00216-006-1100-3.

Guzman, F. (2019) 'Methylphenidate for ADHD: Mechanism of Action and Formulations', Psychopharmacology Institute Open Access Article, pp. 1–9. Available at: https://psychopharmacologyinstitute.com/publication/methylphenidate-for-adhd-mechanism-of-action-and-formulations-2194.

Hadgraft, J. (1999) 'Chapter 4 - Kinetic Modelling and the Skin', in Compton, R. G. and Hancock, G. (eds) *Applications of Kinetic Modelling*. Amsterdam, The Netherlands: Elsevier, pp. 121–132.

Hailat, I. and Helleur, R. J. (2014) 'Direct analysis of sterols by derivatization matrix-assisted laser desorption / ionization time-of-flight mass spectrometry and tandem mass spectrometry', *Rapid Communications in Mass Spectrometry*, 28(2), pp. 149–158. doi: 10.1002/rcm.6766.

Hamm, G., Bonnel, D., Legouffe, R., Pamelard, F., Delbos, J.-M., *et al.* (2012) 'Quantitative mass spectrometry imaging of propranolol and olanzapine using tissue extinction calculation as normalization factor', *Journal of Proteomics*, 75(16), pp. 4952–4961. doi: 10.1016/J.JPROT.2012.07.035.

Hankin, J. A., Barkley, R. M. and Murphy, R. C. (2007) 'Sublimation as a method of matrix application for mass spectrometric imaging', *Journal of the American Society for Mass Spectrometry*, 18(9), pp. 1646–1652. doi: 10.1016/j.jasms.2007.06.010.

Hansen, H. T. and Janfelt, C. (2016) 'Aspects of Quantitation in Mass Spectrometry Imaging Investigated on Cryo-Sections of Spiked Tissue Homogenates', *Analytical Chemistry*, 88(23), pp. 11513–11520. doi: 10.1021/acs.analchem.6b02711.

Haque, T. and Talukder, M. (2018) 'Chemical Enhancer: A Simplistic Way to Modulate Barrier Function of the Stratum Corneum', *Advanced Pharmaceutical Bulletin*, 8(2), pp. 169–179. doi: 10.15171/apb.2018.021.

Hardy, M. H. (1992) 'The secret life of the hair follicle', *Trends in Genetics*, 8(2), pp. 55–61. doi: 10.1016/0168-9525(92)90350-D.

Hart, P. J. *et al.* (2011) 'MALDI-MS imaging of lipids in ex vivo human skin', *Analytical and Bioanalytical Chemistry*, 401(1), pp. 115–125. doi: 10.1007/s00216-011-5090-4.

Harvey, A. *et al.* (2016) 'MALDI-MSI for the analysis of a 3D tissue-engineered psoriatic skin model', *Proteomics*, 16(11–12), pp. 1718–1725. doi: 10.1002/pmic.201600036.

Hengge, U. R. *et al.* (2006) 'Adverse effects of topical glucocorticosteroids', *Journal of the American Academy of Dermatology*, 54(1), pp. 1–18. doi: 10.1016/j.jaad.2005.01.010.

Hewitt, N. J. *et al.* (2013) 'Use of Human In Vitro Skin Models for Accurate and Ethical Risk Assessment : Metabolic Considerations', *Toxicological Sciences*, 133(2), pp. 209–217. doi: 10.1093/toxsci/kft080.

Hillenkamp, F. and Peter-Katalinić, J. (eds) (2007) *MALDI MS : a practical guide*

to instrumentation, methods and applications . Weinheim: Wiley-VCH.

Ho, C. S. *et al.* (2003) 'Electrospray ionisation mass spectrometry: principles and clinical applications.', *The Clinical Biochemist Reviews.*, 24(1), pp. 3–12. Available at: http://www.ncbi.nlm.nih.gov/pubmed/18568044.

Hoffmann, E. and Stroobant, V. (2007) *Mass Spectrometry: Principles and Applications*. 3rd edition. Chichester, UK: John Wiley & Sons, Ltd.

Holle, A. *et al.* (2006) 'Optimizing UV laser focus profiles for improved MALDI performance', *Journal of Mass Spectrometry*, 41, pp. 705–716. doi: 10.1002/jms.1041.

Hossen, M. A. *et al.* (2015) 'Decreased level of phosphatidylcholine (16:0/20:4) in multiple myeloma cells compared to plasma cells: a single-cell MALDI-IMS approach', *Analytical and Bioanalytical Chemistry*, 407(18), pp. 5273–80. doi: 10.1007/s00216-015-8741-z.

Huang, T. *et al.* (2019) 'Chemical Tagging in Mass Spectrometry for Systems Biology', *Analytical Chemistry*, 91, pp. 109–125. doi: 10.1021/acs.analchem.8b04951.

Iribarne, J. V and Thomson, B. A. (1976) 'On the evaporation of small ions from charged droplets', *The Journal of Chemical Physics*, 64(6), pp. 2287–2294. doi: 10.1063/1.432536.

Ishida-Yamamoto, A. and Igawa, S. (2015) 'The biology and regulation of corneodesmosomes', *Cell and Tissue Research*, 360(3), pp. 477–482. doi: 10.1007/s00441-014-2037-z.

Ita, K. B. (2015) 'Chemical Penetration Enhancers for Transdermal Drug Delivery- Success and Challenges', *Current Drug Delivery*, 12(6), pp. 645–651. doi: 10.2174/1567201812666150804104600.

Jadoul, L., Longuespée, R. and Noël, A. (2015) 'A spiked tissue-based approach for quantification of phosphatidylcholines in brain section by MALDI mass spectrometry imaging', *Analytical and Bioanalytical Chemistry*, 407(8), pp. 2095–2106. doi: 10.1007/s00216-014-8232-7.

Jain, A. K., Thomas, N. S. and Panchagnula, R. (2002) 'Transdermal drug

delivery of imipramine hydrochloride. I. Effect of terpenes', *Journal of Controlled Release*, 79(1-3), pp. 93–101. doi: https://doi.org/10.1016/S0168-3659(01)00524-7.

Jang, M. *et al.* (2019) 'Simultaneous determination of methylphenidate and ritalinic acid in hair using LC–MS/MS', *Forensic Science International*, 294, pp. 183–188. doi: https://doi.org/10.1016/j.forsciint.2018.11.021.

Jaskolla, T. W. and Karas, M. (2011) 'Compelling Evidence for Lucky Survivor and Gas Phase Protonation: The Unified MALDI Analyte Protonation Mechanism', *Journal of The American Society for Mass Spectrometry*, 22(6), pp. 976–988. doi: 10.1007/s13361-011-0093-0.

Jirásko, R. *et al.* (2014) 'Distribution study of atorvastatin and its metabolites in rat tissues using combined information from UHPLC/MS and MALDI-Orbitrap-MS imaging', *Analytical and Bioanalytical Chemistry*, 406(19), pp. 4601–4610. doi: 10.1007/s00216-014-7880-y.

Jove, M. *et al.* (2019) 'Precision pharmacology: Mass spectrometry imaging and pharmacokinetic drug resistance', *Critical Reviews in Oncology/Hematology*, 141, pp. 153–162. doi: 10.1016/j.critrevonc.2019.06.008.

Kaletaş, B. K. *et al.* (2009) 'Sample preparation issues for tissue imaging by imaging MS', *Proteomics*, 9(10), pp. 2622–2633. doi: 10.1002/pmic.200800364.

Källback, P. *et al.* (2012) 'Novel mass spectrometry imaging software assisting labeled normalization and quantitation of drugs and neuropeptides directly in tissue sections', *Journal of Proteomics*, 75(16), pp. 4941–4951. doi: 10.1016/j.jprot.2012.07.034.

Källback, P. *et al.* (2016) 'msIQuant − Quantitation Software for Mass Spectrometry Imaging Enabling Fast Access, Visualization, and Analysis of Large Data Sets', *Analytical Chemistry*, 88(8), pp. 4346–4353. doi: 10.1021/acs.analchem.5b04603.

Kanikkannan, N. *et al.* (2000) 'Structure-activity relationship of chemical penetration enhancers in transdermal drug delivery', *Current Medicinal Chemistry*, 7(6), pp. 593–608. doi: 10.2174/0929867003374840.

Kanu, A. B. *et al.* (2008) 'Ion Mobility-Mass Spectrometry.', *Journal of Mass Spectrometry*, 43(1), pp. 1–22. doi: 10.1002/jms.1383.

Karas, M., Bachmann, D. and Hillenkamp, F. (1985) 'Influence of the wavelength in high-irradiance ultraviolet laser desorption mass spectrometry of organic molecules', *Analytical Chemistry*, 57(14), pp. 2935–2939. doi: 10.1021/ac00291a042.

Karas, M., Glückmann, M. and Schäfer, J. (2000) 'Ionization in matrix-assisted laser desorption/ionization: singly charged molecular ions are the lucky survivors', *Journal of Mass Spectrometry*, 35(1), pp. 1–12. doi: 10.1002/(SICI)1096-9888(200001)35:1<1::AID-JMS904>3.0.CO;2-0.

Karas, M. and Hillenkamp, F. (1988) 'Laser desorption ionization of proteins with molecular masses exceeding 10,000 daltons', *Analytical Chemistry*, 60(20), pp. 2299–2301. doi: 10.1021/ac00171a028.

Karas, M. and Krüger, R. (2003) 'Ion Formation in MALDI: The Cluster Ionization Mechanism', *Chemical Reviews*, 103(2), pp. 427–440. doi: 10.1021/cr010376a.

Kaya, I. *et al.* (2018) 'Dual polarity MALDI imaging mass spectrometry on the same pixel points reveals spatial lipid localizations at high-spatial resolutions in rat small intestine', *Analytical Methods*, 10(21), pp. 2428–2435. doi: 10.1039/c8ay00645h.

Kebarle, P. and Verkcerk, U. H. (2009) 'Electrospray: From Ions in solution to Ions in the gas phase, what we know now', *Mass Spectrometry Reviews*, 28(6), pp. 898–917. doi: 10.1002/mas.20247.

Kim, S. H., Shin, C. M. and Yoo, J. S. (1998) 'First application of thermal vapor deposition method to matrix-assisted laser desorption ionization mass spectrometry: determination of molecular mass of bis(p-methyl benzylidene) sorbitol', *Rapid Communications in Mass Spectrometry*, 12(11), pp. 701–704. doi: 10.1002/(SICI)1097-0231(19980615)12:11<701::AID-RCM223>3.0.CO;2-B.

Klerk, L. A. *et al.* (2009) 'Fast and automated large-area imaging MALDI mass spectrometry in microprobe and microscope mode', *International Journal of Mass Spectrometry*, 285(1–2), pp. 19–25. doi: 10.1016/j.ijms.2009.02.032.

Knochenmuss, R. (2006) ‘Ion formation mechanisms in UV-MALDI’, *Analyst*, 131(9), pp. 966–986. doi: 10.1039/b605646f.

Knochenmuss, R. (2013) ‘MALDI ionization mechanisms: the coupled photophysical and chemical dynamics model correctly predicts “temperature”-selected spectra’, *Journal of Mass Spectrometry*, 48(9), pp. 998–1004. doi: 10.1002/jms.3248.

Knochenmuss, R. (2016) ‘The Coupled Chemical and Physical Dynamics Model of MALDI’, *Annual Review of Analytical Chemistry*, 9(1), pp. 365–385. doi: 10.1146/annurev-anchem-071015-041750.

Knochenmuss, R. and Zenobi, R. (2003) ‘MALDI ionization: The role of in-plume processes’, *Chemical Reviews*, 103(2), pp. 441–452. doi: 10.1021/cr0103773.

Koh, C. M. (2013) ‘Preparation of Cells for Microscopy using Chamber Slides and Coverslips’, in Lorsch, J. (ed.) *Laboratory Methods in Enzymology: Cell, Lipid and Carbohydrate*. 1st edition. London, UK: Elsevier/Academic Press Inc, pp. 241–247. doi: 10.1016/B978-0-12-420067-8.00017-9.

Konermann, L. *et al.* (2013) ‘Unraveling the mechanism of electrospray ionization’, *Analytical Chemistry*, 85(1), pp. 2–9. doi: 10.1021/ac302789c.

Krutchinsky, A. N. and Chait, B. T. (2002) ‘On the nature of the chemical noise in MALDI mass spectra’, *Journal of the American Society for Mass Spectrometry*, 13(2), pp. 129–134. doi: 10.1016/S1044-0305(01)00336-1.

Kussmann, M. *et al.* (1997) ‘Matrix-assisted Laser Desorption/Ionization Mass Spectrometry Sample Preparation Techniques Designed for Various Peptide and Protein Analytes’, *Journal of Mass Spectrometry*, 32(6), pp. 593–601. doi: 10.1002/(SICI)1096-9888(199706)32:6<593::AID-JMS511>3.0.CO;2-D.

Lademann, J. *et al.* (2010) ‘Which Skin Model Is the Most Appropriate for the Investigation of Topically Applied Substances into the Hair Follicles?’, *Skin Pharmacology and Physiology*, 23(1), pp. 47–52. doi: 10.1159/000257263.

Lagarrigue, M. *et al.* (2014) ‘Localization and in Situ Absolute Quantification of Chlordecone in the Mouse Liver by MALDI Imaging’, *Analytical Chemistry*, 86(12), pp. 5775–5783. doi: https://doi.org/10.1021/ac500313s.

Laiko, V. V., Baldwin, M. A. and Burlingame, A. L. (2000) ‘Atmospheric pressure matrix-assisted laser desorption/ionization mass spectrometry’, *Analytical Chemistry*, 72(4), pp. 652–657. doi: 10.1021/ac990998k.

Laiko, V. V., Moyer, S. C. and Cotter, R. J. (2000) ‘Atmospheric pressure MALDI/Ion trap mass spectrometry’, *Analytical Chemistry*, 72(21), pp. 5239–5243. doi: 10.1021/ac000530d.

Laizure, S. C. *et al.* (2013) ‘The Role of Human Carboxylesterases in Drug Metabolism : Have We Overlooked Their Importance ?’, *Pharmacotherapy*, 33(2), pp. 210–222.

Lane, M. E. (2013) ‘Skin penetration enhancers’, *International Journal of Pharmaceutics*, 447(1), pp. 12–21. doi: https://doi.org/10.1016/j.ijpharm.2013.02.040.

Laugesen, S. and Roepstorff, P. (2003) ‘Combination of Two Matrices Results in Improved Performance of MALDI MS for Peptide Mass Mapping and Protein Analysis’, *Journal of the American Society for Mass Spectrometry*, 14(9), pp. 992–1002. doi: 10.1016/S1044-0305(03)00262-9.

Lauzon, N. *et al.* (2015) ‘Development of laser desorption imaging mass spectrometry methods to investigate the molecular composition of latent fingermarks’, *Journal of the American Society for Mass Spectrometry*, 26(6), pp. 878–886. doi: 10.1007/s13361-015-1123-0.

Lee, S. *et al.* (2017) ‘Construction of 3D multicellular microfluidic chip for an in vitro skin model’, *Biomedical Microdevices*, 19(2). doi: 10.1007/s10544-017-0156-5.

Lee, Y. J. *et al.* (2012) ‘Use of mass spectrometry for imaging metabolites in plants’, *Plant Journal*, 70(1), pp. 81–95. doi: 10.1111/j.1365-313X.2012.04899.x.

Leite-Silva, V. R. *et al.* (2012) ‘Delivery of drugs applied topically to the skin’, *Expert Review of Dermatology*, 7(4), pp. 383–397. doi: 10.1586/edm.12.32.

Lemaire, R. *et al.* (2006) ‘Solid Ionic Matrixes for Direct Tissue Analysis and MALDI Imaging’, *Analytical Chemistry*, 78(3), pp. 809–819. doi:

10.1021/AC0514669.

Lewis, E. E. L. *et al.* (2018) ‘Examination of the skin barrier repair/wound healing process using a living skin equivalent model and matrix-assisted laser desorption-ionization-mass spectrometry imaging’, *International Journal of Cosmetic Science*, 40(2), pp. 148–156. doi: 10.1111/ics.12446.

Li, B. *et al.* (2014) ‘Natural products in licorice (Glycyrrhiza glabra) rhizome imaged at the cellular level by atmospheric pressure Matrix-Assisted Laser Desorption/Ionization Tandem Mass Spectrometry Imaging’, *The Plant Journal*, 80(1), pp. 161–71. doi: 10.1111/tpj.12608.

Lin, Y., Chen, C. and Wang, G. (2007) ‘Analysis of steroid estrogens in water using liquid chromatography / tandem mass spectrometry with chemical derivatizations’, *Rapid Communications in Mass Spectrometry*, 21(13), pp. 1973–1983. doi: 10.1002/rcm.

Lu, I.-C. *et al.* (2015) ‘Ionization Mechanism of Matrix-Assisted Laser Desorption/Ionization’, *Annual Review of Analytical Chemistry*, 8(1), pp. 21–39. doi: 10.1146/annurev-anchem-071114-040315.

Luxembourg, S. L. *et al.* (2003) ‘Effect of local matrix crystal variations in matrix-assisted ionization techniques for mass spectrometry’, *Analytical Chemistry*, 75(10), pp. 2333–2341. doi: 10.1021/ac026434p.

Luxembourg, S. L. *et al.* (2004) ‘High-spatial resolution mass spectrometric imaging of peptide and protein distributions on a surface’, *Analytical Chemistry*, 76(18), pp. 5339–5344. doi: 10.1021/ac049692q.

Luxembourg, S. L. *et al.* (2006) ‘The molecular scanner in microscope mode’, *Rapid Communications in Mass Spectrometry*, 20(22), pp. 3435–3442. doi: 10.1002/rcm.2747.

Macneil, S. (2007) ‘Progress and opportunities for tissue-engineered skin’, *Nature*, 445(7130), p. 874. doi: 10.1038/nature05664.

Madison, K. C. *et al.* (1987) ‘Presence of intact intercellular lipid lamellae in the upper layers of the stratum corneum’, *Journal of Investigative Dermatology*, 88(6), pp. 714–718. doi: 10.1111/1523-1747.ep12470386.

Mamyrin, B. A. *et al.* (1973) ‘The mass-reflectron, a new nonmagnetic time-of-flight mass spectrometer with high resolution’, *Journal of Experimental and Theoretical Physics*, 37(1), pp. 45–48.

Manevski, N. *et al.* (2015) ‘Phase II Metabolism in Human Skin : Skin Explants Show Full Coverage for Glucuronidation , Sulfation , N -Acetylation , Catechol Methylation , and Glutathione Conjugation’, *Drug Metabolism and Disposition*, 43(1), pp. 126–139.

Marjukka Suhonen, T., A. Bouwstra, J. and Urtti, A. (1999) ‘Chemical enhancement of percutaneous absorption in relation to stratum corneum structural alterations’, *Journal of Controlled Release*, 59(2), pp. 149–161. doi: https://doi.org/10.1016/S0168-3659(98)00187-4.

Marwah, H. *et al.* (2016) ‘Permeation enhancer strategies in transdermal drug delivery’, *Drug Delivery*, 23(2), pp. 564–578. doi: 10.3109/10717544.2014.935532.

Mathes, S. H. and Ruffner, H. (2014) ‘The use of skin models in drug development’, *Advanced Drug Delivery Reviews*, 69, pp. 81–102. doi: 10.1016/j.addr.2013.12.006.

Mead, A. N. *et al.* (2016) ‘Assessing the predictive value of the rodent neurofunctional assessment for commonly reported adverse events in phase I clinical trials.’, *Regulatory Toxicology and Pharmacology : RTP*, 80, pp. 348–57. doi: 10.1016/j.yrtph.2016.05.002.

Medawar, P. B. (1941) ‘Sheets of Pure Epidermal Epithelium from Human Skin’, *Nature*, 148(3765), p. 783. doi: 10.1038/148783a0.

Medzihradszky, K. F. *et al.* (2000) ‘The Characteristics of Peptide Collision-Induced Dissociation Using a High-Performance MALDI-TOF/TOF Tandem Mass Spectrometer’, *Analytical Chemistry*, 72(3), pp. 552–558. doi: 10.1021/ac990809y.

Meisenbichler, C. *et al.* (2019) ‘Improved matrix coating for positive- and negative-ion-mode MALDI-TOF imaging of lipids in blood vessel tissues’, *Analytical and Bioanalytical Chemistry*, 411(15), pp. 3221–3227. doi: 10.1007/s00216-019-01826-x.

Meriaux, C. *et al.* (2010) ‘Liquid ionic matrixes for MALDI mass spectrometry imaging of lipids’, *Journal of Proteomics*, 73(6), pp. 1204–1218. doi: 10.1016/j.jprot.2010.02.010.

Metwally, H., Duez, Q. and Konermann, L. (2018) ‘Chain Ejection Model for Electrospray Ionization of Unfolded Proteins: Evidence from Atomistic Simulations and Ion Mobility Spectrometry’, *Analytical Chemistry*, 90(16), pp. 10069–10077. doi: 10.1021/acs.analchem.8b02926.

Michaels, A. S., Chandrasekaran, S. K. and Shaw, J. E. (1975) ‘Drug permeation through human skin: Theory and in vitro experimental measurement’, *AIChE Journal*, 21(5), pp. 985–996. doi: 10.1002/aic.690210522.

Mitchell, C. A. *et al.* (2015) ‘Lipid changes within the epidermis of living skin equivalents observed across a time-course by MALDI-MS imaging and profiling’, *Lipids in Health and Disease*, 14(1), p. 84. doi: 10.1186/s12944-015-0089-z.

Mitchell, C. A. *et al.* (2016) ‘MALDI MSI analysis of lipid changes in living skin equivalents in response to emollient creams containing palmitoylethanolamide.’, *Methods*, 104, pp. 93–100. doi: 10.1016/j.ymeth.2016.02.001.

van der Molen, R. G. *et al.* (1997) ‘Tape stripping of human stratum corneum yields cell layers that originate from various depths because of furrows in the skin’, *Archives of Dermatological Research*, 289(9), pp. 514–518. doi: 10.1007/s004030050232.

Morikawa-Ichinose, T. *et al.* (2019) ‘Improvement of Sensitivity and Reproducibility for Imaging of Endogenous Metabolites by Matrix-Assisted Laser Desorption/Ionization-Mass Spectrometry’, *Journal of the American Society for Mass Spectrometry*, 30(8), pp. 1512–1520. doi: 10.1007/s13361-019-02221-7.

Moser, K. *et al.* (2001) ‘Passive skin penetration enhancement and its quantification in vitro’, *European Journal of Pharmaceutics and Biopharmaceutics*, 52(2), pp. 103–112. doi: 10.1016/S0939-6411(01)00166-7.

Müller, B. *et al.* (2003) ‘Permeation, metabolism and site of action concentration

of nicotinic acid derivatives in human skin: Correlation with topical pharmacological effect', *European Journal of Pharmaceutical Sciences*, 20(2), pp. 181–195. doi: 10.1016/S0928-0987(03)00179-9.

Murphy, R. C. *et al.* (2011) 'MALDI imaging of lipids after matrix sublimation/deposition', *Biochimica et Biophysica Acta (BBA) - Molecular and Cell Biology of Lipids*, 1811(11), pp. 970–975. doi: 10.1016/j.bbalip.2011.04.012.

Murthy, N. and Shivakumar, H. N. (2010) 'Topical and Transdermal Drug Delivery', in Kulkarni, V. S. (ed.) *Handbook of Non-invasive Drug Delivery Systems*. 1st edition. Oxford: William Andrew, pp. 1–36. doi: 10.1016/B978-0-8155-2025-2.10001-0.

N'Da, D. D. (2014) 'Prodrug strategies for enhancing the percutaneous absorption of drugs', *Molecules*, 19(12), pp. 20780–20807. doi: 10.3390/molecules191220780.

Nafisi, S. and Maibach, H. I. (2018) 'Skin penetration of nanoparticles', in Shegokar, R. and Souto, E. B. (eds) *Emerging Nanotechnologies in Immunology: The Design, Applications and Toxicology of Nanopharmaceuticals and Nanovaccines*. Amsterdam: Elsevier Inc., pp. 47–88. doi: 10.1016/b978-0-323-40016-9.00003-8.

Nakamura, M. *et al.* (2018) 'Alternative test models for skin ageing research', *Experimental Dermatology*, 27(5), pp. 495–500. doi: 10.1111/exd.13519.

Naven, T. J. P. and Harvey, D. J. (1996) 'Cationic derivatization of oligosaccharides with Girard's T reagent for improved performance in matrix-assisted laser desorption/ionization and electrospray mass spectrometry', *Rapid Communications in Mass Spectrometry*, 10(7), pp. 829–834. doi: 10.1002/(SICI)1097-0231(199605)10:7<829::AID-RCM572>3.0.CO;2-Y.

Nemes, Z. and Steinert, P. M. (1999) 'Bricks and mortar of the epidermal barrier', *Experimental & Molecular Medicine*, 31(1), pp. 5–19. doi: 10.1038/emm.1999.2.

Netzlaff, F. *et al.* (2006) 'Comparison of bovine udder skin with human and porcine skin in percutaneous permeation experiments.', *Alternatives to*

laboratory animals : ATLA, 34(5), pp. 499–513. Available at: http://www.ncbi.nlm.nih.gov/pubmed/17121474.

Newton, J. R. A. *et al.* (2017) 'Proteomics and Substrate Based MS Imaging of Xenobiotic Metabolising Enzymes in Ex Vivo Human Skin and a Human Skin Equivalent Model', in *65th ASMS Conference on Mass Spectrometry and Allied Topics, Indianapolis, IN, June 4–8*, p. ThP 297.

Nguyen, S. and Fenn, J. B. (2007) 'Gas-phase ions of solute species from charged droplets of solutions', *Proceedings of the National Academy of Sciences of the United States of America*, 104(4), pp. 1111–1117.

Niehues, H. *et al.* (2018) '3D skin models for 3R research: The potential of 3D reconstructed skin models to study skin barrier function', *Experimental Dermatology*, 27(5), pp. 501–511. doi: 10.1111/exd.13531.

Nilsson, A. *et al.* (2010) 'Fine mapping the spatial distribution and concentration of unlabeled drugs within tissue micro-compartments using imaging mass spectrometry', *PLoS ONE*, 5(7). doi: 10.1371/journal.pone.0011411.

Norlén, L. (2001) 'Skin barrier structure and function: The single gel phase model', *Journal of Investigative Dermatology*, 117(4), pp. 830–836. doi: 10.1046/j.1523-1747.2001.01463.x.

Nowosielski, M. *et al.* (2011) 'Detailed Mechanism of Squalene Epoxidase Inhibition by Terbinafine', *Journal of Chemical Information and Modeling*, 51, pp. 455–462. doi: 10.1021/ci100403b.

Oberacher, H. and Pitterl, F. (2009) 'On the use of ESI-QqTOF-MS/MS for the comparative sequencing of nucleic acids', *Biopolymers*, 91(6), pp. 401–409. doi: 10.1002/bip.21156.

Oertel, R. P. (1977) 'Protein conformational changes induced in human stratum corneum by organic sulfoxides: An infrared spectroscopic investigation', *Biopolymers*, 16(10), pp. 2329–2345. doi: 10.1002/bip.1977.360161017.

Oesch, F. *et al.* (2014) 'Xenobiotic-metabolizing enzymes in the skin of rat, mouse, pig, guinea pig, man, and in human skin models', *Archives of Toxicology*, 88(12), pp. 2135–2190. doi: 10.1007/s00204-014-1382-8.

Oesch, F., Fabian, E. and Landsiedel, R. (2018) ‘Xenobiotica-metabolizing enzymes in the skin of rat, mouse, pig, guinea pig, man, and in human skin models’, *Archives of Toxicology*, 92(8), pp. 2411–2456. doi: 10.1007/s00204-018-2232-x.

Ongpipattanakul, B. *et al.* (1991) ‘Evidence that Oleic Acid Exists in a Separate Phase Within Stratum Corneum Lipids’, *Pharmaceutical Research*, 8(3), pp. 350–354. doi: 10.1023/A:1015845632280.

Osborne, D. W. (2008) ‘Review of changes in topical drug product classification', *Pharmaceutical Technology*, 32(10), p. 66-74.

Otto, A. *et al.* (2008) ‘Effect of penetration modifiers on the dermal and transdermal delivery of drugs and cosmetic active ingredients’, *Skin Pharmacology and Physiology*, 21(6), pp. 326–334. doi: 10.1159/000159265.

Parsons, T. (2002) *An holistic guide to anatomy and physiology*. London: Thomson.

Pathan, I. B. and Setty, C. M. (2009) ‘Chemical Penetration Enhancers for Transdermal Drug Delivery Systems’, *Tropical Journal of Pharmaceutical Research*, 8(2), pp. 173–179. Available at: http://www.tjpr.org.

Petranyi, G., Ryder, N. S. and Stütz, A. (1984) ‘Allylamine derivatives: new class of synthetic antifungal agents inhibiting fungal squalene epoxidase.’, *Science*, 224(4654), pp. 1239–41. doi: 10.1126/science.6547247.

Phan, N. T. N. *et al.* (2016) ‘Laser Desorption Ionization Mass Spectrometry Imaging of Drosophila Brain Using Matrix Sublimation versus Modification with Nanoparticles’, *Analytical Chemistry*, 88(3), pp. 1734–1741. doi: 10.1021/acs.analchem.5b03942.

Pickett, S. *et al.* (2006) ‘Acoustic Droplet Ejection Enables Precise Timing and Positioning for Deposition of Matrix to Optimize MALDI Tissue Imaging’, in *International Mass Spectrometry Conference*. Prague, Czech Republic, p. Number 146.

Pirman, D. A. *et al.* (2013) ‘Quantitative MALDI Tandem Mass Spectrometric Imaging of Cocaine from Brain Tissue with a Deuterated Internal Standard’,

Analytical Chemistry, 85(2), pp. 1081–1089. doi: 10.1021/ac302960j.

Pirman, D. A., Heeren, R. M. A. and Yost, R. A. (2013) 'Identifying Tissue-Specific Signal Variation in MALDI Mass Spectrometric Imaging by Use of an Internal Standard', *Analytical Chemistry*, 85, p. 1090−1096. doi: 10.1021/ac3029618.

Pirman, D. A. and Yost, R. A. (2011) 'Quantitative Tandem Mass Spectrometric Imaging of Endogenous Acetyl-l-carnitine from Piglet Brain Tissue Using an Internal Standard', *Analytical Chemistry*, 83(22), pp. 8575–8581.

Pitt, J. J. (2009) 'Principles and applications of liquid chromatography-mass spectrometry in clinical biochemistry.', *Clinical Biochemist Reviews.*, 30(1), pp. 19–34. Available at: http://www.ncbi.nlm.nih.gov/pubmed/19224008 (Accessed: 2 October 2016).

Poetzsch, M. *et al.* (2014) 'Single hair analysis of small molecules using MALDI-triple quadrupole MS imaging and LC-MS/MS: Investigations on opportunities and pitfalls', *Analytical Chemistry*, 86(23), pp. 11758–11765. doi: 10.1021/ac503193w.

Ponec, M. *et al.* (1988) 'Lipid composition of cultured human keratinocytes in relation to their differentiation.', *Journal of Lipid Research*, 29(7), pp. 949–61. Available at: http://www.ncbi.nlm.nih.gov/pubmed/2457643.

Ponec, M. *et al.* (1997) 'The Formation of Competent Barrier Lipids in Reconstructed Human Epidermis Requires the Presence of Vitamin C', *Journal of Investigative Dermatology*, 109(3), p. 348. doi: 10.1111/1523-1747.ep12336024.

Ponec, M. *et al.* (2000) 'Lipid and ultrastructural characterization of reconstructed skin models', *International Journal of Pharmaceutics*, 203(1–2), pp. 211–225. doi: 10.1016/S0378-5173(00)00459-2.

Porta, T. *et al.* (2015) 'Quantification in MALDI-MS imaging: what can we learn from MALDI-selected reaction monitoring and what can we expect for imaging?', *Analytical and Bioanalytical Chemistry*, 407(8), pp. 2177–2187. doi: 10.1007/s00216-014-8315-5.

Prentice, B. M., Chumbley, C. W. and Caprioli, R. M. (2017) ‘Absolute Quantification of Rifampicin by MALDI Imaging Mass Spectrometry Using Multiple TOF/TOF Events in a Single Laser Shot’, *Journal of the American Society for Mass Spectrometry*, 28(1), p. 136—144. doi: 10.1007/s13361-016-1501-2.

Pretorius, E. *et al.* (2008) ‘In vitro Skin Permeability of Different Terbinafine Hydrochloride Formulations’, *European Journal of Inflammation*, 6(3), pp. 135–140. doi: 10.1177/1721727X0800600306.

Prideaux, B. *et al.* (2007) ‘Sample preparation and data interpretation procedures for the examination of xenobiotic compounds in skin by indirect imaging MALDI-MS’, *International Journal of Mass Spectrometry*, 260(2), pp. 243–251. doi: 10.1016/j.ijms.2006.10.011.

Prideaux, B. *et al.* (2011) ‘High-Sensitivity MALDI-MRM-MS Imaging of Moxifloxacin Distribution in Tuberculosis-Infected Rabbit Lungs and Granulomatous Lesions’, *Analytical Chemistry*, 83(6), pp. 2112–8. doi: 10.1021/ac1029049.

Prideaux, B. and Stoeckli, M. (2012) ‘Mass spectrometry imaging for drug distribution studies’, *Journal of Proteomics*, 75(16), pp. 4999–5013. doi: 10.1016/j.jprot.2012.07.028.

Pringle, S. D. *et al.* (2007) ‘An investigation of the mobility separation of some peptide and protein ions using a new hybrid quadrupole/travelling wave IMS/oa-ToF instrument’, *International Journal of Mass Spectrometry*, 261(1), pp. 1–12. doi: 10.1016/j.ijms.2006.07.021.

Pruniéras, M., Régnier, M. and Woodley, D. (1983) ‘Methods for Cultivation of Keratinocytes with an Air-Liquid Interface’, *Journal of Investigative Dermatology*, 81(s1), p. 28s-33s. doi: 10.1111/1523-1747.ep12540324.

Puolitaival, S. M. *et al.* (2008) ‘Solvent-Free Matrix Dry-Coating for MALDI Imaging of Phospholipids’, *Journal of the American Society for Mass Spectrometry*, 19(6), pp. 882–886. doi: 10.1016/j.jasms.2008.02.013.

Quirke, J. M. E., Adams, C. L. and Van Berkel, G. J. (1994) ‘Chemical Derivatization for Electrospray Ionization Mass Spectrometry. 1. Alkyl Halides,

Alcohols, Phenols, Thiols, and Amines', *Analytical Chemistry*, 66(8), pp. 1302–1315. doi: 10.1021/ac00080a016.

Rademacher, F. *et al.* (2018) 'Skin microbiota and human 3D skin models', *Experimental Dermatology*, 27(5), pp. 489–494. doi: 10.1111/exd.13517.

Rangiah, K. *et al.* (2011) 'Liquid chromatography-mass spectrometry of pre-ionized Girard P derivatives for quantifying estrone and its metabolites in serum from postmenopausal women', *Rapid Communications in Mass Spectrometry*, 25(9), pp. 1297–1307. doi: 10.1002/rcm.4982.

Rao, T. *et al.* (2017) 'Optimization and evaluation of MALDI TOF mass spectrometric imaging for quantification of orally dosed octreotide in mouse tissues', *Talanta*, 165, pp. 128–135. doi: 10.1016/j.talanta.2016.12.049.

Reyzer, M. L. and Caprioli, R. M. (2007) 'MALDI-MS-based imaging of small molecules and proteins in tissues', *Current Opinion in Chemical Biology*, 11(1), pp. 29–35. doi: 10.1016/J.CBPA.2006.11.035.

Rheinwald, J. G. and Green, H. (1977) 'Epidermal growth factor and the multiplication of cultured human epidermal keratinocytes', *Nature*, 265(5593), pp. 421–424. doi: 10.1038/265421a0.

Rodrigues Neves, C. and Gibbs, S. (2018) 'Progress on Reconstructed Human Skin Models for Allergy Research and Identifying Contact Sensitizers', in Ahmed, R. et al. (eds) *Current topics in microbiology and immunology*. Berlin, Germany: Springer, pp. 1–27. doi: 10.1007/82_2018_88.

Rönquist-Nii, Y. and Edlund, P. O. (2005) 'Determination of corticosteroids in tissue samples by liquid chromatography–tandem mass spectrometry', *Journal of Pharmaceutical and Biomedical Analysis*, 37(2), pp. 341–350. doi: https://doi.org/10.1016/j.jpba.2004.10.044.

Rougier, A. *et al.* (1983) 'In vivo correlation between stratum corneum reservoir function and percutaneous absorption', *Journal of Investigative Dermatology*, 81(3), pp. 275–278. doi: 10.1111/1523-1747.ep12518298.

Rougier, A. *et al.* (1990) 'In vivo percutaneous absorption: a key role for stratum corneum/vehicle partitioning', *Archives of Dermatological Research*, 282(8), pp.

498–505. doi: 10.1007/BF00371943.

Ruela, A. L. M. *et al.* (2016) ‘Evaluation of skin absorption of drugs from topical and transdermal formulations’, *Brazilian Journal of Pharmaceutical Sciences*, 52(3), pp. 527–544. doi: 10.1590/s1984-82502016000300018.

Ruffner, H., Graf-Hausner, U. and Mathes, S. (2016) ‘Skin Models for Drug Development and Biopharmaceutical Industry’, in Albanna, M. and Holmes IV, J. H. (eds) *Skin Tissue Engineering and Regenerative Medicine*. London, UK: Academic Press, pp. 357–386. doi: 10.1016/B978-0-12-801654-1.00018-8.

Russo, C. *et al.* (2018) ‘Mass Spectrometry Imaging of 3D Tissue Models.’, *Proteomics*, 18(14), p. e1700462. doi: 10.1002/pmic.201700462.

Ryan, D. J., Spraggins, J. M. and Caprioli, R. M. (2019) ‘Protein identification strategies in MALDI imaging mass spectrometry: a brief review’, *Current Opinion in Chemical Biology*, 48, pp. 64–72. doi: 10.1016/j.cbpa.2018.10.023.

Rzagalinski, I. and Volmer, D. A. (2017) ‘Quantification of low molecular weight compounds by MALDI imaging mass spectrometry – A tutorial review’, *Biochimica et Biophysica Acta (BBA) - Proteins and Proteomics*, 1865(7), pp. 726–739. doi: 10.1016/j.bbapap.2016.12.011.

Sachdeva, V. *et al.* (2010) ‘Transdermal iontophoretic delivery of terbinafine hydrochloride : Quantitation of drug levels in stratum corneum and underlying skin’, *International Journal of Pharmaceutics*, 388, pp. 24–31. doi: 10.1016/j.ijpharm.2009.12.029.

Saeheng, S. *et al.* (2013) ‘In vitro-in vivo correlation study for the dermatopharmacokinetics of terbinafine hydrochloride topical cream’, *Drug Development and Industrial Pharmacy*, 39(9), pp. 1372–1377. doi: 10.3109/03639045.2012.718786.

Sandilands, A. *et al.* (2009) ‘Filaggrin in the frontline: role in skin barrier function and disease.’, *Journal of Cell Science*, 122(Pt 9), pp. 1285–1294. doi: 10.1242/jcs.033969.

Schaefer, H. *et al.* (1980) ‘Principles of Percutaneous Absorption’, in Turner P., Padgham C., Hedges A. (eds) *Clinical Pharmacology & Therapeutics*. London,

UK: Palgrave Macmillan, pp: 395-403, doi: https://doi.org/10.1007/978-1-349-05952-2_44.

Schäfer-Korting, M., Mahmoud, A., *et al.* (2008) 'Reconstructed epidermis and full-thickness skin for absorption testing: influence of the vehicles used on steroid permeation', *Alternatives to laboratory animals : ATLA*, 36(4), p. 441. doi: 10.1177/026119290803600405.

Schäfer-Korting, M., Bock, U., *et al.* (2008) 'The use of reconstructed human epidermis for skin absorption testing: Results of the validation study', *Alternatives to laboratory animals : ATLA*, 36(2), p. 161. doi: 10.1177/026119290803600207.

Schlosser, G. *et al.* (2005) 'MALDI-TOF mass spectrometry of a combinatorial peptide library: Effect of matrix composition on signal suppression', *Journal of Mass Spectrometry*, 40(12), pp. 1590–1594. doi: 10.1002/jms.937.

Schulz, S. *et al.* (2019) 'Advanced MALDI mass spectrometry imaging in pharmaceutical research and drug development', *Current Opinion in Biotechnology*, 55, pp. 51–59. doi: 10.1016/j.copbio.2018.08.003.

Schwamborn, K. and Caprioli, R. M. (2010) 'Molecular imaging by mass spectrometry-looking beyond classical histology', *Nature Reviews Cancer*, 10(9), pp. 639–646. doi: 10.1038/nrc2917.

Schwartz, S. A., Reyzer, M. L. and Caprioli, R. M. (2003) 'Direct tissue analysis using matrix-assisted laser desorption/ionization mass spectrometry: Practical aspects of sample preparation', *Journal of Mass Spectrometry*, 38(7), pp. 699–708. doi: 10.1002/jms.505.

Schweitzer, A., Fahr, A. and Niederberger, W. (1987) 'A simple method for the quantitation of 14C-whole-body autoradiograms', *International Journal of Radiation Applications & Instrumentation. Part A, Applied Radiation & Isotopes*, 38(5), pp. 329–333. doi: 10.1016/0883-2889(87)90019-0.

Seo, J.-E., Kim, S. and Kim, B.-H. (2016) 'In vitro skin absorption tests of three types of parabens using a Franz diffusion cell', *Journal Of Exposure Science And Environmental Epidemiology*, 27(3), pp. 320–325. Available at: https://doi.org/10.1038/jes.2016.33.

Shanks, N. *et al.* (2009) 'Are animal models predictive for humans?', *Philosophy, Ethics, and Humanities in Medicine*, 4(1), p. 2. doi: 10.1186/1747-5341-4-2.

Shanta, S. R. *et al.* (2011) 'Binary matrix for MALDI imaging mass spectrometry of phospholipids in both ion modes', *Analytical Chemistry*, 83(4), pp. 1252–1259. doi: 10.1021/ac1029659.

Shariatgorji, M. *et al.* (2014) 'Direct targeted quantitative molecular imaging of neurotransmitters in brain tissue sections', *Neuron*, 84(4), pp. 697–707. doi: 10.1016/j.neuron.2014.10.011.

Shimma, S. *et al.* (2013) 'Alternative two-step matrix application method for imaging mass spectrometry to avoid tissue shrinkage and improve ionization efficiency', *Journal of Mass Spectrometry*, 48(12), pp. 1285–1290. doi: 10.1002/jms.3288.

Shimma, S. and Sugiura, Y. (2014) 'Effective Sample Preparations in Imaging Mass Spectrometry', *Mass Spectrometry*, 3(S0029). doi: 10.5702/massspectrometry.S0029.

Shroff, R. and Muck, A. (2007) 'Analysis of low molecular weight acids by negative mode matrix-assisted laser desorption/ionization time-of-flight mass spectrometry', *Rapid Communications in Mass Spectrometry*, 21(20), pp. 3295–3300. doi: 10.1002/rcm.

Sindhu, R. *et al.* (2017) 'Skin penetration enhancer's in transdermal drug delivery systems', *Research Journal of Pharmacy and Technology*, 10(6), pp. 1809–1815. doi: 10.5958/0974-360X.2017.00319.5.

Sjövall, P. *et al.* (2014) 'Imaging of Distribution of Topically Applied Drug Molecules in Mouse Skin by Combination of Time-of-Flight Secondary Ion Mass Spectrometry and Scanning Electron Microscopy', *Analytical Chemistry*, 86(7), pp. 3443–3452. doi: 10.1021/ac403924w.

Sleno, L. and Volmer, D. A. (2005) 'Some fundamental and technical aspects of the quantitative analysis of pharmaceutical drugs by matrix-assisted laser desorption/ionization mass spectrometry', *Rapid Communications in Mass Spectrometry*, 19(14), pp. 1928–1936. doi: 10.1002/rcm.2006.

Van Smeden, J. *et al.* (2014) ‘Combined LC/MS-platform for analysis of all major stratum corneum lipids, and the profiling of skin substitutes’, *Biochimica et Biophysica Acta - Molecular and Cell Biology of Lipids*, 1841(1), pp. 70–79. doi: 10.1016/j.bbalip.2013.10.002.

Smith, A. *et al.* (2017) ‘Matrix-assisted laser desorption/ionisation mass spectrometry imaging in the study of gastric cancer: A mini review’, *International Journal of Molecular Sciences*, 18(12). doi: 10.3390/ijms18122588.

Solon, E. G. *et al.* (2010) ‘Autoradiography, MALDI-MS, and SIMS-MS Imaging in Pharmaceutical Discovery and Development’, *The AAPS Journal*, 12(1), pp. 11–26. doi: 10.1208/s12248-009-9158-4.

Solon, E. G. and Kraus, L. (2001) ‘Quantitative whole-body autoradiography in the pharmaceutical industry: Survey results on study design, methods, and regulatory compliance’, *Journal of Pharmacological and Toxicological Methods*, 46(2), pp. 73–81.

Spengler, B., Hubert, M. and Kaufmann, R. (1994) ‘MALDI Ion Imaging and Biological Ion Imaging with a new Scanning UV-Laser Microprobe’, in *42nd ASMS Conference on Mass Spectrometry and Allied Topics, Chicago, IL, May 29- June 3*, p. pp ThP1041.

Sriram, G. *et al.* (2018) ‘Full-thickness human skin-on-chip with enhanced epidermal morphogenesis and barrier function’, *Materials Today*, 21(4), pp. 326–340. doi: 10.1016/j.mattod.2017.11.002.

Stocum, D. L. (2012) *Regenerative biology and medicine*. 2nd edition. London, UK: Elsevier/Academic Press.

Stoeckli, M., Staab, D. and Schweitzer, A. (2007) ‘Compound and metabolite distribution measured by MALDI mass spectrometric imaging in whole-body tissue sections’, *International Journal of Mass Spectrometry*, 260(2–3), pp. 195–202. doi: 10.1016/j.ijms.2006.10.007.

Stokvis, E., Rosing, H. and Beijnen, J. H. (2005) ‘Stable isotopically labeled internal standards in quantitative bioanalysis using liquid chromatography/mass spectrometry: Necessity or not?’, *Rapid Communications in Mass Spectrometry*, 19(3), pp. 401–407. doi: 10.1002/rcm.1790.

Strnad, Š. *et al.* (2019) ‘The use of 1,5-diaminonaphthalene for matrix-assisted laser desorption/ionization mass spectrometry imaging of brain in neurodegenerative disorders’, *Talanta*, 201, pp. 364–372. doi: 10.1016/j.talanta.2019.03.117.

Strohalm, M. *et al.* (2010) ‘mMass 3: A Cross-Platform Software Environment for Precise Analysis of Mass Spectrometric Data’, *Analytical Chemistry*, 82(11), pp. 4648–4651. doi: 10.1021/ac100818g.

Sugibayashi, K. *et al.* (2004) ‘Utility of a Three-Dimensional Cultured Human Skin Model as a Tool to Evaluate the Simultaneous Diffusion and Metabolism of Ethyl Nicotinate in Skin’, *Drug Metabolism and Pharmacokinetics*, 19(5), pp. 352–362. doi: 10.2133/dmpk.19.352.

Sugiura, Y., Shimma, S. and Setou, M. (2006) ‘Thin Sectioning Improves the Peak Intensity and Signal-to-Noise Ratio in Direct Tissue Mass Spectrometry’, *Journal of the Mass Spectrometry Society of Japan*, 54(2), pp. 45–48.

Sun, N. *et al.* (2016) ‘Pharmacokinetic and pharmacometabolomic study of pirfenidone in normal mouse tissues using high mass resolution MALDI-FTICR-mass spectrometry imaging’, *Histochemistry and Cell Biology*, 145(2), pp. 201–211. doi: 10.1007/s00418-015-1382-7.

Swales, J. G. *et al.* (2016) ‘Spatial Quantitation of Drugs in tissues using Liquid Extraction Surface Analysis Mass Spectrometry Imaging’, *Scientific Reports*, 6, p. 37648. doi: 10.1038/srep37648.

Swales, J. G. *et al.* (2019) ‘Mass spectrometry imaging and its application in pharmaceutical research and development: A concise review’, *International Journal of Mass Spectrometry*, 437, pp. 99–112. doi: 10.1016/J.IJMS.2018.02.007.

Tahan, G. P. *et al.* (2016) ‘Determination of parabens in serum by liquid chromatography-tandem mass spectrometry: Correlation with lipstick use’, *Regulatory Toxicology and Pharmacology*, 79, pp. 42–48. doi: https://doi.org/10.1016/j.yrtph.2016.05.001.

Takai, N. *et al.* (2012) ‘Quantitative analysis of pharmaceutical drug distribution in multiple organs by imaging mass spectrometry’, *Rapid Communications in*

Mass Spectrometry, 26(13), pp. 1549–1556. doi: 10.1002/rcm.6256.

Takai, N., Tanaka, Y. and Saji, H. (2014) 'Quantication of Small Molecule Drugs in Biological Tissue Sections by Imaging Mass Spectrometry Using Surrogate Tissue-Based Calibration Standards', *Mass Spectrometry*, 3(1), p. A0025. doi: 10.5702/massspectrometry.A0025.

Taketani, M. *et al.* (2007) 'Carboxylesterase in the liver and small intestine of experimental animals and human', *Life Sciences*, 81(11), pp. 924–932. doi: https://doi.org/10.1016/j.lfs.2007.07.026.

Tannenbaum, J. and Bennett, B. T. (2015) 'Russell and Burch's 3Rs then and now: the need for clarity in definition and purpose', *Journal of the American Association for Laboratory Animal Science : JAALAS*, 54(2), p. 120.

Taudorf, E. H. *et al.* (2015) 'Topically applied methotrexate is rapidly delivered into skin by fractional laser ablation', *Expert Opinion on Drug Delivery*, 12(7), pp. 1059–1069. doi: 10.1517/17425247.2015.1031216.

Teichmann, A. *et al.* (2005) 'Reservoir function of the stratum corneum: Development of an in vivo method to quantitatively determine the stratum corneum reservoir for topically applied substances', *Skin Pharmacology and Physiology*, 18(2), pp. 75–80. doi: 10.1159/000083707.

Teimouri, A., Yeung, P. and Agu, R. (2018) '2D vs. 3D Cell Culture Models for In Vitro Topical (Dermatological) Medication Testing', in Mehanna, R. A. (ed.) *Cell Culture*. London, UK: IntechOpen, pp. 4–20. doi: 10.5772/intechopen.79868.

Teuber, K. *et al.* (2012) '2,4-Dinitrophenylhydrazine as a New Reactive Matrix to Analyze Oxidized Phospholipids by MALDI-TOF Mass Spectrometry', *Analytical Letters*, 45(9), pp. 968–976. doi: 10.1080/00032719.2012.670785.

Thakoersing, V. S. *et al.* (2013) 'Increased presence of monounsaturated fatty acids in the stratum corneum of human skin equivalents', *Journal of Investigative Dermatology*, 133(1), pp. 59–67. doi: 10.1038/jid.2012.262.

Thieme, D., Sachs, H. and Thevis, M. (2008) 'Formation of the N -methylpyridinium derivative to improve the detection of buprenorphine by liquid

chromatography-mass spectrometry', *Journal of Mass Spectrometry*, 43(7), pp. 974–979. doi: 10.1002/jms.

Tholey, A. *et al.* (2002) 'Derivatization of small biomolecules for optimized matrix-assisted laser desorption/ionization mass spectrometry', *Journal of Mass Spectrometry*, 37(9), pp. 963–973. doi: 10.1002/jms.355.

Thomas, A. *et al.* (2012) 'Sublimation of New Matrix Candidates for High Spatial Resolution Imaging Mass Spectrometry of Lipids: Enhanced Information in Both Positive and Negative Polarities after 1,5-Diaminonapthalene Deposition', *Analytical chemistry*, 84(4), pp. 2048–54. doi: 10.1021/ac2033547.

Tjabringa, G. *et al.* (2008) 'Development and validation of human psoriatic skin equivalents', *American Journal of Pathology*, 173(3), pp. 815–823. doi: 10.2353/ajpath.2008.080173.

Tokudome, Y., Katayanagi, M. and Hashimoto, F. (2015) 'Esterase Activity and Intracellular Localization in Reconstructed Human Epidermal Cultured Skin Models', *Annals of Dermatology*, 27(3), pp. 269–274.

Tortora, J. G. and Nielsen, M. (2011) *Principles of Human Anatomy*. 12th edition. United States of America: John Wiley & Sons, Inc.

Touitou, E., Levi-Schaffer, F., *et al.* (1994) 'Modulation of caffeine skin delivery by carrier design: liposomes versus permeation enhancers', *International Journal of Pharmaceutics*, 103(2), pp. 131–136. doi: https://doi.org/10.1016/0378-5173(94)90093-0.

Touitou, E., Alkabes, M., *et al.* (1994) 'Quantitative skin autoradiography: An efficient tool in measuring drug localized in skin layers, hair follicles and glands', in *Proceedings of the International Symposia on Controlled Release Bioactive Materials.* Nice, June 27-30. Deerfield, IL : Controlled Release Society Inc., 21, pp. 431–432. Available at: https://www.scopus.com/inward/record.uri?eid=2-s2.0-0027970716&partnerID=40&md5=ab8bfc1f0f123c8f02a499ffcc0b0d39.

Touitou, E., Meidan, V. M. and Horwitz, E. (1998) 'Methods for quantitative determination of drug localized in the skin', *Journal of Controlled Release*, 56(1), pp. 7–21. doi: https://doi.org/10.1016/S0168-3659(98)00060-1.

Vavrova, K. and Hrabalek, J. Z. and A. (2005) ‘Amphiphilic Transdermal Permeation Enhancers: Structure-Activity Relationships’, *Current Medicinal Chemistry*, 12(19), pp. 2273–2291. doi: http://dx.doi.org/10.2174/0929867054864822.

Vičanová, J. *et al.* (1999) ‘Incorporation of linoleic acid by cultured human keratinocytes’, *Archives of Dermatological Research*, 291(7–8), pp. 405–412. doi: 10.1007/s004030050430.

Vismeh, R., Waldon, D. J. and Zhao, Z. (2012) ‘Localization and Quantification of Drugs in Animal Tissues by Use of Desorption Electrospray Ionization Mass Spectrometry Imaging’, *Analytical Chemistry*, 84(12), p. 5439−5445. doi: 10.1021/ac3011654.

De Vuyst, E. *et al.* (2017) ‘Atopic Dermatitis Studies through In Vitro Models’, *Frontiers in Medicine*, 4(119). doi: 10.3389/fmed.2017.00119.

Walker, R. B. and Smith, E. W. (1996) ‘The role of percutaneous penetration enhancers’, *Advanced Drug Delivery Reviews*, 18(3), pp. 295–301. doi: 10.1016/0169-409X(95)00078-L.

Wang, Y. *et al.* (2016) ‘Critical factors determining the quantification capability of matrix-assisted laser desorption/ionization – time-of-flight mass spectrometry’, *Philosophical Transactions of the Royal Society A*, 374(2079). doi: https://doi.org/10.1098/rsta.2015.0371.

Wang, Z. *et al.* (2015) ‘Organ-on-a-Chip Platforms for Drug Delivery and Cell Characterization: A Review’, *Sensors and Materials*, 27(6), pp. 487–506. doi: 10.18494/SAM.2015.1086.

Weng, N. and Hall, T. D. J. (2002) ‘Systematic Troubleshooting for LC/MS/MS’, *BioPharm*, 15(1), p. 22–26+49.

Wertz, P. W. *et al.* (1989) ‘The role of the corneocyte lipid envelopes in cohesion of the stratum corneum’, *Journal of Investigative Dermatology*, 93(1), pp. 169–172. doi: 10.1111/1523-1747.ep12277394.

Wertz, P. W. (2018) ‘Lipids and the Permeability and Antimicrobial Barriers of the Skin’, *Journal of Lipids*, 2018(5954034), pp. 1–7. doi:

10.1155/2018/5954034.

Wester, R. C. and Maibach, H. I. (2001) ‘In vivo methods for percutaneous absorption measurements’, *Journal of Toxicology - Cutaneous and Ocular Toxicology*, 20(4), pp. 411–422. doi: 10.1081/CUS-120001866.

Wiegand, C., Hewitt, J. and Merk, H. F. (2014) ‘Dermal Xenobiotic Metabolism : A Comparison between Native Human Skin, Four in vitro Skin Test Systems and a Liver System’, *Skin Pharmacology and Physiology*, 27(5), pp. 263–275. doi: 10.1159/000358272.

Wieling, J. (2002) ‘LC-MS-MS experiences with internal standards’, *Chromatographia*, 55(S1), pp. S107–S113. doi: 10.1007/BF02493365.

Wijetunge, C. D. *et al.* (2015) ‘A new peak detection algorithm for MALDI mass spectrometry data based on a modified Asymmetric Pseudo-Voigt model’, *BMC Genomics*, 16(12), pp. 1–12. doi: 10.1186/1471-2164-16-S12-S12.

Wilkinson, W. R. *et al.* (1997) ‘Selection of internal standards for quantitative analysis by matrix-assisted laser desorption-ionization (MALDI) time-of-flight mass spectrometry’, *Fresenius’ Journal of Analytical Chemistry*, 357, pp. 241–248.

Williams, A. C. and Barry, B. W. (2012) ‘Penetration enhancers’, *Advanced Drug Delivery Reviews*, 64, pp. 128–137. doi: 10.1016/j.addr.2012.09.032.

Wolff, M. M. and Stephens, W. E. (1953) ‘A Pulsed Mass Spectrometer with Time Dispersion’, *Review of Scientific Instruments*, 24(8), pp. 616–617. doi: https://doi.org/10.1063/1.1770801.

Xiang, F., Beavis, R. C. and Ens, W. (1994) ‘A method to increase contaminant tolerance in protein matrix-assisted laser desorption/ionization by the fabrication of thin protein-doped polycrystalline films’, *Rapid Communications in Mass Spectrometry*, 8(2), pp. 199–204. doi: 10.1002/rcm.1290080215.

Xie, Y. *et al.* (2010) ‘Development of a Three-Dimensional Human Skin Equivalent Wound Model for Investigating Novel Wound Healing Therapies’, *Tissue Engineering Part C: Methods*, 16(5), pp. 1111–1123. doi: 10.1089/ten.tec.2009.0725.

Xu, H., Timares, L. and Elmets, C. A. (2013) ‘18 - Host defenses in the skin’, in Rich, R. R. et al. (eds) *Clinical Immunology*. 4th edn. Philadelphia, United States: Elsevier Saunders pp. 228–238. Available at: http://www.sciencedirect.com/science/article/pii/B9780723436911000398.

Xu, X. *et al.* (2007) ‘Quantitative Measurement of Endogenous Estrogens and Estrogen Metabolites in Human Serum by Liquid Chromatography−Tandem Mass Spectrometry’, *Analytical Chemistry*, 79(20), pp. 7813–7821. doi: 10.1021/ac070494j.

Yamashita, M. and Fenn, J. B. (1984) ‘Electrospray ion source. Another variation on the free-jet theme’, *The Journal of Physical Chemistry*, 88(20), pp. 4451–4459. doi: 10.1021/j150664a002.

Yang, H. J. *et al.* (2010) ‘Characterization of unknown compounds from stainless steel plates in matrix-assisted laser desorption/ionization mass spectrometry’, *Journal of the American Society for Mass Spectrometry*, 21(12), pp. 2000–2004. doi: 10.1016/j.jasms.2010.08.010.

Yang, J. and Caprioli, R. M. (2011) ‘Matrix Sublimation/Recrystallization for Imaging Proteins by Mass Spectrometry at High Spatial Resolution’, *Analytical Chemistry*, 83(14), pp. 5728–5734. doi: 10.1021/ac200998a.

Yousef, H. and Sharma, S. (2017) ‘Anatomy, Skin (Integument), Epidermis’, in. Treasure Island (FL): StatPearls Publishing.

Zaikin, V. and Halket, J. (2006) ‘Review: Derivatization in mass spectrometry-8. Soft ionization mass spectrometry of small molecules’, *European Journal of Mass Spectrometry*, 12(1), p. 79. doi: 10.1255/ejms.798.

Zaikin, V. and Halket, J. (2009) *A Handbook of Derivatives for Mass Spectrometry*. 1st edition. Chichester, UK: IM Publications.

Zhang, C. *et al.* (2010) ‘CHCA or DHB? Systematic comparison of the two most commonly used matrices for peptide mass fingerprint analysis with MALDI MS’, *Spectroscopy*, 25(2), pp. 48–62.

Zhang, Z. and Michniak-Kohn, B. B. (2012) ‘Tissue engineered human skin equivalents’, *Pharmaceutics*, 4(1), pp. 26–41. doi:

10.3390/pharmaceutics4010026.

Zhao, X. *et al.* (2017) ‘Novel ionic liquid matrices for qualitative and quantitative detection of carbohydrates by matrix assisted laser desorption/ionization mass spectrometry’, *Analytica Chimica Acta*, 985, pp. 114–120. doi: 10.1016/j.aca.2017.07.027.

Zia, H. *et al.* (1991) ‘Cosolvency of Dimethyl Isosorbide for Steroid Solubility’, *Pharmaceutical Research*, 8(4), pp. 502–504. doi: 10.1023/A:1015807413141.